Titre: Title:	Flexible Organic Electrolyte-Gated Transistors Using Liquid and Semi-Solid Electrolytes
Auteur: Author:	Mona Azimi
Date:	2023
Type:	Mémoire ou thèse / Dissertation or Thesis
Référence: Citation:	Azimi, M. (2023). Flexible Organic Electrolyte-Gated Transistors Using Liquid and Semi-Solid Electrolytes [Thèse de doctorat, Polytechnique Montréal]. PolyPublie. https://publications.polymtl.ca/53459/

POLYTECHNIQUE MONTRÉAL

affiliée à l'Université de Montréal

Flexible organic electrolyte-gated transistors using liquid and semi-solid electrolytes

MONA AZIMI

Département de génie chimique

Thèse présentée en vue de l'obtention du diplôme de *Philosophiæ Doctor*

Génie chimique

Juin 2023

POLYTECHNIQUE MONTRÉAL

affiliée à l'Université de Montréal

Cette thèse intitulée:

Flexible organic electrolyte-gated transistors using liquid and semi-solid electrolytes

présentée par **Mona AZIMI**

en vue de l'obtention du diplôme de *Philosophiæ Doctor*

a été dûment acceptée par le jury d'examen constitué de :

Nick VIRGILIO, président
Fabio CICOIRA, membre et directeur de recherche
Julian SELF, membre
Annalisa BONFIGLIO, membre externe

ACKNOWLEDGEMENTS

I would like to express my sincere gratitude to my supervisor, Professor Fabio Cicoira, for his invaluable guidance and support throughout this research project. His extensive knowledge and expertise in the field have significantly influenced the direction and outcome of my research project, contributing greatly to its success. I am grateful for the opportunity to have been supervised by him and for the trust he placed in me to carry out this research work.

I would like to extend my gratitude to the faculty, technical and administrative staff of the Department of Chemical Engineering at Polytechnique Montréal for providing a unique environment for research.

I would like to extend my heartfelt thanks to my friends and colleagues who have been a constant source of support and inspiration throughout my academic journey. This thesis is not only my achievement but also a result of their constant support.

I am sincerely grateful to the Institut de l'Energie Trottier for awarding me the PhD scholarship, which provided me with the financial support to pursue my academic goals.

I would also like to express my appreciation to CMC Microsystems for their financial support through the MNT program.

I would like to express my deepest gratitude to my family for their unwavering support and encouragement throughout my academic journey. Their love, patience, and understanding have been the driving force behind my success.

RÉSUMÉ

Les transistors jouent un rôle essentiel dans la technologie moderne, servant de blocs de construction fondamentaux pour une vaste gamme d'appareils et de systèmes électroniques. Ce sont des composants clés dans les appareils électroniques, tels que les microprocesseurs et les puces de mémoire pour les alimentations, les amplificateurs et les circuits logiques numériques. Les transistors permettent aux appareils électroniques de traiter les informations avec plus de rapidité, d'efficacité et de précision, et ils sont essentiels au développement de technologies telles que les smartphones, les ordinateurs et les systèmes de télécommunications.

Les matériaux organiques gagnent en importance dans la fabrication de transistors en raison de leurs propriétés exceptionnelles et de leurs avantages par rapport aux matériaux inorganiques conventionnels. Parmi les avantages notables, les matériaux organiques sont remarquablement flexibles, ce qui facilite le développement de dispositifs électroniques flexibles et étirables. Cela est particulièrement utile dans des applications telles que l'électronique portable et les dispositifs médicaux. De plus, les matériaux organiques sont relativement bon marché à produire et écologiquement durables, ce qui les distingue des matériaux inorganiques conventionnels.

Cette thèse de doctorat est consacrée à la fabrication et à la caractérisation de transistors à grille électrolyte organique (EGTs). Dans les EGT, le remplacement des diélectriques conventionnels tels que le SiO_2 par un électrolyte permet d'obtenir des basses tensions de fonctionnement (< 1 V) et une haute densité de transporteur de charge (~10^{15} cm^{-2}). Dans la revue de la littérature, divers types d'électrolytes pour EGT sont présentés, cependant, d'autres approches sont nécessaires pour étudier l'effet de l'utilisation de différents types d'électrolyte sur les caractéristiques électriques des EGT.

Dans cette thèse de doctorat, nous avons utilisé des semi-conducteurs organiques de poly[4-(4,4-dihexadecyl-4H-cyclopenta[1,2-b:5,4-b′]dithiophen-2-yl)-alt-[1,2,5]thiadiazolo[3,4-c]pyridine] (PCDTPT) et poly(N-alkyldiketopyrrolo-pyrrole-dithienylthieno[3,2-b]thiophene) (DPP-DTT) et polymère conducteur poly(3,4-éthylènedioxythiophène) sulfonate de polystyrène (PEDOT:PSS) comme matériaux de canal. Les électrolytes des EGT jouent un rôle crucial dans les performances de l'appareil. L'étude des propriétés de l'électrolyte peut aider à diagnostiquer les facteurs qui

affectent la stabilité et la fiabilité des EGT et peut aider à identifier la composition optimale et la structure pour des applications spécifiques.

Tout d'abord, nous avons étudié la caractérisation électrique des EGT basée sur PCDTPT en utilisant un liquide ionique (1-éthyl-3-méthylimidazolium bis (trifluorométhylsulfonyl) imide ([EMIM] [TFSI])) comme l'électrolyte. Nous avons démontré la caractérisation électrique des EGT flexibles, fabriqués sur un substrat de polyimide (PI), à différents rayons de courbure et après plusieurs cycles de flexion. Les appareils ont montré une diminution de 20 % de la valeur de mobilité après 1000 cycles de flexion. Nous avons également démontré comment les EGT peuvent fonctionner comme des phototransistors. Grâce à notre analyse de la photosensibilité des dispositifs EGT flexibles utilisant la lumière solaire simulée, nous avons découvert une amélioration de la densité des porteurs de charge lorsqu'ils sont exposés à une lumière simulée par rapport à celle dans des conditions d'obscurité. La création de porteurs de charge photogénérés dans les semi-conducteurs organiques a entraîné une amélioration de la densité de porteurs de charge et du courant de drain global des dispositifs. Sous illumination, les dispositifs présentaient une valeur de courant de drain plus élevée, environ 1,5 fois supérieure à celle observée dans l'obscurité. Les phototransistors fabriqués fonctionnent à basse tension de fonctionnement (< 1V) par rapport aux phototransistors conventionnels utilisant un matériau diélectrique avec une tension de fonctionnement de plusieurs dizaines de volts.

Deuxièmement, nous avons utilisé des électrolytes en gel semi-solide (c.-à-d. un gel ionique et des hydrogels) comme électrolyte pour les EGT à base de DPP-DTT. Nous avons utilisé deux types d'hydrogels : contenant un agent anti déshydratant (glycérol) et sans agent anti-déshydratant. Tout d'abord, nous avons utilisé la spectroscopie d'impédance (EIS) pour obtenir la caractérisation électrochimique des électrolytes en gel, y compris leurs valeurs de conductivité ionique et de capacité. La caractérisation électrique des EGT à l'aide de différents électrolytes en gel a été obtenue. Nos résultats ont révélé que les dispositifs déclenchés par une capacité spécifique élevée présentaient un courant de drain et une transconductance supérieure par rapport aux autres dispositifs. De plus, nous avons évalué la stabilité opérationnelle des appareils en effectuant des cycles consécutifs de courbes de transfert et de mesures d'impulsions. Les EGT utilisant un gel ionique comme matériau de déclenchement présentaient une stabilité électrique exceptionnelle par rapport aux dispositifs à déclenchement par hydrogel. Notamment, le courant de drain des EGT à

base de gel ionique est resté largement inchangé même après 65 cycles de fonctionnement. De plus, nous avons observé une stabilité électrique améliorée en incorporant du glycérol dans l'hydrogel. La présence de glycérol dans l'hydrogel a significativement amélioré la rétention du courant de drain, l'augmentant de 50% à 90% de son courant initial après 65 cycles. Enfin, nous avons examiné la stabilité mécanique des EGT flexibles sur polyéthylène téréphtalate (PET) sous des états pliés avec des rayons de courbure de 20 mm et 10 mm.

Troisièmement, nous avons fabriqué des transistors électrochimiques organiques plans et verticaux (OECT) imprimés basés sur PEDOT:PSS. Tous les composants des OECT, à l'exception d'un électrolyte, ont été modelés à l'aide de techniques d'impression additive. Des électrolytes semi-solides, à savoir un gel ionique et un organogel, ont été appliqués sur les appareils à l'aide de méthodes de coulage en goutte. Les propriétés électrochimiques des électrolytes ont été évaluées à l'aide d'EIS équipé d'une cellule Swagelok. Nous avons observé un niveau plus élevé de conductivité ionique dans l'organogel par rapport au gel ionique, et cette différence a été attribuée à la plus petite taille des ions présents dans l'organogel. Nous avons effectué une caractérisation électrique des structures planes et verticales en utilisant des gels ioniques et des électrolytes organogels. Nous avons obtenu une transconductance plus élevée pour les OECT en utilisant un organogel par rapport au gel ionique pour les configurations verticales et planaires. De plus, nous avons déterminé les temps de réponse transitoire de ces deux configurations avec gel ionique et organogel en effectuant des mesures d'impulsions. Les dispositifs verticaux ont montré un temps de commutation plus court que celui des dispositifs planaires en raison de la distance de transport réduite des porteurs de charge.

Ce projet de doctorat s'est concentré sur la fabrication et la caractérisation d'EGT à base de matériaux organiques. Nous avons réalisé une application phototransistor d'EGT flexibles basés sur PCDTPT pour comprendre comment le photo-gating module le courant du transistor. De plus, nous avons appliqué différents électrolytes semi-solides (gel ionique et hydrogels) pour les EGT à base de DPP-DTT fonctionnant dans des conditions ambiantes. Nous avons étudié la stabilité de fonctionnement d'appareils utilisant ces différents types d'électrolytes. Nous avons démontré un fonctionnement stable des dispositifs à gel ionique pendant 14 jours dans des conditions ambiantes. De plus, nous avons montré une stabilité opérationnelle améliorée des dispositifs utilisant des dispositifs à déclenchement par hydrogel en ajoutant un agent anti-déshydratant à la formulation

d'hydrogel. De plus, nous avons étudié la stabilité mécanique des EGT en utilisant des électrolytes semi-solides dans des conditions pliées. Enfin, nous avons utilisé une technique d'impression pour modeler les composants des OECT (source, drain, électrodes de grille et matériau actif). Nous avons fabriqué des OECT planaires conventionnels et de nouveaux OECT verticaux basés sur PEDOT:PSS en utilisant une méthode d'impression. Nous avons étudié l'effet de la configuration de l'appareil (réduction d'échelle de la longueur du canal par la structure verticale) sur la valeur de transconductance, en ligne avec l'effet des propriétés de l'électrolyte, telles que la conductivité ionique et la capacité sur la caractérisation électrique et le comportement de commutation des OECT.

ABSTRACT

Transistors play an essential role in modern technology, serving as fundamental building blocks for a vast range of electronic devices and systems. They are key components in electronic devices, such as microprocessors and memory chips to power supplies, amplifiers, and digital logic circuits. Transistors enable electronic devices to process information with greater speed, efficiency, and accuracy, and they are critical to the development of technologies such as smartphones, computers, and telecommunications systems.

Organic materials are gaining significant importance in transistor manufacturing owing to their exceptional properties and advantages over conventional inorganic materials. Among the notable advantages, organic materials are remarkably flexible, which facilitates the development of flexible and stretchable electronic devices. This is particularly useful in applications such as wearable electronics and medical devices. Additionally, organic materials are comparatively inexpensive to produce and environmentally sustainable, setting them apart from conventional inorganic materials.

This PhD thesis is devoted to fabricating and characterizing organic electrolyte-gated transistors (EGTs). In EGTs, replacing conventional dielectrics, like SiO_2, with an electrolyte results in low-operating voltages (< 1 V) and high charge carrier density (~10^{15} cm^{-2}). In the literature review, various types of electrolytes for EGTs are presented, however, further approaches are required to study the effect of using different types of electrolytes on the electrical characteristics of EGTs. We utilized the following p-type organic semiconductors as channel materials: poly[4-(4,4-dihexadecyl-4H-cyclopenta[1,2-b:5,4-b′]dithiophen-2-yl)-alt-[1,2,5]thiadiazolo[3,4-c]pyridine] (PCDTPT) and poly(N-alkyldiketopyrrolo-pyrrole-dithienylthieno[3,2-b]thiophene) (DPP-DTT) and conducting polymer poly(3,4-ethylenedioxythiophene) polystyrene sulfonate (PEDOT:PSS). The electrolytes in EGTs play a crucial role in the performance of the device. Investigating the properties of the electrolyte can help diagnosis the factors that affect the stability and reliability of EGTs and can help in identifying the optimal composition and structure for specific applications.

Firstly, we investigated the electrical characterization of EGTs based on PCDTPT using the ionic liquid, (1-ethyl-3-methylimidazolium bis(trifluoromethylsulfonyl)imide ([EMIM][TFSI])), as an ion gating medium. We demonstrated electrical characterization of flexible EGTs fabricated on a

polyimide (PI) substrate, at various curvature radii and after multiple bending cycles. Devices showed a 20% decrease in mobility value after 1000 bending cycles. We also demonstrated how EGTs can work as phototransistors. Through our analysis of the photosensitivity of flexible EGT devices using simulated solar light, we discovered an improvement in charge carrier density of EGTs when exposed to simulated light compared to that in dark conditions. The creation of photogenerated charge carriers in organic semiconductors resulted in an enhancement of the charge carrier density and overall drain current of the devices. Under illumination, the devices exhibited a higher value of drain current, approximately 1.5 times greater than that observed in the dark condition. Fabricated phototransistors work in low operating voltage (< 1V) compared to conventional phototransistors using dielectric material with an operating voltage of tens of volts.

Secondly, we employed semi-solid gel electrolytes (i.e., ion gel and hydrogels) as gating media for EGTs based on DPP-DTT. We used two types of hydrogels: one containing an anti-dehydrating agent (glycerol) and one without anti-dehydrating agent. We used electrochemical impedance spectroscopy (EIS) to obtain electrochemical characterization of gel electrolytes including their ionic conductivity and capacitance values. Electrical characterization of EGTs using different gel electrolytes were obtained. Our findings revealed that devices gated by high specific capacitance exhibited superior drain current and transconductance compared to other devices. Additionally, we evaluated the operational stability of the devices by conducting consecutive cycles of transfer curves and pulse measurements. EGTs utilizing ion gel as the gating material exhibited exceptional electrical stability when compared to hydrogel-gated devices. Notably, the drain current of the ion gel-based EGTs remained largely unchanged even after 65 operating cycles. Additionally, we observed enhanced electrical stability by incorporating glycerol into the hydrogel. The presence of glycerol in the hydrogel significantly improved the retention of drain current, increasing it from 50% to 90% of its initial current after 65 cycles. Finally, we examined the mechanical stability of flexible EGTs on polyethylene terephthalate (PET) under bent states with bending radii of 20 mm and 10 mm.

Thirdly, we fabricated printed, planar and vertical organic electrochemical transistors (OECTs) based on PEDOT:PSS. All components of the OECTs, except an electrolyte, were patterned using additive printing techniques. Semi-solid electrolytes, namely ion gel and organogel, were applied to the devices using drop-casting methods. The electrochemical properties of the electrolytes were

evaluated using EIS equipped with a Swagelok cell. We observed a higher level of ionic conductivity in organogel compared to ion gel, and this difference was attributed to the smaller size of ions present in the organogel. We conducted an electrical characterization of both planar and vertical structures using ion gel and organogel electrolytes. We obtained higher transconductance for OECTs using organogel compared to ion gel for both vertical and planar configurations. Additionally, we determined the transient response times of these two configurations with ion gel and organogel by performing pulse measurements. Vertical devices showed shorter switching time than that of planar devices due to reduced transport distance of charge carriers.

This PhD project focused on fabrication and characterization of EGTs based on organic materials using liquid and semi-solid electrolytes. We carried out phototransistor application of flexible EGTs based on PCDTPT to understand how photo-gating modulates the transistor current. Additionally, we applied different semi-solid electrolytes (ion gel and hydrogels) for DPP-DTT based EGTs working in ambient conditions. We studied the operational stability of devices using these different types of electrolytes. We demonstrated stable operation of ion gel-gated devices for 14 days in ambient conditions. Furthermore, we showed improved operational stability of devices using hydrogel-gated devices by adding an anti-dehydrating agent to the hydrogel formulation. Additionally, we investigated the mechanical stability of EGTs using semi-solid electrolytes under bent conditions. Lastly, we employed a printing technique to pattern OECTs components (source, drain, gate electrodes, and active material). We fabricated conventional planar OECTs and novel vertical OECTs based on PEDOT:PSS using a printing method. We studied the effect of the device configuration (downscaling of channel length by vertical structure) on the transconductance value, in line with the effect of the properties of the electrolyte, such as ionic conductivity and capacitance on the electrical characterization and switching behavior of the OECTs.

TABLE OF CONTENTS

LIST OF TABLES

LIST OF FIGURES

LIST OF SYMBOLS AND ABBREVIATIONS

$I_{d,dark}$	Drain current in the dark
$I_{d,light}$	Drain current under illumination
p_{light}	Light intensity
V_{gb}	Gate voltages in the backward scan
V_{gf}	Gate voltages in the forward scan
[EMIM][TFSI]	1-Ethyl-3-methylimidazolium bis(trifluoromethylsulfonyl)imide
[PYR_{14}]	1-butyl-1-methylpyrrolidinium
A	Area
a-Si:H	Hydrogenated-amorphous-silicon
AFM	Atomic force microscopy
AgNW	Silver nanowire
BGBC	Bottom-gate/bottom-contact
BGTC	Bottom-gate/top-contact
BHJs	Bulk heterojunctions
BJT	Bipolar junction transistor
C^*	Volumetric capacitance of channel material
C_{CH}	Capacitors created at interface of channel material and electrolyte
CdS	Cadmium sulphide
CDT	Cyclopenta[2,1-b:3,4-b′]dithiophene
C_G	Capacitors created at the interface of gate electrode and electrolyte
$CHCl_3$	Chloroform
C_i	Capacitance of gate dielectric per unit area
CMOS	Complementary metal–oxide–semiconductor
CPE	Constant phase element
CV	Cyclic voltammetry

d	Thickness of the gel
D	Thickness of the dielectric
d_c	Depth
DI	Deionized
DIW	Direct ink writing
DMSO	Dimethyl sulfoxide
DPP	Diketopyrrolopyrrole
DPP-DTT	Poly(N-alkyldiketopyrrolo-pyrrole-dithienylthieno[3,2-b]thiophene)
e	Elementary charge
EA	Electron affinity
ECG	Electrocardiogram
EDS	Energy-dispersive X-ray spectroscopy
EGT	Electrolyte-gated transistor
EIS	Electrochemical impedance spectroscopy
$EMIM^+BF4^-$	1-Ethyl-3-methylimidazolium tetrafluoroborate
EQCM	Electrochemical quartz crystal microbalance
ESR	Equivalent series resistance
f	Frequency
FET	Field-effect transistor
G	Gate electrode
g_m	Transconductance
HMDS	Hexamethyldisilazane
HOMO	Highest occupied molecular orbital
I_0	Initial drain current
I_1	Current coefficient for fitting
I_d	Drain current
$I_{d,lin}$	Drain-source current in the linear region
IoT	Internet of Things
IP	Ionization potential

IPA	Isopropyl alcohol
ITO	Indium tin oxide
k	Dielectric constant
L	Channel length
Li^+	lithium ions
Li^+TFSI^-	Bis(trifluoromethane)sulfonimide lithium salt
$LiClO_4$	Lithium perchlorate
LiOH	Lithium hydroxide
LUMO	Lowest unoccupied molecular orbital
M^+	Cations
MIM	Metal-insulator-metal
MIS	Metal/insulator/semiconductor
MOSFET	Metal-oxide-semiconductor FET
NaClO	Sodium hypochlorite
NaOH	Sodium hydroxide
NMP	N-methyl pyrrolidone
OECT	Organic electrochemical transistor
OFET	Organic field-effect transistor
OLED	Organic light-emitting diode
OPV	Organic photovoltaic
OTFT	Organic thin film transistor
p	Charge carrier density
P	Photosensitivity
P(VPA–AA)	Poly[(vinyl phosphonic acid)-co-(acrylicacid)]
P3CPT	Poly[3-(5-carboxypentyl)thiophene-2,5-diyl]
P3HT	Poly(3-hexylthiophene)
PAN	Polyacrylonitrile
PC	Propylene carbonate
PCB	Printed circuit board

PCBM	Phenyl-C61-butyric acid methyl ester
PCDTPT	Poly[4-(4,4-dihexadecyl-4H-cyclopenta[1,2-b:5,4-b′]dithio-phen-2-yl)-alt-[1,2,5]thiad-iazolo[3,4-c]pyridine]
PDMS	Polydimethylsiloxane
PECVD	Plasma enhanced chemical vapour deposition
PEDOT:PSS	Poly(3,4-ethylenedioxythiophene) polystyrene sulfonate
PEN	Polyethylene naphthalate
PEO	Poly(ethylene oxide)
PET	Polyethylene terephthalate
PI	Polyimide
PMMA	Poly methyl methacrylate
PSS	Polystyrene sulfonate
PSSH	Poly(styrene sulfonic acid)
PSSNa	Poly(styrene sulfonic acid sodium salt)
PTFE	Polytetrafluoroethylene
PVA	Polyvinyl alcohol
PVDF	Polyvinylidene fluoride
PVDF-HFP	Poly(vinylidene fluoride-co-hexafluoropropylene)
PVDF-TrFE	Poly(vinylidene difluoride-trifluoroethylene)
PVP:HDA	Poly(4-vinylphenol) crosslinked with4,4′(hexafluoroisopropylidene) -diphthalic anhydride
R	Photoresponsivity
R_b	Bulk resistance
RIE	Reactive ion etching
r_v	Scan rate
S	Contact area between the electrode and electrolyte
S	Geometrical area of the channel
S/D	Source/drain
SEM	Scanning electron microscopy

SS	Subthreshold swing
t	Time
TFT	Thin film transistor
TGBC	Top-gate/bottom-contact
TGTC	Top-gate/top-contact
TMSiOH	Hydrophilic trimethylsilanol
V_d	Drain-source voltage
V_g	Gate-source voltage
V_{th}	Threshold voltages
W	Channel width
XRD	X-ray diffraction
Z_i	Imaginary part of the impedance
Z_r	Real component of impedance
ε_0	Vacuum permittivity
μ	Carrier mobility
$\mu_{lin,}$	Mobilities in linear regimes
μ_{sat}	Mobilities in saturation regimes
σ	Ionic conductivities
τ	Time constant

LIST OF APPENDICES

CHAPTER 1 INTRODUCTION

1.1 Organic electronics

Organic electronics is an emerging field of science that has received increasing attention in recent years due to its potential to revolutionize the development of electronic devices. The field involves the use of organic materials, such as conducting polymers or small molecules, as semiconductors in electronic devices.

In 1977, Alan J. Heeger, Alan G. MacDiarmid, and Hideki Shirakawa discovered the first conducting polymer, polyacetylene, which exhibited high electrical conductivity upon doping with iodine [1]. This discovery was a breakthrough in the field of materials science and earned them the Nobel Prize in Chemistry in 2000 [2]. The discovery of polyacetylene stimulated the rapid development of new conducting polymers. Researchers quickly synthesized other polymers, including polypyrrole and polythiophene. The invention of conducting polymers led to the development of several types of organic electronic devices, including organic light-emitting diodes (OLEDs), organic photovoltaics (OPVs), and organic transistors [3, 4]. In the early 1980s, OLEDs were invented by Ching W. Tang and Steven Van Slyke at Eastman Kodak [5]. OLEDs are made by layering organic materials between two electrodes, and they emit light when an electric current is applied. OLEDs are used in several applications, including displays and lighting. OPVs are energy harvesting devices that use organic materials to convert sunlight into electricity. OPVs are lightweight, flexible, and low-cost, making them an attractive option for large-scale solar energy production. OPVs can be integrated with other wearable electronic devices to induce self-powering functionality [6]. The development of organic field effect transistor (OFET) began to gain momentum in 1990 and the first flexible OFET were introduced by Garnier et al [7].

FETs are electronic devices with three electrodes (source, drain and gate) that utilize an electric field to control the flow of current through a semiconductor channel. The dielectric layer prevents direct electrical contact between the gate electrode and the channel. The operation of FETs relies on the control of the electric field by the gate terminal. By applying a voltage to the gate, an electric field is created in the channel, which modifies the charge carrier density and controls the flow of current. Transistors can function as amplifiers to amplify input signals, making them essential for various functions in electronic circuits. In FETs, the input signal refers to the voltage applied to the

gate electrode of the transistor. This input signal controls the conductivity of the channel between the source and drain electrodes. By varying the voltage at the gate, the FET can regulate the flow of charge carriers (electrons or holes) in the channel, which in turn affects the output current at the drain electrode. The amplification ability of a transistor, including FETs, is characterized by its transconductance. Transconductance represents the relationship between the change in output current and the corresponding change in input voltage, indicating the transistor's sensitivity to variations in the input signal. Transconductance of transistors can be influenced by device geometry and gate dielectric properties.

In order to advance next-generation electronics, it is imperative that low operating voltage and flexibility be considered as a fundamental requirement. Low operating voltage is necessary to achieve low power consumption for wearable electronic applications. Conventional FETs using metal oxides as gate dielectrics have operating voltage of tens of volts. Utilization of electrolyte as a replacement to metal oxides in electrolyte gated transistors (EGTs) lowers the operating voltage to less than 1 V [8]. Regarding the flexibility properties of transistors traditional silicon based complementary metal–oxide–semiconductor (CMOS) systems cannot meet this requirement due to their rigid and brittle nature. Whereas, organic semiconductors, which are composed of π-bonded molecules or polymers, possess several advantageous characteristics, such as solution processability, lightweight, flexibility, and low processing temperature. These advantages are particularly relevant for the development of wearable electronics and rollable displays, as it allows for the creation of more comfortable and convenient devices [9, 10]. For example, flexible displays can be integrated into clothing or worn as wristbands, providing real-time health monitoring or displaying important information without requiring the use of a traditional screen [11]. Organic electronics also offer potential environmental benefits due to the sustainability of organic materials. Organic materials are typically biodegradable and can be produced from renewable resources, reducing the environmental impact of electronic devices [12]. This is a significant advantage over traditional inorganic materials, which are often difficult to recycle and can have a significant environmental impact over their lifecycle.

1.2 Motivations

The flexibility of organic transistors is a crucial factor that can enable the development of novel electronic devices. The flexibility of these devices allows them to bend, stretch, and conform to irregular surfaces, presenting opportunities for integrating electronic devices into novel applications, such as wearable electronics, flexible displays, and conformable sensors. Furthermore, solution processability, low processing temperature, and environmental friendliness of organic semiconductors make them ideal candidates for flexible devices.

Organic semiconductors, such as poly[4-(4,4-dihexadecyl 4H-cyclopenta[1,2-b:5,4-b′]-dithiophen-2-yl)-alt[1,2,5]thiadiazolo[3,4c]pyridine] (PCDTPT) and poly(N-alkyldiketopyrrolo-pyrrole-dithienylthieno[3,2-b]thiophene) (DPP-DTT) are promising materials for a broad range of applications, including phototransistors, synaptic transistors, and light emitting transistors [13-15]. Electrolytes used as gating media in EGTs can vary in their chemical composition, ionic conductivity, and stability. Different gating media needs to be characterized to determine the most suitable electrolyte for the specific application. Since important electrical parameters of devices such as their transconductance, drain current and ON-OFF ratio, can be influenced by the properties of electrolyte. Moreover, the choice of gating media can influence the long-term stability and reliability of the devices. Some electrolytes may exhibit issues such as electrolyte leakage, or instability under prolonged operation, which can degrade the performance and lifespan of the devices. Investigating the effect of different gating media on device stability and reliability can help identify electrolytes that offer improved stability and long-term performance.

The utilization of additive fabrication techniques such as printing for the fabrication of electronic devices offers several advantages over subtractive photolithography methods, including compatibility with various materials and substrates, fast prototyping for large-scale production, and minimizing material waste. A vertical-channel organic electrochemical transistor (OECT) configuration could offer significant advantages in terms of integration features. The compact device footprint allows for a higher number of transistors to be integrated onto the same substrate [16]. Most of the OECTs reported in the literature have a planar structure with channel lengths typically in the range of tens of microns. However, utilizing a vertical structure can achieve a significantly lower channel length of a few hundred nanometers since the length of the channel is

determined by the active material thickness. Reducing the channel length has the potential to enhance the transconductance value of OECTs to a several hundred millisiemens (mS) [17]. Given the intricacies involved in fabricating vertical structures using photolithography techniques, we used printing techniques as a more convenient and effective approach to fabricate vertical OECTs. These transistors, characterized by short channel lengths, possess a high electric field and deliver high transconductance. As a result, this configuration has the potential to improve the amplification of biological signals. Although vertical devices have been previously demonstrated for OFETs, there are still few reports about vertical OECTs.

1.3 Objectives

This research aims to enhance our understanding of how ion gating media and device configuration influence important figures of merit in EGTs, including their photo sensing properties, electrical properties (such as operating voltage, operational stability, and transconductance), and mechanical properties. The operating voltage of transistors, for example, represents the voltage range within which the device can safely operate. It is crucial to consider the electrochemical stability of the electrolyte and its voltage limits to avoid undesirable reactions. Operational stability refers to the ability of EGT devices to maintain their performance consistently and reliably over an extended operational period. It is a measure of how well the EGT maintains its electrical parameters, including drain current, threshold voltage, mobility, and ON-OFF ratio. Transconductance, on the other hand, quantifies the device's capability to amplify or control the drain current based on the applied input voltage. A higher transconductance value signifies a greater ability to amplify an input signal, resulting in a larger change in output current for a given input voltage change. The mechanical properties of EGT devices can also be influenced by the electrolyte. For instance, the presence of liquid electrolytes introduces challenges related to mechanical stability, as leakage can compromise device integrity and performance. However, semi-solid electrolytes offer a promising solution to mitigate the issue of electrolyte leakage in EGT devices and exhibit better compatibility with the device configuration. Therefore, understanding the impact of the electrolyte on the mechanical properties of EGT devices is essential for ensuring their reliable operation.

By recognizing the significance of electrolyte properties in determining the performance of EGTs, the main objective of this work is to understand the effect of utilization of various ion gating media

with different physical properties (hydrophilic or hydrophobic nature) and electrochemical properties (ionic conductivity and capacitance) on the electrical characterization of EGTs. The findings of this thesis provide a comprehensive understanding of EGTs performance with both accumulation and depletion mode via changing the composition of ion gating media and device configuration and indicate new directions for fabrication of flexible devices.

The specific objectives of this work are:

1. To fabricate flexible, light weight, organic phototransistors with low operating voltage.
2. To utilize semi-solid electrolytes for EGTs and investigate their impact on the electrical and mechanical stability of EGTs.
3. To fabricate planar and vertical OECTs using printing and explore the effect of gating media on device performance.

In order to assess the first specific objective, EGTs based on donor-acceptor conjugated copolymer PCDTPT and using 1-ethyl-3-methylimidazolium bis(trifluoromethylsulfonyl)imide ([EMIM][TFSI]) ionic liquid as a gating media were electrically characterized. The mechanical stability of flexible EGTs, which were fabricated on polyimide (PI) substrates, was evaluated by investigating their electrical characteristics under various bent states with different curvature radii. In order to obtain photo sensing ability of EGTs, they were electrically characterized under illumination of simulated solar light or under dark conditions. We demonstrated that drain current and charge carrier density increased with light and is correlated to the generation of photocurrent. The light weight, flexibility and low operating voltage of fabricated phototransistors make them suitable for bio-medical applications.

To investigate the second specific objective of this work, hydrophobic (ion gel) and hydrophilic (hydrogel) semi-solid electrolytes were prepared. Electrochemical properties of gel electrolytes were measured using electrochemical impedance spectroscopy (EIS). The DPP-DTT organic semiconductor, known for its stability in ambient conditions and aqueous media, was employed as the channel material in EGTs. The electrical stability of the EGTs was assessed through consecutive transfer cycles and the application of ON-OFF pulses to the devices. Additionally, the mechanical stability of flexible devices, fabricated on polyethylene terephthalate (PET) using semi-solid gels as the gating media, was evaluated under bent conditions.

In the third specific objective of our study, we aimed to examine two factors that influence the performance of OECTs. Firstly, we investigated the impact of the OECT configuration, specifically comparing planar and vertical structures. Secondly, we explored the influence of different semi-solid electrolytes, namely ion gel and organogel. OECTs were fabricated using a printing technique. The electrochemical properties of the gel electrolytes were determined using the EIS method and a Swagelok cell. We conducted electrical characterization and studied the transient behavior of both vertical and planar OECTs using the two types of electrolytes.

1.4 Organization of the work

This PhD thesis is comprised of 8 chapters. Chapter 1 provides an overview of the background of organic electronics and outlines the motivation, and objectives of this PhD project. Chapter 2 of this thesis is dedicated to a comprehensive literature review of the history of transistors, FETs and EGTs with a specific focus on their working principles, characteristics, and recent advancements on these devices. Chapter 3 includes the methodology used in this PhD thesis. Chapter 4, 5 and 6 of this thesis consist of articles, where the author is listed as the first author.

Article 1: Mona Azimi, Arunprabaharan Subramanian, Nur Adilah Roslan, Fabio Cicoira, Flexible organic ion-gated transistors with low operating voltage and light-sensing application, *Journal of Physics: Materials*, **2021,** DOI: 10.1088/2515-7639/abd018.

Article 2: Mona Azimi, Arunprabaharan Subramanian, Jiaxin Fan, Francesca Soavi and Fabio Cicoira, Electrical and mechanical stability of flexible, organic electrolyte-gated transistors based on ion gel and hydrogels, *Journal of Materials Chemistry C*, **2023,** DOI: 10.1039/D3TC00410D.

Article 3: Mona Azimi, Chi-hyeong Kim, Jiaxin Fan, and Fabio Cicoira, Effect of Ionic Conductivity of Electrolyte on Printed Planar and Vertical Organic Electrochemical Transistors, *Faraday Discussions*, **2023**, DOI: 10.1039/D3FD00065F.

Chapter 7 provides a general discussion of all work that the author undertook during PhD program.

Chapter 8 discusses the conclusions drawn from all the work presented in the previous chapters. Additionally, this chapter provides an overview of the prospective for future research in the field, building upon the findings and insights gained from the current study.

CHAPTER 2 LITERATURE REVIEW

In this section, we will provide an overview of the history of transistors, with a specific focus on the working principles and components of FETs and EGTs. Additionally, we will discuss recent advancements in the fabrication and characterization of EGTs, highlighting their mechanical flexibility, operational stability, and the influence of configurational structure on device performance.

2.1 History of transistors

The first concept of the FETs was proposed by Lilienfield in 1930 [18] and then in 1948 William Shockley invented the bipolar junction transistor (BJT). BJTs have been used in the design of discrete and integrated circuits. In 1960, Mohamed Atalla and Dawon Kahng used a silicon surface passivation technique and invented the metal-oxide-semiconductor FET (MOSFET) [19]. Compared to BJT technology, MOSFETs can be fabricated with a reduced number of processing steps and offer higher speed and lower dissipation power. The development of MOSFET technology has led to the creation of integrated chips that can hold thousands of reliable transistors. However, the cost of producing these transistors is high and the use of single-crystal silicon substrates limits the creation of large area, flexible, or transparent transistors. In 1961, thin film transistor (TFT) was created using semiconductor material (cadmium sulphide (CdS)) [20]. Furthermore, this concept has been extended to TFTs based on hydrogenated-amorphous-silicon (a-Si:H) where amorphous silicon grows on a heated substrate by plasma enhanced chemical vapour deposition (PECVD) [20]. Thin film transistors based on a-Si:H are widely employed as pixel drive devices in active-matrix liquid-crystal displays on glass substrates. The utilization of MOSFET and a-Si:H-based TFTs have revolutionized the field of electronics, enabling the development of advanced technologies that have transformed the landscape of modern communication, computing, and display systems, despite the fact that a-Si:H TFTs need a lower processing temperature (300 °C) in comparison with MOSFETs (1000 °C). However, this temperature still far above the temperature required for the fabrication of transistors on flexible and lightweight polymeric substrates with glass transition temperatures in the range of 100-200 °C. In contrast, organic materials provide a promising solution for such applications, as they have low processing temperature. Additionally, most organic semiconductors display mechanical flexibility,

making them suitable for flexible electronics. The early stages of research on OFETs date back to the 1980s, Ebisawa et al. reported on a depletion-type metal-insulator-semiconductor field-effect transistor based on poly(acetylene) and poly(siloxane) [21]. The initial efforts laid the foundation for further research in the field of OFETs, driven by the potential of achieving high current modulation and tunable conductivity through the use of novel organic semiconductor materials. Over the following decades, significant advancements were made in terms of device performance. Novel techniques were proposed, and a wide range of organic semiconductors were synthesized, leading to a remarkable increase in the charge carrier mobility of OFETs from 10^{-3} cm^2 V^{-1} s^{-1} in 1989 [22] to 1 cm^2 V^{-1} s^{-1} in 1997 [23]. Through progressive development, modern OFETs now exhibit enhanced performance, with some cases showing mobilities higher than 10 cm^2 V^{-1} s^{-1} [24, 25].

Current research in transistor technology is centered around advancing the field through investigations into novel concepts such as flexibility and stretchability. Flexibility in transistors refers to the ability to withstand bending and twisting, while stretchability refers to the ability to endure stretching and compressing. These properties are crucial for creating electronic devices that can be bent, rolled up, or conform to irregular shapes, offering promising applications in areas such as flexible displays, wearable electronics, and electronic skin [26].

2.2 Field-effect transistor (FETs)

The field-effect transistor (FET) is a three-terminal device that switches or amplifies electrical signal or power. It consists of a gate electrode (G), a dielectric layer, source/drain (S/D) electrodes, and a semiconductor layer (channel material). As shown in Figure 2-1, the device can be configured in four common ways based on the positions of the organic semiconductors and gate dielectrics, namely, bottom-gate/bottom-contact (BGBC), bottom-gate/top-contact (BGTC), top-gate/bottom-contact (TGBC), and top-gate/top-contact (TGTC). The gate electrode modulates the current between source and drain electrodes (I_d), while the source and drain electrodes allow charges to enter and exit the active layer. An insulating layer inhibits current flow between the gate and S/D electrodes. Charges can be transferred in active channel material. In OFETs, the active material is an organic semiconductor that can switch between conductive and non-conductive states through application of a voltage bias on gate electrode [27].

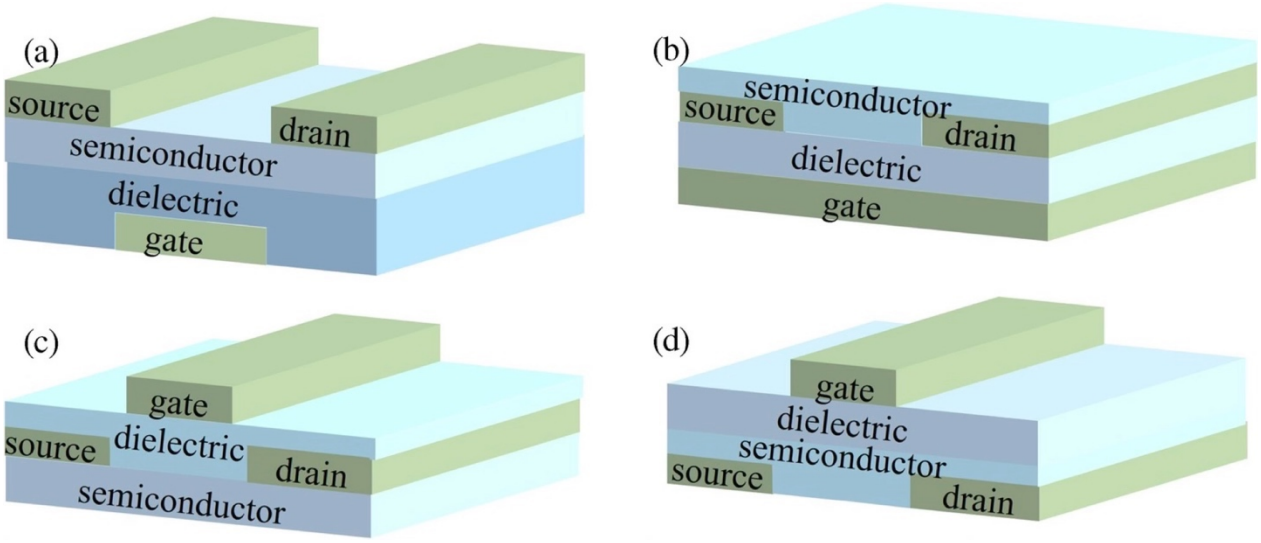

Figure 2-1 Device structures of FETs, BGTC (a), BGBC (b), TGTC (c), TGBC (d). Adapted with permission [27].

2.2.1 Operation of FETs

The transistors operate in two modes called the linear regime and the saturation regime. Figure 2-2 shows a diagrammatic representation of these two modes. When the drain voltage (V_d) is zero, the charge carriers distribute evenly at the interface of semiconductor and dielectric, and there is no current flow ($I_d = 0$). When a small V_d is applied ($V_d << V_g - V_{th}$), there is a linear gradient in the charge density from the source to the drain, and I_d is proportional to V_d. This is known as the linear regime. When V_d increases to the point where a pinch-off occurs at $V_d = V_g - V_{th}$, it results in the creation of a depletion region for charge carriers. This is called the saturation regime, and further increases in V_d will not lead to any further increase in I_d. In the saturation region, a high electric field present in the depletion region drives carriers from the pinch-off point towards the drain. As V_d continues to increase, the pinch-off point approaches the source electrode ($V_d >> V_g - V_{th}$), and the length of the channel (L) undergoes a slight reduction. As a result, the integrated resistance of the channel from the source to the pinch-off point remains mostly the same because of the lack of charge carriers near the drain [28].

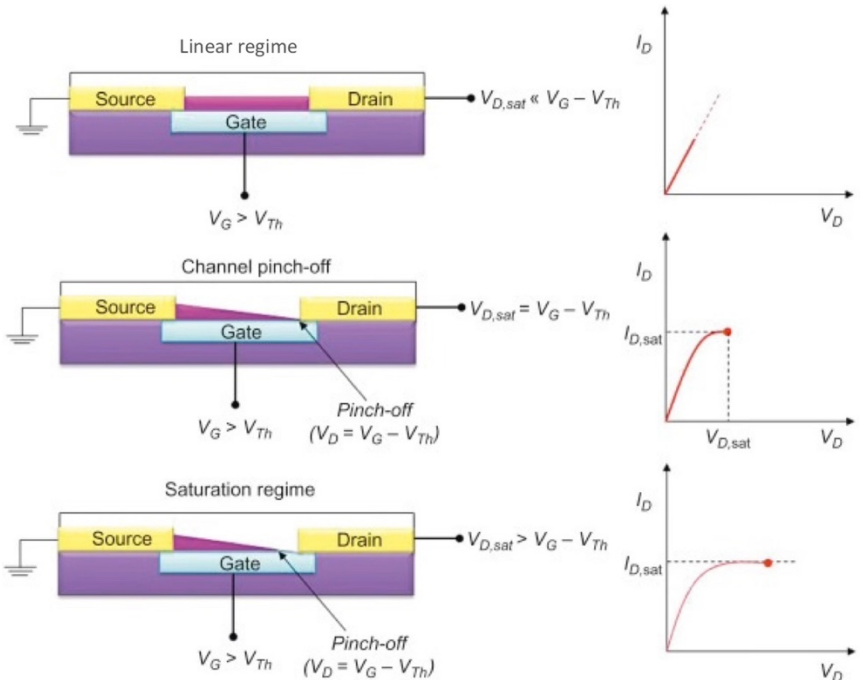

Figure 2-2 Schematic of FETs operating mechanism in linear, pinch-off and saturation region. Adapted with permission [28].

The graph obtained from the I_d versus V_d with different V_g is called output curve. Figure 2-3 (a) shows a typical output curve of FETs. The applied voltages (V_d, V_g) on FETs can be adjusted depending on factors such as the channel geometry, dielectric properties, and the specific requirements of the application. The curve can be divided into linear and saturation regions described by the following equations:

$$I_{d,lin} = \frac{W}{L}\mu_{lin}C_i\left(V_g - V_{th}\right)V_d \quad \text{(Linear)} \qquad (1)$$

$$I_{d,sat} = \frac{W}{2L}\mu_{sat}C_i\left(V_g - V_{th}\right)^2 \quad \text{(Saturation)} \qquad (2)$$

Where W and L are the channel width and length, respectively and C_i is the capacitance of gate dielectric per unit area. V_{th}, V_g, and V_d are the threshold voltage, the voltages at the gate and drain electrodes, respectively, and μ_{lin}, and μ_{sat} are the mobilities in linear and saturation regimes, respectively.

Figure 2-3 (b) shows the transfer curve (plot of I_d against V_g with constant V_d) in linear region and Figure 2-3 (c) is related to transfer curve in saturation region. The onset voltage when I_d experiences

sudden increase (V_{on}) can be obtained from the transfer curve. V_{th} can be achieved by extrapolating the linear section of square root of I_d versus V_g as shown in Figure 2-3 (c). The V_{th} refers to the minimum voltage level that needs to be applied to the gate terminal of a transistor to initiate significant current flow through the channel. It represents the voltage at which the device transitions from OFF-state to ON-state.

The capacitance of gate dielectric can be defined as:

$$C_i = \varepsilon_0 kA/d \qquad (3)$$

Where ε_0 is the vacuum permittivity, k is the dielectric constant, A is the area and d is the thickness of the dielectric.

μ_{lin} can be obtained by a derivative of I_d versus V_g at constant V_d according to the following equation:

$$\mu_{lin} = \frac{L}{WC_iV_d}\frac{dI_{dlin}}{dV_g} \qquad (4)$$

whereas μ_{sat} can be expressed as:

$$\mu_{sat} = \frac{2L}{WC_i}\left(\frac{d\sqrt{I_{dsat}}}{dV_g}\right)^2 \qquad (5)$$

The ON-OFF ratio of a transistor refers to the ratio of the maximum I_d when the transistor is turned ON with respect to the minimum I_d when the transistor is turned OFF. The ON-OFF ratio value can be obtained by dividing the minimum value of drain current ($I_{d,OFF}$) to the maximum value of drain current ($I_{d,ON}$) of transfer curves in the applied gated voltage range as shown in Figure 2-3 (b).

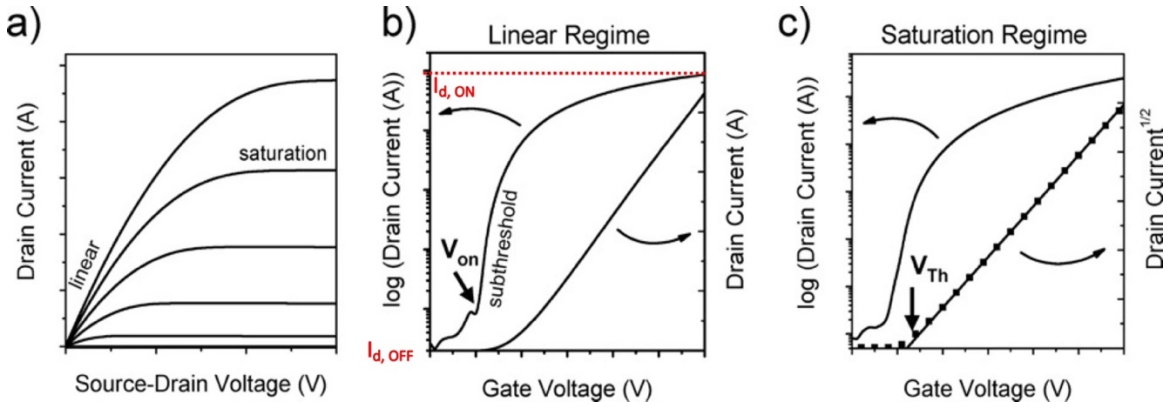

Figure 2-3 Output (a) transfer curve in linear region (b) and transfer curve in saturation region (c). Adapted with permission [29].

Transconductance (g_m) is a measure of how much the drain current of a transistor will change in response to a small change in the gate voltage mathematically it is related to the slope of transfer curve. It quantifies the amplification capability or sensitivity of the device to variations in the input voltage. Higher transconductance leads to greater sensitivity, enabling the device to detect and amplify small variations in the input signal. This is crucial in applications where the sensing system needs to detect and respond to subtle changes, such as in sensors. It is expressed in units of Siemens (S) or Amperes per Volt (A/V) and described as follows:

$$g_m = d(I_d)/d(V_g) \qquad (6)$$

The subthreshold swing quantifies the maximum slope of a transistor when it switches from its OFF-state to ON-state. It serves as a metric for assessing the ability of the channel interface states to be effectively occupied. As such, this parameter is not impacted by the transistor technology and solely depends on the properties of the semiconductor-dielectric interface. The subthreshold swing can be obtained from the logarithmic plot of the I_d versus V_g, at constant V_d and it is expressed as [29]:

$$S = \frac{dV_g}{dlog_{10}(I_d)} \qquad (7)$$

FETs can act as amplifiers by utilizing the field-effect modulation principle and controlling the current flow through the channel. The voltage applied to the gate electrode allows for amplification of the input signal. In an amplification scenario, a small input voltage signal is applied to the gate

electrode. This voltage signal creates an electric field that modifies the conductivity of the semiconductor channel. The change in conductivity results in an amplified output drain current.

Transistors can also function as biosensors and are categorized to two main categories based on the signals they detect. The first category is dedicated to detecting biophysical signals, which include light, cardiac rhythm, brain activity. The second category focuses on detecting biochemicals, such as glucose, enzymes and antibodies. The interaction between the active material of transistor and external stimuli results in a change in the electrical properties of the transistor. This change could manifest as a variation in the drain current value, capacitance, or threshold voltage of the transistor [30].

2.2.2 Channel materials for FETs

The transistor's performance is predominantly determined by the semiconductor channel material, making it a crucial component of the transistor. Semiconducting materials are divided into organic and inorganic materials.

2.2.2.1 Organic semiconductors

Organic semiconductors are molecules based on carbon with a conjugated structure (alternating single and double bands). Organic semiconductors are categorized into small molecules and polymers. Small molecule organic semiconductors can be deposited via thermal evaporation process or solution processes. For polymeric semiconductors solution processing is preferred since their low evaporation temperature limit their deposition through evaporation processes. The double bonds of organic semiconductors consist of σ-bonds and π-bonds formed by the interaction of sp^2 orbitals of two carbon atoms and the overlap of p_z orbitals, respectively. Sp^2- hybridized carbon atoms have three sp^2 orbitals and one perpendicular p_z orbital to sp^2 orbitals (Figure 2-4). Delocalized π molecular orbitals can be formed due to the conjugation (overlap) of the aforementioned π orbitals along the backbone [31].

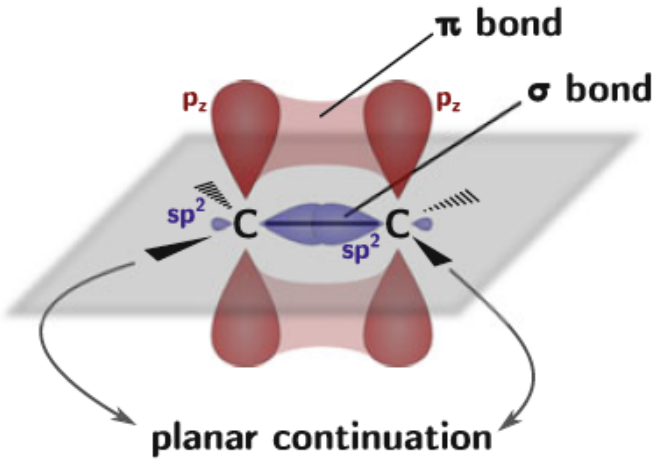

Figure 2-4 The covalent bonding scheme between two carbon atoms with sp^2 hybridization [31].

The electronic structure of organic semiconductors consists of occupied π and σ orbitals and unoccupied π* and σ* orbitals. The ionization potential (IP) and electron affinity (EA) of organic semiconductors can be determined by the energy of (the highest occupied molecular orbital (HOMO) and lowest unoccupied molecular orbital (LUMO) as shown in Figure 2-5 . The π- π interactions between two molecules in conjugated system influence the optical and transport properties (mobility) of organic semiconductors. Conjugated molecules tend to have lower IP and higher EA than non-conjugated molecules. IP is the difference between the vacuum level and the HOMO, while EA is the difference between the vacuum level and LUMO. Molecules with low IP are known as electron-donating molecules that can be oxidized (positively doped) and can form p-type semiconductors. P-type semiconductors are characterized by the presence of positively charged carriers (holes) as the majority carriers. While molecules with high EA are known as electron acceptor and are able to be reduced (negatively doped) and form n-type semiconductors with electrons as the majority charge carriers [32].

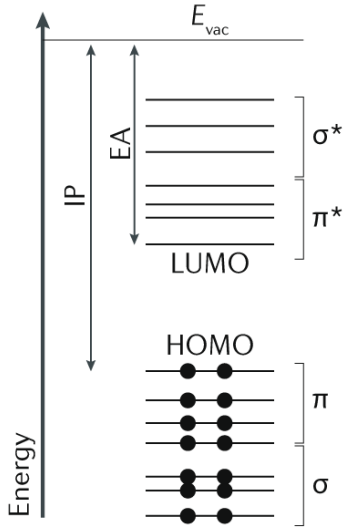

Figure 2-5 Electronic structure of conjugated molecule. Adapted with permission [32].

In this PhD project, we used two types of p-type copolymer semiconductors (PCDTPT and DPP-DTT). The molecular structures of these semiconductors are shown in Figure 2-6.

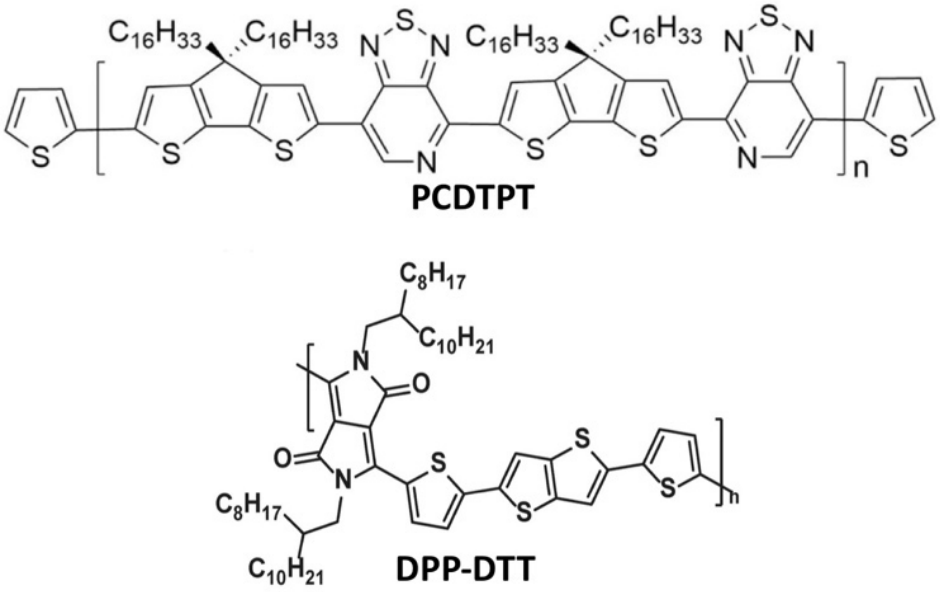

Figure 2-6 Molecular structures of organic semiconductors (PCDTPT and DPP-DTT). Adapted with permission [33, 34].

2.3 Phototransistors

Photodetectors can be broadly classified into two main types: photodiodes and phototransistors. Schemes of typical photodiode and phototransistor structures are shown in Figure 2-7 (a,b). Photodiodes typically feature a vertical structure (Figure 2-7 (a)), with a semiconductor layer sandwiched between electrodes that have an ohmic contact. Phototransistors are light sensing devices with three electrodes as depicted in Figure 2-7 (b). Unlike photodiodes, phototransistors allow the active material to directly receive light without the shielding effect of the electrodes. The presence of gate electrode in phototransistor configuration enables effective amplification of the photocurrent generated by incident light, while simultaneously minimizing unwanted currents that can occur in the absence of light. This combination of features makes the phototransistor well-suited for applications requiring enhanced signal amplification and noise reduction in photo sensing operations. Furthermore, phototransistors combine signal amplification and light sensing in a single device, making them easily integrable into devices and circuits. Figure 2-7 (c,d) shows typical current-voltage curves for photodiodes and phototransistors showing increase of current in light condition compared to dark condition. I_{ph} is correlated to the difference in current for light and dark conditions. In phototransistors transfer curves are affected by the concentration of charge carriers in the channel material, leading to an amplified effect during gate voltage sweep from low to high electric fields [35].

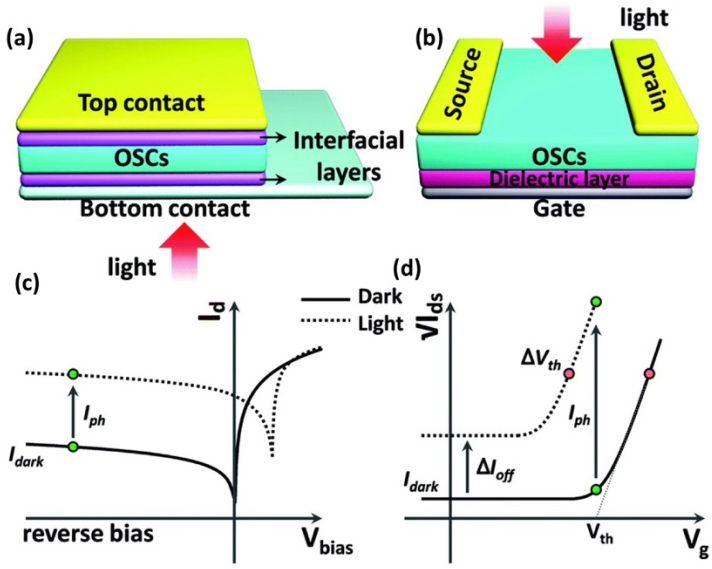

Figure 2-7 Scheme of photodiode configuration (a) and phototransistor (b). Typical current-voltage curves for photodiode (c), and for phototransistor (d). Adapted with permission [35] .

Phototransistors can convert incident light into an electrical signal. This is achieved by modulating the charge carrier in the active material through the presence of light. When light of a specific wavelength is absorbed, excitons are generated and subsequently dissociate into free electrons and holes. These charge carriers can then be collected by the device's electrodes, leading to an increase in the overall drain current of the device. Exciton dissociation can be hindered by the high recombination process. Heterojunction structures has been introduced in order to produce photo-induced charge carriers. Heterojunctions are mixed of donor and acceptor counterparts. In heterojunction structures generated excitons undergo charge transfer state where electrons and holes have low columbic binding and have tendency to dissociate [36].

Charge transport in phototransistors occurs through photovoltaic mode or photoconductive mode. For devices working in accumulation mode, photovoltaic mode of operation is dominant. In the case of p-type channel material by illumination, the excitons dissociate to electron and holes. Holes and electrons move toward the drain and source electrodes, respectively. So, I_d increases and threshold voltage shifts to more positive values. In depletion mode devices the photoconduction mode is governing. In gate voltages higher than threshold voltage, the device is in OFF-state and illumination cause linear enhancement of I_d with optical power [37].

Phototransistors have application in medical imaging and biomedical monitoring. By converting light signals into electrical signals, phototransistors enhance the capabilities of medical imaging, enabling real-time diagnostics, visualization of internal organs, and the study of specific biological processes in a non-invasive manner [35]. Also, they can be employed for energy harvesting from ambient light sources. By converting light energy into electrical energy, phototransistor can be used to power low-power electronic devices or serve as energy-efficient components in energy harvesting systems, such as self-powered sensors or wearable electronics [38].

2.3.1 Figures of merit for phototransistors

Photoresponsivity (R), photosensitivity (P) and response time are the main figure of merits for phototransistors beside the basic electrical characterization of transistors (e.g., mobility, threshold voltage, subthreshold swing). Photoresponsivity shows the ability of phototransistor to transform optical power to electrical current and it is defined as follow:

$$\text{Photoresponsivity (R)} = (I_{d,light} - I_{d,dark})/p_{light}.S \quad (8)$$

Photosensitivity shows the ratio of signal to noise and higher photosensitivity is correlated with easier light detecting ability of devices and it is defined as follow:

$$\text{Photosensitivity (P)} = (I_{d,light} - I_{d,dark})/I_{d,dark} \quad (9)$$

$I_{d,light}$ denote the drain current under illumination, $I_{d,dark}$ denote the drain current in the dark, p_{light} represent the light intensity, and S represent the geometrical area of the channel. The response time of a phototransistor indicates how quickly it reacts to the light, and it can be determined by two main components: rise time and decay time. Rise time represents the interval required for the I_d to increase from 10% to 90% of the saturation value, while decay time refers to the time it takes for the I_d to decrease from 90% to 10% of the saturation current in a dark condition [39]. Various semiconducting materials have been utilized including small molecules, polymer semiconductors to enhance the performance of phototransistors. Also, utilization of electrolyte instead of conventional dielectrics leads to lowering the operating voltage of phototransistor. The subsequent sections of this chapter will provide a more detailed information on transistors using electrolyte as gating media.

Yan et al. showed the performance of a hybrid film of J71:ITIC/PEDOT:PSS organic phototransistor using PAN:LiTFSI ion gel electrolyte with an operating voltage of less than 1.0 V. The device demonstrated outstanding responsivity, reaching up to 6.7×10^6 A/W, and detectivity of 3.6×10^{13} Jones when exposed to 585 nm light with an illumination intensity of 0.5 μW/cm^2 [40].

Sun et al., reported an electrolyte-gated phototransistor with indium tin oxide (ITO) electrodes and based on PCDTPT using [EMIM][TFSI] as an electrolyte. Detectivity of 7.08×10^{11} Jones and the photoresponsivity of 3.56 A/W were obtained under illumination of 885 nm [13].

Vertical structure has been employed for both field effect phototransistors and electrolyte-gated transistors [41, 42]. In vertical structure, the nanoscale channel length and large transconductance enable efficient dissociation, transport, and amplification of photo-generated carriers within the channel, resulting in an enlarged photocurrent output. Yan et al., fabricated vertical electrolyte gated phototransistor based on mixture of CdSe/ZnS and PEDOT:PSS where CdSe/ZnS function as UV sensitive photon-absorbing material and PEDOT:PSS transport charge carriers. Silver nanowire (AgNW) and ITO were employed as electrodes and polyacrylonitrile/[Li^+TFSI^-] as an electrolyte. Phototransistors with a photoresponsivity as high as 2.99×10^7 A/W, detectivity of approximately 1.49×10^{13} Jones, and a rapid response time of around 73 μs have been demonstrated at low operating voltage of 1 V [42].

2.4 Electrolyte-gated transistors

The typical operating voltage of FETs is high (tens of volts) which is correlated to the low capacitance of conventional dielectric materials (5-10 nF cm^{-2}). The specific capacitance of dielectric depends on the thickness and dielectric constant, e.g. 11 nF/cm^2 for 300 nm thick SiO_2. The capacitance of dielectric can be augmented by downscaling the thickness of dielectric or using dielectric with high dielectric constant (e.g. TiO_2 (k~80), ZrO_2 and HfO_2 (k~25)) [43]. However, using dielectric with lower thickness and high dielectric leads to leakage current and decreased charge carrier mobility, respectively.

Another alternative to decrease the operating voltage of transistors is to use electrolytes instead of conventional dielectrics. EGTs are constituted of three terminals (S, D, and G electrodes) similar to FETs. However, in EGTs, channel material and gate electrode are in direct contact with electrolyte. The electrolytes are substances generally composed of mobile ions; cations and anions that are ionically conductive and can move in response to an electric field. The application of a bias voltage to the gate electrode of a device causes ions to migrate within the electrolyte. The active layer of EGTs can consist of conductive polymers or conjugated semiconductors, which allows ions to induce either enhancement or depletion of electronic charges in the channel material. The polarity of the gate voltage determines the type of ions (either cations or anions) accumulated at the gate or channel material, while the magnitude of gate voltage determines the density of accumulated ions. For instance, if a positive gate voltage is applied to EGTs with a p-type channel, anions accumulate at the gate electrode and cations drift toward the channel material, leading to the creation of an electric double layer at interfaces of electrolyte with both channel material and gate electrode (Figure 2-8). The electric double layer consists of the Helmholtz and the diffuse layer. The Helmholtz layer comprised of a layer of solvent molecules and solvated ions while the diffuse layer is made up of free ions. As the distance from the gate or channel material increases, the number of cations or anions decreases. The potential drop at the gate or channel material interface only happens within the double layer, which acts as a dipole, inhibiting electrical current flow. The electric double layer resembles a capacitor with high capacitance, which is inversely proportional to thickness. The capacitance is high (tens of μF cm^{-2}) due to the extremely thin double layer thickness (typically in the range of a few Å). This enables the transistor to operate at low voltages. Two electric double layer capacitors created at the interface of gate electrode and electrolyte (C_G) and at the interface of channel material and electrolyte (C_{CH}) are in series so, the lower capacitance dominates the total capacitance of the circuit. In order to have efficient gating in EGT, C_G should be 10 times higher than C_{CH}. Compared to the dielectric, the utilization of electrolytes delivers several merits such as high transconductance, higher charge carrier

concentration and low operating voltage. Low operating voltage of EGTs makes them an appropriate candidate for several bio-interface applications including biosensors and wearable electronics [44]. EGT devices can utilize a diverse range of gating media, including ionic liquids, ion gels, aqueous electrolytes, polymer electrolytes, and polyelectrolytes, as their ion gating media [45].

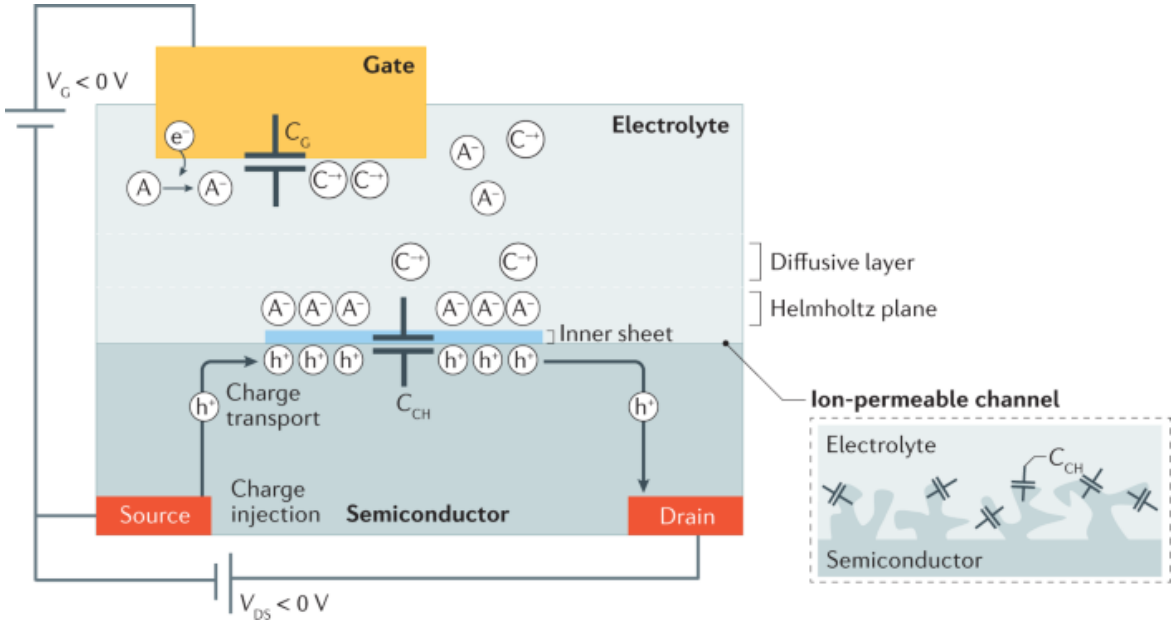

Figure 2-8 Scheme of EGT device with electric double layer capacitances formed at the interface of gate electrode and electrolyte (C_G) and at the interface of channel material and electrolyte (C_{CH}). Adapted with permission [44].

2.4.1 Electrostatic versus electrochemical operation of EGTs

EGTs can operate in two different modes: electrostatic (double layer) and electrochemical. In the electrostatic mode (Figure 2-9 (a)), the active material of the EGT is impermeable to ions, and the modulation of current occurs through electrostatic doping. By applying a gate voltage, an electric double layer is created at the interface between the active material and the electrolyte, and the accumulated charge carriers are modulated by the strength of the electric field. The higher electric field leads to the greater number of accumulated charge carriers. These types of devices operating with electrostatic doping are also known as electric double layer transistors. In the electrochemical mode (Figure 2-9 (b)), the active material of the EGT is permeable to ions, and the modulation of

current occurs through electrochemical doping. By applying a gate voltage, ions from the electrolyte can be penetrated in the channel material, leading to the manipulation of the redox state of the active material. This, in turn, modulates the conductivity of the channel material and the overall current in the EGT [46]. These types of EGTs are known as electrochemical transistors. The key difference between these two operation modes lies in the depth of charge accumulation and the location of charge conduction, whether it takes place at the interface or within the bulk of the material. Principally, electrochemical doping is expected to generate a higher drain current compared to electrostatic doping since ion penetration effectively introduces doping within the bulk of semiconductor. The electrostatic and electrochemical working mechanisms in EGTs has a direct impact on the switching speed of the transistors. Electrostatic doping enables rapid switching in the microsecond range, while electrochemical doping results in switching speeds in the millisecond range [47]. The electrostatic doping mechanism holds great potential for applications demanding low-voltage operation. Conversely, electrochemical doping typically offers a higher charge capacity for a given semiconductor, implying that this doping mechanism may be more suitable for applications requiring high currents. By employing specific materials and techniques to control the doping mechanism of EGTs, the parameters can be finely adjusted to meet the requirements of specific applications. For instance, in high-frequency electronic oscillators, where fast operation is crucial, transistors operating via electrostatic doping are preferred to achieve high switching speeds. On the other hand, the relatively slower process of ion uptake in the semiconducting channel material limits the use of electrochemically driven EGTs in high-frequency electronic circuits. Electrochemically driven EGTs find their applications in memory devices, such as neuromorphic devices, where ions need to be retained in the active channel material for specific and controlled durations [30].

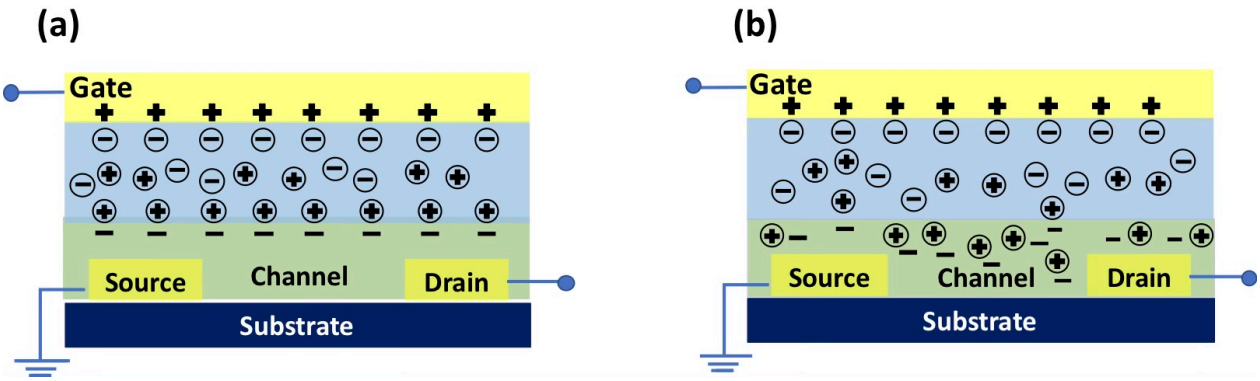

Figure 2-9 Devices working in electrostatic mode (a), and devices working in electrochemical mode (b)

2.4.2 Depletion and accumulation operation

Operation of transistors is categorized into depletion and accumulation (enhancement) depending on the doping level of active channel material. For channel materials that are conductive (doped) in their pristine state, the device is in ON-state without applying V_g. Figure 2-10 (a) shows the scheme of device working in depletion mode. At zero gate voltage when the device is in ON-state (top scheme of Figure 2-10 (a)) the presence of holes in the conducting polymer leads to an increased drain current, resulting in the transistor being in ON-state. When a gate voltage is applied, the holes in the conducting polymer are replaced by cations, causing the transistor to switch to the OFF-state (bottom scheme of Figure 2-10 (a)). According to the output curve of depletion mode (Figure 2-10 (b)), application of gate voltage leads to reduction of drain current. In accumulation mode EGTs, active channel material is based on de-doped semiconductor. Figure 2-10 (c) shows the scheme of device working in accumulation mode. The bottom scheme of Figure 2-10 (c) is related to zero gate voltage where the channel has few mobile holes, and the transistor is OFF. When a gate voltage is applied (top scheme of Figure 2-10 (c)), holes accumulate on the chains of channel material and compensate penetrated anions and device switches to ON-state. According to output curve of accumulation mode devices (Figure 2-10 (d)), at zero gate voltage, the drain current is low. However, when a voltage is applied to the gate electrode, the semiconductor becomes doped, leading to an increase in the drain current. As a result, the device switches to the ON-state [48].

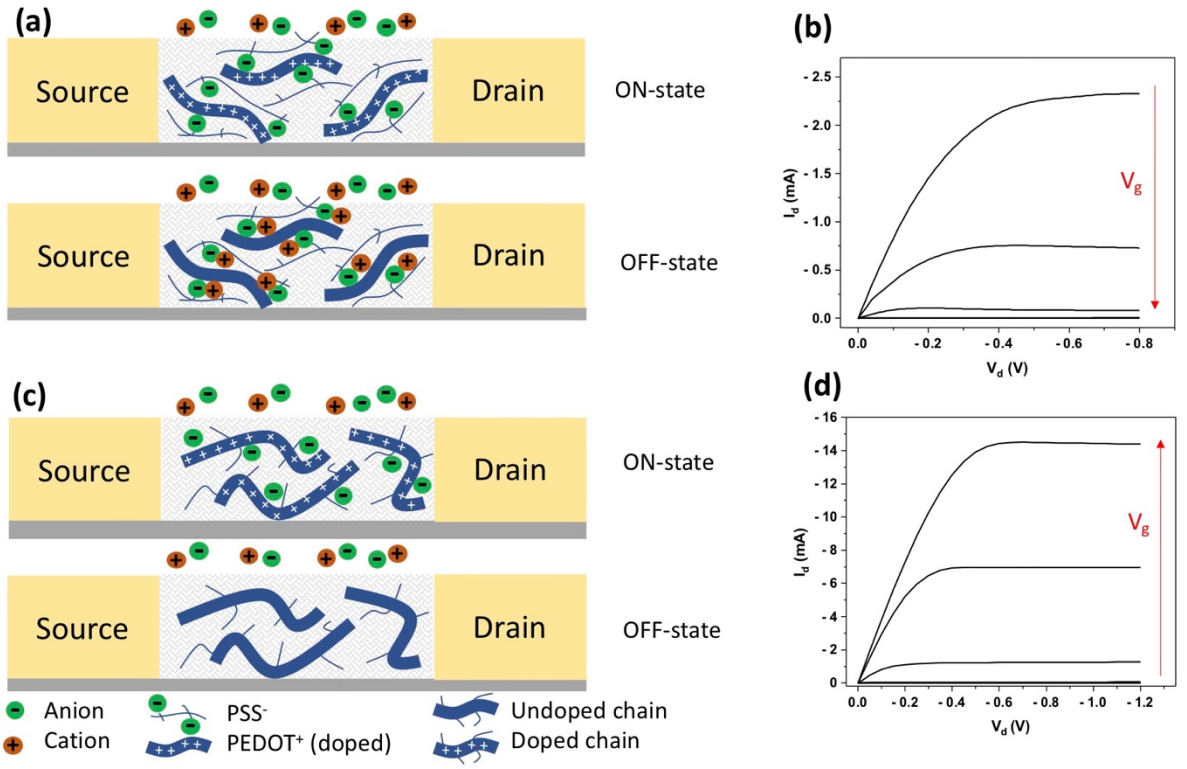

Figure 2-10 Scheme of devices working in depletion mode (top scheme is related to ON-state and bottom scheme is related to OFF-state) (a), Output curve of depletion mode device (b), scheme of devices working is accumulation mode (top scheme is related to ON-state and bottom scheme is related to OFF-state) (c), and output curve of accumulation mode device (d).

PEDOT:PSS conducting polymer is a well-known material used for devices working in depletion mode. PEDOT:PSS is a combination of conjugated polymer and polyelectrolyte dispersion. Molecular structure of PEDOT:PSS is sown in Figure 2-11 (a). PEDOT in its oxidized form exhibits high conductivity; however, it is not soluble in water. On the other hand, when combined with polystyrene sulfonate (PSS), which acts as an insulating agent, PEDOT becomes dispersible in water and forms a stable solution. The sulfonate groups in the polyelectrolyte portion of PEDOT:PSS act as counterions to positively charged polymer chains. PSS serves a critical role in stabilizing the quinoid conformation of PEDOT. The PEDOT:PSS complex can be readily processed due to its high solubility and stability in water. The PEDOT chains within the PEDOT:PSS complex are linked to the PSS chain by electrostatic interactions. The interaction of PSS chains generates a repulsive force that causes the PSS segment to adopt a coiled structure,

within which PEDOT is encapsulated (Figure 2-11(b)). This unique structure prevents the PEDOT chains from coming into direct contact with water [49, 50].

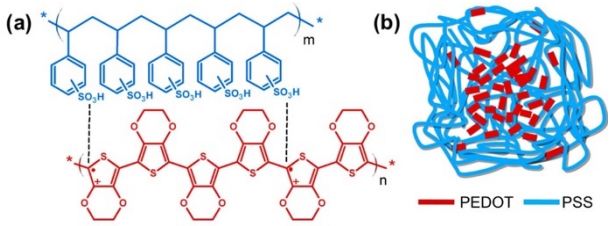

Figure 2-11 Chemical structure (a), and molecular arrangement of PEDOT:PSS (b). Adapted with permission [50].

PEDOT:PSS films possess high conductivity without the application of gate bias. By applying positive V_g, the PEDOT component of PEDOT:PSS is reduced, causing it to become nonconductive. This process is expressed through an equation as follow, where M^+ is the cation of electrolyte and e^- is the electron:

$$\text{PEDOT:PSS}^+ M^+ + e^- \leftrightarrow \text{PEDOT}^+ \text{M:PSS} \qquad (10)$$

The Bernards model provides an understanding of the physics of OECTs. The Bernards model divides the OECT into the electronic circuit and the ionic circuit. The electronic circuit describes the flow of charge carriers in the active material and is governed by Ohm's law. The conductivity of the channel material is assumed to vary during gating and is modeled as a resistor. The ionic circuit is modeled as a resistor (representing the electrolyte) and capacitors at the interface between the gate-electrolyte and channel material-electrolyte. These capacitors represent the charge storage behavior at the gate-electrolyte and channel-electrolyte interfaces. In the Bernards model, efficient gating is characterized by a large voltage drop at the electrolyte-channel material interface, resulting in strong ion injection. These injected ions compensate for the presence of opposite charges in the organic film, leading to changes in the channel conductivity [51]. The I_d value and transconductance in saturation region of depletion mode OECTs can be expressed as follow:

$$I_{d,sat} = \frac{Wd}{2L}\mu_{sat}C^*\left(V_g - V_{th}\right)^2 \qquad (11)$$

$$g_m = \frac{Wd}{l}\mu_{sat}C^*\left(V_g - V_{th}\right) \qquad (12)$$

d represents the thickness of channel material and C^* represents the volumetric capacitance of channel material [52].

2.4.3 Electrolyte materials for EGTs

Various electrolyte materials with distinct chemical compositions and physical properties offer different functionalities for diverse applications. The selection of suitable electrolytes is dependent on the application requirements. Basically, electrolytes are divided into liquid types and solid or semi-solid electrolytes. It is common to use liquid electrolytes in sensors such as biosensors and chemical sensors. Meanwhile, semi-solid electrolytes are commonly employed in electrochemical devices because of their adjustable viscosity and processing temperatures. This allows for a wide range of coating and printing methods. Additionally, semi-solid electrolytes facilitate efficient integration into electrochemical circuit. Semi-solid electrolytes have higher chemical stability and are less prone to evaporation or degradation over time than liquid electrolytes, leading to more stable EGT performance and longer device lifespan. Semi-solid electrolytes can be formulated to have higher mechanical strength and better adhesion to the device substrate than liquid electrolytes, which can prevent electrolyte leakage and improve device reliability [45].

2.4.3.1 Ionic liquids

Ionic liquids are a class of molten salts that exist in a liquid state typically below 100°C. These compounds are composed entirely of ions, unlike traditional liquids that are composed of molecules. They offer multiple benefits, such as low volatility and high thermal stability (up to 350°C). Ionic liquids are widely used for EGTs due to their wide electrochemical stability window (~ 3V). Ionic liquids come in a wide variety of structures and compositions, giving them a diverse range of properties and potential applications. Ionic liquids are categorized according to the type of cations to quaternary ammonium, phosphonium, imidazole, and pyridine-based components. Figure 2-12 shows the molecular structure of some cation and anions of ionic liquids [53]. Choline-based ionic liquids are newer types of ionic liquids that are derived from the natural product choline, which is found in many plants and animals. Jin Jo et. al., used choline based solid electrolytes for poly[3-(5-carboxypentyl)thiophene-2,5-diyl] (P3CPT) based EGTs. They showed that the solid electrolyte based on choline is biodegradable and biocompatible further they showed

the application of EGTs for electrocardiogram (ECG) recordings on human skin and the heart of a rat [54].

Lan et al., studied the effect of two types of ionic liquids (i.e., 1-butyl-1-methylpyrrolidinium [PYR_{14}] and [EMIM][TFSI]) on the doping mechanism of EGTs based on N-type organic semiconductor (phenyl-C_{61}-butyric acid methyl ester (PCBM)). They found that the highly symmetrical and compact arrangement of atoms of [EMIM][TFSI] allows for efficient and rapid diffusion of dopants throughout the bulk of the material. The reduced steric hindrance of [EMIM] enables greater access to the channel material, facilitating the penetration of dopant species in three dimensions. While [PYR_{14}] exhibits a higher degree of steric hindrance, which restricts the diffusion of dopants in the bulk of the channel material. As a result, the doping process in [PYR_{14}] is predominantly confined to the surface, leading to a 2D doping [55].

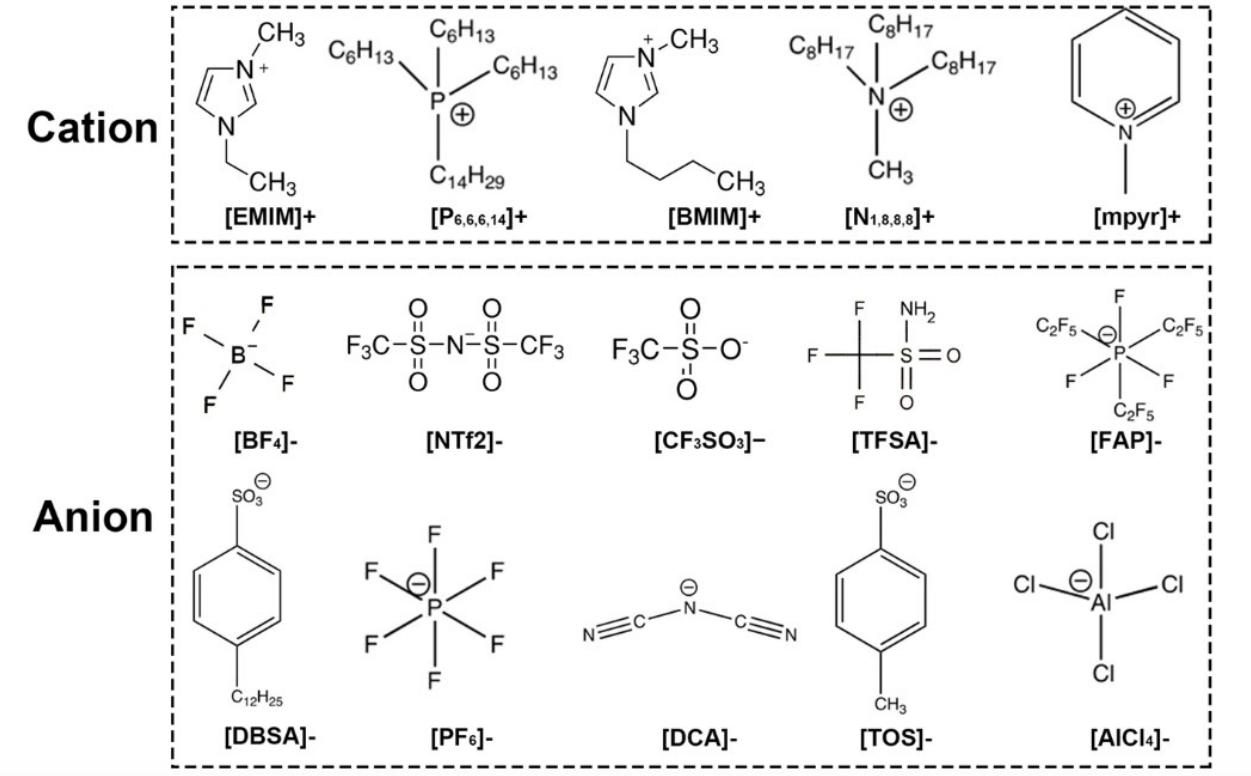

Figure 2-12 Chemical structure of cations and anions of ionic liquids. Adapted with permission [53].

2.4.3.2 Aqueous electrolytes

Aqueous electrolytes consist of dissolved salts in an aqueous solution. NaCl, KCl and PBS are considered as bio-compatible components that have been widely utilized in EGTs for detecting chemical/electrical signals related to physiological activity and monitoring health status [56].

Zhang et.al, investigated the electrical and electrochemical stability of EGTs based DPP-DTT and poly(3-hexylthiophene) (P3HT) using saline (NaCl) solution. They showed that DPP-DTT based EGTs have enhanced mobility and electrochemical stability compared to P3HT EGTs. The inhibition of water absorption and ion doping during prolonged use was attributed to the DPP-DTT's closely interdigitated alkyl side-chains and high crystallinity [57].

Wu et al. investigated the electrical characterization of organic transistors using conjugated polymer (PTDPP-DT) based on diketopyrrolopyrrole (DPP) that is functionalized with polar triethylene glycol side chains. Aqueous electrolytes containing (BF_4^- and Cl^-) were utilized as an electrolyte to figure out the effect of anion on the doping efficiency of semiconducting material. The utilization of $BF4^-$ based aqueous electrolyte in the PTDPP-DT based transistor resulted in impressive performance characteristics. The utilization of $BF4^-$ as the anion in the electrolyte for the PTDPP-DT transistors results in remarkable performance characteristics, including a high transconductance of 21.4 ± 4.8 mS, an ON-OFF ratio of 10^6, and a significantly larger μC* value of 559 ± 65 F cm^{-1} V^{-1} s^{-1}. On the other hand, when the device is gated with a Cl^--based electrolyte, the μC* value was three times lower. The superior performance of the devices using $BF4^-$ was attributed to a larger crystallographic radius of $BF4^-$ compared to smaller Cl^- anions, allowing for efficient doping in the channel material [58].

2.4.3.3 Ion gels

As previously mentioned, ionic liquids are appropriate substances as ion gating media for EGTs. However, their liquid state hinders their practical application. An ion gel is a soft material made of a polymer matrix that contains ionic liquids. The ionic liquids provide the ion conductivity, while the polymer matrix provides the mechanical stability and flexibility of the material. Hence, ion gels are an alternative to ionic liquids where the mechanical stability of the final device is important. The versatility of material selection enables the utilization of diverse polymers in the preparation of ionic gels. Application of copolymers based on poly(vinylidene fluoride) (PVDF) such as

poly(vinylidene fluoride-co-hexafluoropropylene) (PVDF-HFP) and poly(vinylidene difluoride-trifluoroethylene) (PVDF-TrFE) has been shown as a matrix for ion gel due to their thermal and chemical stability and mechanical flexibility [59]. Wu et al., reported on a solid electrolyte composed of PVDF-HFP and 1-Ethyl-3-methylimidazolium tetrafluoroborate ($EMIM^{+}BF4^{-}$). The fabricated devices maintained their performance even under extreme temperatures, operating reliably from -50 to 110 °C which was attributed to the high thermal stability of the channel material and solid electrolyte [60].

Chen et al., reported PVDF-HFP/[EMIM][TFSI] based electrolyte can form fibers through electrospinning and they can be served as a substrate and electrolyte for OECTs based on PEDO:PSS. The devices exhibited a high transconductance of ~0.8 mS, stability over pulsing and time (~1000 cycles and 30 days). The use of a fibrous and porous polymer electrolyte improved interfacial contact with the polymer channel, resulting in more efficient ion injection. They showed the application of fibrous devices for on-skin bioelectronics due to their light weight (0.25 g cm^{-2}), robustness, breathability and waterproof properties [61].

2.4.3.4 Hydrogels

Hydrogels are composed of polymer networks that possess a high affinity for water, which allows them to absorb and retain substantial amounts of water. Hydrogels offer several advantages, such as biodegradability, biocompatibility and nontoxicity. Large amount of water content in hydrogels formulation facilitates ion transport and decreases the driving voltage of EGTs. Self-healing property of hydrogels have gained significant interest for the next generation of electronic devices. This property stems from their ability to restore their mechanical and functional properties when locally damaged [62]. This feature extends the lifespan of products and prevents material failure during use and ensures durability. Generally, hydrogels are made of biomaterials such as cellulose, gelatin, chitosan or biocompatible polymers like polyvinyl alcohol (PVA). The only drawback of hydrogel is their dehydration that may hinder their long-term performance as an electrolyte. Partial substitution of water with anti-dehydrating agent (e.g., organic solvent) is an effective approach to partially inhibit dehydration of hydrogels. These types of hydrogels are known as organohydrogels or organogels. There are three main approaches for incorporating organic solvents into hydrogels:

binary solvent gelation, solvent displacement, and in situ polymerization after infusion with an organogel precursor [63].

Jin et al., reported OECTs based on PEDOT:PSS and using gelatin based hydrogel as an electrolyte. In order to adjust the ionic species concentration in gelatin-based hydrogel, acidic (malic acid) or basic (sodium hydroxide) additives were added to the formulation of the hydrogel. It has been shown that the conductivity of PEDOT:PSS is influenced by the pH level of the hydrogel with which it comes into contact. Application of OECTs with gelatin hydrogels were also shown as electrochemical logic gate circuits such as NOT, NOR and NAND [64].

Cunha et al., reported reusable, sticky and conformable hydrogels based on cellulose. The process of preparation of cellulose hydrogel involves dissolving microcrystalline cellulose and carboxymethyl cellulose in an aqueous lithium hydroxide (LiOH)/urea solvent system at a low temperature (<−8 °C), and subsequently regenerating cellulose using acetic acid. They utilized cellulose hydrogels for EGTs based on indium–gallium–zinc-oxide fabricated on paper. The devices showed ON-OFF ratio of 10^6 and saturation mobility of 26 $cm^2\ V^{-1}\ s^{-1}$ [65]. The same group used sodium hydroxide (NaOH) solution instead of LiOH solution in the formulation of hydrogel. They demonstrated healing ability of prepared hydrogel through the creation of physically crosslinked domains and reversible hydrogen bonding. The hydrogen bonding is facilitated by hydroxyl or amide groups, allowing for efficient reestablishment of the network [66].

2.4.3.5 Polymer electrolytes

Polymer electrolytes are a class of materials that are composed of an ion-coordinating polymer with a dissolved salt. Poly(ethylene oxide) (PEO) is the most studied ion-coordinating polymer in polymer electrolytes. The backbone of PEO contains oxygen lone pairs that can efficiently coordinate with positive ions, such as lithium ions (Li^+). Polymers such as PVA or polycarbonate can be utilized for preparation of polymer electrolytes. $LiClO_4$ is a widely used salt for polymer electrolytes. Polymer electrolytes can be produced by applying a solution containing both polymer and salt onto the targeted area and subsequently drying it [67, 68].

2.4.3.6 Polyelectrolytes

Polyelectrolytes are macromolecules that contain ionizable groups. Depending on the nature of the charge present in the polymer, they can be classified as either polycations or polyanions. One possible way for preparation of polyelectrolytes is to polymerize one of the ions of ionic liquid [69]. Poly(styrene sulfonic acid) (PSSH), poly[(vinyl phosphonic acid)-co-(acrylicacid)] [P(VPA–AA)] with H^+ counterion and poly(styrene sulfonic acid sodium salt) (PSSNa), with Na^+ as the counterion are used as a gating media for transistors [70-72].

Polyelectrolytes are electrolytes that are noteworthy for their ability to enable rapid switching in EGTs. Laiho et al., showed EGTs based on polyelectrolyte (poly(vinylphosphonic acid-co-acrylic acid) (P(VPA-AA)) gating media are able to operate in both electrostatic mode and electrochemical mode by varying the gate voltage. Consequently, switching properties of devices can also be optimized by changing the mode of operation since, electrostatic mode is faster than electrochemical mode of operation [73]. Natural polymer derivates such as chitosan, carboxymethyl cellulose and other cellulose derivates are also used as a polyelectrolyte.

Berggren et.al., controlled the mode of operation (from electrochemical to electrostatic doping) of organic electrochemical transistors using a polyelectrolyte, i.e., polyanionic proton-conducting electrolyte. Due to the immobile nature of the anions in the ion-gating medium, it resists the diffusion of anions into the organic semiconductor when the gate is negatively biased. This effect prevents the electrochemical doping in the channel [74].

2.4.4 Mechanical flexibility

One significant benefit of utilizing organic semiconductors is their capability to be applied for flexible electronic circuits. The polycrystalline structures of organic semiconductors are formed by relatively weak van-der-Waals bonds, which can withstand greater mechanical strain than covalent bonds [75]. This property makes them an ideal choice for constructing flexible electronics. Moreover, their low processing temperatures, allow for the use of inexpensive plastic foils and even paper as substrates [76, 77]. Morphology and crystallinity of polymeric organic semiconductors have a significant effect on the mobility and the mechanical stretchability of devices [78]. Flexible OFETs have been developed for a broad range of applications, including

rollable displays, bendable smart cards, and conformable sensors [26]. However, conventional dielectrics used in OFETs often require high operating voltages, which are not suitable for wearable electronics. In this context, low operating voltage and low energy consumption are essential prerequisites. Flexible EGTs that employ semi-solid or solid electrolytes may serve as suitable candidates, as they can offer a combination of low operating voltage and mechanical flexibility. For instance Yawson et al., fabricated flexible EGTs based on P3HT and using ionic gel based on P(VDF-TrFE):P(VDF-HFP) and [EMIM][TFSI] on poly(ethylene naphthalate) (PEN) substrate (Figure 2-13 (a)). Transfer curves of devices in ambient conditions and during 30000 bending cycles (with bending radius of 6 mm) were obtained (Figure 2-13 (b)). The sensitivity of P3HT to oxygen resulted in an increase in both ON drain current and OFF current. Initially, the mobility value was increased, but after 5 hours of bending stress, it decreased slightly while still remaining higher than the initial mobility value (Figure 2-13 (c)) [79].

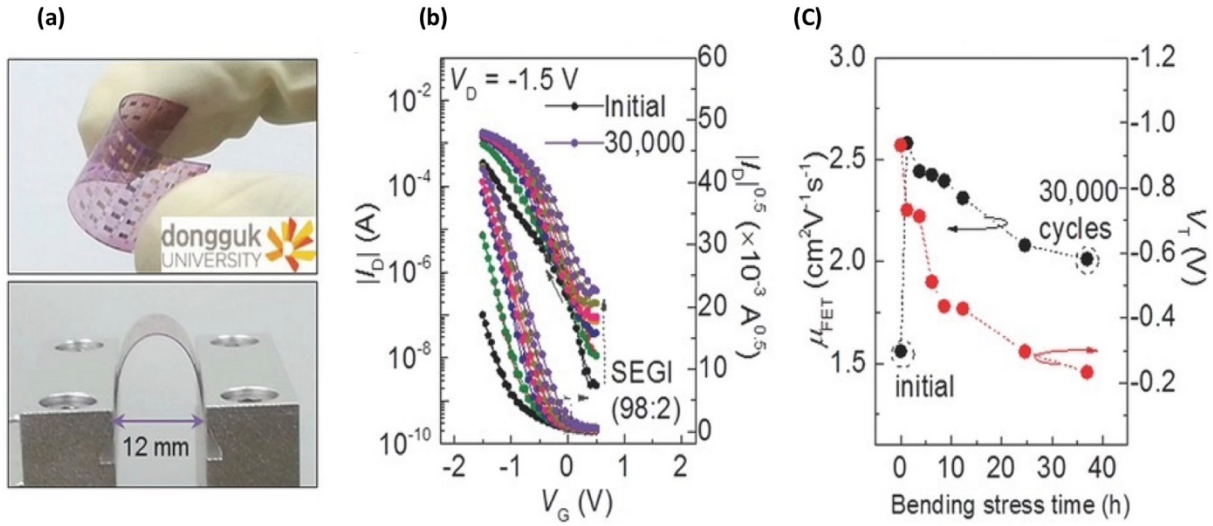

Figure 2-13 Image of flexible EGT at bending radius of 6 mm (a), transfer curves during continuous bending cycles (b), saturation mobility and threshold voltage variation versus bending stress time (c). Adapted with permission [79].

Jin Jo et al., reported EGTs based on P3CPT and using electrolyte with edible components (levan polysaccharide and choline-based ionic liquid). They also used levan polysaccharide as a substrate of EGTs (Figure 2-14 (a)). The electrical characterization of devices was evaluated under strain values of 0.28%, 0.33%, 0.77%, and 1.11% and stretching values of 5%, 10%, 15%, and 20%. Figure 2-14 (b) presents the ON/OFF currents of transistors under different mechanical

deformations. Bending the device slightly changed both ON and OFF currents, but maintained the ON-OFF ratio above 10^2, even at 1.11% strain. Stretching in the vertical direction caused little change in the ON-OFF ratio up to 5% strain, while stretching over 10% decreased the ratio significantly. Bending reduced the field-effect mobility from 0.98 to 0.41 $cm^2\ V^{-1}\ s^{-1}$. The threshold voltage remained almost the same under 5% vertical stretching, with a maximum of 75 µV (Figure 2-14 (c)). The transconductance of the transistors slightly decreased from 2.1 to 1.1 mS under bending. Transconductance value decreased from 0.86 to 0.06 mS under 5% and 20% stretching, respectively (Figure 2-14 (d)) [54].

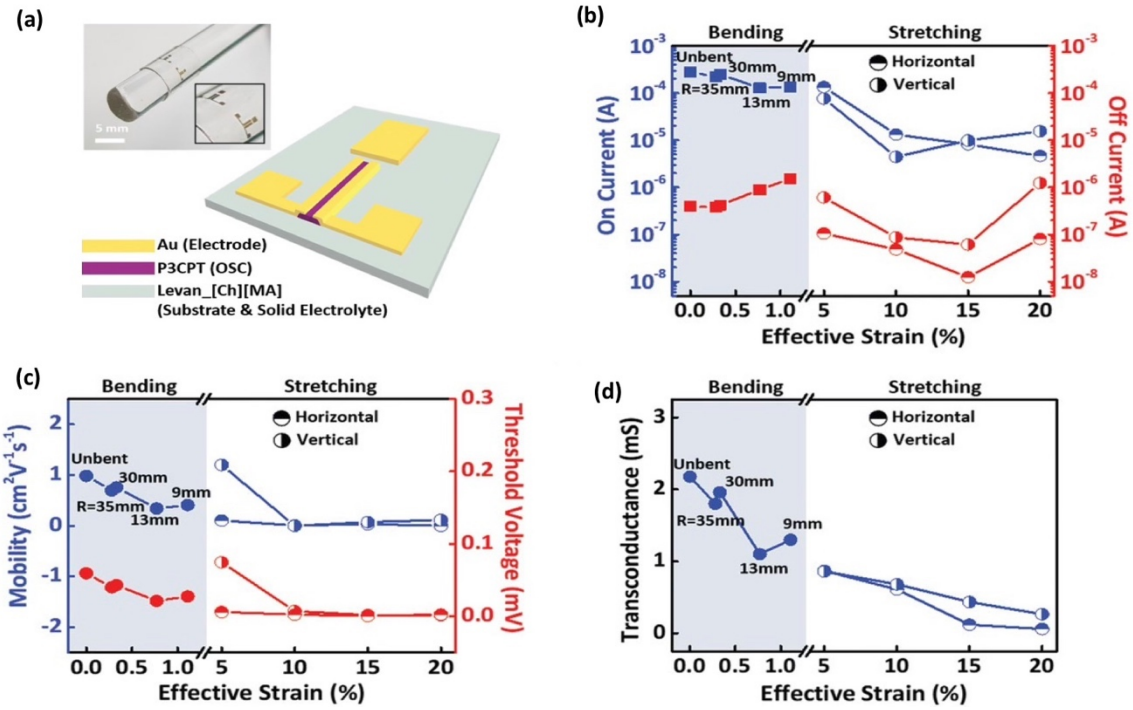

Figure 2-14 Schematic and photographic image of flexible EGTs using levan polysacharid as electrolyte and substrate (a), ON-current and OFF-current variation versus strain and stretch (b), mobility and threshold voltage versus bending (c), maximum transconductance versus mechanical strain and stretch (d). Adapted with permission [54].

2.4.5 Operational stability

Investigating the stability of EGTs can help to identify the key factors affecting their performance and guide the design and fabrication of more stable devices. Zhang et al. investigated the operational stability of EGTs based on P3HT and DPP-DTT using saline (NaCl) aqueous electrolyte. Evaluation of the operational stability of EGTs were performed by obtaining

consecutive transfer curves of P3HT and DPP-DTT EGTs in a an electrolyte for an extended period of 5 days (Figure 2-15 (a,b)). The mobility of DPP-DTT EGT remained remarkably stable, even after soaking in a saline solution for 5 days. Contrary to DPP-DTT, P3HT showed a substantial reduction in mobility and ON-OFF current ratio (30% and 10%), respectively. This indicates lower stability of EGTs based on P3HT compared to DPP-DTT in aqueous electrolyte. (Figure 2-15 (c)). The stability of EGTs was also evaluated by cycling devices between ON-state and OFF-state. As shown in Figure 2-15 (d) minimal fluctuations in the ON and OFF currents of DPP-DTT EGTs even after undergoing 200 ON-OFF cycles. In contrast, P3HT experienced a notable decrease in the ON current and an increase in the OFF current. From magnified cycling curves, it is obvious that DPP-DTT EGTs can be rapidly regulated at either the ON or OFF state. However, I_d at ON and OFF states of the P3HT device exhibits continuous changes throughout the duration of the test [57].

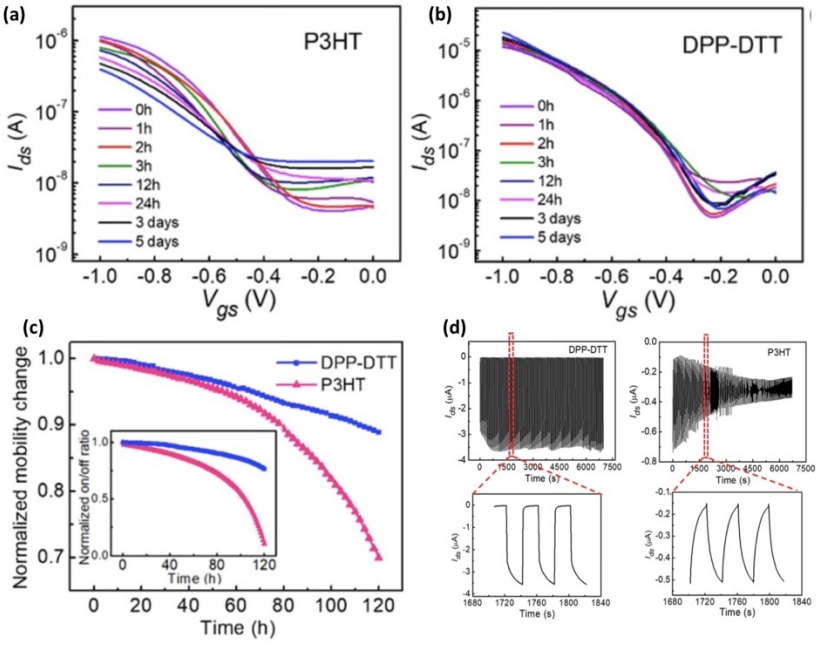

Figure 2-15 Transfer curves of P3HT (a), and DPP-DTT EGTs tested over 5 days (b), normalized mobility and ON-OFF ratio of EGTs over testing time (c), and cycling stability test of EGTs under 200 bias cycles (d). Adapted with permission [57].

Na et al., claimed that the stability of EGTs can be deteriorated by the unintentional electrochemical doping phenomena such as ion migration and charge transfer. This process leads to device degradation due to ion penetration into the semiconducting layer. They showed that the stability of

EGTs based on P3HT and using ion gel as an electrolyte was improved by adding small amount of ionic liquid in the solution of P3HT. The dispersion of ionic liquid nanodroplets in the active layer of the blend played a crucial role in maintaining local charge balance, leading to a reduction in slow electrochemical transport processes under applied biases. As a result, devices with nanodroplet-embedded blends exhibited higher current levels and enhanced stability against operational bias stress over 150 cycles [80].

Cherukupally et al. conducted a study investigating the stability of printed EGTs that were based on In_2O_3 and utilized three types of solid electrolytes. The solid electrolytes used in the study were ion gel based on (PVDF-TrFE) and [EMIM][TFSI], as well as PVA with two different molecular weights (13-23 kDa and 89-98 kDa) and $LiClO_4$, using dimethyl sulfoxide (DMSO) and propylene carbonate as the solvent and plasticizer, respectively. The drain current of devices using three different electrolytes were reported for as prepared devices and after 1 month and 8 months after fabrication (Figure 2-16). The findings indicated that, while the ion gel-gated devices initially exhibited higher levels of saturated drain currents, they also experienced significant performance degradation over time, particularly within the first month. In contrast, the $CSPE_{PVA,89k}$ gated devices demonstrated minimal variation in device performance and exhibited excellent stability which is correlated to better solvent uptake of polymeric chains with high molecular weight [81].

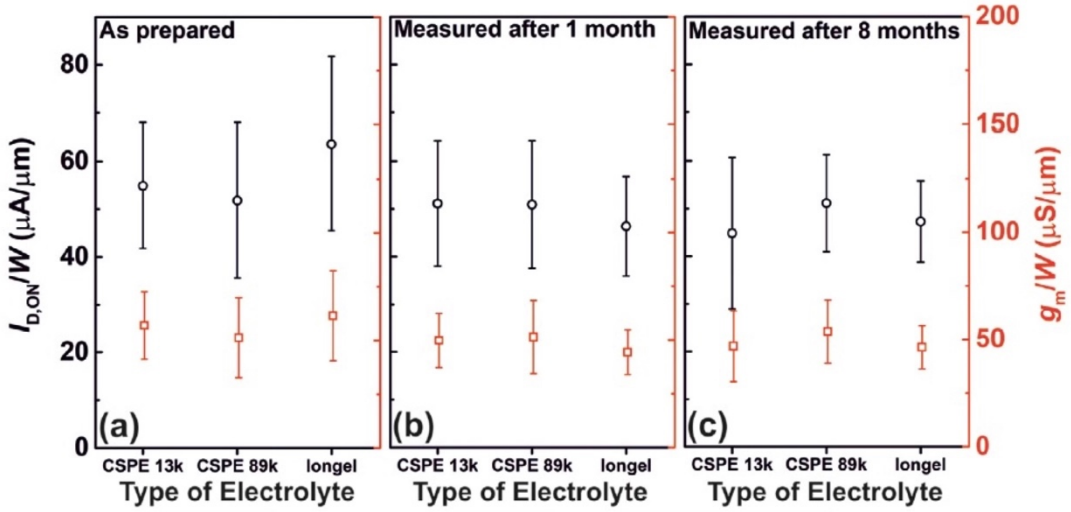

Figure 2-16 The normalized I_d with respect to channel width and transconductance values (normalized by channel width) for devices gated with different electrolytes in as prepared condition (a), after 1 month (b), and after 8 months (c). Adapted with permission [81].

2.4.6 Printing method for EGTs

Printing is an additive patterning method. Additive patterning refers to the process of adding material onto a surface in a controlled manner to create the desired pattern or structure. This process involves depositing layers of material on top of each other until the desired shape is achieved. Conventional photolithography patterning is subtractive method that involves removing material from a surface to create the desired pattern or structure. This process typically starts with a bulk material or a coated substrate, which is then selectively removed using various techniques such as etching. One key advantage of subtractive patterning is that it can achieve high resolution features with high precision, making it suitable for applications where a lower channel length is required. Printing methods are generally more cost-effective than photolithography since they do not require expensive equipment and facilities. The scalability of printing methods allows for the production of a large quantity of EGTs, which can be fabricated on various substrates, including non-planar and flexible surfaces. This flexibility is especially beneficial for applications that require conformal EGTs, such as biomedical sensors or wearable electronics. The photolithography process (Figure 2-17) typically involves depositing active material on substrates, followed by thermal treatment. The semiconductor is then patterned using photolithography and etching, and a photoresist is applied and developed. Metal contacts are deposited through electron-beam evaporation and lifted off. In contrast, printing processes involve depositing metal contacts and semiconductor using liquid ink, which reduces the number of steps required. Metal contacts are deposited using a printer such as a screen printer, inkjet printer, or aerosol jet printer, and thermal treatment is applied for maximum conductivity. The printer is then aligned to print the active channel material [44].

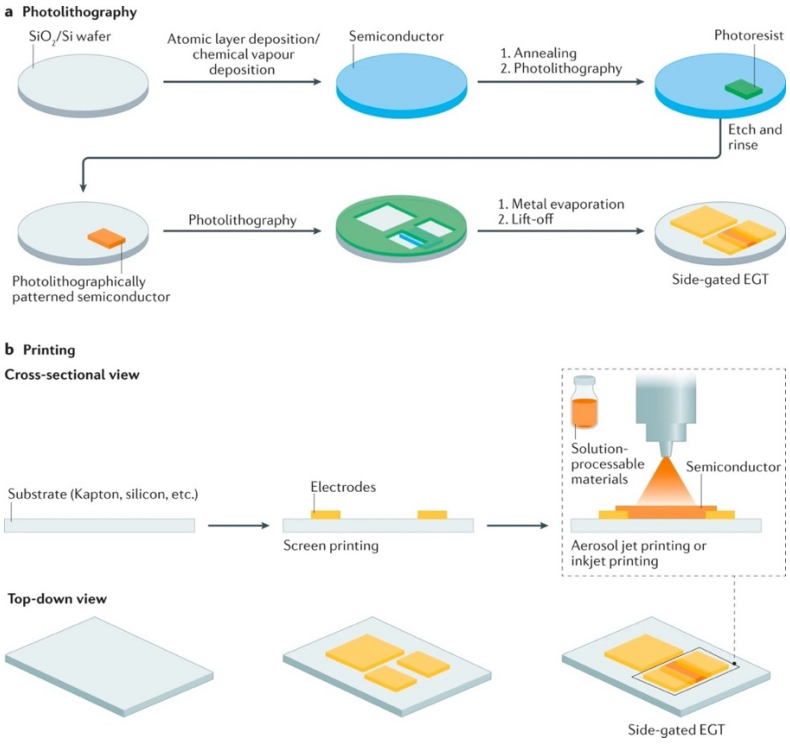

Figure 2-17 Fabrication by photolithography technique (a) and printing technique (b). Reproduced with permission [44].

The prevalent printing technologies for fabrication of OECTs include inkjet printing, screen printing, and 3D printing, each with its unique features [82, 83]. Inkjet printing stands out as a non-contact fabrication process that allows for the direct deposition of small particle size solutions onto the substrates. Notably, inkjet printing eliminates the requirement for a mask, as it can precisely produce patterned films without using mask. This is achieved through the use of an ink cartridge that enables accurate ejection of the solution in a designated area using jet technology. Among various printing techniques, screen printing is known for its fast patterning using a mesh mask and a squeegee. The mask acts as a barrier, preventing the paste from reaching the substrate, while the open areas of the mesh allow the inks to be applied and fill the desired pattern. Screen printing, while offering fast fabrication of OECTs, presents certain limitations, such as generation of waste from residual inks on the mask, that leads to increased process costs [84].

2.4.7 Vertical configuration OFETs and EGTs

The most extensively reported OFETs typically employ a conventional planar device structure, in which the source and drain electrodes are positioned laterally, with a channel material between them. In planar structure, current flow direction is perpendicular to the gate electric field whereas in vertical structure, transfer path of charge carriers is in same direction as electric field as shown in Figure 2-18 [85]. Planar OFETs possess the disadvantage of relatively large channels, which typically measure in micrometers or even larger scales. Reducing the channel size is challenging due to limitations arising from the device geometry and fabrication techniques. Therefore, low current density and operating speeds are often observed, significantly restricting their potential applications in various fields. Vertical OFETs were first introduced in 2004 and quickly gained significant attention due to their much shorter channel length compared to planar structures [86]. The channel length of vertical OFETs can be reduced to a few tens of nanometers, as the thickness of the channel material is equal to channel length. In vertical structure due to the presence of a source between the gate/gate dielectric and the semiconductor layer, the source electrode shields the gate field in semiconductors. However, in the architecture proposed by Ma and coworkers, this issue was addressed by using very thin metal for the source electrode along with utilization of dielectric with high-*k*, allowing for elevated electric field [86]. A more recent and even simpler design of the source electrode was realized by using a carbon nanotube or graphene mesh that allows for effective gate-field penetration and alleviates the issue of source shielding [87-89]. This innovative design provides a solution to the challenge of source shielding in semiconductor devices in a more straightforward manner. Vertical OFETs have the ability to provide high current density and operate at high frequencies while using low operating voltages so, they are an ideal choice for transistor circuits used to drive organic light-emitting diode pixels in displays. These characteristics make them highly practical for use in organic electronics [90]. Vertical structures offer an extra benefit of being able to easily integrate with a photodetector or a light-emitting diode to form an integrated optoelectronic with simplified production procedure [91].

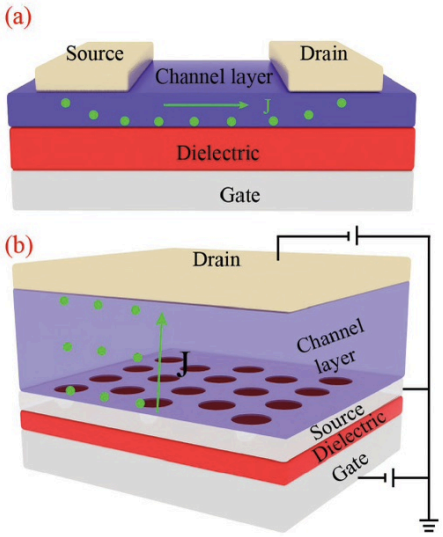

Figure 2-18 Schematic of planar OFET (a), and vertical OFET. Adapted with permission [85].

2.4.7.1 Recent advancements in EGTs and OECTs with vertical structure

Lenz et al., fabricated vertical EGTs based on PDPP with source and drain electrodes produced using electron-beam lithography. The length of the channel was equal to the thickness of the SiO_2. The layers of SiO_2 and titanium between the contacts were removed by etching with HF acid. The depth (d_c) could be determined by the etch time. The next step was to apply the organic semiconductor (PDPP) using spin-coating. Excess semiconductor material was removed using reactive ion etching (RIE), which left the semiconductor only between the contacts. Finally, a drop of liquid electrolyte ([EMIM][TFSI]) was cast onto the transistor to complete the device as shown in Figure 2-19. The channel length of 40 nm provides current densities exceeding 2 MA cm^{-2} at −0.3 V bias, and an ON-OFF ratio of 10^8. Furthermore, the transistor demonstrated exceptional operation at low voltages, with a minimum of just 10 μV [92].

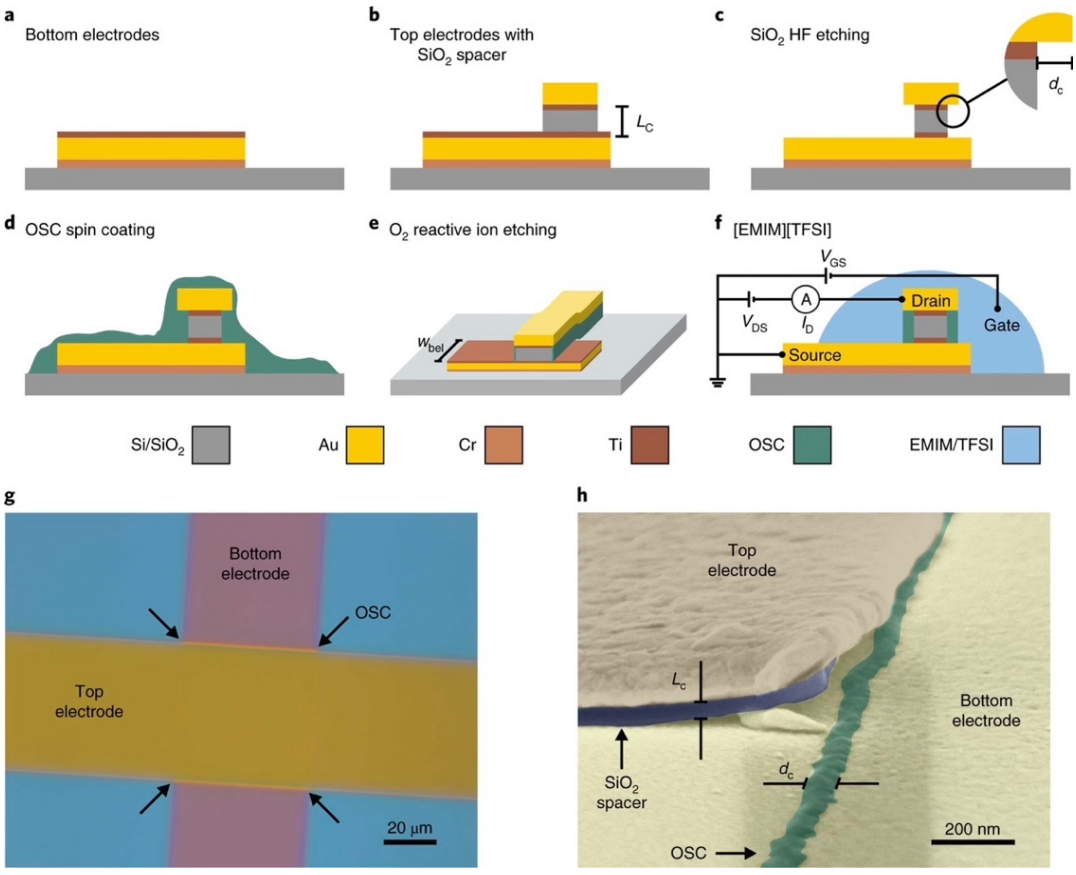

Figure 2-19 Fabrication of vertical structure device (a-f), microscopy image of vertical structure without electrolyte (g), and coloured cross-sectional SEM image of vertical structure (h). Adapted with permission [92].

Huang et al. demonstrated vertical OECTs based on p-type and n-type semiconducting polymer (gDPP-g2T and Homo-gDPP). The fabrication process for the devices included creating Au electrodes, achieved through thermal evaporation and masking. An ion-conducting semiconductor channel was deposited using spin-coating and photopatterning Figure 2-20 (a). Transfer characteristics and g_m and subthreshold swing (SS) plots for both p-type and n-type vertical OECTs were demonstrated in Figure 2-20 (b,c) and (d,e), respectively. The p-type devices demonstrated transconductance value of 226.1 µS µm^{-2}, while the n-type devices yielded transconductance values of up to 112.4 µS µm^{-2}. The vertical structure utilizing p-type and n-type semiconductors yielded transconductance values that were notably higher (18 and 100 times, respectively) compared to planar OECTs [93].

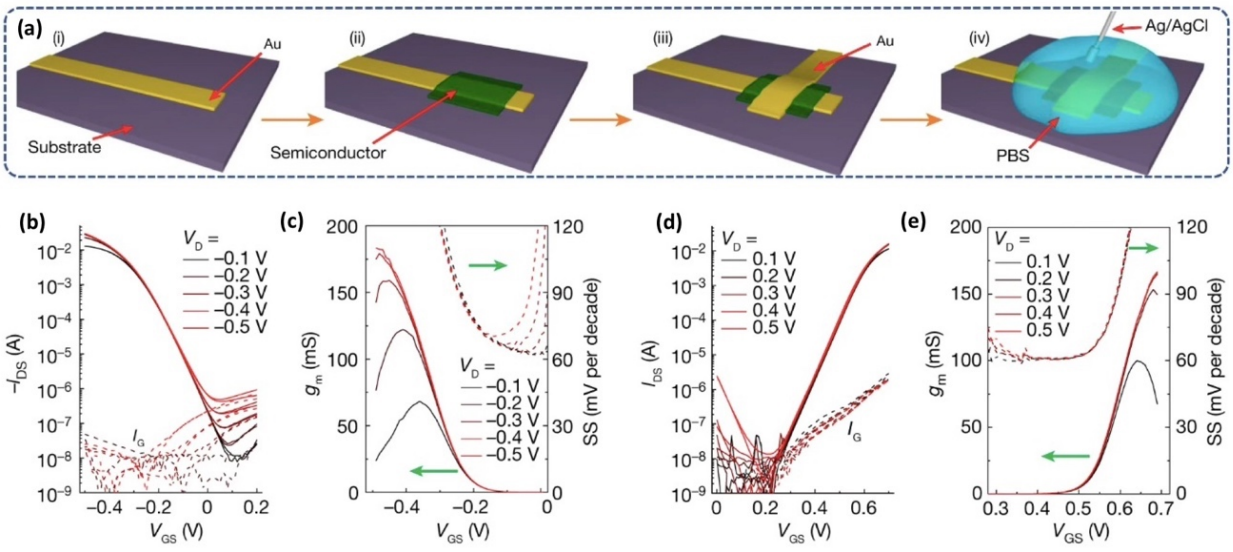

Figure 2-20 Process flow of fabrication of vertical OECTs using thermal evaporation of metal contacts through shadow mask and photopatterning of semiconductor (a), Transfer curve, transconductance and subthreshold swing versus gate voltage for p-type (b,c) and n-type (d,e) OECTs. Adapted with permission [93].

Donahue et al. used a step-edge configuration to fabricate vertical OECTs based on PEDOT:PSS. The separation distance between the top and bottom contacts (channel length) was defined by the thickness of a parylene-C separator layer. This design allowed for high resolution in the sub-micrometer range, enabling the variation of channel length down to 450 nm. Figure 2-21 (a) depicts a significant increase in transconductance for the vertical OECT, demonstrating impressive values of up to 24 mS with a channel length of 450 nm. Remarkably, this performance was achieved while utilizing less than half of the substrate area compared to the planar OECT. Figure 2-21 (b-e) display SEM images of both planar and vertical OECTs, along with schematic illustrations highlighting the width and length of the transistors [16].

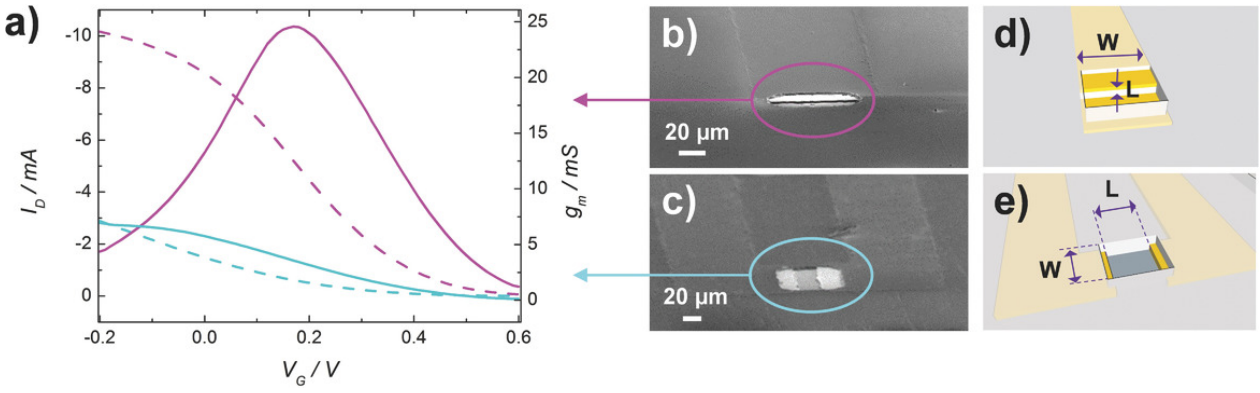

Figure 2-21 Transfer curves (dashed lines), transconductance versus gate voltage (solid lines) for vertical and planar OECTs, SEM images (b,c) and schematic of vertical and planar structures (d,e). Adapted with permission [16].

Yun et al. reported on vertical OECTs based on PEDOT:PSS, which utilized ITO and AgNW as the bottom and top electrodes, respectively, and a thermally evaporated Au electrode as the gate electrode. Figure 2-22 (a,b) show the schematic of the vertical device and SEM images of silver nanowires. An ion gel based on polyacrylonitrile (PAN) and Bis(trifluoromethane)sulfonimide lithium salt (Li^+TFSI^-) was used as an electrolyte. Figure 2-22 (c) shows the SEM of vertical OECTs where the conducting polymer PEDOT:PSS, which served as the active layer, was positioned between AgNW and ITO. In Figure 2-22 (d), the transfer curves and corresponding transconductance curves of the vertical OECTs are compared with planar structures. The vertical OECTs demonstrated ON-state current of 18.61 ± 1.21 mA and peak transconductance of 64.25 ± 1.49 mS. These values are almost 5 times higher than that of planar devices [94].

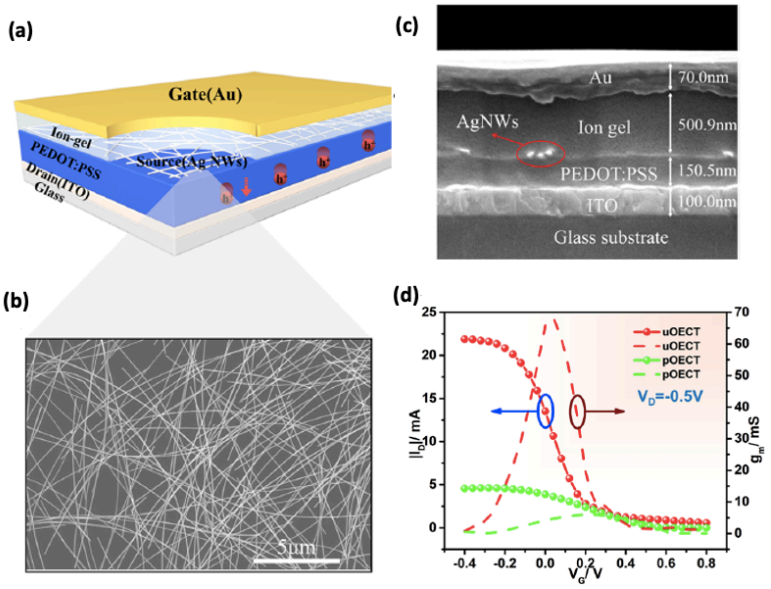

Figure 2-22 Schematic of vertical OECT (a), SEM of silver nanowires (b), cross section image of vertical OECTs (c), Transfer curve and transconductance versus V_g for vertical and planar OECTs. Adapted with permission [94].

Koutsouras et al. have reported on a vertical OECT based on PEDOT:PSS, in which the vertical channel is created through electrodeposition, allowing for channel lengths below 100 nm. The schematic representation of devices from different views, and its 3D illustration, are shown in Figure 2-23 (a-e). The detailed fabrication procedure is shown in Figure 2-23 (f). The proposed manufacturing method enables precise control of the transistor's geometry (W and d) by using a straightforward photolithography step. Additionally, the organic polymer thickness determines the transistor channel precisely through an electrodeposition process. This is also significant as it makes it possible to achieve channel lengths less than 100 nm. These features results in an extremely high transconductance of 275 mS, which is unachievable with traditional planar OECTs [17].

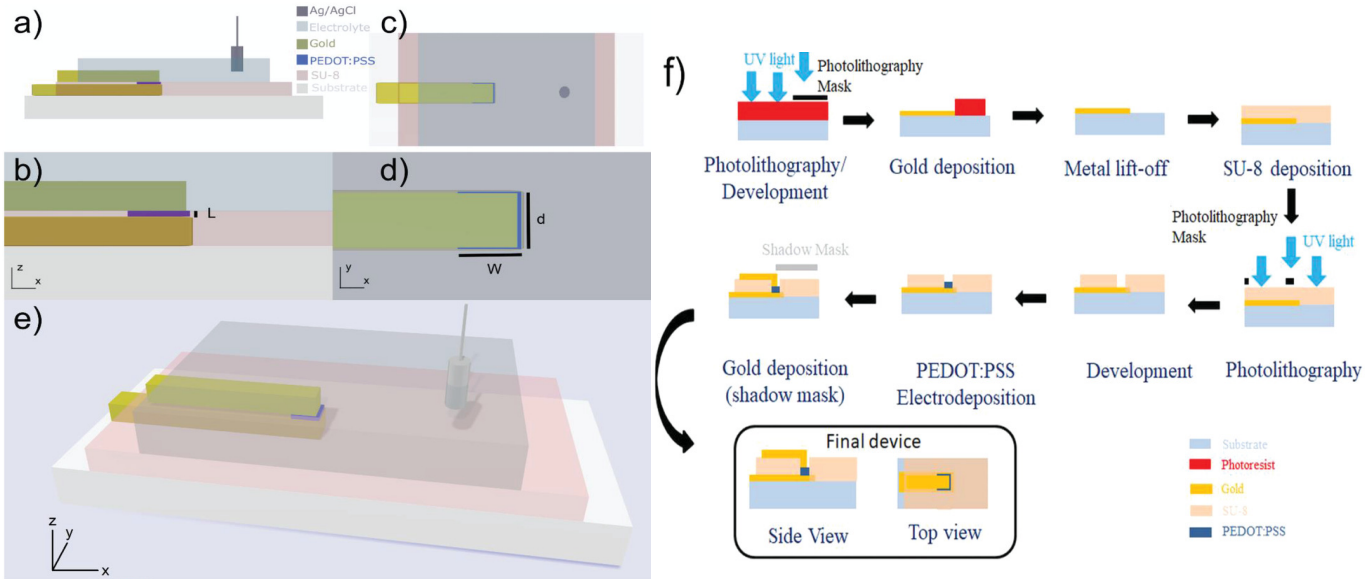

Figure 2-23 Schematic representation of vertical OECTs from different views (a-e), process flow of fabrication of vertical OECTs using electropolymerized PEDOT:PSS channel (f). Adapted with permission [17].

CHAPTER 3 METHODOLOGY

In this chapter, various techniques are addressed, including microfabrication for gold patterning on substrates, patterning of OECTs components (electrodes and channel material) via printing, solution processing for deposition of transistor channel materials, preparation of semi-solid electrolytes, preparation of gate electrodes, device assembly, and evaluation of properties of active channel materials and electrical testing of transistors.

3.1 Substrates

The substrate for a transistor is a material upon which the component of transistor is deposited. Typically, the substrate is a thin, flat, and rigid, flexible or stretchable material that provides mechanical support for the transistor. Some commonly used substrate materials for transistors include glass, silicon dioxide, and plastics such as PET or PI. The choice of substrate material can have a substantial influence on the performance and properties of the organic transistor, and careful selection is necessary to ensure optimal device performance.

Two different types of substrates were utilized for fabrication of transistors: rigid substrates including (SiO_2/ Si) and glass substrates and flexible substrates such as PET and PI. The SiO_2/ Si substrate, provided by WaferPro, consists of wet thermal oxide (~200 nm) grown on the polished Boron-doped silicon with a crystal orientation of <100> with a thickness of approximately 500 μm and an electrical conductivity of ~650 S/cm. SiO_2/ Si substrate has smooth, uniform surface with high thermal stability. On the other hand, polymeric substrates were used for flexible transistor preparation. In particular, PET substrates with a thickness of 175 μm were supplied from Policrom and PI sheets with a thickness of 125 μm were purchased from Polyonics. Before depositing materials on the substrates, we performed three cycles of ultrasonication to clean them. We immersed them in a solution of isopropanol for 10 minutes, and another 10 minutes in acetone, and then 10 more minutes in isopropanol (for flexible substrates we skipped sonication in acetone). After that, we exposed the substrate surfaces to UV-Ozone treatment for 15 minutes. This step helped to eliminate any remaining organic contaminants and also improved the adhesion of the channel material films to the substrate surface [95]. The UV-Ozone cleaner we used was a Jelight

Model 30, which features a low-pressure mercury vapor lamp with a lamp intensity of approximately 30 mW/cm2, emitting a wavelength of around 254 nm.

3.2 Contact electrodes preparation

We used microfabrication to pattern Au source and drain electrodes of EGTs. For OECTs, fabrication, printing was employed. All the electrodes of OECTs (S, D, and G) were patterned by printing of silver ink on substrate.

3.2.1 Microfabrication

Microfabrication technique includes photolithography, etching and metal deposition to create desired patterns on substrates. Photolithography is a process used in the fabrication of electronic to create patterns on a substrate. It involves using UV light to create patterns from a mask or photomask onto a light-sensitive material, such as photoresist on the substrate.

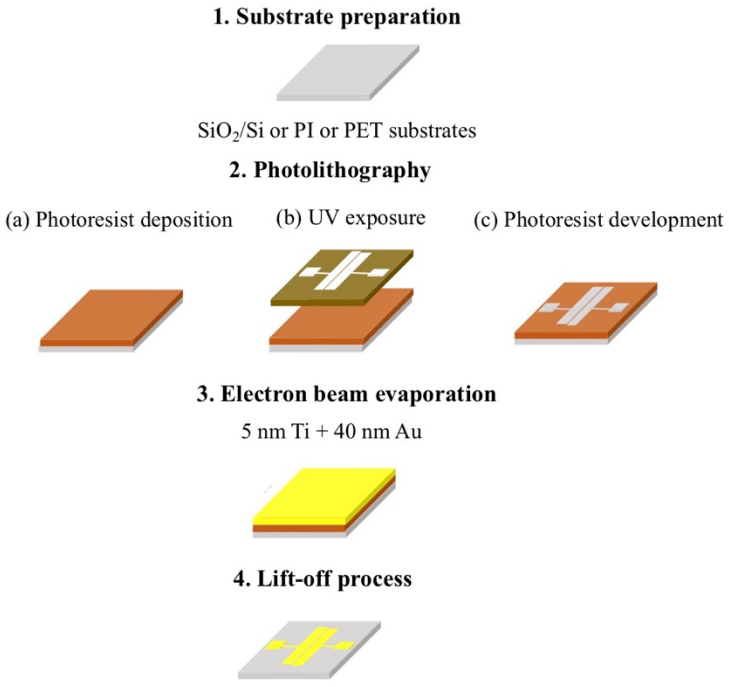

Figure 3-1 Schematic representation of Au electrodes patterning on the substrates.

To pattern the substrates using photolithography the substrates were first treated by hexamethyldisilazane (HMDS) coating. In the lithography process, HMDS was utilized to modify

the surface of a Si wafer using a silane coupling reaction. When HMDS reacts with the surface, it produces a hydrophilic trimethylsilanol (TMSiOH) layer on the surface. This modification simplifies the process of coating the Si wafer surface with photoresist.

In the lithography process, a Si wafer was uniformly coated with positive photoresist, AZ 900 MIR, using a spin-coater at a speed of 3000 rpm. The coated substrate was then heated at 110 ˚C for 60 seconds before being placed under a photomask with desired pattern. Using a Karl Suss MA6 mask aligner, the wafer was exposed to i-line UV light at 365 nm. Following the exposure, the wafer was further heated at 90 ˚C for 60 seconds, and the wafer was then immersed in a developer solution, AZ726, to dissolve the UV-exposed areas. AZ726 is an aqueous solution of 3 % of tetramethylammonium hydroxide. Developing process results in a substrate containing photoresist pattern of unexposed area. To create the metal contacts, a substrate containing a patterned photoresist was coated with a 5 nm layer of Ti to improve Au adhesion, and then a 40 nm layer of Au was deposited via e-beam evaporation at a rate of 0.5 Å/s. Following the deposition of the metal contacts, any excess metal was eliminated through a lift-off process, where the substrates were immersed in Remover 1165 (comprising 90-99% of 1-Methyl-2-pyrrolidinone) for 4 h at 60 ˚C. The photoresist-covered areas of the substrate that have not been exposed to UV are removed, leaving Ti/Au in the desired configuration adhered to the silicon substrate. The process flow for fabricating metal electrodes was shown in Figure 3-1. We used top gate bottom contact configuration for EGTs based on PCDTPT and DPP-DTT where the active material is deposited on the patterned gold contacts.

3.2.2 Printing

A printed circuit board (PCB) printer with direct ink writing (DIW) technology was used to pattern OECT devices based on PEDOT:PSS on the substrates. Initially, the desired patterns were plotted using a DipTrace software, schematic and PCB design software. After creating the pattern file using the pattern editor, the design was transferred into the Voltera V-One software. The PCB printer was equipped with an ink cartridge and a nozzle size of 100 µm, which was used to print the Ag ink and PEDOT:PSS inks. Silver paste (Ag PASTE 520 EI, Chimet) was used to pattern S, D, and G electrodes. The PEDOT:PSS ink (Clevios™ SV3, Heraeus) was used to pattern an active channel material of OECTs. Before printing substrates were cleaned as it is mentioned before and

exposed to UV-ozone to eliminate contamination. Once the ink cartridge has been loaded the Voltera controller moves the ink cartridge to the designated locations on the substrate, and then prints a layer of ink with a specific pattern, as determined by the Voltera V-One software. We used printing method to fabricate planar and vertical OECTs. Initially, the silver gate electrode was printed onto the surface and heated at 130°C for 20 minutes. Next, the electrode was transformed into an Ag/AgCl gate electrode [96, 97]. Following this, the S, D electrodes and channel material (PEDOT:PSS) were printed and heated, sequentially.

3.3 Thin film deposition

We employed a solution processing approach for the preparation of thin films, which is a versatile method for depositing uniform thin films of organic semiconductors, such as small molecules and polymers, on various substrates with the desired thickness ranging from a few nanometers to several micrometers at a low cost. To prepare the semiconducting polymer solution, the semiconducting material was dissolved in a suitable solvent, specifically chloroform in this PhD work, and left overnight to dissolve to obtain the desired concentration of 2.5 mg/ml. Once the solution was prepared, it could be dispensed onto the substrate. The substrate was first placed on a rotating chuck and fixed by applying a vacuum. The semiconducting solution was then dispensed onto the center of the substrate using either a pipette or a syringe, with a sufficient volume of solution to cover the entire substrate. Finally, the substrate rotation speed was accelerated centrifugally to spread the solution over the substrate with a uniform thickness. The speed and duration of spinning were determined based on the solution's properties, such as viscosity and concentration, as well as the desired film thickness. After the spinning process was completed, the substrate was allowed to dry for a few seconds, leaving a thin film deposited on the substrate (Figure 3-2) [98]. Subsequently, the substrates were placed on a hotplate to further anneal the semiconductor. The annealing temperature significantly affects the morphology and crystallinity of the semiconducting film [99]. In this PhD work, we used Laurell spin-coater (WS-650HZB-23NPPB/UD3) for deposition of organic semiconducting film.

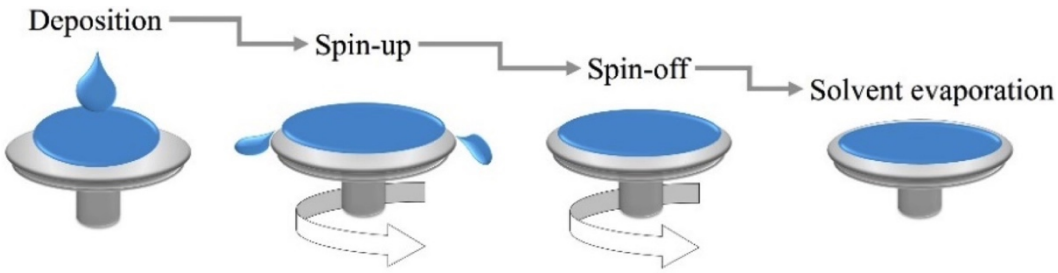

Figure 3-2 Scheme of the spin-coating. Adapted with the permission [98].

3.4 Ion-gating medium

3.4.1 Ionic liquid

In this study room temperature ionic liquid ([EMIM] [TFSI]) is used as an ion gating medium for EGTs and phototransistors based on PCDTPT. [EMIM] [TFSI] demonstrates a high level of ionic conductivity, with a value of 6.63 mS/cm. It also possesses favorable properties such as a density of 1.52 g/cm^3, a viscosity of 39.4 cP, with an anodic limitation of 2.6 V and a cathodic limitation of -2.1 V [100, 101]. The introduction of water into the ionic liquid results in its contamination, leading to a reduction in the electrochemical potential window of the ionic liquid. Before proceeding with device fabrication, the ionic liquid underwent a purification process involving vacuum treatment (10^{-6} Torr) and overnight heating at 60 ˚C to ensure its purity [101]. We used hydrophobic polyvinylidene fluoride (PVDF) membrane with thickness and pore size of 25 µm and 220 nm, respectively to confine the ionic liquid. By immersing the membrane in an ionic liquid, it can adsorb the ionic liquid [95].

3.4.2 Semi-solid gel electrolytes

In this study, three types of semi-solid gel electrolytes were utilized, which include ion gel, hydrogels (with and without an anti-dehydrating agent), and organogel. The ion gel was prepared by blending PVDF-HFP with an ionic liquid ([EMIM][TFSI]) in acetone. PVDF-HFP, a semi-crystalline and hydrophobic copolymer that has excellent film-forming capability, was added to acetone in a weight ratio of 1:15 and stirred for 2 hours at 50°C to attain a homogeneous solution. The ionic liquid, added at a ratio of 4:1 w/w in relation to PVDF-HFP, was then stirred for an additional 2 hours at 50°C [102]. For EGTs based on DPP-DTT, the ion gel was deposited onto the

devices using a spin coating method, while for organic OECTs based on PEDOT:PSS, a drop casting method was used to deposit the ion gel. Hydrogels were based on hydrophilic PVA and were produced utilizing a freezing/thawing technique, which induces physical crosslinking of polymer chains without the need for crosslinking agents. A solution of 16 wt % PVA was prepared by dissolving PVA in deionized (DI) water at 95°C for 1 hour until it turned transparent. The solution was then poured into a glass petri dish and placed in a freezer at -15°C for 3 hours, followed by thawing at room temperature for 24 hours. The resulting gel had a thickness of approximately 1000 μm and was subsequently cut into desired shapes. We used blade to precisely cut the gels with dimension of (0.4×0.8 cm). It is important to note that the capacitance of electrolyte is independent of the thickness of the electrolyte, but it is dependent on the thickness of the electric double layer and area of electrolyte [103]. Finally, the PVA hydrogel pieces were swollen in three different aqueous solutions of NaCl (containing glycerol as an anti-dehydrating agent and without an anti-dehydrating agent). Solvent displacement was utilized to introduce an anti-dehydrating agent in the formulation of hydrogels. The hydrogels were placed on devices using the cut and stick method. Organogel was prepared using binary solvent gelation of PVA in a mixture of water and DMSO. The PVA-based organogel was prepared by dissolving 10 wt % of PVA in a mixture of water (containing 0.1M NaCl) and DMSO (50 v/v%). The resulting solution was then drop-casted onto the OECTs, and the devices were placed in a freezer at -15°C for 3 hours [97].

3.5 Gate electrode preparation

The gate electrode used for the EGT devices was carbon paper coated with activated carbon, chosen for its high surface area which enables efficient current modulation. Two types of activated carbon inks were utilized in the fabrication process. For ion gel-gated devices, a hydrophobic solution of activated carbon with concentration of 28 mg mL^{-1} and PVDF with concentration of 1.4 mg mL^{-1} in NMP was employed. For hydrogel-gated devices device, mixture of activated carbon with same concentration as before and Nafion with concentration of 2.4 mg mL^{-1} in isopropyl alcohol was used to prepare the ink. The activated carbon ink was dropped on carbon paper pieces and then heated at 60 °C for 5 hours to remove the solvent.

3.6 Device Assembly

Figure 3-3 (a) presents the schematic diagram of EGT devices based on organic semiconductors, namely PCDTPT and DPP-DTT. The contact electrodes (S,D) are patterned using photolithography method. The fabrication process involves spin coating the organic semiconductors onto prepatterned substrates, followed by placing the ion gating media (such as ionic liquid soaked PVDF membrane or hydrogels) onto the channel area. Subsequently, a carbon paper gate electrode is deposited on top of the gating media. In Figure 3-3 (b,c), the printed planar and vertical OECTs based on PEDOT:PSS are depicted. The silver ink is used to print the S, D, and G electrodes. To create an Ag/AgCl electrode, the gate electrode is treated with a 5% NaClO solution. The channel material is made of PEDOT:PSS (Clevios SV3 STAB). All OECT components, except the electrolyte, are printed. Once the printing process is complete, the electrolyte (ion gel and organogel) is applied onto the devices using the drop casting method.

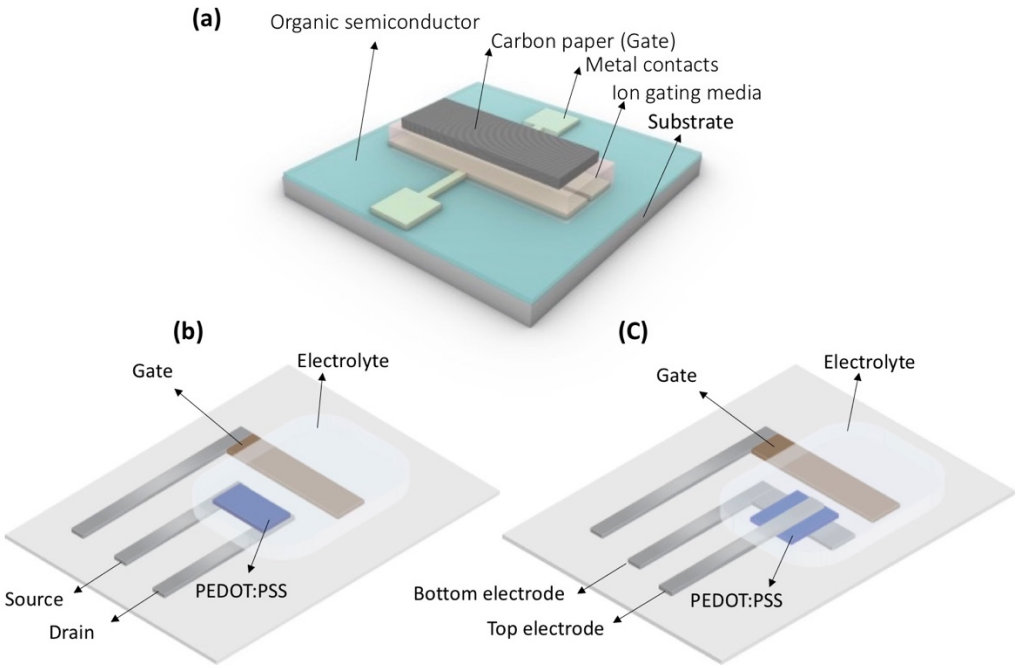

Figure 3-3 Schematic representation of EGTs based on organic semiconductor (a), OECTs with planar configuration (b), and vertical configuration (c).

3.7 Film characterization of organic semiconductors

3.7.1 Atomic force microscopy

Atomic force microscopy (AFM) is an imaging technique that used to obtain topography of surfaces at the nanoscale level. It works by scanning a sharp-tipped cantilever over the surface. As the tip is moved, it experiences forces that are related to the topography, composition, and other physical and chemical properties of the sample. These forces cause the cantilever to bend, and the extent of this movement is measured by a laser beam that is directed onto the cantilever. AFM can be operated in a variety of modes, such as contact, non-contact and tapping modes, depending on the application and properties of the sample. In contact mode, the tip is in constant contact with the surface and experiences a constant force, while in non-contact mode, the tip oscillates above the surface and measures the forces between the tip and the sample without making physical contact. In tapping mode, cantilever oscillate at or close to its resonance frequency. This causes the tip to tap the sample surface. As the tip taps the surface, it makes brief contact with it, producing a small interaction force. The tip then rebounds, which reduces the interaction force and allows the tip to avoid sticking to the surface [104].

In this PhD, tapping mode AFM was utilized to study the surface topology of the organic semiconductor films (PCDTPT, DPP-DTT) at ambient conditions. Microscopy was performed in tapping mode and scan rate of 1Hz. We utilized Digital Instruments Dimension 3100 with tip radius of less than 10 nm.

3.7.2 Scanning electron microscopy

Scanning electron microscopy (SEM) utilizes an accelerated electron beam to create signals from the surface of a sample. Atoms of sample interact with electrons, and the resulting signals are detected by specialized detectors. These signals are collected by a variety of detectors positioned at different angles relative to the sample. When the primary electron beam strikes the sample surface, low-energy electrons are emitted from the surface. They provide information about the topography and morphology of the surface. Backscattered electrons are higher-energy electrons that are scattered back toward the detector when they interact with the atoms of the sample. X-rays

are produced when the primary electron beam interacts with the atoms of the sample. They can be detected using an energy-dispersive X-ray spectroscopy (EDS) detector and used to identify the chemical elements present in the sample [105, 106].

In this PhD study, we used (JEOL FEG-SEM) to obtain cross sectional images of OECTs with vertical configuration. Also, we obtained EDX analysis of vertical OECTs.

3.7.3 X-ray diffraction

X-ray diffraction (XRD) is a non-destructive technique that is commonly used to study the crystallographic structure of materials. It involves exposing a sample to a beam of X-rays and analyzing the pattern of X-rays that are scattered by the sample. The X-ray beam interacts with the atoms in the sample, causing the X-rays to be scattered in different directions. The pattern of scattering depends on the arrangement of atoms in the sample, which is known as the crystal structure. The crystal structure of the sample can be determined by analyzing the pattern of X-ray scattering [107].

In this PhD work, we analyzed the crystallographic structure of the DPP-DTT films using X-ray diffractometer, Malvern PanAlytical Empyrean 3 with CuKα source with $\lambda = 1.54178$ Å.

3.7.4 Stylus Profilometry

A stylus profilometer is a type of surface metrology tool used to measure the shape and texture of a surface. It works by using a small stylus that is dragged across the surface of the sample being measured, and the motion of the stylus is recorded by a sensor. As the stylus moves along the surface, it measures the height of the surface relative to a reference plane. Results of profilometer shows surface roughness, waviness, and other important surface characteristics.

The thickness of the semiconductor films was measured using the Dektak 150 (Veeco, USA) stylus profilometer (with a tip radius of 12.5 μm and a force of 10 mg) in this PhD study.

3.7.5 Cyclic voltammetry and electrochemical impedance spectroscopy

Cyclic voltammetry (CV) is an electrochemical technique that involves the application of a varying potential waveform to an electrochemical cell, while measuring the resulting current. The technique

is commonly used to study the redox behavior of electroactive species, and provides information about the thermodynamic and kinetic properties of the electrochemical reaction. The cyclic voltammetry experiment involves sweeping the potential of the working electrode while recording the current. The resulting current-potential curve, also known as a voltammogram, provides information about the electrochemical reaction mechanism, including the oxidation and reduction potentials, the peak current density, and the electron transfer rate. A three-electrode system is a common setup used in electrochemistry to measure the electrochemical behavior of a sample. The system consists of three electrodes: working, reference, and counter electrodes. The working electrode is the electrode on which the electrochemical reaction takes place, and it is used to measure the current flowing in and out of the cell. The reference electrode is used to measure the potential of the working electrode, and it serves as a stable reference point for the electrochemical measurement. The counter electrode is used to complete the circuit and provide a current flow opposite to that of the working electrode, thus ensuring that the current in the system is balanced. In contrast, a two-electrode system only has a working electrode and a counter electrode that acts also as a reference electrode by maintaining constant potential. The potential of the working electrode is measured relative to the counter electrode in this configuration. During a CV experiment, the voltage applied to the working electrode is swept back and forth between two set values, causing the potential of the electrode to vary cyclically. As the potential of the working electrode changes, the electrochemically active material in the working electrode undergoes oxidation or reduction reactions. These reactions result in the flow of current between the working and reference electrodes, which is depicted in CV plots [108, 109].

In the transistor configuration, we conducted CV where the active channel material (organic semiconductors) acted as the working electrode. The ion-gating medium functioned as the electrolyte, and the counter and quasi-reference electrode consisted of activated carbon on carbon paper. The activated carbon electrode served as a quasi-reference electrode. It has high capacitance (with a specific capacitance of approximately 100 F/g). By utilizing CV, we could gain insights into the mode of operation of EGTs and their safe operating voltage [100, 110]. We conducted Electrochemical impedance spectroscopy (EIS) on electrolytes. We fabricated metal-insulator-metal (MIM) configuration. In MIM configuration gold acted as the working electrode and carbon paper acted as the reference and counter electrodes, respectively. We also employed Swagelok cell

for electrochemical characterization of ion gel and organogel used for OECTs. The testing cell consisted of a Teflon cylinder containing an electrolyte solution and two stainless-steel electrodes. A two-electrode configuration consisting of two stainless-steel electrodes separated by an electrolyte was utilized to perform the EIS [111].

In this work, we used versaSTAT4 (Princeton Applied Research) potentiostat to conduct the CV and EIS.

3.8 Device characterization

3.8.1 Electrical characteristics

In this PhD study, we have focused on p-type channel materials. For devices that operate in accumulation mode, negative voltages were applied to the gate and drain electrodes. This negative bias causes anions to accumulate at electrolyte-semiconductor interface, while cations accumulate at the gate electrode. The accumulation of negative ions in the semiconductor increases the number of electronic charge carriers (holes) in the channel material, causing the device to turn on. This ionic-electronic modulation results in a change in channel conductivity, which in turn modulates the I_d. In contrast, for devices that operate in depletion mode, we applied a positive voltage to the gate electrode. This causes cations to accumulate at the interface between the semiconductor and electrolyte, resulting in a decrease in the number of holes in the channel material. This decrease in holes leads to a lower current, causing the transistor to turn off. Transistor characteristics of EGTs are measured using a semiconductor parameter analyzer (Keysight B1500A controlled by EasyEXPERT software) with a micropositioner. The devices were tested to measure their typical electrical characterizations (output and transfer characteristics). To determine the output characteristics, the V_d is varied at a specified scan rate while the V_g is kept constant. On the other hand, to measure the transfer characteristics, the V_g is varied at a specific scan rate while keeping the V_d constant. Throughout both tests, the I_d and I_g were recorded. For pulse measurements of devices, the gate voltage is systematically varied between the ON-state and OFF-state for a specific duration at a constant V_d, while I_d is recorded as a function of time. The source of illumination utilized for obtaining the electrical characterization of phototransistors was a compact solar

simulator class AAA, specifically the SLB-300A model, which can simulate solar light with a power density of 1 KW/m^2, an AM 1.5 spectrum, and a wavelength of 400 nm to 1100 nm.

CHAPTER 4 ARTICLE 1 : FLEXIBLE ORGANIC ION-GATED TRANSISTORS WITH LOW OPERATING VOLTAGE AND LIGHT-SENSING APPLICATION

Mona Azimi[1], Arunprabaharan Subramanian[1], Nur Adilah Roslan[2], Fabio Cicoira[1]*

[1] Department of Chemical Engineering, Polytechnique Montréal, H3T 1J4, Canada.

[2] Department of Physics, Faculty of Science, University Putra Malaysia, 43400 UPM Serdang, Selangor Darul Ehsan, Malaysia.

* Corresponding author: fabio.cicoira@polymtl.ca

Journal of Physics: Materials, Submittted 04 September 2020, Published 07 January 2021

KEYWORDS: Ion-gated transistor, Donor-acceptor conjugated copolymer, Poly[4-(4,4-dihexadecyl4H-cyclopenta[1,2-b:5,4-b′]-dithiophen-2-yl)alt[1,2,5]thiadiazolo[3,4c]pyridine] (PCDTPT), Flexible organic electronic devices.

4.1 Abstract

Ion-gated transistors are attracting significant attention due to their low operating voltage (<1 V) and modulation of charge carrier density by ion-gating media. We report flexible organic ion-gated transistors based on a high mobility donor-acceptor conjugated copolymer. Along with the low operating voltage of ion-gated transistor it has advantageous features, including flexibility and light-sensing application. We fabricated ion-gated transistors based on poly[4-(4,4-dihexadecyl 4H-cyclopenta[1,2-b:5,4-b′]-dithiophen-2-yl)-alt[1,2,5]thiadiazolo[3,4c]pyridine] (PCDTPT) and the ionic liquid [1-ethyl-3 methylimidazolium bis(trifluoromethylsulfonyl)imide] ([EMIM][TFSI]) as the ion-gating medium. Electrical characteristics of [EMIM][TFSI] gated transistors on rigid (SiO_2/Si) and flexible (polyimide (PI)) substrates were obtained and very similar mobility values (~0.9 $cm^2V^{-1}s^{-1}$) and ON-OFF ratio of ~10^5 were calculated for both of the substrates. Flexible ion-gated transistors showed good mechanical stability at different bending curvature radii and under repetitive bending cycles. Mobility of flexible ion-gated transistors were remained almost same in flat and bent state, and after 1000 times of bending cycles mobility decreased by 20% of its initial value. Photosensitivity of ion-gated transistors were evaluated under solar simulator light

under vacuum condition. The photosensitivity and photoresponsivity values of 0.4 and 93 AW^{-1} were obtained for flexible phototransistors based on PCDTPT.

4.2 Introduction

Flexible organic electronic devices have aroused a great deal of interest for various novel applications, including wearable devices, flexible displays and sensor systems, due to light weight, ability to withstand mechanical deformation, printability, ease of processing and easy skin attachment [112]. Organic thin film transistors (OTFTs) are considered as the essential building blocks of electronic systems. Conjugated organic semiconductors have been extensively explored as active materials in flexible devices due to their low temperature processing, tunable energy levels, charge transport properties, and compatibility with fabrication processes over large areas, such as roll-to-roll, screen and inkjet printing [113, 114]. Polymer substrates such as polyimide (PI) polytetrafluoroethylene (PTFE), polyethylene terephthalate (PET), and polyethylene naphthalate (PEN) are the most commonly utilized for flexible electronics [115]. Ion-gated organic transistors are a category of devices with low operating voltage (<1V), where charge carrier density in the active material is modulated by exploiting an ionic gating medium, which is in direct contact with the channel material. Metal oxides as well as organic conjugated semiconductors, are being exploited as active materials for ion-gated transistors [68, 95, 101, 116-123]. The use of ionic gating media, instead of brittle oxide-based dielectrics, e.g. silicon, aluminum or hafnium oxides, is attractive for the fabrication of high-performance flexible transistors.

Organic phototransistors encompass light detection, light switching and signal amplification in a single device and typically show higher photosensitivity and lower noise current with respect to organic photodiodes, due the presence of the gate electrode that amplifies the photogenerated electrical signal [124, 125]. Light absorption by the semiconductor layer leads to the generation of excitons with a binding energy of a few hundred meV, which are dissociated into free charges by the applied electric field and detected as an increase in source-drain current. The flux of free charges in the semiconductor layer is correlated with the intensity and wavelength of the absorbed light [126]. Conformable phototransistors are attractive for applications in curved image sensors, which are a crucial components in bio-inspired imaging systems, artificial compound eyes and artificial retinas [127, 128]. One of the drawbacks of organic phototransistors is their high driving

voltage (typically higher than 20 V), which leads to high energy consumption [129]. Making use of low-voltage ion-gated transistors is a feasible way to effectively reduce energy consumption [130]. In addition to the low operating voltage of ion-gated transistors and modulation of charge carrier density by ion-gating media they have merits including flexibility, printability and bio-sensing applications [131].

In recent years, several donor-acceptor conjugated semiconductors with narrow band gap and high mobility have been synthesized [132]. Intermolecular charge transfer in these materials leads to very narrow band gaps, which improve the harvest of incident photons. Furthermore, strong π–π stacking causes high charge carrier mobility. Therefore, single-component donor-acceptor conjugated semiconductors as substitutes for bulk heterojunctions (BHJs) and bilayer systems are of great significance [35]. Poly[4-(4,4-dihexadecyl4H-cyclopenta[1,2-b:5,4-b′]-dithiophen-2-yl) alt[1,2,5]thiadiazolo[3,4c]pyridine](PCDTPT) is a donor-acceptor conjugated copolymer with a cyclopenta[2,1-b:3,4-b′]dithiophene (CDT) donor unit, and a [1,2,5]thiadiazolo[3,4-c]pyridine (PT) acceptor unit (Figure 4-1 (a)). Lowest unoccupied molecular orbital (LUMO) and highest occupied molecular orbital (HOMO) of PCDTPT are -3.7 eV and -5.16 eV, respectively. Strong electronic delocalization between donor and acceptor units enhances charge transport along the PCDTPT chain. Outstanding performance of PCDTPT as an active material for organic field effect transistors (OFETs) has been reported [133-135]. Alignment of polymer chains induced by nanogrooved substrates leads to a hole mobility higher than 20 $cm^2V^{-1}s^{-1}$ [133]. PCDTPT based OFETs, with a bottom gate bottom contact configuration, were fabricated on rigid and flexible substrates and showed a mobility of ∼20 $cm^2\ V^{-1}\ s^{-1}$ and 10.5 $cm^2\ V^{-1}\ s^{-1}$, respectively [136]. Film nanomorphology was controlled by using a nanogrooved polymer dielectric poly(4-vinylphenol) cross-linked with 4,4′-(hexafluoroisopropylidene)- diphthalic anhydride (PVP:HDA). Photo-sensing ability of PCDTPT has been reported for a multilevel optical memory with a vertical configuration, using a mixture of CdSe/ZnS quantum dots and poly methyl methacrylate (PMMA) as floating gate electrode. Photoresponsivity and photosensitivity value of the vertical device at a light wavelength of 830 nm and intensity of 70 mW cm^{-2} were 104 AW^{-1} and 200, respectively, which are higher than that of a planar device [137]. This improvement is related to the very short channel length (tens of nanometers), which leads to an easier dissociation of photogenerated excitons. Photoresponsivity of the blend PCDTPT: [6,6]-phenyl C61-butyric acid methyl ester

(PCBM) (BHJ) showed an improvement with respect to pure PCDTPT both for planar and vertical configurations [41].

Here, we demonstrate PCDTPT flexible ion-gated transistors using PI as a substrate. PI has good chemical and thermal stability, making it an appropriate candidate for flexible devices. [1-ethyl-3 methylimidazolium bis (trifluoromethylsulfonyl) imide] ([EMIM][TFSI]) was used as gating medium. Charge carrier mobilities of ∼0.9 $cm^2V^{-1}s^{-1}$ and ON-OFF ratios of $\sim 10^5$ were obtained for devices on rigid (SiO_2/Si) and flexible substrates. Electrical characteristics of flexible devices under different bending radii and several bending cycles showed good mechanical flexibility. We used these devices as phototransistors based on PCDTPT, which showed a photosensitivity of 0.4 and a photoresponsivity of 93 AW^{-1} at V_g= -1 V.

4.3 Experimental

4.3.1 Materials

PCDTPT (M_w= 50KDa, PDI=2) was purchased from 1-Material-Organic Nano Electronic and chloroform ($CHCl_3$) was purchased from Acros Organics. The ionic liquid ([EMIM][TFSI]) with viscosity of 39.4 mPa·s and ionic conductivity of 6.63 $mS \cdot cm^{-1}$ was supplied by IoLiTec and purified under vacuum ($\sim 10^{-5}$ Torr) at 60 °C for 24 h before use. PI sheets (PolyFLE™ XF-102) with a thickness of 125 μm were purchased from Polyonics. Polydimethylsiloxane (PDMS) (SYLGARD™ 184) was supplied by Dow Chemical Company. Carbon paper (Spectracarb 2050), activated carbon (Norit CA1, Sigma-Aldrich, 28 mg mL^{-1}), polyvinylidene fluoride (PVDF) (Kynar HSV900), and N-methyl pyrrolidone (NMP) (Fluka, >99.0%) were used for gate electrode fabrication.

4.3.2 Device fabrication

Activated carbon was chosen as gate electrode since its high surface area enables transistors to modulate current efficiently [138]. In order to prepare gate electrodes, carbon paper (6×3 mm^2) was immersed in a solution of activated carbon (28 mg mL^{-1}) and PVDF (1.4 mg mL^{-1}) in NMP. Carbon paper pieces coated with activated carbon ink were heated at 60 °C for 5 h to remove solvent. Source and drain electrodes (channel width/length (W/L) = 4000 μm/10 μm) were

patterned on SiO_2/Si substrate by photolithography and lift-off. For photolithography on SiO_2/Si substrate, a positive tone photoresist (AZ900) was spin-coated on substrates at 3000 rpm for 1 min. Samples were soft baked (at 90˚C for 1.5 mins) and exposed to UV light through a photo mask in a Karl Suss mask aligner (MA-6). Next, a post-exposure bake was carried out at 115 ˚C for 1.5 mins and the photoresist was developed in AZ-726 (MicroChem) developer for 60 seconds. Finally, samples were rinsed with deionized water several times in order to remove excess developer and dried with a N_2 flow. After metal deposition (40 nm gold and 5 nm titanium as adhesion layer), samples were immersed in PG remover to strip out the photoresist and sonicated in IPA, acetone, and IPA for 5, 10, and 5 min sequentially. For photolithography on flexible substrates, PI sheets were cleaned by ultrasonication in acetone, isopropyl alcohol (IPA), and deionized (DI) water for 10 min each. PDMS (elastomer/curing agent (10:1wt.%)) was spin coated (500 rpm for 30s) on glass slides and heated at 100 °C for 15 min. Then PI sheets (75 mm×50 mm) were laminated on semi-cured PDMS and heated at 100 °C for 15 min. This step was performed to ensure a flat surface during photolithography. The following steps were performed as described for the rigid substrates.

PCDTPT solution (2.5 mg mL^{-1}) in $CHCl_3$ was prepared and stirred overnight. Next, PCDTPT films were deposited on prepatterned substrates inside a glovebox (< 5 ppm O_2, H_2O) by spin coating at 1000 rpm for 1 min and then heated at 200 °C for 10 min on a hotplate.

[EMIM][TFSI] was dropped on PVDF hydrophobic membrane (Durapore GVHP 01300 with a pore size of 0.22 μm, 9×4 mm^2). The color of the membrane changed from white to transparent by absorbing ionic liquid, then the membrane containing ionic liquid was placed on PCDTPT film. We used PVDF membrane soaked with ionic liquid for constructing ionic gating media in order to prevent leakage of ionic liquid for the application in a flexible device. Carbon paper was placed on top of the PVDF membrane for the transistor device, while for the phototransistor it was placed in a position not covering the channel active material [101].

4.3.3 Characterization

Atomic force microscopy (AFM) images were taken in ambient conditions with a Digital Instruments Dimension 3100 equipped with etched silicon cantilevers (ACTA from Applied NanoStructures, Inc.) with a resonance frequency of 300 kHz, a spring constant of 40 N/m, and a tip radius <10 nm. Imaging was performed in tapping mode and scan rate of 1Hz and images were

analyzed by Nanoscope software. Cyclic voltammetry was performed with a VERSASTAT 4 (Princeton Applied Research) potentiostat under N_2 in a glovebox. The experimental condition was a two-electrode configuration such that the PCDTPT film in channel area acted as the working electrode and an activated carbon gate electrode (with high surface area and specific capacitance of about 100 $F \cdot g^{-1}$) acted as counter and quasi-reference electrode. Transistor characterizations were conducted by semiconductor parameter analyzer (Agilent B1500A) and electrical probe station in a glovebox. We performed characterization of 3 devices in the same conditions. Optoelectronic measurements were performed at room temperature in a cryostat probe station ($P \sim 10^{-4}$ Torr). A solar simulator (SLB-300A Compact Solar Simulator Class AAA) with a light power of 100 $mWcm^{-2}$ and wavelength range of 400 nm–1100 nm was used to evaluate the device characteristics under illumination.

4.4 Results and Discussion

AFM images (Figure 4-1(b)) show that PCDTPT films on SiO_2/Si have a porous structure, which can be explained by the rapid evaporation of the processing solvent (chloroform), upon heating at 200 °C, due to its low boiling point (61.2 °C). The presence of the pores favors an effective contact of the ionic liquid with the semiconductor film during ion gating [139]. Films on PI substrates show pores smaller than that of SiO_2/Si, likely because of the greater affinity of PCDTPT to hydrophobic substrates [140, 141]. The root mean square (rms) surface roughness of the PCDTPT films is ∼11 nm on SiO_2/Si and ∼7 nm on PI.

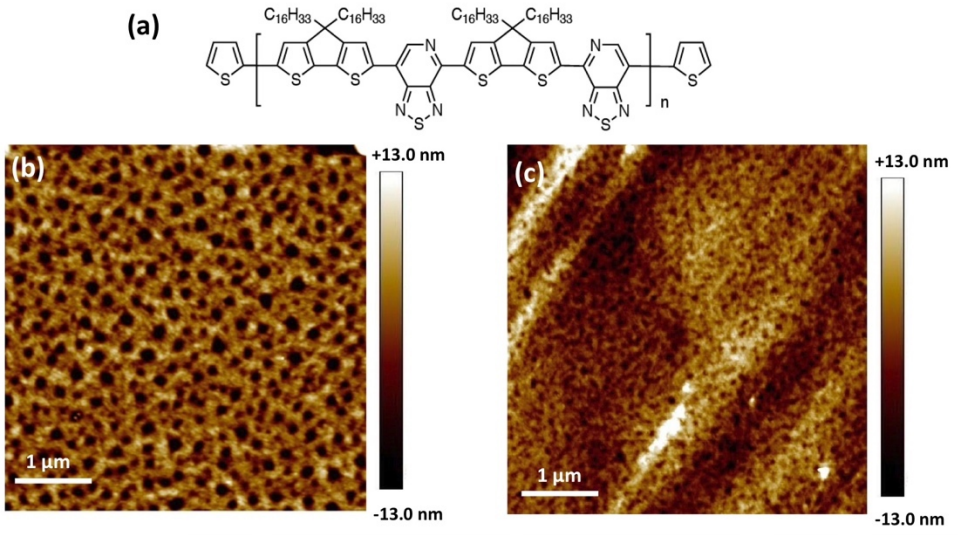

Figure 4-1 Molecular structure of PCDTPT (a), AFM images of spin coated PCDTPT films on: SiO_2/Si substrate (b), and PI substrate (c). The height scale bars in AFM images show the relative height of each point.

In order to obtain the electrochemical characteristic of PCDTPT film in transistor configuration, we performed cyclic voltammetry measurement at different scan rates (Figure 4-2). No significant redox reactions were observed in the range of 0 V to -1 V. For forward scan, a broad anodic peak in the interval of 0 V to 1.5 V was observed at all scan rates and it became more significant at higher scan rates. In the backward scan, a cathodic peak with a slightly negative shift compared to the anodic peak was observed in the voltage range of 1 V to 0.25 V. The current increases upon increasing the scan rate and the peak currents are linearly dependent on the square root of the potential, which indicates a diffusion-limited response [108]. Since there is a linear dependence between peak current versus scan rate, the electrochemical processes in PCDTPT are (pseudo) capacitive [142]. Overall, these results show that PCDTPT is electrochemically active in the presence of [EMIM][TFSI] ionic liquid and undergoes doping and de-doping reactions.

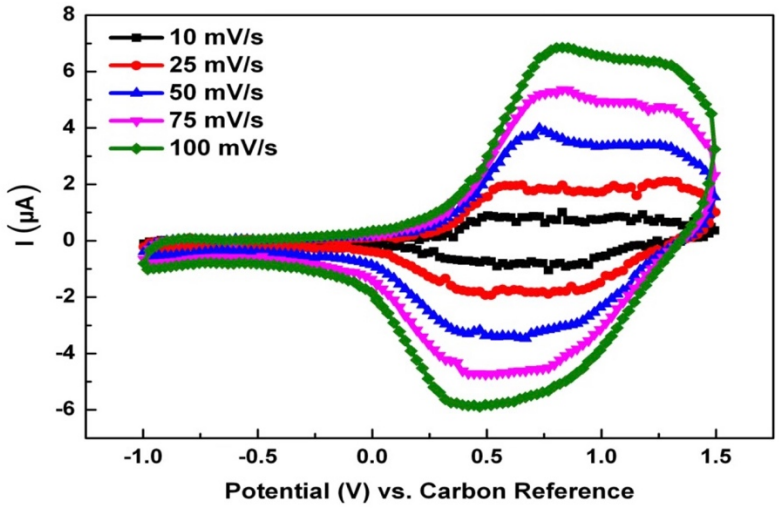

Figure 4-2 Cyclic voltammetry of PCDTPT films in transistor configuration at different scan rates. [EMIM][TFSI] acts as electrolyte, activated carbon coated carbon paper as counter and quasi-reference electrode, and PCDTPT film as working electrode.

PCDTPT ion-gated transistors on rigid and flexible substrates are capable of operating in enhancement mode at low voltage (<1.2 V) and show typical *p*-type characteristics. Output and transfer characteristics of ion-gated transistors on SiO_2/Si substrate are presented in Figure 4-3 (a-c).

The charge carrier mobility is extracted from $\mu = \frac{L}{W}\frac{I_d}{V_d\, pe}$, where L is the channel length (10 μm) and w the channel width (4000 μm), I_d is the drain-source current, V_d is the drain-source voltage and p the charge carrier density [143]. The charge density (p) was obtained from $p = \frac{Q}{eA} = \frac{\int I_g dV_g}{r_v eA}$, where Q is the total accumulated charge, which can be calculated by integration of the gate current (I_g) versus V_g (Figure 4-3 (b), blue graph), A is the area of the interface between the active layer and the ionic liquid (4 mm × 9 mm), r_v is the scan rate of V_g and e is the elementary charge. We obtained a charge carrier density of ~2×10^{14} cm^{-2}, which led to a mobility of 0.98 ± 0.10 $cm^2\ V^{-1}\ s^{-1}$ (the error represents the standard deviation of mobility values of 3 devices (transistor characteristics of 2 more devices is shown in FigureS1)). The ON-OFF ratio was ~10^5. The transconductance, i.e. the derivative of drain current (I_d) versus gate voltage (V_g), showed a maximum of 5 mS at V_g = -0.45 V (Figure 4-3 (d)). This value is among the highest previously reported values for organic semiconductor based, e.g., (poly(3-hexylthiophene) (P3HT)) ion gated

transistor devices [144, 145]. We correlate the high value of transconductance with the effective penetration of ions in the porous films [146] .

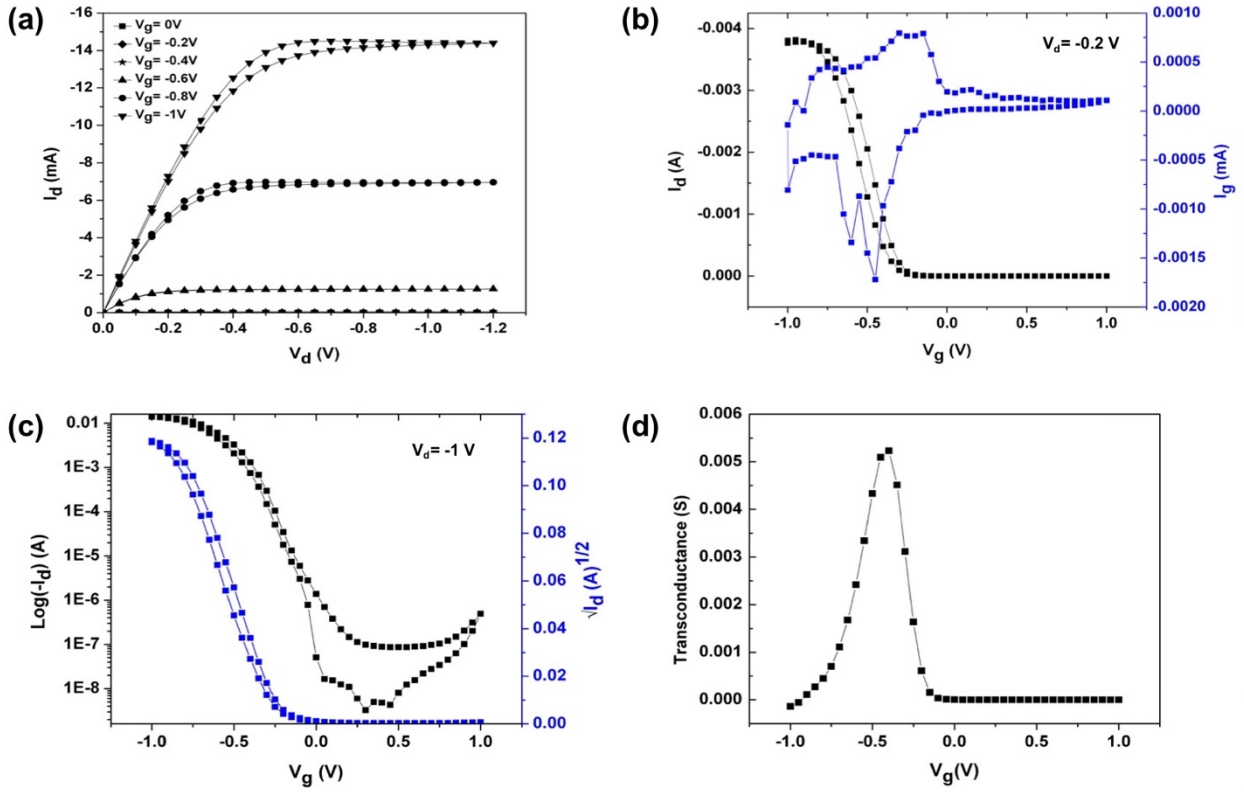

Figure 4-3 Electrical characteristics of [EMIM][TFSI] gated PCDTPT transistor fabricated on SiO_2/Si substrate and measured in N_2-purged glovebox (O_2 and H_2O < 3 ppm) with a scan rate of 50 mV/s. Output characteristic (a), transfer characteristics in the linear region (V_d = -0.2 V); left Y axis is related to drain-source current and right Y axis is related to gate-source current (b), transfer characteristics in the saturation region (V_d = -1 V); left Y axis shows drain-source current and right Y axis is the square root of drain-source current (c), transconductance plot versus gate-source voltage (d).

We fabricated ion gated transistors on flexible PI substrate, as shown in Figure 4-4 (a), and evaluated their performance under different bending conditions. Flat devices (Figure 4-4 (b)) show a mobility of 0.86 ± 0.06 $cm^2\ V^{-1}\ s^{-1}$, very similar to that of rigid devices (repeatability tests for 2 other devices in same condition is shown in Figure S2). A slight decrease in current was observed when the devices were bent perpendicularly to the channel width, with curvature radii R~20 mm and R~10 mm (Figure 4-4 (c, d)). Transfer curves obtained under different bending conditions

(Figure 4-4 (e, f)) showed that the threshold voltage increased from ~-0.2 V for flat devices to ~-0.25 V for R~20 mm and to ~-0.3 V for R~10 mm. The ON-OFF ratio was ~10^5 for all devices.

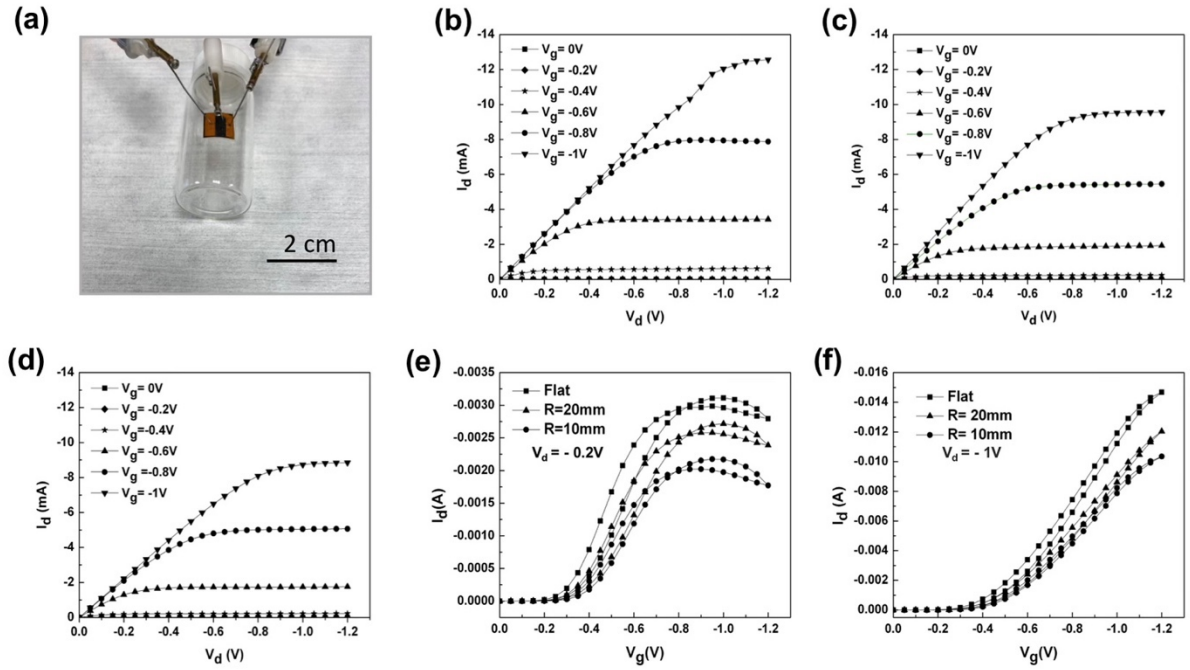

Figure 4-4 Photograph of a flexible device (a), output characteristic of [EMIM][TFSI] gated transistor on PI substrate in flat condition (b), under curvature radius of R~20 mm (c), and R~10 mm (d). Transfer characteristic in flat and different bending conditions in linear (V_d = -0.2 V) (e), and n saturation (V_d = -1 V) regime (f). The scan rate was of 50 mV/s.

The mobility at different curvature radii (Figure 4-5 (a)) remained almost unchanged with respect to the flat state and were 0.72 ± 0.04 and 0.79 ± 0.03 $cm^2 V^{-1} s^{-1}$ for flat, R~20 mm and R~10 mm curvature radii (values averaged on 3 devices and error representing the standard deviation). Along with electrical characterization in varied curvature radius we tested the device under repetitive bending cycles. The mobility as a function of the number of bending cycles is shown in Figure 4-5 (b). Mobility values in repetitive bending up to 1000 cycles decreased from 0.86 ± 0.06 to 0.68 ± 0.04 $cm^2 V^{-1} s^{-1}$, i.e. just 20 % with respect to the flat state. Optical microscopy images of PCDTPT films after 1000 bending cycles show no significant cracks (Figure S3).

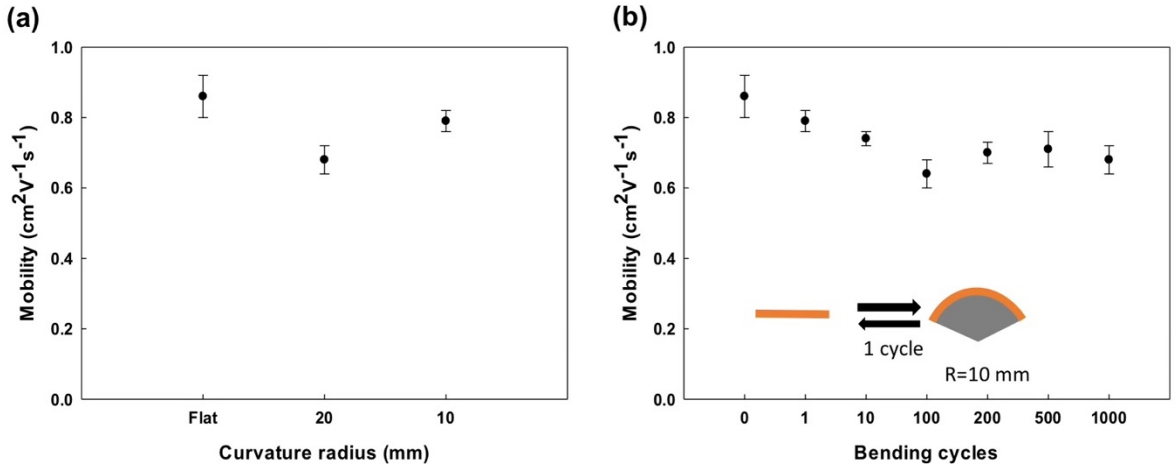

Figure 4-5 Mobility variation versus different bending curvature (a), Mobility values in different bending cycles with curvature radius of R∼10 mm (b). The error bars represent the standard deviation of the mobility values obtained from 3 devices.

In order to evaluate light-sensing application of ion-gated transistors we tested the devices in dark and light conditions. The scheme of a phototransistor is shown in Figure 4-6 (a). The activated carbon gate was positioned in a position that was not covering the channel area, so the light could be absorbed by the semiconducting layer. According to output and transfer characterization (Figure 4-6 (b, c)), the PCDTPT film is photosensitive. The values of charge carrier density in dark and illumination conditions are $(2.19 \pm 0.05)\times10^{14}$ cm^{-2} and $(2.47 \pm 0.02)\times10^{14}$ cm^{-2}, respectively (I_g versus V_g curves are shown in Figure 4-6 (d)). The mobility increased from 0.78 ± 0.03 cm^2 V^{-1} s^{-1} in the dark to 0.87 ± 0.05 cm^2 V^{-1} s^{-1} under illumination. As these devices were briefly exposed to air before measurements, their mobility values are lower than those of devices tested in glovebox. Phototransistors were evaluated for their photosensitivity $= (I_{d,light} - I_{d,dark})/I_{d,dark}$ and photoresponsivity $= (I_{d,light} - I_{d,dark})/p_{light}.S$ [39], where $I_{d,light}$ is the drain-source current in illumination and $I_{d,dark}$ is the drain-source current in the dark, p_{light} is the light intensity and S is the geometrical area of channel (4000 μm × 10 μm).

Photosensitivity and photoresponsivity versus V_g, shown in Figure 4-6 (e), increased by increasing V_g and reached the value of 0.4 and 93 AW^{-1} at V_g= -1 V, respectively. Previously reported photoresponsivity for PCDTPT based phototransistor with planar OFET configuration was 56 AW^{-1} upon application of a V_g of -30 V [41]. Although our obtained values for photosensitivity and photoresponsivity are lower than other organic phototransistors, our devices are operated at

significantly lower voltage (<1 V). The dynamic photosensitivity behavior of ion-gated phototransistors determines their response speed. The transient characteristics (drain current versus pulsed illumination) of a PCDTPT phototransistor are shown in Figure 4-6 (f). The measurement was started at t= 0 s and after the current (I_d) became stable (at t= 300 s) the device was exposed to light. We obtained rise time and fall time from the transient curve. Rise time is defined as the response speed of a phototransistor device under illumination, and as time passed the photocurrent increased from 10% to 90% of maximum value. Fall time is defined as the time needed for the current to decrease from 90% of maximum value to 10% by removing the light source [147]. We obtained a rise time of ∼15 s and a fall time of ∼20 s, which are higher values compared to phototransistors with OFET configuration [41], which are ∼ 3s and 0.05 s. Longer response time of ion-gated phototransistors is due to the slow motion of ions[148]. We also fabricated phototransistor device on SiO_2/Si substrate (Figure S4), which show similar photosensitivity and photoresponsivity (0.7, 31 AW^{-1}, respectively).

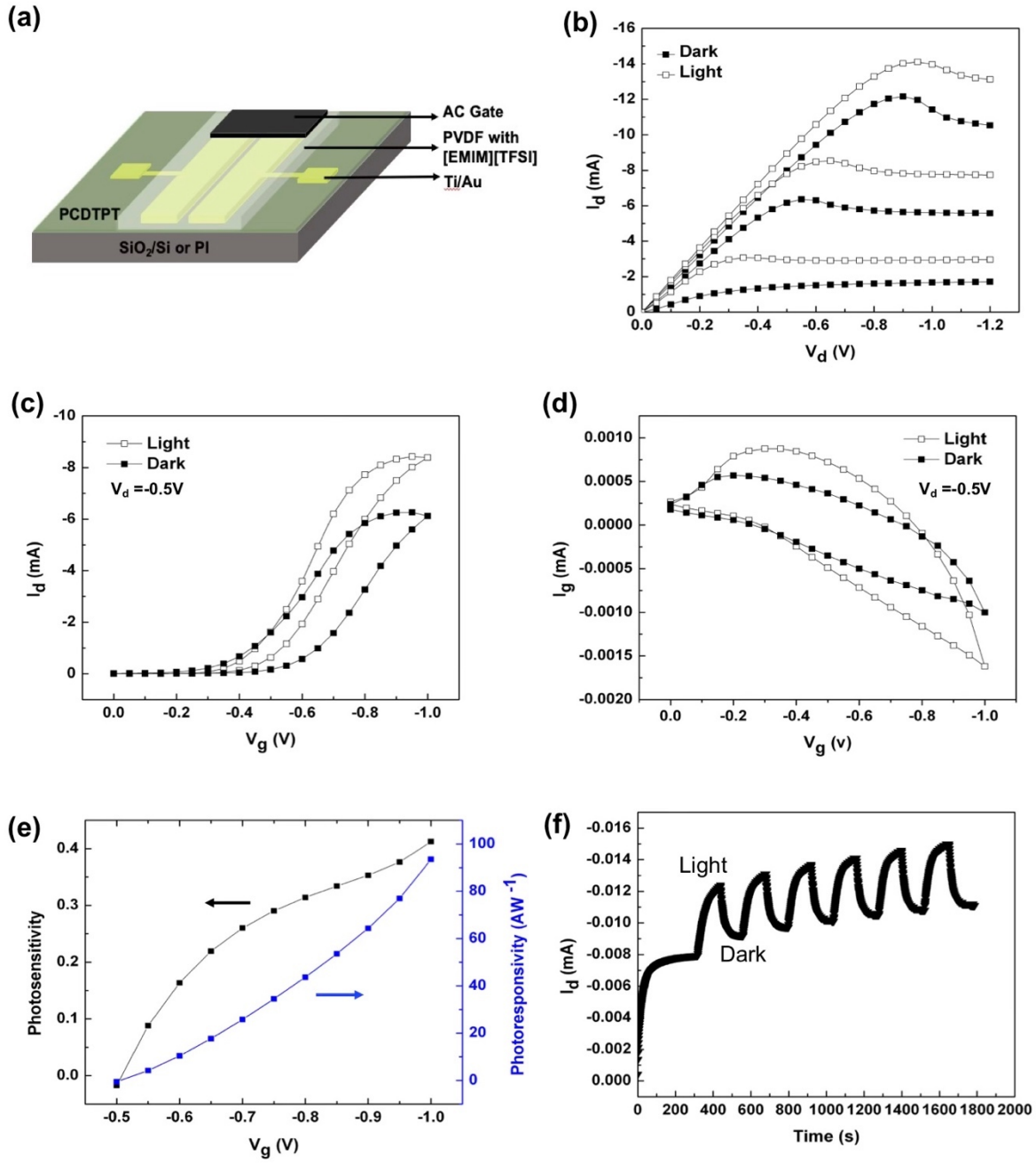

Figure 4-6 Scheme of [EMIM][TFSI] gated phototransistor (a), output characteristic of flexible phototransistor (on PI substrate) at V_g = -1, -0.8, -0.6 V in dark and under solar simulator light in vacuum condition (b), transfer characteristic at V_d = -0.5 V in dark and light condition (c), plot of gate-source current versus gate voltage at V_d = -0.5 V (d), photosensitivity and photoresponsivity curves versus gate voltage at V_d = -0.5 V(e), and dynamic photoresponse behavior at V_g = -0.2 V and V_d = -0.2V (f).

4.5 Conclusions

We demonstrated fabrication of flexible ion-gated transistor and phototransistor based on donor-acceptor conjugated copolymer (PCDTPT) operating at low voltages (< 1 V). Cyclic voltammetry showed that application of ionic liquid ([EMIM][TFSI]) as ion-gating media which is in direct contact with an organic semiconducting layer led to doping/de-doping reactions in a permeable semiconducting copolymer layer. Designed devices on both flexible and rigid substrates exhibited high mobility values. Ion-gated transistors fabricated on PI substrate showed good mechanical flexibility at different curvature radii and repetitive bending cycles. Evaluation of the photosensitivity of flexible ion-gated devices under simulated solar light showed enhancement of charge carrier mobility of devices under illumination. Phototransistors with ion-gated configuration showed photosensitivity of 0.4 and responsivity of 93 AW^{-1}. Development of low-weight flexible transistor with low operating voltages enlightens application of such kinds of devices for novel flexible electronic and optoelectronic devices. On the long-term, flexible ion-gated transistors and phototransistors offer great promises for optical sensor application and bio-inspired imaging systems.

4.6 Acknowledgments

This work is supported to a NSERC Discovery Grant awarded to FC. MA. and AS are grateful for financial support from the Institut de l'Energie Trottier through PhD scholarships. NA Roslan is grateful to the Canada ASEAN scholarship for internship. This work was supported by CMC Microsystems through the MNT program.

CHAPTER 5 ARTICLE 2 : ELECTRICAL AND MECHANICAL STABILITY OF FLEXIBLE, ORGANIC ELECTROLYTE-GATED TRANSISTORS BASED ON ION GEL AND HYDROGELS

Mona Azimi[1], Arunprabaharan Subramanian[1], Jiaxin Fan[1], Francesca Soavi[2] and Fabio Cicoira[*1]

[1] Department of Chemical Engineering, Polytechnique Montréal, H3T 1J4, Montreal, Canada.

[2] Dipartimento di Chimica "Giacomo Ciamician", Università di Bologna, Via Selmi 2, Bologna 40126, Italy.

Journal of Materials Chemistry C, Submitted 04 February 2023, Published 01 March 2023

* Corresponding author: fabio.cicoira@polymtl.ca

5.1 Abstract

Electrolyte-gated transistors (EGTs) have been widely investigated for applications in bioelectronics owing to their low operating voltage and mixed ionic-electronic conduction. The ion-gating media play a primary role in determining the operating voltage and electrical stability of these devices. In this study, we employed an ion gel based on an ionic liquid and hydrogels based on polyvinyl alcohol (PVA) as the gating media for EGTs using an organic semiconductor, poly(N-alkyldiketopyrrolo-pyrrole-dithienylthieno[3,2-b]thiophene) (DPP-DTT), as the channel material. The device characteristics revealed that ion gel-gated transistors showed superior electrical stability over hydrogel-gated transistors because hydrogels undergo dehydration over time. After 65 cycles of pulse measurements, the drain current of the ion gel-gated devices did not show any significant change, whereas it decreased to ~50 % of the initial value for the hydrogel-gated devices. By adding glycerol as an anti-dehydrating agent, the current decreased by only ~10 % under the same conditions, demonstrating improved operational stability. Finally, we fabricated flexible EGTs on polyethylene terephthalate (PET), which can be operated under different bending radii.

5.2 Introduction

Electrolyte-gated transistors (EGTs), which exploit mixed ionic-electronic transport, have applications in flexible and printed electronics, bioelectronics, and neuromorphic devices [149, 150]. EGTs can be operated at low voltages owing to the high electrical double-layer capacitance at the semiconductor/electrolyte interface. Different types of semiconductors have been used for EGTs, including organic small molecules and polymers, carbon nanomaterials, and metal oxides [151, 152]. A variety of materials are used for EGTs gating media, including aqueous saline solutions, ionic liquids, polymer electrolytes, polyelectrolytes, ion gels and hydrogels [153-155]. These materials differ in their physical state (e.g., solid, gel, or liquid), electrochemical stability, ionic conductivity, and mechanical properties. Aqueous electrolytes, which are used in most bioelectronic applications, have the disadvantages of limited electrochemical stability (~1.2 V) and rapid evaporation, leading to device degradation. Ionic liquids have a negligible evaporation rate and a wide electrochemical stability window (~3 V) [45]. However, their liquid state remains an obstacle for integration into solid-state devices. Solid-state gating can be achieved with polymer electrolytes, that is, salts dispersed in a polymer matrix; polyelectrolytes, that is, macromolecules bearing ionic groups; ion gels, that is, mixtures of ionic liquids with polymers; and hydrogels, that is, cross-linked three-dimensional networks of hydrophilic polymeric chains that swell in water [45]. Among these materials, ion gels and hydrogels are the most suited for flexible and stretchable EGTs because of their softer nature and superior mechanical properties [65, 156]. Ion gels show negligible evaporation rate, wide electrochemical stability window, and, owing to their hydrophobic nature, are compatible with most organic semiconductors. Moreover, they exhibit versatility for processing via printing techniques [111, 121], and can be utilized as ion-exchange layers to facilitate the penetration of ions into the hydrophobic semiconductor material [157]. Hydrogel electrolytes are of particular interest for flexible electronics, since their crosslinked polymer structure enables high water absorption and mechanical softness [158]. Hydrogels based on biomaterials such as gelatin, cellulose and agarose or biodegradable materials, such as polyvinyl alcohol (PVA), have been used for the fabrication of sustainable devices [12, 66]. PVA hydrogels have been used as healable electrolytes, which retrieved 95% of their initial ion sensitivity after healing and showed 86% retention of drain current after 1000 cycles [62]. The major concern about hydrogels is their dehydration over time, which impacts the device electrical stability. The

dehydration process can be inhibited by incorporating non-volatile organic polyols (e.g., ethylene glycol, glycerol) to improve the water retention ability via formation of multiple hydrogen bonds, thus permitting the fabrication of EGTs suitable for long-term electrophysiological monitoring [159]. There are two methods to introduce organic solvents in the formulation of hydrogels: i) gelation of the matrix polymer in a mixture of water and organic solvents, and ii) solvent displacement, achieved by immersion of the hydrogel in polyol-based solvents [63].

To expand the use of EGTs for practical applications, it is critical to improve their electrical stability over time, which mostly depends on active materials, ion-gating media, and metal contacts. Most studies to date have focused on the chemical stability of active materials or metal electrodes for long-term applications [160, 161], while the influence of different gating media on the electrical stability of EGTs has yet to be sufficiently explored. Non-aqueous (semi-solid) electrolytes present unique advantages over their aqueous counterparts for applications in flexible and stretchable electronics. Possible applications include wearable devices for health monitoring, artificial skin and implantable electronics. These applications require continuous stability over time, as well as intimate contact with curved surfaces that undergo frequent mechanical deformation. Aqueous electrolytes typically do not meet these requirements owing to their fluid nature and high volatility under ambient conditions.

Dasgupta *et al.* [81], reported the long-term stability of EGTs based In_2O_3 using different types of polymer electrolytes. The polymer electrolytes were composed of PVA (molecular weights of 13k and 89k), dimethyl sulfoxide (DMSO), propylene carbonate (PC), and lithium perchlorate ($LiClO_4$). They showed that high-molecular-weight PVA improved the stability of hydrogels owing to better water uptake. It has been reported that the normalized transconductance of EGTs gated with high molecular weight PVA changed from 51 ± 19 (for as prepared device) to 51 ± 17 and 54 ± 14 μS μm^{-1} after one month and 8 months, respectively. The normalized transconductance for low molecular weight PVA decreased from 57 ± 16 (for as prepared device) to 50 ± 13 and 47 ± 17 μS μm^{-1} after one month and 8 months post-fabrication, respectively. However, the operational stability of EGTs based on organic semiconductors and the use of different gating media has not yet been reported.

Zaumseil *et al.*[162] found that the replacement of the acidic hydrogen of the imidazolium salt with a methyl group improved the stability of ZnO based EGTs. The operational stability of EGTs based

on DPP-DTT in aqueous electrolytes has been reported previously. After 5 days in ambient conditions, the initial mobility value of 0.15 $cm^2 V^{-1} s^{-1}$ decreased by less than 10 %, while similar devices based on poly(3-hexylthiophene) (P3HT) showed a 30 % decrease [57]. Electrical stability of ion gel gated EGTs based on pristine P3HT and its mixture with ionic liquid (1-Ethyl-3-methylimidazolium bis(trifluoromethylsulfonyl)imide ([EMIM][TFSI])) has also been studied. The hole mobility decreased by 70 % for neat P3HT devices after 150 switching cycles, whereas the mobility of EGTs based on the blend of semiconductor with ionic liquid retained 90 % of its initial value [80].

In this study, we used hydrogel ion-gating media for the DPP-DTT-based EGTs. We investigated the electrical stability of EGTs by focusing on the effects of ion-gating media, including ion gels and hydrogels. The ion gel was based on poly(vinylidene fluoride-co-hexafluoropropylene) (PVDF-HFP) (IUPAC name:1,1-difluoroethene, 1,1,2,3,3,3-hexafluoroprop-1-ene) and the ionic liquid ([EMIM][TFSI]). PVDF-HFP was selected as the matrix polymer owing to its film-forming ability and high tensile strength. Hydrogels are based on PVA, a sustainable material whose gelation occurs through a freezing/thawing process, leading to the formation of hydrogen bonds without additional chemical crosslinkers. We observed superior electrical stability for ion gel-gated devices compared to devices gated by hydrogels, which, without an anti-dehydrating agent, exhibited electrical degradation over time owing to the fast evaporation of water. The addition of high-boiling point glycerol to the hydrogel formulation significantly improved the electrical stability of the devices. Furthermore, changes in the drain current and mobility under different bending radii were monitored to evaluate the flexibility of the devices. This study contributes to the understanding of the effect of different gating media on the electrical characteristics and operational stability of EGTs based on organic semiconductors. The development of flexible EGTs with reasonable operational stability promises the future application of novel flexible electronics.

5.3 Experimental

5.3.1 Materials and methods

The organic semiconductor (DPP-DTT) was purchased from Ossila; chloroform ($CHCl_3$) was purchased from Acros Organics; PVDF-HFP (Mw~400,000, Mn~130,000) and PVA

(Mw~89,000-98,000, 99+ % hydrolysed) were purchased from Millipore Sigma. The ionic liquid ([EMIM][TFSI]) (viscosity of 39.4 mPa·s and ionic conductivity of 6.63 $mS \cdot cm^{-1}$) was supplied by IoLiTec and purified under vacuum (~10^{-5} Torr) at 60 °C for 24 h before use. Carbon paper (Spectracarb 2050) coated with carbon ink was used as the gate electrode. The electrical resistivity of the carbon paper is 5.4 mΩcm (as declared by the supplier) and its roughness ~18 μm, as reported in the literature [163]. The Carbon ink contains activated carbon (Norit CA1, Millipore Sigma, 28 mg mL^{-1}), polyvinylidene fluoride (PVDF, Millipore Sigma) (IUPAC name: 1,1-difluoroethene), Nafion, and N-methyl pyrrolidone (NMP, Fluka, >99.0 %).

5.3.2 Morphology and structure

The topographical characteristics of the organic semiconductor thin films were obtained by Atomic Force Microscopy (AFM) under ambient conditions using a Digital Instruments Dimension 3100 (resonance frequency of 300 kHz, spring constant of 40 N m^{-1}, and tip radius <10 nm). Tapping mode with a scan rate of 1 Hz was used for imaging, and the Nanoscope software was used to analyze the images. The XRD pattern of the thin film was obtained using a Malvern Pan-Alytical Empyrean 3 diffractometer with a CuKα (λ = 1.54178 Å) beam.

5.3.3 Synthesis of ion gels and hydrogels

The ion gel was prepared from a mixture of PVDF-HFP, which acted as the host matrix, and an ionic liquid ([EMIM][TFSI]) in acetone. PVDF-HFP is a hydrophobic and semi-crystalline copolymer with good film-forming ability.63 PVDF-HFP was added to acetone at a weight ratio of (1:15) and stirred for 2 h at 50 °C to obtain a homogenous solution. The ionic liquid (ratio of 4:1 w/w with respect to PVDF-HFP) was added to the solution, which was stirred for 2 h at 50 °C. The resulting gel was directly spin-coated (500 rpm, 30s, thickness ~130 μm) onto the device for use as a transistor gating medium. PVA hydrogels were prepared using a freezing/thawing method, which leads to the physical crosslinking of polymer chains without the use of crosslinking agents. 16 wt % PVA was dissolved in deionized (DI) water at 95 °C in an oil bath for 1 h. When the solution became transparent, it was cast into a glass petri dish and kept in a freezer (-15 °C) for 3 h and then at room temperature for 24 h. The resulting gel (thickness ~1000 μm) was cut to desired shapes and swelled in three different solutions:0.5M aqueous NaCl (PVA/W (0.5)), mixture of

water/glycerol (50/50) (%v) with a concentration of 0.5 M NaCl (PVA/W+Gl (0.5)), and mixture of water/glycerol solution with concentration of 0.7 M NaCl (PVA/W+Gl (0.7)). The different thicknesses of the gating media are due to the difference in processing: ion-gel electrodes were directly spin-coated on the devices, while hydrogels were applied manually on the devices after casting and solidification on a different substrate. As expected, spin coating led to a significantly lower thickness.

5.3.4 Electrochemical characterization of gels

The electrochemical properties of the ion gel and hydrogels were evaluated by Electrochemical Impedance Spectroscopy (from 10^5 Hz to 1 Hz) using a VERSASTAT 4 potentiostat (Princeton Applied Research). To extract the ionic conductivities, an MIM structure was adopted, using gold as the bottom electrode and activated carbon-coated carbon paper as the top electrode (Figure 5-2 (a)), where gold acted as the working electrode and carbon paper acted as the reference and counter electrodes, respectively. For CV measurements in the transistor configuration, we used a two-electrode configuration, where DPP-DTT films served as the working electrode, carbon paper as the counter and quasi-reference electrodes, and gels as the electrolyte, with a scan rate of 50 mV s^{-1} or 10 mV s^{-1} between -1V and +1 V versus the carbon quasi-reference. The current density in the CV curves was normalized to the geometric area of the semiconductor in contact with the electrolyte.

The ionic conductivities (σ) of the gels were calculated using Equation (1):[164]

$$\sigma = \frac{1}{R_b} . \frac{d}{S} \qquad (1)$$

where d (cm) is the thickness of the gel and S (cm^2) is the contact area between the electrode and electrolyte. R_b is the bulk resistance (Ω), which is equal to the value of Z_r in the high-frequency region (10^5 Hz), as shown in Figure 5-2 (c). The thicknesses of the gels were measured using optical microscopy.

The specific capacitance (F cm^{-2}) of the gels was obtained using Equation (2):[164]

$$C = \frac{-1}{2\pi f Z_i A} \qquad (2)$$

where f (Hz) is the frequency, Z_i (ohm) is the imaginary part of the impedance (from Nyquist plots (Figure 5-2 (b)), and A (cm^{-2}) is the area of the activated carbon paper top contact (0.4 cm× 0.8 cm).

5.3.5 Fabrication and characterization of EGTs

Au source and drain electrodes (channel width/length (W/L) = 4000 μm/10 μm) were patterned on Si/SiO_2 and PET substrates by photolithography and lift-off, as reported elsewhere [155]. The DPP-DTT solution (2.5 mg mL^{-1}) in $CHCl_3$ was prepared and stirred overnight at room temperature. DPP-DTT films (thickness 65± 5 nm) were obtained by spin coating the prepatterned substrates (1000 rpm, 1 min), followed by heating at 100 °C for 20 min on a hotplate. The ion gel and hydrogels were prepared as previously described and applied to semiconductor-coated electrodes.

Carbon paper coated with activated carbon was used as the gate electrode because of its high surface area, which leads to efficient current modulation [110]. We used two types of activated carbon inks: a hydrophobic solution of activated carbon (28 mg mL^{-1}) and PVDF (1.4 mg mL^{-1}) in NMP for ion gel-gated devices, and a hydrophilic solution of activated carbon (28 mg mL^{-1}) and Nafion (2.4 mg mL^{-1}) in isopropyl alcohol for hydrogel-gated devices. Carbon paper pieces (4×8 mm^2) were coated with activated carbon ink via drop casting and heated at 60 °C for 5 h to remove the solvent. Finally, they were placed on a gel electrolyte solution.

Transistor characterization was performed using a semiconductor parameter analyzer (Agilent B1500A). The charge carrier mobility ($cm^2\ V^{-1}\ s^{-1}$) of the devices was obtained from the linear transfer characteristics using Equation (3):

$$\mu_{lin} = \frac{L\, I_{d,lin}}{W\, e\, p\, V_d} \qquad (3)$$

where L is the channel length (10 μm), $I_{d,lin}$ is the drain-source current in the linear region, W is the channel width (4000 μm), e is the elementary charge (1.6×10^{-19} C), V_d is the drain-source voltage, and p is the charge carrier density. p (cm^{-2}) was calculated from the linear transfer characteristics using Equation (4):

$$p = \frac{\int I_{gs} dV_g}{r_v e A} \qquad (4)$$

where r_v is the scan rate and A (cm^2) is the electrolyte area in contact with the semiconductor [165].

We evaluated the hysteresis of the devices using Equation (5):

$$W = |V_{gf}(I_d)| - |V_{gb}(I_d)| \qquad (5)$$

where $V_{gf}(I_d)$ and $V_{gb}(I_d)$ are related to the gate voltages in the forward and backward scans at a given drain current [166].

5.4 Results and Discussion

5.4.1 Structural and Topographical Characterization

The chemical structures of the materials used for the EGTs and the device structure are shown in Figure 5-1 (a) side view of the device structure is shown in Figure S1a). The ion gel (PVDF-HFP/IL) was a mixture of PVDF-HFP and [EMIM][TFSI] (Figure 5-1 (a)). The hydrogels were mixtures of PVA and aqueous NaCl (0.5 M or 0.7M), with or without glycerol (Figure 5-1 (b)). The hydrogel formulations are listed in Table 5-1. To evaluate the effect of ion-gating media on EGTs performance, we maintained the same device dimensions. To investigate the effect of glycerol on the electrical stability and performance of the devices, the composition of the swelling solution was varied.

Table 5-1. Chemical composition of hydrogels

Hydrogel	Swelling solution
PVA/W (0.5)	NaCl 0.5M in H_2O
PVA/W+Gl (0.5)	NaCl 0.5M in H_2O /glycerol (50/50) (%v/v)
PVA/W+Gl (0.7)	NaCl 0.7M in H_2O /glycerol (50/50) (%v/v)

The semiconductor DPP-DTT was used as the channel material (Figure 5-1 (c)). The choice of semiconductor is critical for achieving electrical stability in the transistors. DPP-DTT exhibited stable transistor characteristics in aqueous electrolytes [57, 151]. Height micrographs obtained from atomic force microscopy (AFM) revealed that DPP-DTT films on Si/SiO_2 (Figure 5-1 (d)) consist of well-ordered and homogeneously distributed lamellae, with a root mean square (rms) surface roughness of 3.5 ± 0.4 nm, which is similar to previously reported observations [57, 167]. The X-ray diffraction (XRD) pattern (Figure S1b) revealed semi-crystalline characteristics, with a first-order lamellar stacking peak (100) at $2\theta = 4.65°$, corresponding to an interlayer alkyl side chain

distance of ~10 nm. This is in sufficient agreement with the findings of Lei *et al.*[168] and Zhang *et al.* [169], who observed the (100) peak positioned at 2θ= 4.45°.

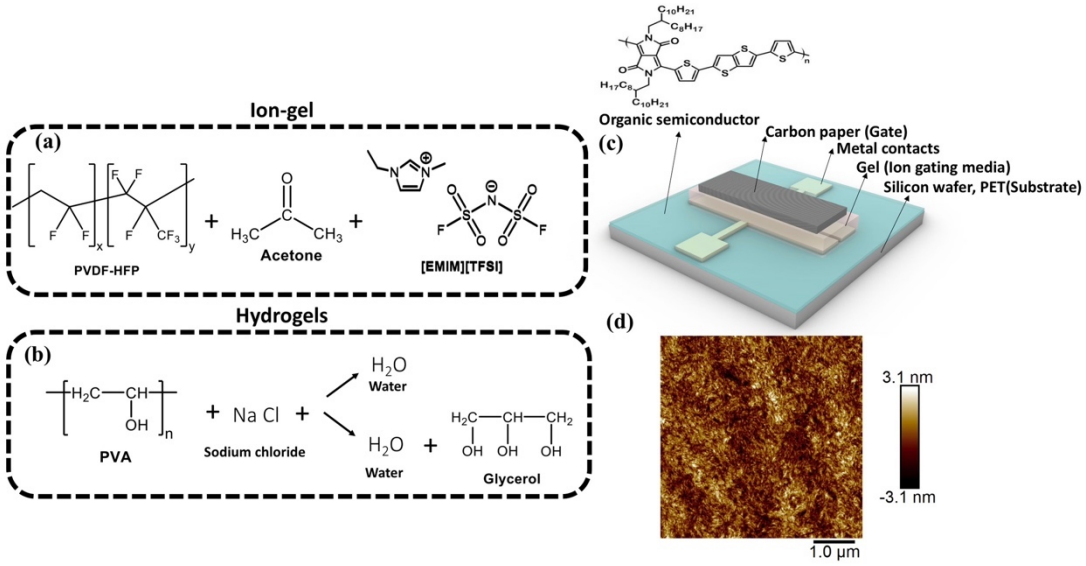

Figure 5-1 Molecular structures of the materials used for ion gels (a) and hydrogels (b), scheme of device and molecular structure of the organic semiconductor (DPP-DTT) (c), AFM image of spin-coated DPP-DTT film on Si/SiO_2 substrate (d).

5.4.2 Electrochemical Properties of Ion gel and Hydrogels

Electrochemical characterization of the ion-gating media was performed in a metal-insulator-metal (MIM) configuration (Figure 5-2 **(**a)), see experimental section for details) to determine their ionic conductivity and capacitance, as well as stability over time. In MIM structures, the electrolyte is sandwiched between two conductor layers. Although Au is commonly used as the contact material in such structures, other conductive materials such as indium tin oxide (ITO) can be used. For example, Kim *et al.* [80], used ITO as the bottom contact and aluminum as the top contact. We chose Au as the bottom electrode and conductive carbon paper coated with activated carbon as the top electrode. This material, which has a high surface area, high capacitance, and wide electrochemical stability window, is commonly used as a gate electrode in EGTs [110, 152, 154, 155], and can be directly laminated on the gel electrolyte without the need of thermal evaporation. The Nyquist plots (imaginary component, Z_i, versus the real component of impedance, Z_r) show

tilted straight lines that are related to the typical behavior of electrolytes in contact with the solid electrodes. The high-frequency region of the Nyquist plots (Figure 5-2 (b)) does not show a semicircle, which indicates non-Faradaic processes at the gel/electrode interface [170, 171]. The behavior of Z_r at high frequencies (Figure 5-2 (c)) reveals that the equivalent series resistance (ESR) of the ion gel and PVA/W(0.5) are almost similar and lower than those of glycerol-containing hydrogels. The ESR value includes the contributions of the bulk resistance of the electrolyte and the interfacial resistance between the electrolyte and the electrode. The absence of a semi-circular region at high frequencies (10^5 Hz) indicates that the interfacial resistance is negligible compared with the bulk resistance [172, 173]. The higher ESR value in glycerol-based hydrogels is likely due to the presence of glycerol, which is an insulating material. Figure 5-2 (d) shows the impedance versus the frequency of the electrolytes. The decrease in impedance by increasing the frequency is related to the formation of an electric double-layer [172, 174]. The impedance at high frequencies, which is related to the bulk resistance of electrolytes, is higher for hydrogels containing glycerol. For all gels, the phase angle is ~-45° or lower at frequencies lower than 10 Hz (Figure 5-2 (e)), which indicates a non-ideal capacitive behavior (a phase angle of -90° indicates purely capacitive behavior). The ion gel shows higher phase angles at low frequency (1 Hz) with respect to hydrogels. For hydrogels with and without glycerol and a lower concentration of NaCl (0.5 M) the phase angle was ~-50°. At higher NaCl concentration (0.7 M), the phase angle increased to ~-60°, which indicates an improved capacitive behavior. At frequencies higher than 10 Hz, the hydrogels with glycerol showed lower phase angles, likely due to the hindrance effect of glycerol, which inhibits double layer formation [174].

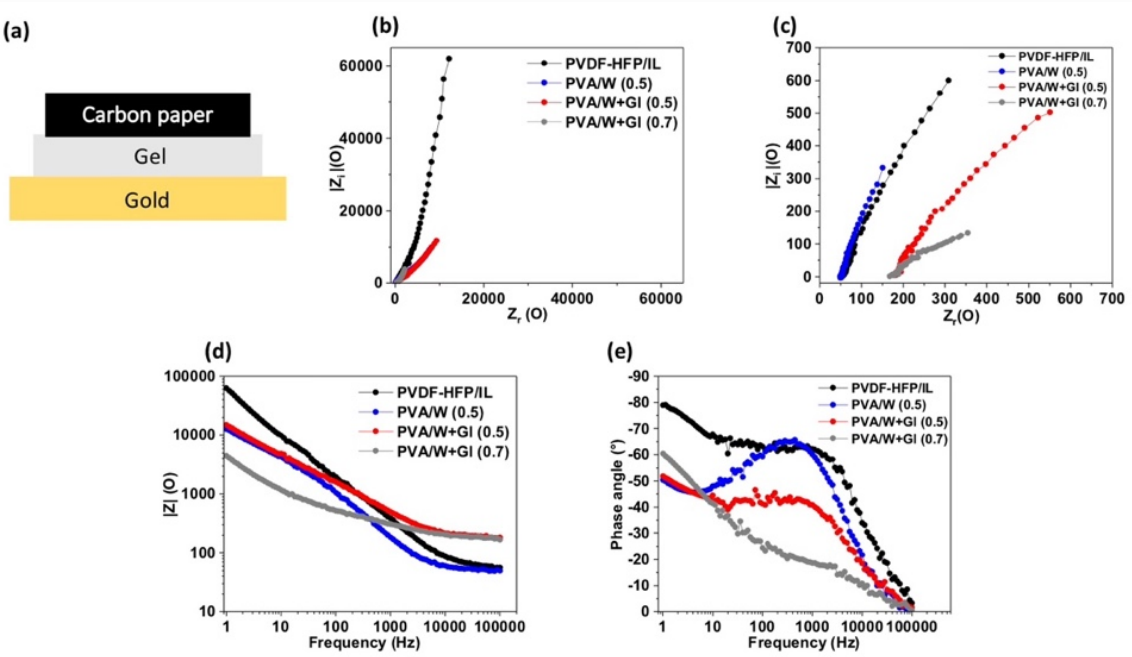

Figure 5-2 MIM structure (a), Nyquist plots of gels (b), magnified Nyquist plots at high frequencies (c), Bode plot (impedance versus frequency) (d), Bode plot (phase angle versus frequency) The sample compositions are listed in Table 5-1.

We extracted the ionic conductivity and capacitance of the MIM assembled with gels from Equations (1) and (2) (experimental section). The values, summarized in Table 5-2**,** are comparable with those reported for state-of-the-art systems featuring ion gels and hydrogels (Table S1) [54, 65, 79, 80, 121, 175]. Our measurements yielded the capacitance of the electric double layer at the interface between the Au electrode (working electrode) and the electrolyte, which does not depend on the thickness of the electrolyte [8, 176]. Capacitance values from the MIM structure provide insight into the capacitive behavior of electrolytes in EGTs. However, they are not directly related to the device performance (see next paragraph for details). The ionic conductivity depends on the ion concentration and mobility, as well as on the viscosity of the material [164]. Hydrogels show higher ionic conductivity than ion gels because the large amount of water present in the material (typically over 70 %) facilitates ion transport [64, 177]. The addition of glycerol increases the viscosity, leading to a decrease in ionic conductivity [178], [179]. The equivalent circuit model of our system (inset of Figure S2) consists of a resistor and a constant phase element (CPE) in series. Resistance includes both ionic and electronic contributions. The CPE accounts for the electric double-layer, and α is a parameter accounting for the electrolyte behavior (α=1 corresponds to an

ideal capacitor). The parameters obtained from the fitting are listed in Table S2. The ion gel and PVA/W(0.5) showed a resistance value lower than that of glycerol-containing hydrogels. The higher resistance observed in hydrogels containing glycerol is related to the presence of glycerol, which is an insulating material. Comparing the α values of the electrolytes reveals that the ion gel (α~0.8) behaves more like an ideal capacitor than the hydrogels (α~0.5). This is likely due to the presence of water molecules in hydrogels, which inhibits ideal capacitor behavior. The highest CPE value is found for PVA/W+Gl(0.7), in agreement with its highest capacitance.

Table 5-2. Ionic conductivity and capacitance values of MIM devices obtained from EIS measurements. (The thicknesses of ion gel and hydrogels are ~130 μm and 1000 μm, respectively.) The values were averaged for three samples, and the errors represent the standard deviation.

Gels	Ionic conductivity (mS cm^{-1})at 10^5Hz	Effective Capacitance (μF cm^{-2}) at f=1Hz
PVDF-HFP/IL	0.6±0.1	4.5±0.8
PVA/W (0.5)	9.4±3.5	28.6±7.9
PVA/W+Gl (0.5)	2.7±0.3	30.5±6.5
PVA/W+Gl (0.7)	3.1±0.5	51.2±15.4

5.4.3 Characterization of Ion gel and Hydrogel Gated Transistors

The electrical characteristics of the ion gel and hydrogel-gated transistors are shown in Figure 5-3**.** The figures of merit are summarized in Table 5-3 (values averaged for six devices and error bars corresponding to standard deviation). The output curves show p-type enhancement mode operation (Figure 5-3 (a, a b, c, and d)). The transfer curves ($|I_d|$ versus V_d) in the saturation region (V_d= -0.8 V) show ON-OFF ratios of ~10^2-10^3 between 0 and -1 V, in agreement with reports for other EGTs based on DPP-DTT (see Table 5-3 for details) [57]. The transconductance ($g_m = \partial I_d / \partial V_g$) depends on the device geometry, applied voltage, charge carrier mobility, and capacitance [180]. The transconductance versus V_g plots (Figure 5-3 (e, f, g, and h)) reveal that the highest value is shown by the PVA/W+Gl (0.7) gated device. This result can be ascribed to the high capacitance of this gating medium, which leads to large current modulation and a higher ON state current. The transfer curves in the linear region (V_d= -0.2 V) are shown in Fig. S3. Smoother transconductance curves were obtained at lower scan rates (10 mV s^{-1}, Figure S4). The gate current versus gate voltage plots

are shown in Figure S5. The leakage current was approximately three orders of magnitude smaller than the drain current. Patterning the semiconductor, gel electrolyte, or concentric source-drain electrodes is a possible strategy to decrease the gate leakage current [101, 181, 182]. The leakage current in our devices can be attributed to the unpatterned semiconductor layer, which has been spin coated all over the surface (1 cm×1 cm). In terms of the configuration of devices, it has been shown that the top gate configuration has higher gate leakage current with respect to the planar gate configuration [183].

The charge carrier density and mobility values were calculated using Eqs. (3) and (4). The values of transconductance and mobility are among the highest reported for state-of-the-art organic EGTs [57, 80, 151, 175, 184]. Specifically for EGTs based on DPP-DTT semiconductor, Zhang *et al.* [57] obtained mobility and ON-OFF ratio of 0.15 $cm^2\ V^{-1}\ s^{-1}$ and 3×10^2, respectively, using a NaCl solution as an electrolyte. Tong *et al.* [151] reported a mobility of 0.18 $cm^2\ V^{-1}\ s^{-1}$ and an ON-OFF ratio of 3×10^3 for EGTs based on DPP-DTT using deionized water as an electrolyte. PVA/W (0.5) gated transistors exhibited a lower drain current with respect to devices gated with glycerol-based hydrogel, which can be explained by the rapid dehydration of the hydrogel (note that the time interval between the assembly of the device and measurement was the same (20 min) for all devices). Devices based on PVA/W+Gl (0.7) hydrogels showed the best performance in terms of output current and transconductance owing to the high capacitance of the ion gating medium.

The capacitance values reported for MIM structures are related to the electrolyte/gold-electrode interface. However, in the transistor configuration, two electrical double layer capacitors are formed: one at the gate/electrolyte interface and the other at the semiconductor/electrolyte interface. As these two capacitors are in series, the total capacitance in the transistor configuration is given by : $C_{total} = \frac{1}{{}^{1}/_{C_{ch}} + {}^{1}/_{C_g}}$, where C_{ch} is the capacitance at the interface between the channel and the electrolyte and C_g is the capacitance at the interface between the electrolyte and the gate electrode [185]. In the transistor configuration, the drain current is directly proportional to C_{tot}. Thus, we cannot expect to observe a proportional relationship between the capacitance obtained from the MIM structure and drain current of the transistor.

We obtained the hysteresis width, that is, the gate voltage shift corresponding to the reference drain current in the forward and backward scans, according to Equation (5). Normally, the average value

between the maximum and minimum drain currents in the transfer curves (-2 mA for PVA/W (0.5) and -5mA for PVA/W+Gl(0.7)) is considered as the reference drain current to evaluate the hysteresis. The PVA/W (0.5)-gated devices had a larger hysteresis width (~0.3 V) than those gated with glycerol-containing gels (~0.1 V). The hysteretic behavior in EGTs is due to the slow movement of ions in the electrolyte to form an electric double layer at the gate/electrolyte and electrolyte/semiconductor interfaces. In ion gel or hydrogel electrolytes ions have lower conductivity (10^{-5}- 10^{-2} S/cm) compared to aqueous electrolytes (e.g., 0.01 M NaCl aqueous solution with 10^{-3} S/cm) [8]. The size of ions is another parameter affecting the hysteresis of EGTs. Larger ions have poor polarization efficiency and slower movement, which contribute to higher hysteresis [186]. In practical applications, electrolytes with higher ionic conductivity (aqueous electrolytes) and small ion size could have a significant effect on the reduction of hysteresis. In addition to the electrolyte properties, the characteristics of the semiconducting film, such as the morphology and thickness of the film, influence the hysteresis of EGTs [187]. The position and area of the gate electrode also determine the hysteresis; a larger gate electrode and closer position to the channel result in smaller hysteresis [188]. So, hysteresis is less pronounced in the top-gated configuration than in the side-gated configuration. We observed hysteresis for both the ion-gated and hydrogel-gated devices. However, the hysteresis for hydrogels without an anti-dehydrating agent was higher than that for glycerol-based hydrogels because of the high rate of water dehydration. The dried hydrogel can show poor polarization efficiency and slow migration of ions within the electrolyte to reach the electrolyte/semiconductor [189]. So, the higher hysteresis of the PVA/W (0.5) transistor is due to the instability and degradation in the performance of the device due to the dehydration of the hydrogel.

EGTs have two operating regimes for EGTs; electrostatic and electrochemical. In the electrostatic mode, the channel material is not permeable to ions, and by applying a gate voltage, ions accumulate at the interface of the semiconductor/electrolyte, and an electric double-layer forms at the interface. In the electrochemical mode, ions can permeate the bulk of the semiconductor, so doping can occur in three dimensions. Electrochemical doping leads to reversible electrochemical oxidation and reduction reactions [8].

To further investigate and understand the working mechanism of EGTs with ion-gel electrolytes, we performed cyclic voltammetry (CV). CV is widely used to investigate the redox properties of

materials (i.e., the redox potential and stability of redox states). Studying the interaction between the active material and the dopant agent reveals information about the doping mechanism. To investigate the electrochemical properties of semiconductors with semi-solid electrolytes, the metal/insulator (ion gel)/semiconductor (MIS) structure is an appropriate configuration instead of a conventional electrochemical cell. In the MIS structure, the organic semiconductor is in contact with a semi-solid electrolyte. Performing CV with this configuration revealed the redox properties of the semiconductor with the proposed electrolyte. In our experimental design, we first performed CV measurements using the MIM structure to study the electrochemical activity of the electrolyte in the applied potential range to eliminate interference. As expected, an almost capacitive behavior was observed for the MIM structure (Figure S6 a), indicating that there was no electron transfer between the ion gel electrolyte and the Au electrode; hence, the process was non-faradaic. However, in the case of the MIS structure (Figure S6 (b)), we observed an almost reversible faradaic peak at V=0.5 V. In the forward scan, the anodic current peak was 25 μA, whereas in the backward scan, the cathodic current peak reached only -5 μA. The anodic and cathodic currents are not equal, which is attributed to the fact that only a fraction of the molecules that were oxidized in the forward scan were then reduced during the reverse scan. Principally, faradaic processes are paralleled by the insertion of ions to the bulk of the active material; however, considering the large size of [EMIM][TFSI] ions and well-ordered morphology of DPP-DTT, we hypothesize that the redox process is confined at the interface of the electrolyte and semiconductor film. Based on the electrochemical and transistor characterizations, the coexistence of interface-confined electrochemical doping and electrostatic doping is proposed.

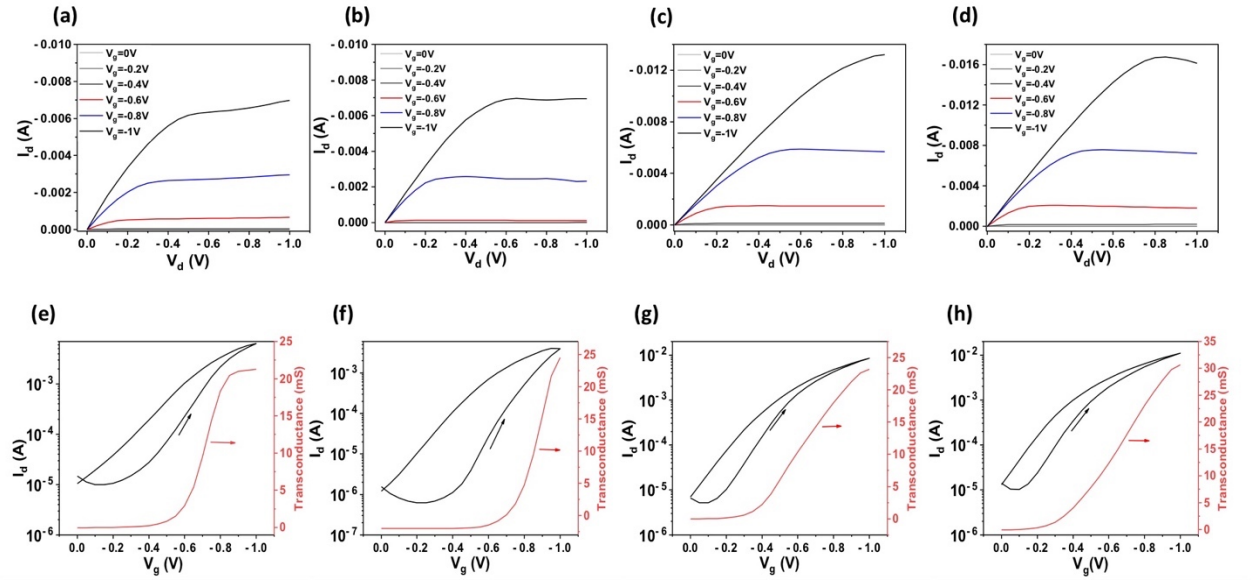

Figure 5-3 Output curves of PVDF-HFP/IL, PVA/W (0.5), PVA/W+Gl (0.5), and PVA/W+Gl (0.7) gated transistors (a, b, c, d) obtained at six different gate voltages (0 V<V_g< -1 V with interval of 0.2 V). Transfer curves (log scale) in the saturation region (V_d= -0.8 V) (right Y-axis represents transconductance (e, f, g, h). Scan rate is 50 mV s^{-1}.

Table 5-3 Figures of merit for ion gel and hydrogel-gated transistors. The charge carrier density and mobility values were obtained using Eqs. (3) and (4), respectively. The values were averaged for the six devices, and the errors represent standard deviations.

Gel	Charge carrier density (cm^{-2})	Mobility (cm^2 V^{-1} s^{-1})	ON-OFF ratio	Threshold voltage (v)	g_m (mS)	I_d (mA) at V_g = -1V, V_d= -0.2V	I_d (mA) at V_g = -1V, V_d= -0.8 V
PVDF-HFP/IL	2.2±0.1 E14	0.79 ±0.07	~5×10^2	-0.6±0.1	25±4	2.2±0.6	6.6±1.2
PVA/W (0.5)	4.8±0.6 E14	0.60±0.19	~4×10^3	-0.6±0.1	22±3	3.1±0.8	5.2±1.4
PVA/W+Gl (0.5)	5.1±0.3 E14	0.88±0.10	~8×10^3	-0.5±0.2	30±5	3.8±0.5	11.4±0.7
PVA/W+Gl (0.7)	5.6±0.5 E14	1.12±0.17	~7×10^3	-0.5±0.2	34±5	4.5±0.6	14.9±1.1

5.4.4 Electrochemical stability of ion-gating media

To study the effect of different gating media on the electrical stability of EGTs, we evaluated the electrochemical stability of the ion-gating media over time using EIS. As shown in Figure S7a, the Nyquist plots of the ion gel over two weeks did not change, and the real component of impedance at high frequency (Figure S7d), which correlates with ionic conductivity, did not change

significantly. For PVA/W (0.5), the value of Z_r at high frequency (and therefore the ionic conductivity) doubled after 30 min and increased by a factor of four after 60 min (Figure S7 b, e), likely due to water evaporation. For the glycerol-containing hydrogels (Figure S7 c, f), the Nyquist plots remained stable over two days, which shows that the incorporation of glycerol was efficient in increasing the water retention ability of the hydrogel. In 3rd day the Z_r value at a high frequency increased by two times. Accordingly, the ionic conductivity decreased by 2 times.

5.4.5 Electrical stability of EGTs based on ion gel and hydrogels

We evaluated the electrical stability of the ion gel and hydrogel-gated devices by measuring 20 consecutive transfer curves, sweeping V_g from 0 V to -1 V, and backward (Figure 5-4 **(**a-c)). The ion gel (PVDF-HFP/IL)-gated devices showed no significant changes in current, threshold voltage, and ON-OFF ratio over 20 cycles (Figure 5-4 (a)).

Devices based on PVA/W (0.5) hydrogels show a ~45 % decrease in drain current and a threshold voltage shift from -0.7 V to -0.8 V after 20 cycles (Figure 4b). For PVA/W+Gl (0.7) hydrogel, the current decreased only by ~5 %, with no significant change in threshold voltage (Figure 5-4 (c)). We further investigated the electrical stability (transient behavior) of the devices using square-wave pulse measurements varying V_g from 0 V to −0.8 V, with a pulse length of 5 s, at V_d = −0.2 V (Figure 5-4 (d-f)). After 65 ON-OFF cycles (~1000 s), the PVDF-HFP/IL gel gated devices maintained ~98 % of their drain current (Figure 5-4 (d)), whereas the PVA/W (0.5) gated devices exhibited a decline of ~50 % (Figure 5-4e). The devices gated with glycerol-containing hydrogels (Figure 5-4 (f), S8) maintained ~90 % of their initial current during 65 cycles. As DPP-DTT is stable in aqueous media, [57] the observed performance decrease is caused by the dehydration of the hydrogel. The fast dehydration of hydrogels without an anti-dehydrating agent is a weak point of these ion-gating media, which can be prevented, at least partially, by the addition of glycerol (normal boiling point of 290 °C). The effectiveness of glycerol in partially preventing dehydration was confirmed by measuring the normalized mass (m/m_0) (where m is the mass of the dehydrated hydrogel, and m_0 is its initial mass) versus time (Figure S9b). One hour after removal from the swelling solution, the hydrogel without glycerol lost ~45 % of its mass, whereas that containing glycerol only lost ~15 %. Optical images of freshly prepared hydrogels and 24 h after removal

from the swelling solution (Figure S9a, top and bottom) show that the PVA/W (0.5) hydrogel completely dehydrated after one day, while PVA/W+Gl (0.7) retained its structure. Magnified five cycles of pulse measurements in the time scale of 200-250 s are shown in Figure S10 to highlight the switching properties of the devices, which are mainly governed by ionic transport and time of electric double-layer formation [8]. Ion gel-gated transistor showed a slower switching speed with respect to the hydrogels, as highlighted by the transient curves (Figure S10a). For ion gel-gated devices, the drain current did not reach the steady state in either the ON or OFF states after 5 s of gate bias application. This indicates slow kinetics for the processes of electric double-layer formation as a consequence of the slow ion motion of bulky $[TFSI]^-$ ions. For hydrogel-gated transistors, the OFF current stabilizes after a 5 s pulse at V_g= 0 V, while a longer time (> 5 s) is needed to stabilize the ON current (Figure S10 b,c). The faster switching OFF time of hydrogel-gated devices is due to the smaller size of the $[Cl]^-$ ions and facile ion transport toward the gate electrode in the OFF state. The electrical stability of EGTs was evaluated over a longer time span. The ion gel-gated devices were stable for over two weeks without any significant change in the drain current (Figure S11a). Devices gated by PVA/W (0.5) showed a ~60 % decrease in the drain current within 1 h (Figure S11b). The addition of glycerol led to improved electrical stability, i.e., the drain current remained almost unchanged for 2 days and decreased by 40 % on 3rd day (Figure S11c).

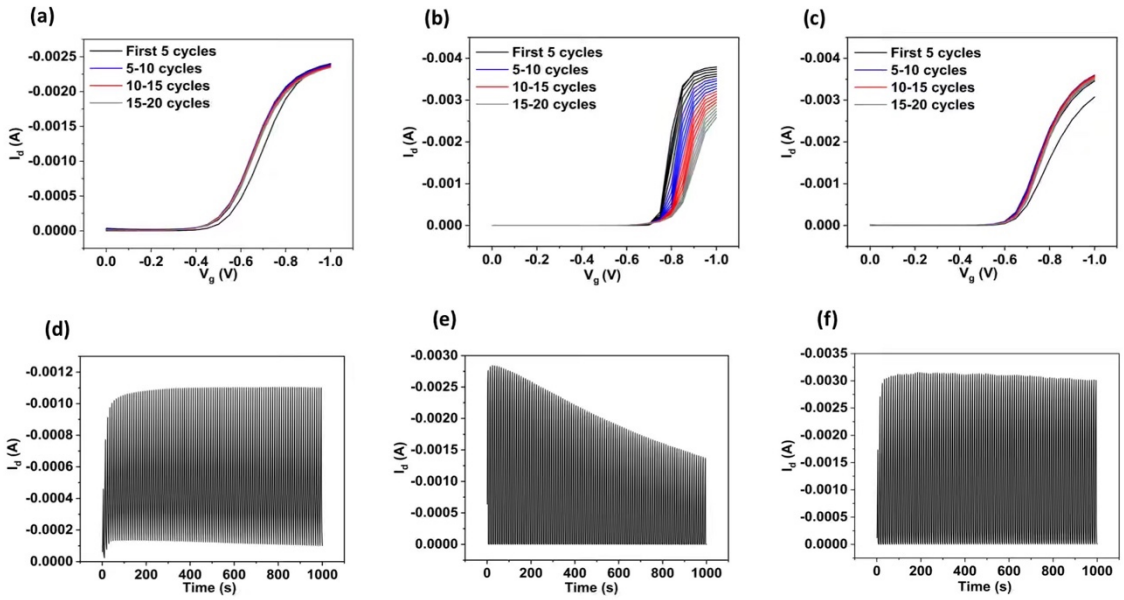

Figure 5-4 Sequence of 20 transfer curves (V_d =−0.2 V) for PVDF-HFP/IL, PVA/W (0.5) and PVA/W+Gl (0.7) gated transistor (a, b, c) (only forward scans are plotted for clarity); pulse measurements with V_d =−0.2 V and square pulse V_g varied from 0 to -0.8 V (pulse duration = 5 s) for PVDF-HFP/IL, PVA/W (0.5) and PVA/W+Gl (0.7) gated transistor (d,e, f).

5.4.6 Electrical characterization of EGTs in bent state

Gel electrolytes are of great interest for use in flexible electronic devices because of their superior mechanical properties compared to aqueous electrolytes. Semi-solid electrolytes, including ion gels, hydrogels, and polymer electrolytes, have been reported for applications in organic and inorganic flexible and stretchable EGTs [54, 96, 190, 191]. Recently, Kim *et al.* reported fully stretchable OECTs based on PEDOT-PSS, using printed hydrogels as the gating media [96]. Biodegradable and biocompatible ion gels have been utilized for flexible EGTs with an application for electrocardiogram recording [54]. Agarose based hydrogel have also been used to fabricate flexible pressure sensors with long-term stability and sensitivity in the low-pressure regime (for several hundred pascals) [156]. Therefore, electrical measurements were performed under bending to evaluate the mechanical stability of gel-gated EGTs. Flexible EGTs were fabricated on polyethylene terephthalate (PET). The flexibility of the devices was evaluated by measuring the transfer curves in the linear region (V_d= -0.2 V) in the bent states (Figure 5-5). Bending radius of 20 mm and 10 mm corresponds to tensile strain of ~0.9 % and ~0.45 %, respectively (where tensile

strain is defined as $\varepsilon = D/2R$, where D is the thickness of substrate (175 μm) and R is bending radius) [187]. As DPP based polymer is potentially applicable for stretchable devices [192], we assume that current changes during bending only depend on the gating media. PVDF-HFP/IL gated transistor showed a small change (less than 10 %) in the drain current upon bending (Figure 5-5 (a)). For PVA/W (0.5) gated devices, the transfer curves reveal a significant decrease (~50 %) in drain current in the bent state (R~10 mm) with respect to the flat state (Figure 5-5 (b)). The PVA/W+Gl (0.7) (Figure 5-5 (c)) EGTs showed a slight decrease in the drain current in bent states with respect to the PVA/W (0.5) gated devices. As the ion gel and PVA/W+Gl (0.7) gated transistors showed stable performance over time, the decrease in their drain current upon bending was mainly caused by mechanical effects. Since the time to perform the electrical characterization of devices in bent state is rather long (~40 minutes), in the case of PVA/W (0.5)-gated devices, the significant decrease in current in bent states is likely due to both mechanical effects and dehydration. The threshold voltage of ion gel-gated devices did not change significantly upon bending, while that of hydrogel-gated devices increased by ~30%. The increased stability of ion gel-gated devices upon bending can be explained by the stronger adhesion of the gating medium on the devices, as a result of its lower thickness and hydrophobicity. Figure 5-5 (d) illustrates the changes in the hole mobility of the transistors when changing from a flat to bent state. There was no significant change in the mobility of the PVDF-HFP/IL-gated transistors. PVA/W (0.5) and PVA/W+Gl (0.7) gated devices experienced ~50 % and ~10 % decreases in mobility values in bent state. These results suggest that DPP-DTT has reasonable flexibility, as reported elsewhere[193], and is a good candidate for other flexible electronic applications.

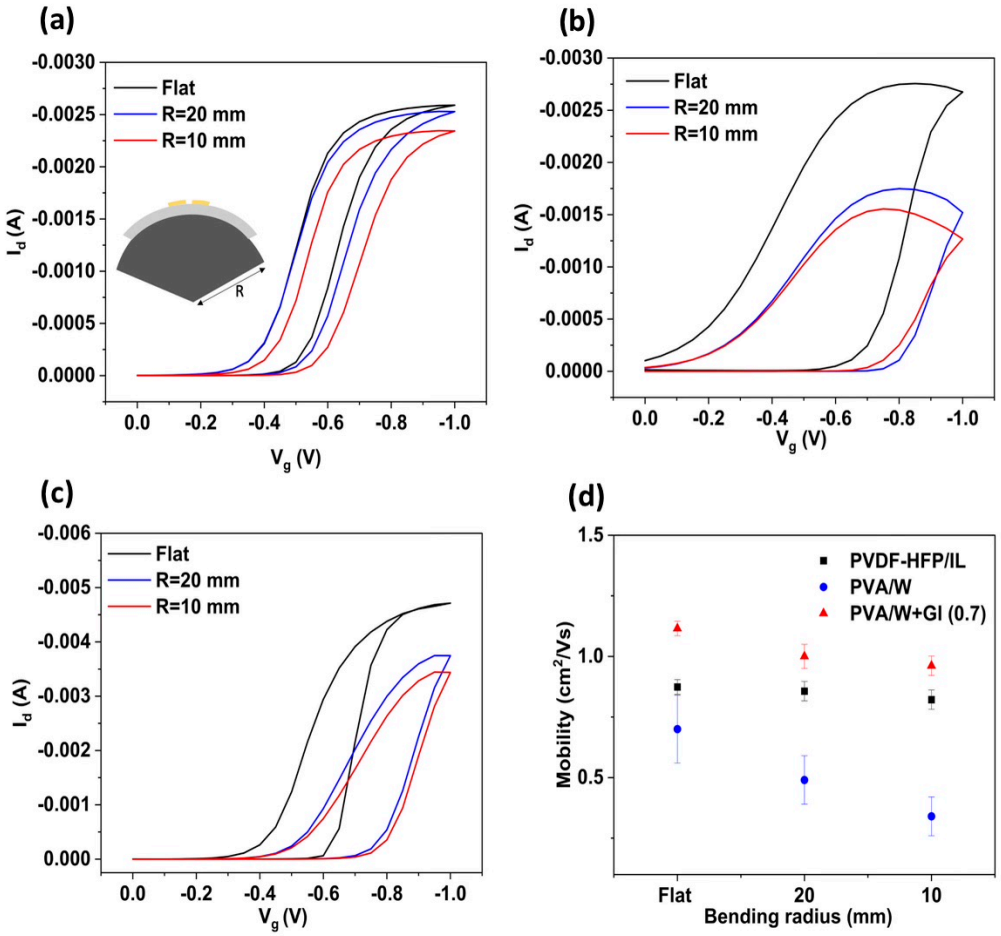

Figure 5-5 Transfer curves (V_d= -0.2 V) of PVDF-HFP/IL (inset is related to the scheme of bending) (a), PVA/W (0.5) (b), and PVA/W+Gl (0.7) (c) gated transistors in different bent states. Hole mobility of three different gel-gated transistors in bent and unbent conditions (error bars represent the standard deviation for three different samples).

5.5 Conclusions

In summary, we demonstrated EGTs based on a p-type ambient-stable DPP-DTT organic semiconductor using ion gels and hydrogels as gating media. Devices based on ion gels showed higher electrical stability than hydrogel-based devices and maintained 98 % of the initial current after 20 consecutive cycles. However, devices gated by hydrogels without an anti-dehydrating agent exhibited a 45 % decrease in drain current after 20 cycles owing to the dehydration of the hydrogel. The incorporation of glycerol into the hydrogel significantly improved its electrical stability and decreased the current by only 5 % after 20 cycles. We tested the electrical stability of

the devices over a long period of time, and the ion-gel-gated transistor showed stable operation within 2 weeks. The hydrogels without an anti-dehydrating agent showed the weakest performance, where the drain current decreased by 60 % after 1 h compared to the initial measurement. Glycerol-based hydrogels showed improved electrical stability, and the drain current was stable for 2 days. Flexible EGTs fabricated on PET substrates are also investigated. No significant changes were observed in the electrical characteristics of the ion-gel-based devices in the bent state, which was attributed to the physicochemical stability of the ion gel and its good adhesion to the substrate. We observed a significant drain current decline in the case of PVA/W(0.5) when compared to PVA/W+Gl (0.7), because the evaporation of water had a synergistic effect on the current drop in parallel with bending. Our results provide insights into the electrical stability of ion gel and hydrogel-gated devices. Moreover, these findings pave the way for realizing the compositional formulation of non-volatile and environmentally friendly electrolytes for use as gating media in electrolyte-gated devices.

5.6 Author Contributions

Mona Azimi: Formal analysis; investigation; methodology; writing original draft. Arunprabaharan Subramanian: Formal analysis; validation; review and editing. Francesca Soavi: writing –review and editing. Jiaxin Fan: Formal analysis; investigation during the revision process. Fabio Cicoira: Conceptualization; data curation; funding acquisition; project administration; resources; supervision; validation; writing, review and editing.

5.7 Acknowledgements

This work was supported by the Natural Sciences and Engineering Research Council of Canada (NSERC) through a discovery grant, and by Defence Research and Development Canada through an IDEaS Micronet (CFPMN1-008) awarded to the FC. MA and AS are grateful for the financial support from the Institut de l'Energie Trottier for the PhD scholarship. JF acknowledges NSERC for a postdoctoral fellowship. This work was supported by CMC Microsystems through the MNT program.

CHAPTER 6 ARTICLE 3 : EFFECT OF IONIC CONDUCTIVITY OF ELECTROLYTE ON PRINTED PLANAR AND VERTICAL ORGANIC ELECTROCHEMICAL TRANSISTORS

Mona Azimi[1], Chi-hyeong Kim[1], Jiaxin Fan[1], Fabio Cicoira[1*]

[1] Department of Chemical Engineering, Polytechnique Montréal, Montreal, Quebec, Canada

Faraday Discussions, Submitted 11 March 2023, Published 06 April 2023

[*] Corresponding Author: fabio.cicoira@polymtl.ca

6.1 Abstract

Conducting polymers with mixed electronic/ionic transport are attracting a great deal of interest for their application in organic electrochemical transistors (OECTs). Ions play a crucial role in OECT performance. The concentration and mobility of ions in the electrolyte influence the current flow in the OECT and its transconductance. This study examines the electrochemical properties and ionic conductivity of two semi-solid electrolytes, ion gels, and organogels, with diverse ionic species and properties, as determined by electrochemical impedance spectroscopy (EIS). Our results indicate that the organogels exhibited higher ionic conductivities than the ion gels. Furthermore, the geometry of OECTs plays an important role in determining their transconductance. Thus, this study employs a novel approach for fabricating vertical-configuration OECTs with significantly shorter channel lengths than those of their planar counterparts. This is achieved through a printing method that offers advantages, such as design versatility, scalability, expedited production time, and reduced cost relative to traditional microfabrication methods. The transconductance values obtained for the vertical OECTs were significantly (approximately 50 times) higher than those of the planar devices because of their shorter channel lengths. Finally, the impact of different electrolytes on the performance of both planar and vertical OECTs was studied, and devices gated by organogels demonstrated improved transconductance and switching speed (almost two times higher) than those gated by ion gels.

6.2 Introduction

Organic electrochemical transistors (OECTs) are of great interest for numerous bioelectronic applications, such as the recording of electrophysiological signals and detection of analytes [194-198], because of their low operating voltages and stability in aqueous media. In OECTs, the current is modulated via doping or de-doping of the bulk channel material with the electrolyte ions. This property makes these devices effective as ion-electron transducers. Poly(3,4-ethylenedioxythiophene) polystyrene sulfonate (PEDOT:PSS) is a well-known active material for OECTs because it displays mixed ionic and electronic conductivity, self-healing, stretchability, electrochemical activity, and stability in aqueous environments over a wide pH range, which is necessary for its application in biological systems [199-203].

Current modulation in OECTs based on PEDOT:PSS is achieved via the reversible reduction of PEDOT:PSS ($PEDOT^+PSS^-+M^++e^-\leftrightarrow PEDOT^0+PSS^-M^+$), which involves the diffusion of cations (M^+) provided by the electrolyte into the channel material upon application of a positive gate bias.

Transconductance is a key metric for OECTs because it measures the sensitivity of the device's output current to changes in the gate voltage. It is expressed as a derivative of the drain current with respect to gate voltage ($g_m = \partial I_d / \partial V_g$). The transconductance of OECTs depends on the device geometry (length, width, and thickness of the channel material) and active material properties [199], according to the following relationship*:*

$$g_m = \frac{wd}{l} \mu \, C^* \, (V_g - V_{th}) \qquad (1)$$

where *w, d,* and *l* are the channel width, thickness, and length, respectively*;* μ is the carrier mobility*;* C^* is the capacitance per unit volume of the channel*;* and V_g and V_{th} are the gate and threshold voltages, respectively [52]. Equations 1 is derived from Bernards model. This model describes the OECT channel as a combination of an electronic and an ionic circuit [51] and assumes that the contact resistance is much lower than the channel resistance and, hence, can be neglected. This model predicts a constant transconductance at low gate voltage (linear region). However, experimental data indicates a non-monotonic relationship between transconductance and gate voltage. To resolve this discrepancy, another model has been recently proposed to consider the contact resistance [204]. By comparing devices with low conductivity films, based on pristine

PEDOT:PSS, with highly conductive ones, based on PEDOT:SS and conductivity enhancers, the model showed that the contact resistance is the dominant factor (5-10 times larger than channel resistance) for highly conductive films.

The properties of the active material can be optimized by mixing PEDOT:PSS with ionic liquids, which leads to the formation of highly ordered PEDOT-rich domains, resulting in higher conductivity and transconductance [205, 206]. Because the transconductance is directly proportional to the channel width-to-length ratio, it can be enhanced by downscaling the channel length of the device [207]. The use of vertical OECTs represents an interesting approach to achieving this goal, in which the channel length corresponds to the thickness of the active channel material sandwiched between the vertically stacked source-drain electrodes. Conversely, downscaling the channel length of planar OECTs, that is, the distance between the source and drain electrodes, requires complex high-resolution photolithography procedures. Vertical OECTs with short channel lengths deliver a high transconductance and improved signal amplification. Most OECTs reported to date have planar structures, and there are few reports on vertical OECTs [16, 17, 94, 208].

The first reported vertical OECTs based on PEDOT:PSS were fabricated using both sides of a plastic or paper substrate [208]. Carbon paste was used to fabricate the top and bottom electrodes (source and drain, respectively) on both sides of the substrate. The fabrication was achieved by screen printing on polyethylene terephthalate (PET) and inkjet printing on paper. ON-OFF ratios of 4000 and 280 were obtained for the OECTs fabricated on PET and paper substrates, respectively. PEDOT:PSS vertical OECTs were also fabricated using photolithography [16]. The channel length was defined by the thickness (down to 450 nm) of the Parylene-C layer separating the vertical source and drain electrodes. These devices exhibited a transconductance of up to ~60 mS. Vertical OECTs based on PEDOT:PSS with nanoscale channel lengths (down to 100 nm) have been reported to mimic biological synapses [94]. Indium tin oxide (ITO) and silver nanowires were used as the drain and source electrodes, respectively, and transconductance values up to ~70 mS were obtained. Recently, electropolymerization has been used for the deposition of a PEDOT:PSS channel material on photolithographically patterned gold bottom electrodes, followed by gold deposition using a shadow mask as the top electrode [17]. Transconductances in the range of 30-275 mS were reported for these devices, depending on the channel length and width. Vertical

structures have also been reported with semiconducting active channel materials such as diketopyrrolopyrrole–terthiophene donor–acceptor polymer (PDPP) and poly(3-hexylthiophene) (P3HT) [92, 209]. Vertical OECTs based on p-type (gDPP-g2T) or n-type (Homo-gDPP) materials have also been used for complementary circuit applications with current densities of 1 kA cm^{-2} and transconductances of 200-400 mS [93].

The electrical characteristics of OECTs are significantly influenced by the electrolyte properties (i.e., ion size, ionic conductivity, and capacitance). High ionic conductivity improves the response time of the OECT, making it more suitable for high-frequency applications. Conversely, low ionic conductivity results in slower ion transport, leading to a reduced OECT performance. Therefore, optimizing the ionic conductivity of the electrolyte is crucial to enhance the performance of OECTs. The typical ranges of ionic conductivities for polyelectrolytes and gels are 10^{-4} -10^{-1} and 10^{-2}-10 mS cm^{-1}, respectively [8]. Larger ions exhibit slower motion and lower ionic conductivity because of the larger activation energy required for ion hopping [210]. Studies on the effect of the cation size (i.e., Li^+, Na^+, K^+, Cs^+) on the response time of OECTs based on PEDOT:PSS have shown that electrolytes with smaller cations lead to faster response times [211]. Recently, gel electrolytes have been extensively studied for OECTs owing to their advantages over traditional liquid and solid electrolytes. They exhibit a unique balance of ionic conductivity, mechanical stability, and the ability to maintain a stable interface with electrodes, making them ideal for OECTs [53, 96]. Additionally, they can be easily integrated with other materials and can conform to various shapes, making them suitable for flexible and stretchable devices [96, 102, 212]. The molecular weight of the polymeric matrix, its functional end groups, and temperature affect the ionic conductivity of the gel electrolytes [213]. The main categories of gel electrolytes are ion gels, which consist of mixtures of ionic liquids in polymeric matrices, and organogels, which consist of networks of hydrophilic polymer chains dissolved in a mixture of water and organic solvents (often acting as anti-dehydrating agents) [63].

In this study, we fabricated planar and vertical OECTs using a printed circuit board (PCB) printer. We printed all components (top, bottom, gate electrodes, and active channel material) of the devices. Vertical OECTs showed shorter response times and higher transconductance than planar structures because of the shorter channel lengths. To understand the effect of ionic conductivity on the performance of OECTs, we employed two types of electrolytes: ion gels and organogels. The

ionic conductivities of the electrolytes were measured by electrochemical impedance spectroscopy (EIS). OECTs with organogel electrolytes showed a faster response time with respect to the ion gel-gated devices, which was attributed to the higher ionic conductivity. This study contributes to the development of a new pathway for fabricating vertical OECTs by using a facile and cost-effective printing technique. More specifically, the utilization of different electrolytes with varying ionic conductivities broadens the knowledge of the effect of electrolytes on the performance of OECTs and offers great promise for fabricating OECTs with high transconductance and high switching speed.

6.3 Experimental

6.3.1 Materials

PEDOT:PSS (Clevios SV3 STAB) was purchased from Heraeus. The material has a viscosity of 1.5-6 Pa.s and a sheet resistance of 700 Ω sq^{-1} (as declared by the supplier). The SV3 ink contained propane-1,2-diol, 2-2'-oxydiethanol, and other additives at lower concentrations. Silver ink (Ag Paste 520 EI) was purchased from Chimet Spa. NaCl (≥99.5%), PVA with a molecular weight of 89000-98000 and PVDF-HFP with a molecular weight of 400,000 were purchased from Millipore Sigma. Dimethyl sulfoxide (DMSO) was purchased from Caledon Ltd. Sodium hypochlorite (NaClO) solution (5% w/v) was purchased from LabChem Inc. The ionic liquid ([EMIM][TFSI]) (viscosity of 39.4 mPa·s and ionic conductivity of 6.63 $mS \cdot cm^{-1}$) was supplied by IoLiTec. Soda-lime glass slides with a thickness of 1 mm were supplied by Corning (USA).

6.3.2 Fabrication of OECTs

OECTs were patterned on glass substrates using a PCB printer (Voltera V-One). Prior to printing, the glass substrates were sequentially sonicated in acetone, isopropyl alcohol (IPA), and deionized water for 15 min and dried with a stream of nitrogen gas. To further remove contaminants and increase the adhesion of the silver ink, it was exposed to UV ozone for 20 min. First, the Ag gate electrode was printed followed to heating at 130°C for 20 min on the built-in heating stage of the printer. Subsequently, to obtain a Ag/AgCl gate electrode, the silver gate electrode was chlorinated by exposing it to a 5 % NaClO solution and rinsed with deionized water for 10 min [96]. The use

of Ag/AgCl as a nonpolarizable electrode contributes to effective gating because of the minimized voltage drop at the gate/electrolyte interface [176]. Subsequently, for planar configuration, the source and drain electrodes were patterned and baked at 130°C for 20 min. After homogenizing the ink for 5 min using a planetary mixer (THINKY ARM-310), a PEDOT:PSS channel was patterned between the source and drain electrodes, followed by heating at 130°C for 30 min. For the vertical configuration, after chlorination of the gate electrode, the bottom electrode, PEDOT:PSS, and top electrode were printed and baked consecutively. Finally, ~50 µL of the ion gel or organogel electrolyte were applied to the OECTs by drop casting.

6.3.3 Preparation of ion gel and organogel electrolytes

The ion gel was prepared from a mixture of PVDF-HFP (acting as the polymer matrix), and an ionic liquid ([EMIM][TFSI]) in acetone. Acetone and PVDF-HFP were mixed in a sealed vial at a weight ratio of (1:15 w/w) and stirred for 2 h at 50 °C until complete dissolution. The ionic liquid (4:1 w/w) with respect to PVDF-HFP was added to the solution, which was stirred for 12 h at room temperature. The resulting solution was drop-casted onto the device and left for a few minutes under an ambient atmosphere to allow the evaporation of acetone.

The PVA-based organogel was prepared by dissolving PVA powder (10 wt %) in a mixture of water and DMSO (50 v/v%). First, PVA was dissolved in 20 mL of 0.1 M (NaCl) aqueous solution at 95 °C in an oil bath for 1 h. When the solution became transparent, 20 mL DMSO was added, and the solution was stirred for 1h. DMSO was added to the organogel formulation as an anti-dehydrating agent. Afterward, the viscous polymeric solution was drop-casted on the OECTs, and the devices were kept in a freezer (-15 °C) for 3 h to allow physical crosslinking of the polymer chains [214].

6.3.4 Electrochemical characterization of ion gel and organogel

Electrochemical impedance spectroscopy (EIS) of the electrolytes was performed using a VERSASTAT 4 (Princeton Applied Research) potentiostat and a Swagelok cell (purchased from the Beyond Battery Company). The cell contained two stainless-steel electrodes and a Teflon body filled with the testing electrolyte. The ion gel (thickness of ~ 1.5 mm) was cast inside the cell and kept under ambient conditions to allow the evaporation of acetone, after which the top stainless-

steel electrode was fixed. For the organogel electrolytes, after casting the solution (thickness ~ 1.5 mm), the cell was kept in a freezer (-15 °C) for 3 h to form the gel. EIS tests were performed using a two-electrode configuration, where one of the stainless steel electrodes acted as the working electrode and the other acted as both the counter and reference electrodes. The ionic conductivity (σ) of the gels was calculated using the following equation:

$$\sigma = \frac{1}{R_b} \cdot \frac{d}{S} \qquad (2)$$

where d (cm) is the thickness of the gel, S (cm^2) is the contact area between the electrode and electrolyte, and R_b is the bulk resistance (Ω), which is equal to the real impedance (Z_r) in the high-frequency region (10^5 Hz) [164].

6.3.5 Device characterization

Transistor characterization was conducted using an Agilent B1500A source-measure unit under ambient conditions. The transfer curves ($I_d - V_g$) were obtained at a constant drain voltage (V_d= -0.2 V). The gate voltage (V_g) was swept from -0.5 V to 1.5 V (with 10 mV/s steps) for ion gel electrolyte and from -0.5 to 0.8 V (with 10 mV/s steps) for organogel electrolytes. to avoid exceeding the electrochemical stability window of water. Output curves ($I_d - V_d$) were obtained by sweeping V_d from 0 V to -0.8 V with V_g changing from 0 to 1 V (with 0.2 V intervals) for the planar structure and from 0.4 to 1 V (with 0.2 V intervals) for the vertical structure. The transconductance is obtained from the first derivative of I_d with respect to V_g. The transient response of OECTs was obtained by applying square-wave pulses and varying V_g from 0 V to 1.5 V for the Ion gel and from 0 V to 0.8 V for the organogel, with a pulse length of 50 s, at constant V_d = −0.2 V. Cross-sectional images of the vertical structure were obtained using field-emission scanning electron microscopy (FE-SEM; JEOL, JSM-7500F).

6.4 Results and discussion

Figure 6-1 (a) shows the chemical compositions of the materials employed as electrolytes for OECTs. The ion gel is based on poly (vinylidene fluoride)-co-hexafluoropropylene (PVDF-HFP) and the ionic liquid ([EMIM][TFSI]). PVDF-HFP is a semi-crystalline hydrophobic copolymer with a high tensile strength and good thermal and chemical stability [215]. The organogel was

based on hydrophilic polyvinyl alcohol (PVA) as a matrix polymer, dissolved in an aqueous NaCl solution, and DMSO as an anti-dehydrating solvent. These semi-solid electrolytes have been utilized as gating media in our previous studies and have shown reasonable ambient stability and mechanical strength for flexible and stretchable devices [96, 102]. Schemes of planar and vertical OECTs are shown in Figure 6-1 (b,c). Optical images of the printed planar and vertical devices are shown in Figure S1. The color difference between the source/drain electrodes and the gate electrode is due to chlorination of the gate electrode. In the vertical structure, the source and drain electrodes were stacked perpendicularly and a PEDOT:PSS layer was printed between them. Cross-sectional scanning electron microscopy (SEM) images Figure 6-1 (d) of the vertical structure revealed a thickness of ~2 µm of the PEDOT:PSS layer sandwiched between silver source-drain electrodes. Energy dispersive X-ray (EDX) mapping (Figure S2) of Ag and S indicated that no significant contamination occurred between the Ag and PEDOT:PSS layers.

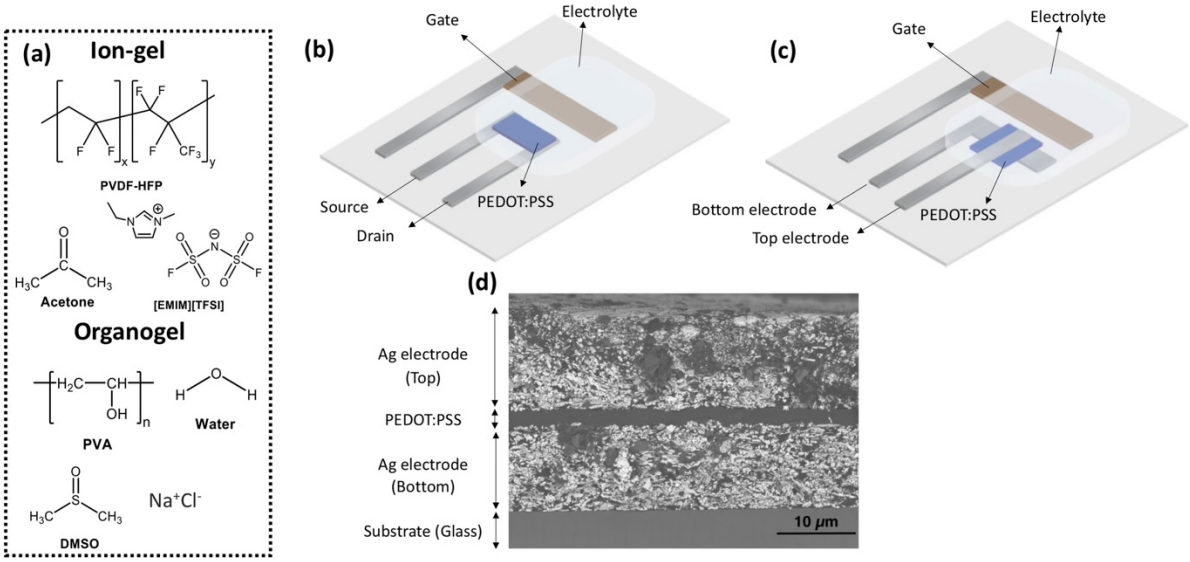

Figure 6-1 Molecular structures of the materials used for ion-gels and organogels (a), scheme of planar (b), and vertical OECT (c), SEM image of the cross-section of the vertical structure (d).

Solution processability allows the printing of PEDOT:PSS for different applications such as OECTs fabrication. Several printing techniques such as inkjet printing and screen printing have been employed for planar OECTs with channel lengths ranging from hundreds of microns to a few

millimeters [96, 216-219]. Obtaining a short channel length with a planar structure via printing is challenging and requires high-resolution patterning, whereas a vertical configuration allows channels in the range of a few microns without the need for complex fabrication procedures. The smallest reported channel length for printed planar OECTs is 118 μm, which results in a transconductance of approximately 30 mS [216]. The vertical OECTs reported to date have mostly been fabricated using microfabrication techniques. The device properties of recently reported vertical OECTs are summarized in Table 6-1. In this study, we used a printing method to pattern the electrodes (source, drain, and gate) and channel material of the vertical and planar structures.

Table 6-1. Reported figures of merit of OECTs in vertical configuration.

Channel material	**Electrode material**	**Fabrication method**	**Channel length**	**Electrolyte**	**g_m (mS)**	**ON-OFF ratio** **V_g, V_d**	**Ref**
PEDOT:PSS (SV3), Clevios P Jet HC	Carbon paste	Screen printing and Inkjet printing	100 nm	Poly quaternary imidazolium chloride	-	4000 (PET substrate) 280 (paper substrate) $0 < V_g < +1$ V or $0 < V_g < +1.5$ V $V_d = 1$ V	[208]
PEDOT:PSS (Clevios,PH1000)	Gold	Photolithography	450 nm - 1.4 µm	NaCl aqueous solution	20-57	$-2 < V_g < +0.6$ V $-0.6 < V_d < 0$ V	[16]
PEDOT:PSS (Clevios,PH1000)	ITO and silver nanowire	Spin coating of silver nanowires	150 nm	Ion gel (Polyacrylonitrile (PAN)/LiTFSI)	68	1000 $-0.4 < V_g < +0.8$ V $V_d = -0.5$ V	[94]
PEDOT:PSS	Gold	Photolithography and electropolymerization	210 nm	NaCl aqueous solution	30-275	$-0.6 < V_g < +1$ V $-0.6 < V_d < 0$ V	[17]
Diketopyrrolopyrrole –terthiophene (PDPP)	Gold	Electron-beam lithography	40 nm	Ionic liquid ([EMIM][TFSI])	11.7	10^8 $-1.2 < V_g < -0.6$ V $-0.6 < V_d < 0$ V	[92]
Poly(3-hexylthiophene (P3HT)	ITO and silver	Thermal evaporation by shadow mask	300 nm	Polymer electrolyte (PMMA, PEO, $LiCF3SO_3$)	1	10^4 $-6 < V_g < +6$ V $-1 < V_d < 0$ V	[209]
p-type (gDPP-g2T) and n-type (Homo-gDPP)	Gold	Thermal evaporation and photopatterning	100 nm	PBS	200-400	10^6 $-0.4 < V_g < +0.2$ V (p-type) $0 < V_g < +0.6$ V (n-type) $-0.5 < V_d < -0.1$ V (p-type) $0.1 < V_d < +0.5$ V (n-type)	[93]
PEDOT:PSS (SV3)	Silver ink	PCB printer	~2 µm	Ion gel and organogel	50-130	6×10^3 (ion gel) 2×10^2 (organogel) $-0.5 < V_g < +1.5$ V (ion gel) $-0.5 < V_g < +0.8$ V (organogel) $-0.8 < V_d < 0$ V	This work

6.4.1 Electrochemical characterization of electrolytes

The electrochemical properties of the electrolytes were studied in a stainless-steel Swagelok cell (inset of Figure 6-2 (a)). The tilted straight line of the Nyquist plots (imaginary impedance, Z_i, versus real impedance, Z_r, Figure 6-2 (a)) indicates the typical behavior of an electrolyte in contact with a solid electrode. At high frequencies, the Nyquist plots do not show a semicircular region (Figure 6-2 (b)), which indicate a non-faradaic process and negligible interfacial resistance at gel/electrode interface [170]. The value of Z_r at high frequencies is related to the total ionic and electronic resistance. The ion gel showed higher resistance than the organogel. The ionic conductivities, calculated using equation (2), were 0.7 ±0.1 mS cm^{-1} and 2.4 ±0.2 mS cm^{-1} for the ion gel and organogel, respectively (error bars represent standard deviation obtained from three samples). The ionic conductivity of the ion gel is comparable to previously reported values [102]. The lower ionic conductivity of the ion gel can be correlated with the larger ion size. The size of $[EMIM]^+$ in ion gel is 8 Å, whereas the size of Na^+ is 1 Å and 2.3 Å in the non-hydrated and hydrated forms, respectively. Figure 6-2 (c) shows the total impedance of the electrolytes versus frequency (1- 10^5 Hz). The impedance of the organogel was four times lower than that of the ion gel. The lower impedance of the organogel reflected a higher capacitance, which correlated with the differences in the ion sizes of these electrolytes.

Larger ions have a lower charge density, which means they interact less strongly with the charged surface and are less likely to be adsorbed in the Stern layer, leading to lower capacitance [220, 221]. As shown in Figure 6-2 (d), for both the ion gel and organogel, the phase angle at low frequencies reached values higher than 45°, indicating their capacitive behavior (a phase angle of 90° corresponds to an ideal capacitive behavior). The Inset of Figure S3a shows the equivalent circuit model for our system, which consists of a resistor and constant phase element (CPE). The ionic and electronic contributions are included in the resistance. CPE represents the electric double layer, and α is related to the electrolyte behavior (α=1 corresponds to purely capacitive behavior). The modelled and obtained data were well matched by comparing the experimental data and equivalent circuit models (Figure S3, fitting parameters listed in Table S2). The ion gel has a higher resistance than the organogel, which is attributed to the larger ion size. The organogel showed a higher CPE value than that of the ion gel. Several factors contribute to the capacitance, including the electrode surface area, size and concentration of ions in the electrolyte, and dielectric constant.

The capacitance of the double layer depends on the amount of charge stored at the interface. Ions with a smaller ionic radius can pack more closely together at the interface, resulting in a greater concentration of charges and a higher capacitance [221]. In addition, the presence of water in the organogel formulation facilitates ion motion in the electrolyte. All these factors contribute to the higher ionic conductivity and capacitance of the organogel compared to those of the Ion gel.

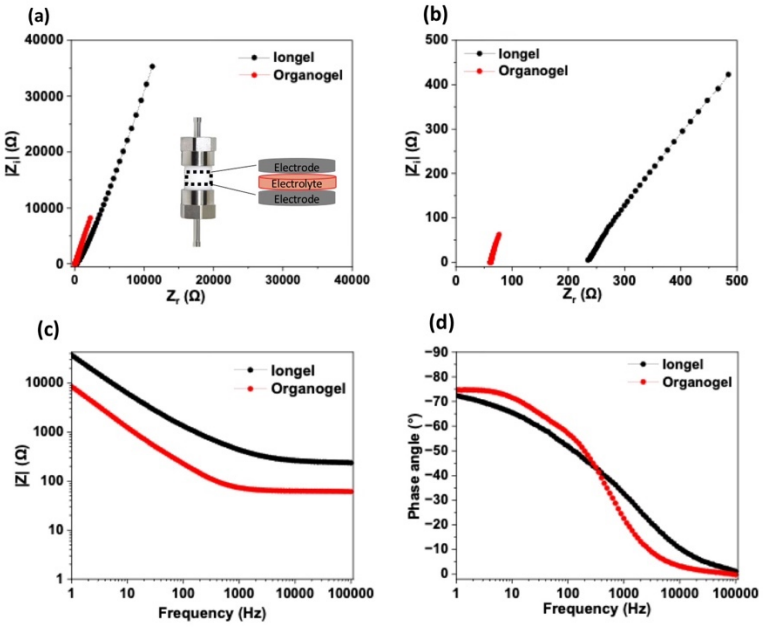

Figure 6-2 Nyquist plot for ion gels and organogels (inset is a Swagelok cell setup with two electrodes for electrochemical characterization of electrolytes (a), magnified Nyquist plots at high frequency (b), Bode plot (impedance versus frequency) (c), and Bode plot (phase angle versus frequency) for ion gels and organogels (d). EIS measurements were repeated for the three samples.

6.4.2 Electrical characterization of planar OECTs

Electrical characterization of the planar OECTs was performed using the two electrolytes. The output and transfer curves of OECTs with the ion gel electrolyte and organogel are shown in Figure 6-3 (a, b) and Figure 6-3 (c, d). The transfer curves for the two additional samples are shown in Figure S4. According to the output curves, the magnitude of the drain current (I_d) decreases with an increase in the gate voltage (V_g) arising from the de-doping of PEDOT:PSS upon the injection of cations, indicating that these devices operate in the depletion regime. The drain current increases

with an increase in the drain voltage in the linear regime and saturates with further increases owing to the channel pinch-OFF. The output curves of OECTs with the two types of electrolytes (Figure 6-3 (a,c)) show a clear difference in the modulation behavior. ON-OFF ratios of ~ 2×10^4 and 10^2 were obtained for the ion gel and organogel-gated devices, respectively. The broad electrochemical stability window of the ionic liquid permits the application of a higher gate voltage (1.5 V) compared to organogels (0.8 V), which leads to a lower OFF current. The transconductance curves (right Y-axis of Figure 6-3 (b,d)) show a typical bell-shaped dependence on V_g. The transconductance of organogel-gated devices is 2.6±0.6 mS, while that of ion gel-gated ones is 1.5±0.1 mS (error bars represent standard deviation obtained from three samples). The normalized values of transconductance with respect to the width of device (W=1 mm) are 2.6±0.6 S m^{-1} and 1.5±0.1 S m^{-1} for organogel and ion gel-gated devices, respectively. Organogel-gated OECTs exhibit a lower operating voltage than ion gel-gated ones. According to the transfer curves (Figure 6-3 (b, d)) the OFF-state was achieved at V_g =1.5 V for the ion gel-gated OECTs and at V_g =0.8 V for the organogel-gated ones. The lower operating voltage of organogel-gated OECTs compared to those gated by ion gel can be correlated with several factors, including the ion size, nature of the electrolyte (hydrophilicity or hydrophobicity), and capacitance of the electrolyte. The smaller ion size and higher capacitance of the organogel compared to the ion gel leads to a larger amount of charge storage at the channel material/electrolyte interface, and consequently, lowers the operating voltage.

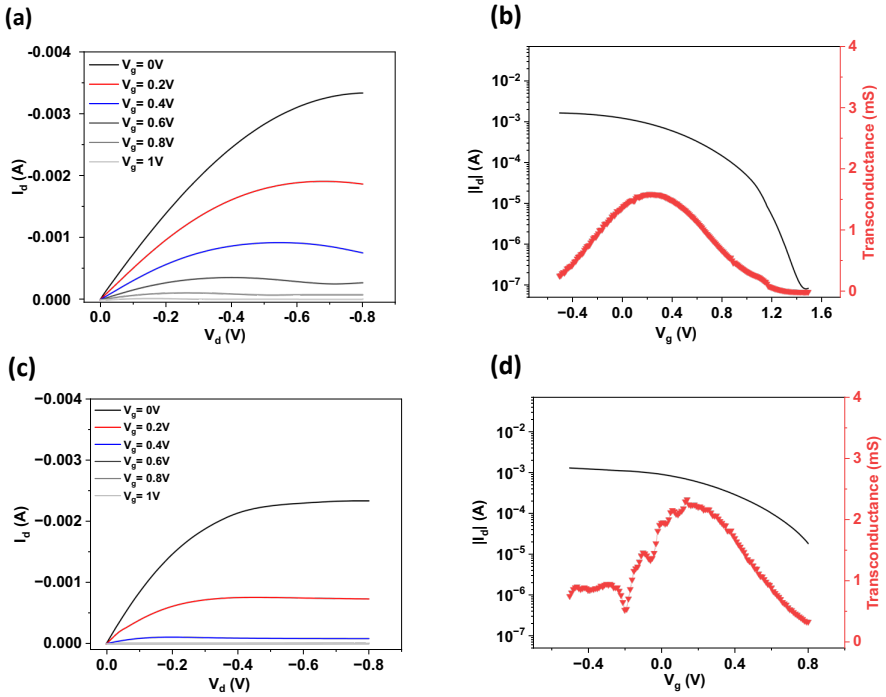

Figure 6-3 Output and transfer characteristics (V_d= -0.2 V) of planar OECTs using ion gel (a,b) and organogel (c,d) as the electrolyte. (Electrical characterizations were repeated on three devices.)

6.4.3 Electrical characterization of vertical OECTs

The output and transfer characteristics of vertical OECTs using ion gel and organogel were obtained in the same range of V_d and V_g as those of the planar devices (Figure 6-4 (a,b) and (c,d)). The transfer curves of the two additional samples are shown in Figure S5. As expected, the ON-state current for vertical OECTs was higher than that for planar ones, due of the shorter distance between the electrodes. Transconductance values of 60±10 mS for ion gels and 110±25 mS for the organogels were obtained (error bars represent standard deviation computed based on three samples). The normalized values of transconductance with respect to width of device (W=2 mm) is 30±5 S m^{-1} and 55±12 S m^{-1} for organogel and ion gel-gated devices, respectively. As for planar devices, vertical organogel-gated devices exhibit higher transconductance, which is attributed to the higher ionic conductivity of the organogel. A high transconductance means that a small change in the gate voltage can produce a large change in the output current, which is desirable for many applications, such as sensing and amplification. In vertical structures, the reduced channel length

increases the charge carrier concentration, resulting in a higher drain current for a given gate voltage as well as a higher transconductance. A high transconductance indicates a large change in drain current for a small change in gate voltage, making the vertical OECTs more sensitive to changes in gate voltage. The ON-OFF ratios were ~6×10^3 for the ion gel and ~2×10^2 for organogel-gated devices. The OFF current of the vertical OECTs was higher than that of the planar ones, in accordance with previously reported observations [94]. A shorter channel length results in a lower electrical resistance across the channel, which further increases the OFF current. In general, reducing the channel length is a trade-off between a higher OFF current and improved device performance, such as a higher transconductance and faster switching speed. In the vertical structure, part of the active material is covered by the top electrode, which may hinder close coupling with the electrolyte. However, vertical structures with short channel lengths can deliver high transconductance, leading to an enhanced amplification of biological signals. A possible method to reduce the screening of the active material by the top electrode is to reduce the width of the top electrode or to use the step-edge vertical configuration proposed by Malliaras et al., where the active channel is not covered by the top electrode [16].

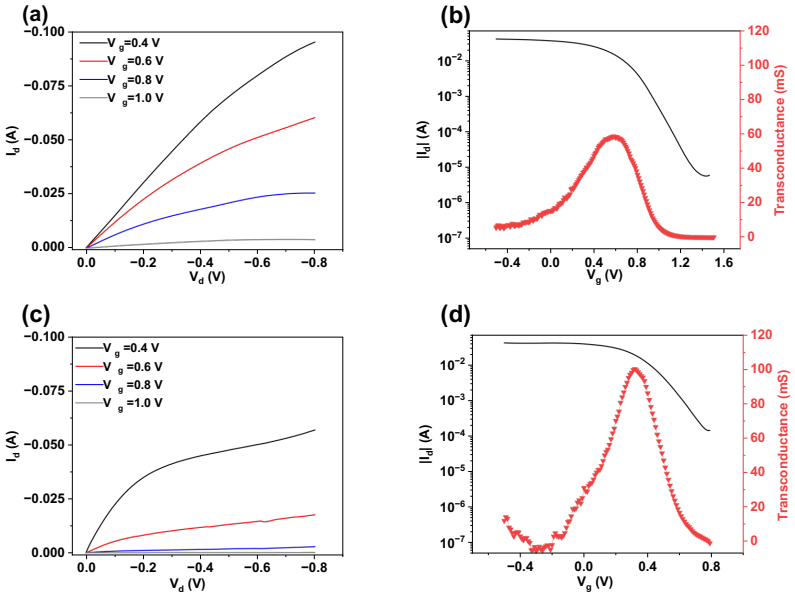

Figure 6-4 Output and transfer curves (V_d= -0.2 V) of the vertical structure using ion gels (a,b), and output and transfer curves (V_d= -0.2 V) of the vertical structure using an organogels as the electrolyte (Electrical characterizations were repeated on three devices.).

6.4.4 Transient behaviour of planar and vertical OECTs

To study the switching behavior of OECTs, we measured the transient response of both vertical and planar devices with the two electrolytes (Figure 6-5). Square-wave pulses were applied at a constant $V_d = -0.2$ V, varying V_g from 0 V to 1.5 V for the ion gel and from 0 V to 0.8 V for the organogel with a pulse length of 50 s. By applying a positive voltage to the gate electrode in pulse measurements, the channel material is reduced to its OFF-state, whereas by setting V_g back to 0 V, the channel material is re-oxidized to its conductive state. The transient responses were fitted using monolithic rise and decay models based on the following equation:

$$I_d = I_1 \exp(t/\tau) + I_0 \qquad (3)$$

where I_d is the drain current, I_1 is the current coefficient for fitting, t is the time, τ is the time constant, and I_0 is the initial drain current. The time constants indicate the speeds of the doping and de-doping processes in the channel material. The transient response of OECTs depends on various factors, including device dimensions (channel length and channel width) and electrolyte properties. In a vertical structure, the short channel length reduces the transport distance of charge carriers and results in higher electric field within the channel. Enhanced electric field leads to faster charge carrier and ions drift velocities. These effects contribute to a faster device transient response. Although ions must penetrate from the sides of the active channel material in vertical OECTs, which may impede ion transportation, both our results and previously reported finding suggest that vertical structures have a faster response than planar structures [94]. As also observed by Huang et al., through varying the channel length of vertical OECTs based on p-type gDPP-g2T and n-type homo-gDPP, the transient response time is faster for shorter channel length [93]. Thus, shortening the channel length has significant impact on achieving fast switching. The size of the ions in an electrolyte can affect the switching time of OECTs. In general, smaller ions tend to diffuse faster through the electrolyte and reach the OECT active layer, resulting in faster switching times. The mobility of ions in the electrolyte affects the switching time of OECTs. Ions with smaller sizes have a higher mobility, allowing them to move more easily through the electrolyte and reach the active layer. Ion mobility is also influenced by the viscosity of the electrolyte; lower viscosity allows for faster ion transport [222]. The response times of the vertical and planar OECTs using these two types of electrolytes are summarized in Table 6-2. The values of the response time

obtained were higher than those of previously reported vertical OECTs. This is correlated with the relatively higher thickness (~ 2 µm) of the PEDOT:PSS layer in our OECTs. In previously reported vertical OECTs, spin coating or electropolymerization methods were employed for the deposition of the PEDOT:PSS layer, which resulted in lower thicknesses (in the range of hundreds of nanometers) and shorter response times [16, 17]. In addition, the drain-current response time is asymmetric for the injection and extraction of cations. The drain response to cation extraction (OFF-ON state) was slower than that to cation injection (ON-OFF state). However, the origin of this asymmetry is not well understood. Some studies have correlated the response time asymmetry of OECTs with the presence of a dissipation process, such as a viscoelastic element within the conducting path across the channel. The development of this pathway can be caused by various processes, such as relaxation of the intrachain arrangement during the doping and de-doping processes, which affect the hole mobility [211]. In general, our findings indicate that vertical OECTs exhibit a response time four times shorter than that of their planar counterparts. Moreover, when comparing OECTs with different gating media for each configuration, those gated by the organogel exhibited shorter response times. The response time of devices with an ion gel is twice as high as that of organogel-gated devices. The longer response time of OECTs using ion gel can be attributed to factors such as larger ion size and lower ionic conductivity.

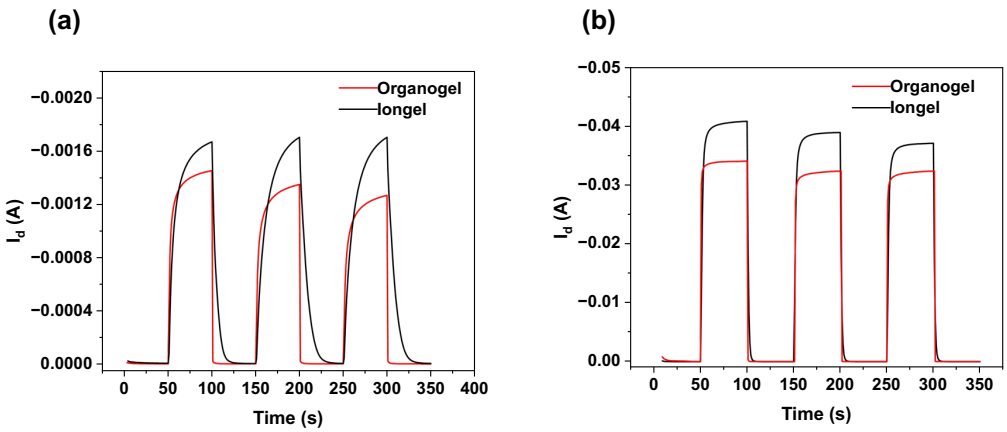

Figure 6-5 Transient response of planar (a) and vertical (b) using Ion gel and organogel electrolytes (V_g was pulsed from 0 V to 1.5 V for the ion gel and from 0 V to 0.8 V for the organogel).

Table 6-2. Response times of planar and vertical OECTs using organogels and ion gel electrolytes (error bars are related to response times obtained from three cycles of transient curves).

Device		**τ_{OFF-ON} (s)**	**τ_{ON-OFF} (s)**
Planar	Ion gel	7.32 ± 1.12	5.02 ± 1.22
	Organogel	4.04 ± 0.60	2.31 ± 0.65
Vertical	Ion gel	2.08 ± 0.53	1.19 ± 0.38
	Organogel	1.57 ± 0.48	0.55 ± 0.10

As vertical OECTs with organogel electrolytes have shown superior transconductance and faster response times than other devices, we conducted a long-term stability test on this device (Figure S6). We evaluated the long-term stability by plotting the transfer curves (V_d= -0.2 V) for 18 days after fabrication and storing the device under ambient conditions. As shown in Figure S6a, the device performance was almost stable until 10 d after fabrication. However, after 10 d, the OFF current began to increase, and by 18 d, the device lost its modulation property. This phenomenon can be attributed to the dehydration of the organogel over time. We believe that the introduced organogel demonstrated improved stability compared with previously reported gels [102]. We also investigated the stability of organogel-gated vertical OECTs during 10,000 s of pulse cycling (Figure S6b). Remarkably, even after approximately 65 ON-OFF cycles, the ON current decreased by only 25% compared to its initial value. We hypothesize that this is likely due to the trapping of cations in the bulk of the channel material during several cycles (doping and de-doping) of OECTs or the degradation of PEDOT:PSS over repetitive ion injection and extraction [48, 223]. These effects can lead to a lower channel conductivity and, thus, a lower ON-current.

6.5 Conclusions

We investigated the effect of different types of electrolytes on the performance of printed organic electrochemical transistors (OECTs) based on PEDOT:PSS. The organogel exhibited four times

higher ionic conductivity and capacitance than those of the ion gel. A printing technique was used to fabricate all components of OECTs (except the electrolyte) and novel vertical-structure OECTs. Printing is a promising technique for the fabrication of organic electronic devices because it is compatible with various materials and substrates and provides fast prototyping for large-scale production. The vertical OECTs showed approximately 50 times higher transconductance than the planar ones because of the shorter channel length. OECTs using the organogel electrolyte showed a higher transconductance value for both the vertical and planar structures because of their higher ionic conductivity. Furthermore, OECTs using organogels as electrolytes showed a response time that was two times faster than that of the ion gel-gated devices for both configurations. A comparison of the response times of the vertical and planar OECTs revealed an almost four-times faster response for the vertical configuration than for the planar configuration. In conclusion, our study demonstrates the importance of selecting an appropriate electrolyte for OECTs and highlights the potential of printing techniques and novel vertical device architectures for the development of high-performance organic electronic devices.

6.6 Acknowledgements

This work was supported by the Natural Sciences and Engineering Research Council of Canada (NSERC) through a Discovery Grant (RGPIN-2017-06319) and a Defence Research and Development Canada Grant (IDEaS Micronet CFPMN1-008) awarded to FC. MA is grateful for financial support from the Institut de l'Energie Trottier for the PhD scholarship. JF acknowledges NSERC for a postdoctoral fellowship. This work was supported by CMC Microsystems through the MNT program.

CHAPTER 7 GENERAL DISCUSSION

Transistors that employ organic semiconductors and utilize electrolytes as a gating medium have garnered significant interest in recent years due to their potential to operate at low voltages while inducing high carrier densities in the active channel material. The underlying mechanism responsible for this behavior is attributed to the formation of an electrical double layer at the interface of the active channel material and the electrolyte. The double layer, consisting of a compact layer and a diffuse layer, acts as a capacitor with a large specific capacitance of tens of microfarads per square centimeter [102, 154]. The electric double layer capacitance is defined as:

$$C = \varepsilon_r \varepsilon_0 \frac{A}{\lambda} \qquad (1)$$

Where λ is the thickness of the electric double layer, A is the area of electrolyte and $\varepsilon_r, \varepsilon_0$ are relative and vacuum permittivities, respectively. According to Equation (1), capacitance depends on the thickness of the electric double layer. The electric double layer's thickness typically ranges from a few nanometers, which is much thinner than the conventional dielectric used in FETs. As a result, this leads to an increased capacitance. With a high capacitance, the transistor can store a larger amount of charge for a given voltage. Consequently, a smaller voltage applied to the gate can achieve the desired charge accumulation in the electric double layer, effectively controlling the conductivity of the transistor channel. In contrast, OFETs typically require higher voltages to operate as their specific capacitance is much lower, usually in the range of tens of nanofarads per square centimeter for example the capacitance of 300 nm SiO_2 dielectric is 11 $nF.cm^{-2}$ [103]. These advantageous features of EGTs make them well-suited for a diverse range of advanced technology applications, such as sensors, neuromorphic, and memory devices [224-226]. The lower operating voltage of EGTs results in reduced power consumption, which, in turn, extends the life cycle of the devices without the need for frequent power supply replacements.

This thesis explores the electrochemical and charge carrier transport properties of p-type organic semiconductors, specifically PCDTPT and DPP-DTT, which were utilized as channel materials in this study. EGTs based on these semiconductors operate in accumulation mode, and the application of a negative gate voltage leads to the accumulation of anions at the interface of the semiconductor and electrolyte. P-type semiconductors generally exhibit greater stability than their n-type counterparts, as excess electrons in n-type semiconductors are susceptible to reacting with oxygen

or other oxidizing agents, leading to the formation of electron traps or defect states that can compromise the material's stability [227]. To attain satisfactory performance in EGTs (i.e., low operating voltage (<1 V), high transconductance (in the range of tens of mS), reliable operational stability over long time and mechanical stability), each component of the device, including the active channel material, contact electrodes, and electrolyte, must be meticulously optimized to align with the intended target applications of these devices.

We also investigated OECTs operating in depletion mode, which utilized the organic conducting material PEDOT:PSS as the channel material. PEDOT:PSS has demonstrated excellent performance in biological environments, owing to its stability in aqueous media. PEDOT exhibits high electro-optical and electrical properties, and PEDOT:PSS, in particular, is renowned for its water-dispersibility. This is due to the use of PSS as a dopant, which facilitates the formation of gel-like particles with PSS shells, enabling stable aqueous dispersions [49]. The solution processability of PEDOT:PSS makes it to be compatible with different printing technologies including screen printing, spray printing, aerosol-jet printing, and inkjet printing [84].

The first specific objective of this study was to examine the light sensing capabilities of EGTs. Therefore, the selection of an active channel material with a suitable bandgap is crucial. The bandgap of the material determines the energy level of photons that it can absorb, and it needs to align with the desired range of light wavelengths for the intended application. Various materials possess different bandgap energies, enabling the selection of materials that are sensitive to specific regions of the electromagnetic spectrum. For instance, PCDTPT exhibits a prominent absorption peak at approximately 890 nm, making it a material sensitive to near-infrared light [13]. By leveraging the unique optical absorption properties of the semiconducting material, we conducted electrical measurements in both dark and light environments, enabling us to comprehensively assess the efficacy of ion-gating under varying conditions. we utilized a liquid electrolyte, specifically an ionic liquid, as the ion gating medium for EGTs based on PCDTPT. It should be noted that liquid electrolytes have a higher susceptibility to leakage. This can happen when the device is bent or exposed to mechanical stress, thereby compromising the overall integrity of the device. Consequently, this leakage can potentially result in performance degradation, characterized by a decrease in drain current and the mobility of charge carriers.

Considering the limitations of liquid electrolytes for flexible EGTs we aimed to use semi-solid gel electrolytes in the second part of our study. Clearly, finding appropriate formulation and processing technique of semi-solid gel electrolytes is challenging. The formulation of semi-solid gel electrolytes requires selecting suitable components that can provide the desired ionic conductivity, stability, and compatibility with the device. It involves choosing the right combination of solid and liquid components, such as polymer binders, electrolyte salts, and solvents, to achieve the desired ion transport characteristics. Moreover, Electrolytes are susceptible to various degradation mechanisms, such as electrochemical reactions, evaporation, and contamination, which can result in changes in the transistor's electrical characteristics over time. Understanding and mitigating these degradation mechanisms are crucial to ensuring the stable operation of EGTs in real-world applications. Since DPP-DTT is stable in aqueous media we aimed to use both hydrophilic (hydrogel) and hydrophobic (ion gel) electrolytes for devices. Ion gels consisting of PVF-HFP and [EMIM][TFSI] were utilized, as well as hydrogel electrolytes composed of PVA and NaCl as ionic species. First, we investigated the electrical characterization of hydrogel without anti-dehydrating agent and ion gel. The devices using hydrogel without anti-dehydrating agent showed unstable performance over time due to fast evaporation of water. So, we needed to find a formulation to hinder dehydration of hydrogel. Utilization of non-volatile organic polyols (e.g., ethylene glycol, glycerol) is a method to hinder the dehydration of hydrogel through formation of multiple hydrogen bonds which can cause improved water retention ability of hydrogels. So, we added glycerol to the swelling solution of the hydrogels, in this method water molecules in hydrogel can be displaced by glycerol molecules. We obtained electrical stability of devices using hydrogel containing glycerol and we observed improvement in their electrical stability. We demonstrated mechanical stability of EGTs using different gating media and we observed better mechanical stability of ion gel-gated devices compared to hydrogel gated ones. This was correlated to better adhesion of ion gel to device substrate due to its hydrophobic nature.

Finally in the last part (3rd article) we considered using semi-solid electrolytes for OECTs based on PEDOT:PSS and working in depletion mode. More importantly we demonstrated the effect of configuration of device (vertical and planar) on the main figure of merits of OECTs, such as their transconductance, ON-OFF ratio and switching response. We used printing method for fabrication of OECTs. The most challenging aspect of this work involved optimizing the thickness of the

channel material to prevent short circuits between the top and bottom electrodes. This means that printing needs to be done precisely to obtain well-defined vertical structure without any contamination of silver ink in the channel area. Such short circuit can lead to a non-functional device and hinder the desired modulating effect of the gate electrode. In our work we confirmed creation of vertical structure by SEM images and their EDX mapping, providing strong evidence for the successful realization of the intended vertical structure without any silver contamination in the channel region. We demonstrated electrical characterization of OECTs and we obtained 50 times higher transconductance for vertical OECTs compared to planar ones. One limitation of this study was the resolution of the printer. We believe that employing alternative printers with inkjet technology could enable the fabrication of smaller devices, specifically reducing their width. Additionally, by utilizing such printers, it may be possible to decrease the thickness of the channel material to below 2 μm, surpassing the channel length achievable in our study using the printer with direct ink writing technology. In addition to the fact that vertical structure enhances amplification ability of OECTs through increasing the transconductance they can offer reduced footprint. By adopting a vertical architecture, OECTs can achieve better space utilization and higher integration levels on a given substrate. The implementation of a vertical geometry in OECTs fabricated through printing methods has the potential to drive the advancement of the industry and optimize device performance. This progress can result in the creation of electronic circuits that are compact, facilitating the production of smaller and highly portable OECT-based devices. Additionally, the utilization of printing techniques for OECT fabrication brings notable advantages, including the scalability required for mass production in the industry. The use of printing methods enables high-speed fabrication on a large industrial scale, further contributing to the efficiency and cost-effectiveness of the manufacturing process.

The material selection and processing methods described in this PhD thesis for EGTs are capable of fabricating highly performing and reliable devices. The incorporation of organic materials as channel materials in these devices has resulted in a reasonable degree of flexibility. Meanwhile, the use of electrolytes instead of dielectric materials has enabled us to achieve low operating voltage devices. Moreover, the utilization of semi-solid electrolytes is particularly attractive for use in EGTs, where reliability and longevity are of utmost importance. These findings will have a significant influence on future techniques used for fabricating flexible organic EGTs with high

performance. Our printed vertical OECTs have a significant impact on achieving devices with high transconductance, suitable for use in biosensors with high sensitivity. The results of this PhD research project, along with the outlined methods and material selection for constructing organic EGTs, will lay a strong foundation for the development of the next generation of organic electronic devices.

CHAPTER 8 CONCLUSION AND RECOMMENDATIONS

In this PhD work, we have demonstrated the fabrication and characterization of EGTs based on organic semiconductors and OECTs based on conducting polymers. Our focus was on the utilization of different types of ion-containing gating media, including ionic liquid and semi-solid gel electrolytes, and the further investigation of the possible applications of EGTs. We conducted an in-depth investigation into the effect of electrolyte composition and its properties on the electrical characterization of EGT and OECT devices. EGTs based on organic semiconductors (PCDTPT, DPP-DTT) functioned in p-type enhancement mode, while OECTs based on conducting PEDOT:PSS operated in depletion mode. Our research revealed the effectiveness of using semi-solid electrolytes in obtaining devices with low operating voltage. These findings demonstrated the potential for future research to explore the use of semi-solid electrolytes in the development of more efficient EGT and OECT devices.

We investigated the electrical characterization of EGTs based on the p-type donor-acceptor conjugated copolymer PCDTPT. We fabricated both rigid (SiO_2/Si) and flexible (PI) EGTs using the ionic liquid [EMIM][TFSI] as an ion gating medium. AFM images of the thin films on both rigid and flexible substrates showed a porous structure of the solution-processed thin films. The charge carrier mobility and ON-OFF ratio values were found to be similar for both the rigid and flexible devices, indicating the possibility of using these devices for flexible organic electronic applications. We conducted CV measurements on the EGTs, which showed that PCDTPT is electrochemically active in the presence of the [EMIM][TFSI] ionic liquid and undergoes doping and de-doping reactions. The charge carrier mobility and the ON-OFF ratio values were approximately 0.9 $cm^2\ V^{-1}\ s^{-1}$ and 10^5, respectively, for the rigid and flexible devices. The mobility values in the bent state (R=10 mm) and during repetitive bending cycles decreased by only 10% and 20%, respectively, compared to the flat state. We demonstrated the light sensing application of the EGTs by conducting electrical characterizations under both dark and simulated light conditions. The mobility increased from $0.78 \pm 0.03\ cm^2\ V^{-1}\ s^{-1}$ in the dark to $0.87 \pm 0.05\ cm^2\ V^{-1}\ s^{-1}$ under illumination. The phototransistors with ion-gated configuration showed a photosensitivity of 0.4 and a responsivity of 93 AW^{-1}. In the future it would be worthwhile to investigate photo-sensing ability of vertical EGTs based on PCDTPT. Vertical structures with lower channel length offer efficient dissociation of photogenerated charge carriers leading to higher photocurrent output.

We fabricated EGTs based on p-type DPP-DTT semiconductor and using semi-solid gel electrolytes. We investigated the effect of using different electrolytes on the electrical characterization, operational and mechanical stability of EGTs. We utilized two types of gel electrolytes (i.e., ion gel and hydrogels containing anti-dehydrating agent and without anti-dehydrating agent). Ion gel was based on PVDF-HFP and [EMIM][TFSI] whereas hydrogels were based on hydrophilic PVA. We utilized glycerol as an anti-dehydrating agent in the formulation of hydrogels in order to study its effect on inhibiting dehydration of hydrogel and consequently on operational stability of EGTs. Electrochemical characterization of gel electrolytes was obtained by performing EIS on MIM structures. EIS results exhibited high specific capacitance for hydrogels with glycerol, especially for the sample with higher ionic species (NaCl) concentration (0.7 M versus 0.5 M). Higher values of ionic conductivity were obtained for hydrogels compared to that of ion gel which is correlated to the presence of water in the formulation of hydrogels that can facilitate ion transport within the electrolyte. Higher specific capacitance of hydrogels with glycerol and containing higher amount of ionic species concentration, exhibit an elevated drain current when employed in EGTs. The electrical stability of the ion gel and hydrogel-gated devices were assessed by conducting 20 successive transfer curve measurements. Our analysis revealed that the ion gel-gated devices exhibited no notable reduction in their current, threshold voltage, or the on-off ratio during the 20 cycles. The use of hydrogels without glycerol for EGT devices resulted in a reduction of approximately 45% in drain current. On the other hand, the use of hydrogel containing glycerol only led to a minor decrease of approximately 5% in current, with no noticeable shift in the threshold voltage. We performed pulse cycling for EGTs to further study their stability. After undergoing approximately 65 on-off cycles (equivalent to around 1000 seconds), the devices that were gated with ion gel maintained approximately 98% of their drain current. On the other hand, the devices gated with hydrogels without glycerol and with glycerol experienced a decline of approximately 50% and 10%, respectively. Moreover, the long-term electrical stability of EGTs was assessed and compared. Ion-gel gated devices displayed remarkable stability for more than two weeks, exhibiting no significant change in the drain current. Conversely, devices using hydrogel without anti-dehydrating agent as an electrolyte showed a rapid decline in drain current, with a decrease of approximately 60% within an hour. However, the introduction of glycerol resulted in an improvement in electrical stability, as the drain current

remained nearly unchanged for two days and declined by 40% on the third day. To assess the mechanical stability of gel-gated EGTs, we conducted electrical measurements while subjecting them to bending. The EGTs were fabricated on PET substrates to make them flexible. The mobility of ion gel-gated transistors did not exhibit any notable alteration. However, the mobility values of devices gated by hydrogel without and with glycerol were reduced by approximately 50% and 10%, respectively, when subjected to bending. We correlated improved durability of ion gel-gated devices under bending to the enhanced adhesion of the ion gel to the devices due to its lower thickness and greater hydrophobicity. Our results clearly revealed that partially substitution of water with organic solvents improved the electrical stability of EGTs. We hypothesize that complete removal of the fast-evaporating elements of gels (i.e., water) and replacement with organic solvents having high boiling points could potentially improve the stability of EGTs. It would be worthwhile to understand the doping mechanism in EGTs using different electrolytes (containing different ionic species) with methods such as electrochemical quartz crystal microbalance (EQCM). In the EQCM method, a semiconductor material is used as the working electrode in contact with an electrolyte solution containing dopant ions. A voltage bias is applied to the working electrode to induce doping, and the changes in the mass and viscoelastic properties of the semiconductor material during the doping process are monitored using the QCM. The frequency and dissipation changes measured by the QCM can provide information about the doping kinetics, dopant concentration, and changes in the mechanical properties of the semiconductor material, which can help in understanding the doping mechanism (electrostatic versus electrochemical) of semiconductors.

We have successfully fabricated both planar and vertical OECTs based on PEDOT:PSS using a PCB printer with DIW technology. All components, including the top, bottom, gate electrodes, and active channel material, were printed. Semi-solid gel electrolytes, specifically ion gel and organogel, were used for printed OECTs and were applied by the drop casting method. The electrochemical properties of the gels were tested using EIS methodology equipped with a Swagelok cell. Ionic conductivity values of 0.7 ±0.1 mS cm^{-1} and 2.4 ±0.2 mS cm^{-1} were obtained for the ion gel and organogel, respectively. The lower ionic conductivity of the ion gel was attributed to the larger ion size. Planar OECTs with organogel and ion gel-gated devices showed transconductance values of 2.6±0.6 mS and 1.5±0.1 mS, respectively. The higher ionic

conductivity of the organogel resulted in devices with higher transconductance. We observed that organogel-gated OECTs had a lower operating voltage than those gated by the ion gel, which was attributed to the smaller size of ions, the electrolyte's hydrophilicity or hydrophobicity, and the capacitance of the electrolyte. Notably, the organogel exhibited a smaller ion size and higher capacitance than the ion gel, resulting in a larger amount of charge storage at the interface between the channel material and electrolyte.

We also investigated the electrical properties of vertical OECTs using two types of gels. Vertical OECTs showed transconductance values of 60±10 mS and 110±25 mS for devices gated by ion gel and organogel, respectively. The vertical OECTs demonstrated a significantly higher transconductance value than planar devices. This was related to their shorter channel length compared to planar devices. We obtained the transient response of OECTs by applying square-wave pulses at a constant $V_d = -0.2$ V, varying V_g from 0 V to 1.5 V for the ion gel and from 0 V to 0.8 V for the organogel with a pulse length of 50 s. The response times of vertical and planar OECTs were compared, revealing a four-fold increase in response speed for vertical structures compared to the planar configuration. OECTs utilizing organogels as electrolytes demonstrated significantly faster response times than ion gel-gated devices, with a speed that was twice as fast in both configurations. Vertical OECTs with their shorter channel lengths exhibited superior performance compared to planar structures, including shorter response times and higher transconductance. This study presents a novel approach to fabricate vertical OECTs using a facile and cost-effective printing technique. It also sheds light on the significance of electrolyte selection in OECT performance. The utilization of different electrolytes with varying ionic conductivities expands our understanding of the effects of electrolytes on OECT performance and offers promising opportunities for fabricating OECTs with enhanced transconductance and switching speed. In a vertical structure, charge transport occurs perpendicular to the substrate, which can reduce the impact of mechanical deformations, such as stretching or bending, on device performance. Work is in progress to fabricate vertical OECTs on flexible and stretchable substrates to evaluate their mechanical stability in comparison to planar structures. It would be advantageous to investigate alternative printing methods, such as inkjet printing, for the fabrication of vertical OECTs. Unlike PCB printers, inkjet printing employs inks with lower viscosity, which can yield a

thinner PEDOT:PSS layer. Consequently, the vertical structure can have a shorter channel length, potentially improving the device's transconductance.

Overall, our results demonstrate possible applications of EGTs as a phototransistor as well as importance of selection of electrolytes for EGTs and exploring new configuration of OECTs in order to enhance their performance in terms of transconductance and response time. Our first article provides valuable insights into the electrical characterization of EGTs and their light sensing application as well as investigation on the flexibility of EGT devices. In our second article we focused on utilization of semi-solid electrolytes instead of liquid electrolytes. Semi-solid electrolytes provide improved durability compared to liquid electrolytes, which are prone to evaporation and leakage. Semi-solid electrolytes can be tailored to specific requirements, such as flexibility, shape, and size, enabling versatile applications in flexible electronics. We highlighted the importance of selection of electrolyte and its role on the electrical characterization and operational stability of EGTs. Our third article highlights the potential of printing techniques and novel vertical device architectures for the development of high-performance organic electronic devices. The utilization of different electrolytes with varying ionic conductivities not only broadens the understanding of electrolyte effects on OECT performance but also offers promising avenues for fabricating OECTs with improved transconductance and response time. Further research in this area may lead to the development of OECTs with advanced performance characteristics for a wide range of applications.

REFERENCES

[1] H. Shirakawa, E. J. Louis, A. G. MacDiarmid, C. K. Chiang, and A. J. Heeger, "Synthesis of electrically conducting organic polymers: halogen derivatives of polyacetylene,(CH) x," *Journal of the Chemical Society, Chemical Communications,* no. 16, p. 578, 1977.

[2] A. J. Heeger, "Semiconducting and metallic polymers: the fourth generation of polymeric materials (Nobel lecture)," *Angewandte Chemie International Edition,* vol. 40, no. 14, p. 2591, 2001.

[3] S. Günes, H. Neugebauer, and N. S. Sariciftci, "Conjugated polymer-based organic solar cells," *Chemical reviews,* vol. 107, no. 4, p. 1324, 2007.

[4] M. Gross, D. C. Müller, H.-G. Nothofer, U. Scherf, D. Neher, C. Bräuchle, and K. Meerholz, "Improving the performance of doped π-conjugated polymers for use in organic light-emitting diodes," *Nature,* vol. 405, no. 6787, p. 661, 2000.

[5] C. W. Tang and S. A. VanSlyke, "Organic electroluminescent diodes," *Applied Physics Letters,* vol. 51, no. 12, p. 913, 1987.

[6] J. Tong, S. Xiong, Y. Zhou, L. Mao, X. Min, Z. Li, F. Jiang, W. Meng, F. Qin, and T. Liu, "Flexible all-solution-processed all-plastic multijunction solar cells for powering electronic devices," *Materials Horizons,* vol. 3, no. 5, p. 452, 2016.

[7] F. Garnier, G. Horowitz, X. Peng, and D. Fichou, "An all-organic" soft" thin film transistor with very high carrier mobility," *Advanced Materials,* vol. 2, no. 12, p. 592, 1990.

[8] S. H. Kim, K. Hong, W. Xie, K. H. Lee, S. Zhang, T. P. Lodge, and C. D. Frisbie, "Electrolyte-gated transistors for organic and printed electronics," *Advanced Materials,* vol. 25, no. 13, p. 1822, 2013.

[9] M. T. Lee, C. S. Chan, Y. H. Chen, C. Y. Lin, A. T. Huang, J. H. Tao, and C. H. Wu, "Toward a Foldable Organic Light-emitting Diode Display," in *Flexible Flat Panel Displays*, D. R. Cairns, D. J. Broer, and G. P. Crawford Eds., Second ed., 2023, ch. 9, p. 149.

[10] X. Xu, Y. Zhao, and Y. Liu, "Wearable Electronics Based on Stretchable Organic Semiconductors," *Small,* vol. 19, no. 20, p. 2206309, 2023.

[11] D. Yin, Z.-Y. Chen, N.-R. Jiang, Y.-F. Liu, Y.-G. Bi, X.-L. Zhang, W. Han, J. Feng, and H.-B. Sun, "Highly transparent and flexible fabric-based organic light emitting devices for unnoticeable wearable displays," *Organic Electronics,* vol. 76, p. 105494, 2020.

[12] F. Torricelli, I. Alessandri, E. Macchia, I. Vassalini, M. Maddaloni, and L. Torsi, "Green materials and technologies for sustainable organic transistors," *Advanced Materials Technologies,* vol. 7, no. 2, p. 2100445, 2022.

[13] J. Sun, J. Jiang, Y. Deng, Y. Wang, L. Li, Z. Lou, Y. Hou, F. Teng, and Y. Hu, "Ionic Liquid-Gated Near-Infrared Polymer Phototransistors and Their Persistent Photoconductivity Application in Optical Memory," *ACS applied materials & interfaces,* vol. 14, no. 51, p. 57082, 2022.

[14] X. Wang, W. Lu, P. Wei, Z. Qin, N. Qiao, X. Qin, M. Zhang, Y. Zhu, L. Bu, and G. Lu, "Artificial Tactile Recognition Enabled by Flexible Low-Voltage Organic Transistors and Low-Power Synaptic Electronics," *ACS applied materials & interfaces,* vol. 14, no. 43, p. 48948, 2022.

[15] M. Ullah, K. Tandy, J. Li, Z. Shi, P. L. Burn, P. Meredith, and E. B. Namdas, "High-mobility, heterostructure light-emitting transistors and complementary inverters," *ACS Photonics,* vol. 1, no. 10, p. 954, 2014.

[16] M. J. Donahue, A. Williamson, X. Strakosas, J. T. Friedlein, R. R. McLeod, H. Gleskova, and G. G. Malliaras, "High-Performance Vertical Organic Electrochemical Transistors," *Advanced Materials,* vol. 30, no. 5, p. 1705031, 2018.

[17] D. A. Koutsouras, F. Torricelli, and P. W. Blom, "Submicron Vertical Channel Organic Electrochemical Transistors with Ultrahigh Transconductance," *Advanced Electronic Materials,* vol. 9, no. 2, p. 2200868, 2023.

[18] L. J. Edgar, "Method and apparatus for controlling electric currents," ed: Google Patents, 1930.

[19] M. Atalla and E. Tannenbaum, "Impurity redistribution and junction formation in silicon by thermal oxidation," *Bell System Technical Journal,* vol. 39, no. 4, p. 933, 1960.

[20] P. K. Weimer, "The TFT a new thin-film transistor," *Proceedings of the IRE,* vol. 50, no. 6, p. 1462, 1962.

[21] F. Ebisawa, T. Kurokawa, and S. Nara, "Electrical properties of polyacetylene/polysiloxane interface," *Journal of applied physics,* vol. 54, no. 6, p. 3255, 1983.

[22] G. Horowitz, D. Fichou, X. Peng, Z. Xu, and F. Garnier, "A field-effect transistor based on conjugated alpha-sexithienyl," *Solid State Communications,* vol. 72, no. 4, p. 381, 1989.

[23] Y.-Y. Lin, D. Gundlach, S. Nelson, and T. Jackson, "Stacked pentacene layer organic thin-film transistors with improved characteristics," *IEEE Electron Device Letters,* vol. 18, no. 12, p. 606, 1997.

[24] Y. Yamashita, F. Hinkel, T. Marszalek, W. Zajaczkowski, W. Pisula, M. Baumgarten, H. Matsui, K. Müllen, and J. Takeya, "Mobility exceeding 10 cm2/(V· s) in donor–acceptor polymer transistors with band-like charge transport," *Chemistry of Materials,* vol. 28, no. 2, p. 420, 2016.

[25] S. Zhou, Y. Tong, H. Li, X. Zhao, Q. Tang, and Y. Liu, "A High Mobility of Up to 13 $cm^2V^{-1}s^{-1}$ in Dinaphttho-Thieno-Thiophene Single-Crystal Field-Effect Transistors via Self-Assembled Monolayer Selection," *IEEE Electron Device Letters,* vol. 41, no. 5, p. 757, 2020.

[26] K. Liu, B. Ouyang, X. Guo, Y. Guo, and Y. Liu, "Advances in flexible organic field-effect transistors and their applications for flexible electronics," *Npj Flexible Electronics,* vol. 6, no. 1, p. 1, 2022.

[27] X. Zhang, Z. Pu, X. Su, C. Li, H. Zheng, and D. Li, "Flexible organic field-effect transistors-based biosensors: progress and perspectives," *Analytical and Bioanalytical Chemistry,* vol. 415, p. 1607, 2023.

[28] C. M. Hussain, *Handbook of nanomaterials for industrial applications*. Elsevier, 2018.

[29] J. Zaumseil and H. Sirringhaus, "Electron and ambipolar transport in organic field-effect transistors," *Chemical reviews,* vol. 107, no. 4, p. 1296, 2007.

[30] X. Bu, H. Xu, D. Shang, Y. Li, H. Lv, and Q. Liu, "Ion-gated transistor: An enabler for sensing and computing integration," *Advanced Intelligent Systems,* vol. 2, no. 12, p. 2000156, 2020.

[31] R. Schlesinger, *Energy-level control at hybrid inorganic/organic semiconductor interfaces*, First ed. Springer, 2017.

[32] M. Fahlman, S. Fabiano, V. Gueskine, D. Simon, M. Berggren, and X. Crispin, "Interfaces in organic electronics," *Nature Reviews Materials,* vol. 4, no. 10, p. 627, 2019.

[33] K. Gu, J. Onorato, S. S. Xiao, C. K. Luscombe, and Y.-L. Loo, "Determination of the molecular weight of conjugated polymers with diffusion-ordered NMR spectroscopy," *Chemistry of Materials,* vol. 30, no. 3, p. 570, 2018.

[34] R. Venkatesh, Y. Zheng, A. L. Liu, H. Zhao, C. Silva, C. J. Takacs, M. A. Grover, J. C. Meredith, and E. Reichmanis, "Overlap concentration generates optimum device performance for DPP-based conjugated polymers," *Organic Electronics,* vol. 117, p. 106779, 2023.

[35] C. Wang, X. Zhang, and W. Hu, "Organic photodiodes and phototransistors toward infrared detection: materials, devices, and applications," *Chemical Society Reviews,* vol. 49, no. 3, p. 653, 2020.

[36] A. Li, L. Yan, M. Liu, I. Murtaza, C. He, D. Zhang, Y. He, and H. Meng, "Highly responsive phototransistors based on 2, 6-bis (4-methoxyphenyl) anthracene single crystal," *Journal of Materials Chemistry C,* vol. 5, no. 22, p. 5304, 2017.

[37] X. Huang, D. Ji, H. Fuchs, W. Hu, and T. Li, "Recent progress in organic phototransistors: Semiconductor materials, device structures and optoelectronic applications," *ChemPhotoChem,* vol. 4, no. 1, p. 9, 2020.

[38] P. C. Chow and T. Someya, "Organic photodetectors for next-generation wearable electronics," *Advanced Materials,* vol. 32, no. 15, p. 1902045, 2020.

[39] K. J. Baeg, M. Binda, D. Natali, M. Caironi, and Y. Y. Noh, "Organic light detectors: photodiodes and phototransistors," *Advanced Materials,* vol. 25, no. 31, p. 4267, 2013.

[40] Y. Yan, X. Wu, Q. Chen, Y. Liu, H. Chen, and T. Guo, "High-performance low-voltage flexible photodetector arrays based on all-solid-state organic electrochemical transistors for photosensing and imaging," *ACS applied materials & interfaces,* vol. 11, no. 22, p. 20214, 2019.

[41] G. Zhang, J. Zhong, Q. Chen, Y. Yan, H. Chen, and T. Guo, "High-Performance Organic Phototransistors With Vertical Structure Design," *IEEE Transactions on Electron Devices,* vol. 66, no. 4, p. 1815, 2019.

[42] Y. Yan, Q. Chen, X. Wang, Y. Liu, R. Yu, C. Gao, H. Chen, and T. Guo, "Vertical channel inorganic/organic hybrid electrochemical phototransistors with ultrahigh responsivity and fast response speed," *ACS applied materials & interfaces,* vol. 13, no. 6, p. 7498, 2021.

[43] J. Robertson, "High dielectric constant oxides," *The European Physical Journal-Applied Physics,* vol. 28, no. 3, p. 265, 2004.

[44] F. Torricelli, D. Z. Adrahtas, Z. Bao, M. Berggren, F. Biscarini, A. Bonfiglio, C. A. Bortolotti, C. D. Frisbie, E. Macchia, and G. G. Malliaras, "Electrolyte-gated transistors for enhanced performance bioelectronics," *Nature Reviews Methods Primers,* vol. 1, no. 1, p. 66, 2021.

[45] W. Huang, J. Chen, G. Wang, Y. Yao, X. Zhuang, R. M. Pankow, Y. Cheng, T. J. Marks, and A. Facchetti, "Dielectric materials for electrolyte gated transistor applications," *Journal of Materials Chemistry C,* vol. 9, no. 30, p. 9348, 2021.

[46] K. D. Dorfman, D. Z. Adrahtas, M. S. Thomas, and C. D. Frisbie, "Microfluidic opportunities in printed electrolyte-gated transistor biosensors," *Biomicrofluidics,* vol. 14, no. 1, p. 011301, 2020.

[47] J. Lee, L. G. Kaake, J. H. Cho, X.-Y. Zhu, T. P. Lodge, and C. D. Frisbie, "Ion gel-gated polymer thin-film transistors: Operating mechanism and characterization of gate dielectric capacitance,

switching speed, and stability," *The Journal of Physical Chemistry C,* vol. 113, no. 20, p. 8972, 2009.

[48] E. Zeglio and O. Inganäs, "Active materials for organic electrochemical transistors," *Advanced Materials,* vol. 30, no. 44, p. 1800941, 2018.

[49] T. Horii, Y. Li, Y. Mori, and H. Okuzaki, "Correlation between the hierarchical structure and electrical conductivity of PEDOT/PSS," *Polymer Journal,* vol. 47, no. 10, p. 695, 2015.

[50] C. M. Palumbiny, C. Heller, C. J. Schaffer, V. Körstgens, G. Santoro, S. V. Roth, and P. Müller-Buschbaum, "Molecular reorientation and structural changes in cosolvent-treated highly conductive PEDOT: PSS electrodes for flexible indium tin oxide-free organic electronics," *The Journal of Physical Chemistry C,* vol. 118, no. 25, p. 13598, 2014.

[51] D. A. Bernards and G. G. Malliaras, "Steady-state and transient behavior of organic electrochemical transistors," *Advanced Functional Materials,* vol. 17, no. 17, p. 3538, 2007.

[52] J. Rivnay, P. Leleux, M. Ferro, M. Sessolo, A. Williamson, D. A. Koutsouras, D. Khodagholy, M. Ramuz, X. Strakosas, and R. M. Owens, "High-performance transistors for bioelectronics through tuning of channel thickness," *Science advances,* vol. 1, no. 4, p. e1400251, 2015.

[53] D. Wang, S. Zhao, R. Yin, L. Li, Z. Lou, and G. Shen, "Recent advanced applications of ion-gel in ionic-gated transistor," *Npj Flexible Electronics,* vol. 5, no. 1, p. 13, 2021.

[54] Y. J. Jo, H. Kim, J. Ok, Y. J. Shin, J. H. Shin, T. H. Kim, Y. Jung, and T. i. Kim, "Biocompatible and biodegradable organic transistors using a solid-state electrolyte incorporated with choline-based ionic liquid and polysaccharide," *Advanced Functional Materials,* vol. 30, no. 29, p. 1909707, 2020.

[55] T. Lan, F. Soavi, M. Marcaccio, P.-L. Brunner, J. Sayago, and C. Santato, "Electrolyte-gated transistors based on phenyl-C 61-butyric acid methyl ester (PCBM) films: bridging redox properties, charge carrier transport and device performance," *Chemical Communications,* vol. 54, no. 43, p. 5490, 2018.

[56] A. Giovannitti, R. B. Rashid, Q. Thiburce, B. D. Paulsen, C. Cendra, K. Thorley, D. Moia, J. T. Mefford, D. Hanifi, and D. Weiyuan, "Energetic control of redox-active polymers toward safe organic bioelectronic materials," *Advanced Materials,* vol. 32, no. 16, p. 1908047, 2020.

[57] Y. Zhang, Q. Zeng, Y. Shen, L. Yang, and F. Yu, "Electrochemical stability investigations and drug toxicity tests of electrolyte-gated organic field-effect transistors," *ACS Applied Materials & Interfaces,* vol. 12, no. 50, p. 56216, 2020.

[58] X. Wu, Q. Liu, A. Surendran, S. E. Bottle, P. Sonar, and W. L. Leong, "Enhancing the electrochemical doping efficiency in diketopyrrolopyrrole-based polymer for organic electrochemical transistors," *Advanced Electronic Materials,* vol. 7, no. 1, p. 2000701, 2021.

[59] A. Melianas, T. Quill, G. LeCroy, Y. Tuchman, H. v. Loo, S. Keene, A. Giovannitti, H. Lee, I. Maria, and I. McCulloch, "Temperature-resilient solid-state organic artificial synapses for neuromorphic computing," *Science advances,* vol. 6, no. 27, p. eabb2958, 2020.

[60] X. Wu, S. Chen, M. Moser, A. Moudgil, S. Griggs, A. Marks, T. Li, I. McCulloch, and W. L. Leong, "High Performing Solid-State Organic Electrochemical Transistors Enabled by Glycolated Polythiophene and Ion-Gel Electrolyte with a Wide Operation Temperature Range from− 50 to 110° C," *Advanced Functional Materials,* vol. 33, no. 3, p. 2209354, 2023.

[61] S. Chen, K. Hou, T. Li, X. Wu, Z. Wang, L. Wei, and W. L. Leong, "Ultra-Lightweight, Highly Permeable, and Waterproof Fibrous Organic Electrochemical Transistors for On-Skin Bioelectronics," *Advanced Materials Technologies,* vol. 8, no. 1, p. 2200611, 2023.

[62] J. Ko, X. Wu, A. Surendran, B. T. Muhammad, and W. L. Leong, "Self-healable organic electrochemical transistor with high transconductance, fast response, and long-term stability," *ACS applied materials & interfaces,* vol. 12, no. 30, p. 33979, 2020.

[63] Z. Wu, X. Yang, and J. Wu, "Conductive hydrogel-and organohydrogel-based stretchable sensors," *ACS Applied Materials & Interfaces,* vol. 13, no. 2, p. 2128, 2021.

[64] Y. J. Jo, K. Y. Kwon, Z. U. Khan, X. Crispin, and T.-i. Kim, "Gelatin Hydrogel-Based Organic Electrochemical Transistors and Their Integrated Logic Circuits," *ACS Applied Materials & Interfaces,* vol. 10, no. 45, p. 39083, 2018.

[65] I. Cunha, R. Barras, P. Grey, D. Gaspar, E. Fortunato, R. Martins, and L. Pereira, "Reusable cellulose-based hydrogel sticker film applied as gate dielectric in paper electrolyte-gated transistors," *Advanced Functional Materials,* vol. 27, no. 16, p. 1606755, 2017.

[66] I. Cunha, J. Martins, D. Gaspar, P. G. Bahubalindruni, E. Fortunato, R. Martins, and L. Pereira, "Healable Cellulose Iontronic Hydrogel Stickers for Sustainable Electronics on Paper," *Advanced Electronic Materials,* vol. 7, no. 3, p. 2001166, 2021.

[67] S. A. Singaraju, T. T. Baby, F. Neuper, R. Kruk, J. A. Hagmann, H. Hahn, and B. Breitung, "Development of fully printed electrolyte-gated oxide transistors using graphene passive structures," *ACS Applied Electronic Materials,* vol. 1, no. 8, p. 1538, 2019.

[68] Y. Zhu, G. Liu, Z. Xin, C. Fu, Q. Wan, and F. Shan, "Solution-processed, electrolyte-gated In2O3 flexible synaptic transistors for brain-inspired neuromorphic applications," *ACS applied materials & interfaces,* vol. 12, no. 1, p. 1061, 2019.

[69] W. Qian, J. Texter, and F. Yan, "Frontiers in poly (ionic liquid) s: syntheses and applications," *Chemical Society Reviews,* vol. 46, no. 4, p. 1124, 2017.

[70] H. Sinno, S. Fabiano, X. Crispin, M. Berggren, and I. Engquist, "Bias stress effect in polyelectrolyte-gated organic field-effect transistors," *Applied Physics Letters,* vol. 102, no. 11, p. 50, 2013.

[71] L. Du, D. He, Y. Liu, M. Xu, Q. Wang, Q. Xin, and A. Song, "Low-voltage, flexible IGZO transistors gated by PSSNa electrolyte," *IEEE Electron Device Letters,* vol. 39, no. 9, p. 1334, 2018.

[72] L. Herlogsson, X. Crispin, S. Tierney, and M. Berggren, "Polyelectrolyte-gated organic complementary circuits operating at low power and voltage," *Advanced Materials,* vol. 23, no. 40, p. 4684, 2011.

[73] A. Laiho, L. Herlogsson, R. Forchheimer, X. Crispin, and M. Berggren, "Controlling the dimensionality of charge transport in organic thin-film transistors," *Proceedings of the National Academy of Sciences,* vol. 108, no. 37, p. 15069, 2011.

[74] L. Herlogsson, X. Crispin, N. D. Robinson, M. Sandberg, O. J. Hagel, G. Gustafsson, and M. Berggren, "Low-voltage polymer field-effect transistors gated via a proton conductor," *Advanced materials,* vol. 19, no. 1, p. 97, 2007.

[75] P. Heremans, A. K. Tripathi, A. de Jamblinne de Meux, E. C. Smits, B. Hou, G. Pourtois, and G. H. Gelinck, "Mechanical and electronic properties of thin-film transistors on plastic, and their integration in flexible electronic applications," *Advanced Materials,* vol. 28, no. 22, p. 4266, 2016.

[76] C.-J. Lee, Y.-C. Chang, L.-W. Wang, and Y.-H. Wang, "Biodegradable materials for organic field-effect transistors on a paper substrate," *IEEE Electron Device Letters,* vol. 40, no. 2, p. 236, 2019.

[77] S. Lai, Y. Vlamidis, N. Mishra, P. Cosseddu, V. Mišeikis, P. C. Ricci, V. Voliani, C. Coletti, and A. Bonfiglio, "A Flexible, Transparent Chemosensor Integrating an Inkjet-Printed Organic Field-Effect Transistor and a Non-Covalently Functionalized Graphene Electrode," *Advanced Materials Technologies,* vol. 6, no. 12, p. 2100481, 2021.

[78] B. O'Connor, E. P. Chan, C. Chan, B. R. Conrad, L. J. Richter, R. J. Kline, M. Heeney, I. McCulloch, C. L. Soles, and D. M. DeLongchamp, "Correlations between mechanical and electrical properties of polythiophenes," *ACS nano,* vol. 4, no. 12, p. 7538, 2010.

[79] B. Nketia-Yawson, S. J. Kang, G. D. Tabi, A. Perinot, M. Caironi, A. Facchetti, and Y. Y. Noh, "Ultrahigh mobility in solution-processed solid-state electrolyte-gated transistors," *Advanced Materials,* vol. 29, no. 16, p. 1605685, 2017.

[80] Y. Na and F. S. Kim, "Nanodroplet-embedded semiconducting polymer layers for electrochemically stable and high-conductance organic electrolyte-gated transistors," *Chemistry of Materials,* vol. 31, no. 13, p. 4759, 2019.

[81] N. Cherukupally, M. Divya, and S. Dasgupta, "A comparative study on printable solid electrolytes toward ultrahigh current and environmentally stable thin film transistors," *Advanced Electronic Materials,* vol. 6, no. 12, p. 2000788, 2020.

[82] M. Massetti, S. Zhang, P. C. Harikesh, B. Burtscher, C. Diacci, D. T. Simon, X. Liu, M. Fahlman, D. Tu, and M. Berggren, "Fully 3D-printed organic electrochemical transistors," *Npj Flexible Electronics,* vol. 7, no. 1, p. 11, 2023.

[83] U. Boda, I. Petsagkourakis, V. Beni, P. Andersson Ersman, and K. Tybrandt, "Fully Screen-Printed Stretchable Organic Electrochemical Transistors," *Advanced Materials Technologies,* p. 2300247, 2023.

[84] S. Chen, A. Surendran, X. Wu, S. Y. Lee, M. Stephen, and W. L. Leong, "Recent technological advances in fabrication and application of organic electrochemical transistors," *Advanced Materials Technologies,* vol. 5, no. 12, p. 2000523, 2020.

[85] J. Liu, Z. Qin, H. Gao, H. Dong, J. Zhu, and W. Hu, "Vertical organic field-effect transistors," *Advanced Functional Materials,* vol. 29, no. 17, p. 1808453, 2019.

[86] L. Ma and Y. Yang, "Unique architecture and concept for high-performance organic transistors," *Applied Physics Letters,* vol. 85, no. 21, p. 5084, 2004.

[87] M. A. McCarthy, B. Liu, R. Jayaraman, S. M. Gilbert, D. Y. Kim, F. So, and A. G. Rinzler, "Reorientation of the high mobility plane in pentacene-based carbon nanotube enabled vertical field effect transistors," *ACS nano,* vol. 5, no. 1, p. 291, 2011.

[88] J. S. Kim, B. J. Kim, Y. J. Choi, M. H. Lee, M. S. Kang, and J. H. Cho, "An organic vertical field-effect transistor with underside-doped graphene electrodes," *Advanced Materials,* vol. 28, no. 24, p. 4803, 2016.

[89] Y. Liu, H. Zhou, N. O. Weiss, Y. Huang, and X. Duan, "High-performance organic vertical thin film transistor using graphene as a tunable contact," *ACS nano,* vol. 9, no. 11, p. 11102, 2015.

[90] H. Hlaing, C.-H. Kim, F. Carta, C.-Y. Nam, R. A. Barton, N. Petrone, J. Hone, and I. Kymissis, "Low-voltage organic electronics based on a gate-tunable injection barrier in vertical graphene-organic semiconductor heterostructures," *Nano Letters,* vol. 15, no. 1, p. 69, 2015.

[91] H. Yu, Z. Dong, J. Guo, D. Kim, and F. So, "Vertical organic field-effect transistors for integrated optoelectronic applications," *ACS applied materials & interfaces,* vol. 8, no. 16, p. 10430, 2016.

[92] J. Lenz, F. Del Giudice, F. R. Geisenhof, F. Winterer, and R. T. Weitz, "Vertical, electrolyte-gated organic transistors show continuous operation in the MA cm−2 regime and artificial synaptic behaviour," *Nature nanotechnology,* vol. 14, no. 6, p. 579, 2019.

[93] W. Huang, J. Chen, Y. Yao, D. Zheng, X. Ji, L.-W. Feng, D. Moore, N. R. Glavin, M. Xie, and Y. Chen, "Vertical organic electrochemical transistors for complementary circuits," *Nature,* vol. 613, no. 7944, p. 496, 2023.

[94] Y. Yan, Q. Chen, X. Wu, X. Wang, E. Li, Y. Ke, Y. Liu, H. Chen, and T. Guo, "High-performance organic electrochemical transistors with nanoscale channel length and their application to artificial synapse," *ACS Applied Materials & Interfaces,* vol. 12, no. 44, p. 49915, 2020.

[95] A. Subramanian, B. George, S. R. Bobbara, I. Valitova, I. Ruggeri, F. Borghi, A. Podestà, P. Milani, F. Soavi, and C. Santato, "Ion-gated transistors based on porous and compact TiO2 films: Effect of Li ions in the gating medium," *AIP Advances,* vol. 10, no. 6, p. 065314, 2020.

[96] C.-H. Kim, M. Azimi, J. Fan, H. Nagarajan, M. Wang, and F. Cicoira, "All-printed and stretchable organic electrochemical transistors using a hydrogel electrolyte," *Nanoscale,* vol. 15, no. 7, p. 3263, 2023.

[97] M. Azimi, C.-h. Kim, J. Fan, and F. Cicoira, "Effect of Ionic Conductivity of Electrolyte on Printed Planar and Vertical Organic Electrochemical Transistors," *Faraday Discussions,* 2023.

[98] J. Shojaeiarani, D. S. Bajwa, N. M. Stark, T. M. Bergholz, and A. L. Kraft, "Spin coating method improved the performance characteristics of films obtained from poly (lactic acid) and cellulose nanocrystals," *Sustainable Materials and Technologies,* vol. 26, p. e00212, 2020.

[99] J. S. Bangsund, T. R. Fielitz, T. J. Steiner, K. Shi, J. R. Van Sambeek, C. P. Clark, and R. J. Holmes, "Formation of aligned periodic patterns during the crystallization of organic semiconductor thin films," *Nature materials,* vol. 18, no. 7, p. 725, 2019.

[100] X. Meng, F. Quenneville, F. d. r. Venne, E. Di Mauro, D. Işık, M. Barbosa, Y. Drolet, M. M. Natile, D. Rochefort, and F. Soavi, "Electrolyte-gated WO3 transistors: electrochemistry, structure, and device performance," *The Journal of Physical Chemistry C,* vol. 119, no. 37, p. 21732, 2015.

[101] I. Valitova, P. Kumar, X. Meng, F. Soavi, C. Santato, and F. Cicoira, "Photolithographically patterned TiO2 films for electrolyte-gated transistors," *ACS applied materials & interfaces,* vol. 8, no. 23, p. 14855, 2016.

[102] M. Azimi, A. Subramanian, J. Fan, F. Soavi, and F. Cicoira, "Electrical and mechanical stability of flexible, organic electrolyte-gated transistors based on iongel and hydrogels," *Journal of Materials Chemistry C,* vol. 11, no. 14, p. 4623, 2023.

[103] K. Hong, S. H. Kim, K. H. Lee, and C. D. Frisbie, "Printed, sub-2V ZnO electrolyte gated transistors and inverters on plastic," *Advanced Materials,* vol. 25, no. 25, p. 3413, 2013.

[104] D. E. Ashkenaz, W. Paige Hall, C. L. Haynes, E. M. Hicks, A. D. McFarland, L. J. Sherry, D. A. Stuart, K. E. Wheeler, C. R. Yonzon, and J. Zhao, "Coffee cup atomic force microscopy," *Journal of Chemical Education,* vol. 87, no. 3, p. 306, 2010.

[105] J. Cazaux, "Recent developments and new strategies in scanning electron microscopy," *Journal of microscopy,* vol. 217, no. 1, p. 16, 2005.

[106] K. D. Vernon-Parry, "Scanning electron microscopy: an introduction," *III-Vs Review,* vol. 13, no. 4, p. 40, 2000.

[107] M. Ermrich and D. Opper, "XRD for the analyst," *Getting acquainted with the principles. Second. Panalytical,* 2013.

[108] N. Elgrishi, K. J. Rountree, B. D. McCarthy, E. S. Rountree, T. T. Eisenhart, and J. L. Dempsey, "A practical beginner's guide to cyclic voltammetry," *Journal of Chemical Education,* vol. 95, no. 2, p. 197, 2018.

[109] A. W. Colburn, K. J. Levey, D. O'Hare, and J. V. Macpherson, "Lifting the lid on the potentiostat: a beginner's guide to understanding electrochemical circuitry and practical operation," *Physical Chemistry Chemical Physics,* vol. 23, no. 14, p. 8100, 2021.

[110] J. Sayago, F. Soavi, Y. Sivalingam, F. Cicoira, and C. Santato, "Low voltage electrolyte-gated organic transistors making use of high surface area activated carbon gate electrodes," *Journal of Materials Chemistry C,* vol. 2, no. 28, p. 5690, 2014.

[111] J. Jeong, G. C. Marques, X. Feng, D. Boll, S. A. Singaraju, J. Aghassi-Hagmann, H. Hahn, and B. Breitung, "Ink-Jet Printable, Self-Assembled, and Chemically Crosslinked Ion-Gel as Electrolyte for Thin Film, Printable Transistors," *Advanced Materials Interfaces,* vol. 6, no. 21, p. 1901074, 2019.

[112] S. Yuvaraja, A. Nawaz, Q. Liu, D. Dubal, S. G. Surya, K. N. Salama, and P. Sonar, "Organic field-effect transistor-based flexible sensors," *Chemical Society Reviews,* vol. 49, no. 11, p. 3423, 2020.

[113] J. Kim, T. Hassinen, W. H. Lee, and S. Ko, "Fully solution-processed organic thin-film transistors by consecutive roll-to-roll gravure printing," *Organic Electronics,* vol. 42, p. 361, 2017.

[114] M. Sadeghi, P. Delparastan, A. Pierre, and A. C. Arias, "Printed Flexible Organic Transistors with Tunable Aspect Ratios," *Advanced Electronic Materials,* vol. 6, no. 2, p. 1901207, 2020.

[115] W. Gao, H. Ota, D. Kiriya, K. Takei, and A. Javey, "Flexible electronics toward wearable sensing," *Accounts of chemical research,* vol. 52, no. 3, p. 523, 2019.

[116] G. V. D. O. Silva, A. Subramanian, X. Meng, S. Zhang, M. S. Barbosa, B. Baloukas, D. Chartrand, J. C. Gonzáles, M. O. Orlandi, and F. Soavi, "Tungsten oxide ion-gated phototransistors using ionic liquid and aqueous gating media," *Journal of Physics D: Applied Physics,* vol. 52, no. 30, p. 305102, 2019.

[117] I. Valitova, M. M. Natile, F. Soavi, C. Santato, and F. Cicoira, "Tin dioxide electrolyte-gated transistors working in depletion and enhancement modes," *ACS applied materials & interfaces,* vol. 9, no. 42, p. 37013, 2017.

[118] T. Lan, F. Bélanger, F. Soavi, and C. Santato, "Ambient-stable, ion-gated poly [N-9′-heptadecanyl-2, 7-carbazole-alt-5, 5-(4′, 7′-di-2-thienyl-2′, 1′, 3′-benzothiadiazole)](PCDTBT) transistors and phototransistors," *Organic Electronics,* vol. 74, p. 265, 2019.

[119] H. Xu, Q. Zhu, Y. Lv, K. Deng, Y. Deng, Q. Li, S. Qi, W. Chen, and H. Zhang, "Flexible and Highly Photosensitive Electrolyte-Gated Organic Transistors with Ionogel/Silver Nanowire Membranes," *ACS applied materials & interfaces,* vol. 9, no. 21, p. 18134, 2017.

[120] P. Balakrishna Pillai, A. Kumar, X. Song, and M. M. De Souza, "Diffusion-controlled faradaic charge storage in high-performance solid electrolyte-gated zinc oxide thin-film transistors," *ACS applied materials & interfaces,* vol. 10, no. 11, p. 9782, 2018.

[121] F. Zare Bidoky, B. Tang, R. Ma, K. S. Jochem, W. J. Hyun, D. Song, S. J. Koester, T. P. Lodge, and C. D. Frisbie, "Sub-3 V ZnO electrolyte-gated transistors and circuits with screen-printed and photo-crosslinked ion gel gate dielectrics: new routes to improved performance," *Advanced Functional Materials,* vol. 30, no. 20, p. 1902028, 2020.

[122] X. Meng, I. Valitova, C. Santato, and F. Cicoira, "Tin dioxide ion-gated transistors," in *Tin Oxide Materials*, M. O. Orlandi, Ed.: Elsevier, 2020, ch. 16, p. 477.

[123] H. W. Son, J. H. Park, M.-S. Chae, B.-H. Kim, and T. G. Kim, "Bilayer indium gallium zinc oxide electrolyte-gated field-effect transistor for biosensor platform with high reliability," *Sensors and Actuators B: Chemical,* vol. 312, p. 127955, 2020.

[124] H. J. Nam, J. Cha, S. H. Lee, W. J. Yoo, and D.-Y. Jung, "A new mussel-inspired polydopamine phototransistor with high photosensitivity: signal amplification and light-controlled switching properties," *Chemical Communications,* vol. 50, no. 12, p. 1458, 2014.

[125] Y. Zhang, Y. Yuan, and J. Huang, "Detecting 100 fW cm− 2 light with trapped electron gated organic phototransistors," *Advanced Materials,* vol. 29, no. 5, p. 1603969, 2017.

[126] Z. A. Lamport, H. F. Haneef, S. Anand, M. Waldrip, and O. D. Jurchescu, "Tutorial: organic field-effect transistors: materials, structure and operation," *Journal of Applied Physics,* vol. 124, no. 7, p. 071101, 2018.

[127] H. Xu, J. Liu, J. Zhang, G. Zhou, N. Luo, and N. Zhao, "Flexible organic/inorganic hybrid near-infrared photoplethysmogram sensor for cardiovascular monitoring," *Advanced Materials,* vol. 29, no. 31, p. 1700975, 2017.

[128] J. Huang, J. Du, Z. Cevher, Y. Ren, X. Wu, and Y. Chu, "Printable and flexible phototransistors based on blend of organic semiconductor and biopolymer," *Advanced functional materials,* vol. 27, no. 9, p. 1604163, 2017.

[129] G. Wang, K. Huang, Z. Liu, Y. Du, X. Wang, H. Lu, G. Zhang, and L. Qiu, "Flexible, Low-Voltage, and n-Type Infrared Organic Phototransistors with Enhanced Photosensitivity via Interface Trapping Effect," *ACS applied materials & interfaces,* vol. 10, no. 42, p. 36177, 2018.

[130] L. Q. Guo, H. Han, L. Q. Zhu, Y. B. Guo, F. Yu, Z. Y. Ren, H. Xiao, Z. Y. Ge, and J. N. Ding, "Oxide Neuromorphic Transistors Gated by Polyvinyl Alcohol Solid Electrolytes with Ultralow Power Consumption," *ACS applied materials & interfaces,* vol. 11, no. 31, p. 28352, 2019.

[131] L. Kergoat, B. Piro, M. Berggren, G. Horowitz, and M.-C. Pham, "Advances in organic transistor-based biosensors: from organic electrochemical transistors to electrolyte-gated organic field-effect transistors," *Analytical and bioanalytical chemistry,* vol. 402, no. 5, p. 1813, 2012.

[132] M. Kim, S. U. Ryu, S. A. Park, K. Choi, T. Kim, D. Chung, and T. Park, "Donor–acceptor-conjugated polymer for high-performance organic field-effect transistors: a progress report," *Advanced Functional Materials,* vol. 30, no. 20, p. 1904545, 2020.

[133] H. R. Tseng, H. Phan, C. Luo, M. Wang, L. A. Perez, S. N. Patel, L. Ying, E. J. Kramer, T. Q. Nguyen, and G. C. Bazan, "High-mobility field-effect transistors fabricated with macroscopic aligned semiconducting polymers," *Advanced Materials,* vol. 26, no. 19, p. 2993, 2014.

[134] Y. Hu, Z. D. Rengert, C. McDowell, M. J. Ford, M. Wang, A. Karki, A. T. Lill, G. C. Bazan, and T.-Q. Nguyen, "Doping polymer semiconductors by organic salts: Toward high-performance solution-processed organic field-effect transistors," *ACS nano,* vol. 12, no. 4, p. 3938, 2018.

[135] Y. Park, J. W. Jung, H. Kang, J. Seth, Y. Kang, and M. M. Sung, "Single-Crystal Poly [4-(4, 4-dihexadecyl-4H-cyclopenta [1, 2-b: 5, 4-b′] dithiophen-2-yl)-alt-[1, 2, 5] thiadiazolo [3, 4-c] pyridine] Nanowires with Ultrahigh Mobility," *Nano letters,* vol. 19, no. 2, p. 1028, 2019.

[136] B. H. Lee, B. B. Hsu, S. N. Patel, J. Labram, C. Luo, G. C. Bazan, and A. J. Heeger, "Flexible organic transistors with controlled nanomorphology," *Nano letters,* vol. 16, no. 1, p. 314, 2016.

[137] X. Wu, S. Lan, D. Hu, Q. Chen, E. Li, Y. Yan, H. Chen, and T. Guo, "High performance flexible multilevel optical memory based on a vertical organic field effect transistor with ultrashort channel length," *Journal of Materials Chemistry C,* vol. 7, no. 30, p. 9229, 2019.

[138] H. Tang, P. Kumar, S. Zhang, Z. Yi, G. D. Crescenzo, C. Santato, F. Soavi, and F. Cicoira, "Conducting polymer transistors making use of activated carbon gate electrodes," *ACS applied materials & interfaces,* vol. 7, no. 1, p. 969, 2015.

[139] D. M. Tartakovsky and M. Dentz, "Diffusion in porous media: phenomena and mechanisms," *Transport in Porous Media,* vol. 130, no. 1, p. 105, 2019.

[140] R. Williams and A. M. Goodman, "Wetting of thin layers of SiO2 by water," *Applied Physics Letters,* vol. 25, no. 10, p. 531, 1974.

[141] C. F. Soon, W. I. W. Omar, N. Nayan, H. Basri, M. B. Narawi, and K. S. Tee, "A bespoke contact angle measurement software and experimental setup for determination of surface tension," *Procedia Technology,* vol. 11, p. 487, 2013.

[142] J. B. Allen and R. F. Larry, *Electrochemical methods fundamentals and applications*. John Wiley & Sons, 2001.

[143] Y. Xia, J. H. Cho, J. Lee, P. P. Ruden, and C. D. Frisbie, "Comparison of the mobility–carrier density relation in polymer and single-crystal organic transistors employing vacuum and liquid gate dielectrics," *Advanced Materials,* vol. 21, no. 21, p. 2174, 2009.

[144] J. H. Cho, J. Lee, Y. Xia, B. Kim, Y. He, M. J. Renn, T. P. Lodge, and C. D. Frisbie, "Printable ion-gel gate dielectrics for low-voltage polymer thin-film transistors on plastic," *Nature materials,* vol. 7, no. 11, p. 900, 2008.

[145] D. Braga, N. C. Erickson, M. J. Renn, R. J. Holmes, and C. D. Frisbie, "High-transconductance organic thin-film electrochemical transistors for driving low-voltage red-green-blue active matrix organic light-emitting devices," *Advanced functional materials,* vol. 22, no. 8, p. 1623, 2012.

[146] H. Sun, M. Vagin, S. Wang, X. Crispin, R. Forchheimer, M. Berggren, and S. Fabiano, "Complementary Logic Circuits Based on High-Performance n-Type Organic Electrochemical Transistors," *Advanced Materials,* vol. 30, no. 9, p. 1704916, 2018.

[147] T. Han, M. Shou, L. Liu, Z. Xie, L. Ying, C. Jiang, H. Wang, M. Yao, H. Deng, and G. Jin, "Ultrahigh photosensitive organic phototransistors by photoelectric dual control," *Journal of Materials Chemistry C,* vol. 7, no. 16, p. 4725, 2019.

[148] X. Ren, F. Yang, X. Gao, S. Cheng, X. Zhang, H. Dong, and W. Hu, "Organic Field-Effect Transistor for Energy-Related Applications: Low-Power-Consumption Devices, Near-Infrared Phototransistors, and Organic Thermoelectric Devices," *Advanced Energy Materials,* vol. 8, no. 24, p. 1801003, 2018.

[149] N. Wang, A. Yang, Y. Fu, Y. Li, and F. Yan, "Functionalized organic thin film transistors for biosensing," *Accounts of Chemical Research,* vol. 52, no. 2, p. 277, 2019.

[150] H. Ling, D. A. Koutsouras, S. Kazemzadeh, Y. Van De Burgt, F. Yan, and P. Gkoupidenis, "Electrolyte-gated transistors for synaptic electronics, neuromorphic computing, and adaptable biointerfacing," *Applied Physics Reviews,* vol. 7, no. 1, p. 011307, 2020.

[151] A. Doumbia, J. Tong, R. J. Wilson, and M. L. Turner, "Investigation of the Performance of Donor–Acceptor Conjugated Polymers in Electrolyte-Gated Organic Field-Effect Transistors," *Advanced Electronic Materials,* vol. 7, no. 9, p. 2100071, 2021.

[152] A. Subramanian, M. Azimi, C. Y. Leong, S. L. Lee, C. Santato, and F. Cicoira, "Solution-Processed Titanium Dioxide Ion-Gated Transistors and Their Application for pH Sensing," *Frontiers in Electronics,* vol. 3, p. 813535, 2022.

[153] Z. Liu, Z. Yin, J. Wang, and Q. Zheng, "Polyelectrolyte dielectrics for flexible low-voltage organic thin-film transistors in highly sensitive pressure sensing," *Advanced functional materials,* vol. 29, no. 1, p. 1806092, 2019.

[154] M. Azimi, A. Subramanian, N. A. Roslan, and F. Cicoira, "Flexible organic ion-gated transistors with low operating voltage and light-sensing application," *Journal of Physics: Materials,* vol. 4, no. 2, p. 024001, 2021.

[155] A. Subramanian, M. Azimi, C. Santato, and F. Cicoira, "Combining Aqueous Solution Processing and Printing for Fabrication of Flexible and Sustainable Tin Dioxide Ion-Gated Transistors," *Advanced Materials Technologies,* vol. 7, no. 2, p. 2100843, 2022.

[156] Q. Zhang, F. Leonardi, R. Pfattner, and M. Mas-Torrent, "A Solid-State Aqueous Electrolyte-Gated Field-Effect Transistor as a Low-Voltage Operation Pressure-Sensitive Platform," *Advanced Materials Interfaces,* vol. 6, no. 16, p. 1900719, 2019.

[157] C. G. Bischak, L. Q. Flagg, and D. S. Ginger, "Ion exchange gels allow organic electrochemical transistor operation with hydrophobic polymers in aqueous solution," *Advanced Materials,* vol. 32, no. 32, p. 2002610, 2020.

[158] Y. J. Jo, J. Ok, S. Y. Kim, and T. i. Kim, "Stretchable and soft organic–ionic devices for body-integrated electronic systems," *Advanced Materials Technologies,* vol. 7, no. 2, p. 2001273, 2022.

[159] H. Lee, S. Lee, W. Lee, T. Yokota, K. Fukuda, and T. Someya, "Ultrathin organic electrochemical transistor with nonvolatile and thin gel electrolyte for long-term electrophysiological monitoring," *Advanced functional materials,* vol. 29, no. 48, p. 1906982, 2019.

[160] A. Campos, S. Riera-Galindo, J. Puigdollers, and M. Mas-Torrent, "Reduction of charge traps and stability enhancement in solution-processed organic field-effect transistors based on a blended n-type semiconductor," *ACS Applied Materials & Interfaces,* vol. 10, no. 18, p. 15952, 2018.

[161] Q. Zhang, F. Leonardi, S. Casalini, I. Temiño, and M. Mas-Torrent, "High performing solution-coated electrolyte-gated organic field-effect transistors for aqueous media operation," *Scientific reports,* vol. 6, no. 1, p. 1, 2016.

[162] S. Thiemann, S. Sachnov, S. Porscha, P. Wasserscheid, and J. Zaumseil, "Ionic liquids for electrolyte-gating of ZnO field-effect transistors," *The Journal of Physical Chemistry C,* vol. 116, no. 25, p. 13536, 2012.

[163] G. Karimi, X. Li, and P. Teertstra, "Measurement of through-plane effective thermal conductivity and contact resistance in PEM fuel cell diffusion media," *Electrochimica Acta,* vol. 55, no. 5, p. 1619, 2010.

[164] K. H. Seol, S. J. Lee, K. G. Cho, K. Hong, and K. H. Lee, "Highly conductive, binary ionic liquid–solvent mixture ion gels for effective switching of electrolyte-gated transistors," *Journal of Materials Chemistry C,* vol. 6, no. 41, p. 10987, 2018.

[165] Y. Xia, J. Cho, B. Paulsen, C. D. Frisbie, and M. J. Renn, "Correlation of on-state conductance with referenced electrochemical potential in ion gel gated polymer transistors," *Applied Physics Letters,* vol. 94, no. 1, p. 4, 2009.

[166] A. Di Bartolomeo, L. Genovese, F. Giubileo, L. Iemmo, G. Luongo, T. Foller, and M. Schleberger, "Hysteresis in the transfer characteristics of MoS2 transistors," *2D Materials,* vol. 5, no. 1, p. 015014, 2017.

[167] P. Ghamari, M. R. Niazi, and D. F. Perepichka, "Controlling Structural and Energetic Disorder in High-Mobility Polymer Semiconductors via Doping with Nitroaromatics," *Chemistry of Materials,* vol. 33, no. 8, p. 2937, 2021.

[168] Y. Lei, B. Wu, W.-K. E. Chan, F. Zhu, and B. S. Ong, "Engineering gate dielectric surface properties for enhanced polymer field-effect transistor performance," *Journal of Materials Chemistry C,* vol. 3, no. 47, p. 12267, 2015.

[169] Y. Zhang, W. Liu, Y. Liu, C. Wang, G. Zhu, and W. Song, "Directly written DPP-DTT/SrTiO 3 organic/inorganic heterojunctions for anisotropic self-powered photodetectors," *Journal of Materials Chemistry C,* vol. 9, no. 43, p. 15654, 2021.

[170] A. Allison and H. Andreas, "Minimizing the Nyquist-plot semi-circle of pseudocapacitive manganese oxides through modification of the oxide-substrate interface resistance," *Journal of Power Sources,* vol. 426, p. 93, 2019.

[171] M. Singh, K. Manoli, A. Tiwari, T. Ligonzo, C. Di Franco, N. Cioffi, G. Palazzo, G. Scamarcio, and L. Torsi, "The double layer capacitance of ionic liquids for electrolyte gating of ZnO thin film transistors and effect of gate electrodes," *Journal of Materials Chemistry C,* vol. 5, no. 14, p. 3509, 2017.

[172] J. Kang, J. Wen, S. H. Jayaram, A. Yu, and X. Wang, "Development of an equivalent circuit model for electrochemical double layer capacitors (EDLCs) with distinct electrolytes," *Electrochimica Acta,* vol. 115, p. 587, 2014.

[173] X. Wang, C. Gong, D. He, Z. Xue, C. Chen, Y. Liao, and X. Xie, "Gelled microporous polymer electrolyte with low liquid leakage for lithium-ion batteries," *Journal of Membrane Science,* vol. 454, p. 298, 2014.

[174] A. F. Visentin and M. J. Panzer, "Poly (ethylene glycol) diacrylate-supported ionogels with consistent capacitive behavior and tunable elastic response," *ACS Applied Materials & Interfaces,* vol. 4, no. 6, p. 2836, 2012.

[175] B. Nketia-Yawson, G. D. Tabi, and Y.-Y. Noh, "Polymer electrolyte blend gate dielectrics for high-performance ultrathin organic transistors: toward favorable polymer blend miscibility and reliability," *ACS Applied Materials & Interfaces,* vol. 11, no. 19, p. 17610, 2019.

[176] G. Tarabella, C. Santato, S. Y. Yang, S. Iannotta, G. G. Malliaras, and F. Cicoira, "Effect of the gate electrode on the response of organic electrochemical transistors," *Applied physics letters,* vol. 97, no. 12, p. 205, 2010.

[177] B. Pal, S. Yang, S. Ramesh, V. Thangadurai, and R. Jose, "Electrolyte selection for supercapacitive devices: A critical review," *Nanoscale Advances,* vol. 1, no. 10, p. 3807, 2019.

[178] J. B. Segur and H. E. Oberstar, "Viscosity of glycerol and its aqueous solutions," *Industrial & Engineering Chemistry,* vol. 43, no. 9, p. 2117, 1951.

[179] M. B. A. Rahman, K. Jumbri, M. Basri, E. Abdulmalek, K. Sirat, and A. B. Salleh, "Synthesis and physico-chemical properties of new tetraethylammonium-based amino acid chiral ionic liquids," *Molecules,* vol. 15, no. 4, p. 2388, 2010.

[180] M. Di Lauro, M. Berto, M. Giordani, S. Benaglia, G. Schweicher, D. Vuillaume, C. A. Bortolotti, Y. H. Geerts, and F. Biscarini, "Liquid-Gated Organic Electronic Devices Based on High-Performance Solution-Processed Molecular Semiconductor," *Advanced Electronic Materials,* vol. 3, no. 9, p. 1700159, 2017.

[181] K.-J. Baeg, D. Khim, D.-Y. Kim, J. B. Koo, I.-K. You, W. San Choi, and Y.-Y. Noh, "High mobility top-gated poly (3-hexylthiophene) field-effect transistors with high work-function Pt electrodes," *Thin Solid Films,* vol. 518, no. 14, p. 4024, 2010.

[182] C. Santato, F. Cicoira, P. Cosseddu, A. Bonfiglio, P. Bellutti, M. Muccini, R. Zamboni, F. Rosei, A. Mantoux, and P. Doppelt, "Organic light-emitting transistors using concentric source/drain electrodes on a molecular adhesion layer," *Applied physics letters,* vol. 88, no. 16, p. 163511, 2006.

[183] R. Morais, D. H. Vieira, M. dos Santos Klem, C. Gaspar, L. Pereira, R. Martins, and N. Alves, "Printed in-plane electrolyte-gated transistor based on zinc oxide," *Semiconductor Science and Technology,* vol. 37, no. 3, p. 035007, 2022.

[184] B. Nketia-Yawson, G. D. Tabi, J. W. Jo, and Y. Y. Noh, "Solid-State Electrolyte Dielectrics Based on Exceptional High-k P (VDF-TrFE-CTFE) Terpolymer for High-Performance Field-Effect Transistors," *Advanced Materials Interfaces,* vol. 7, no. 17, p. 2000842, 2020.

[185] N. Delavari, K. Tybrandt, M. Berggren, B. Piro, V. Noël, G. Mattana, and I. Zozoulenko, "Nernst–Planck–Poisson analysis of electrolyte-gated organic field-effect transistors," *Journal of Physics D: Applied Physics,* vol. 54, no. 41, p. 415101, 2021.

[186] S. J. Lee, K. G. Cho, S.-H. Jung, S. Kim, J.-K. Lee, and K. H. Lee, "High-Mobility Low-Hysteresis Electrolyte-Gated Transistors with a DPP-Benzotriazole Copolymer Semiconductor," *Macromolecular Research,* vol. 28, no. 7, p. 683, 2020.

[187] S. H. Kim, K. Hong, K. H. Lee, and C. D. Frisbie, "Performance and stability of aerosol-jet-printed electrolyte-gated transistors based on poly (3-hexylthiophene)," *ACS Applied Materials & Interfaces,* vol. 5, no. 14, p. 6580, 2013.

[188] V. Kaphle, S. Liu, C. M. Keum, and B. Lüssem, "Organic electrochemical transistors based on room temperature ionic liquids: performance and stability," *physica status solidi (a),* vol. 215, no. 24, p. 1800631, 2018.

[189] M. J. Panzer and C. D. Frisbie, "Polymer electrolyte-gated organic field-effect transistors: Low-voltage, high-current switches for organic electronics and testbeds for probing electrical transport at high charge carrier density," *Journal of the American Chemical Society,* vol. 129, no. 20, p. 6599, 2007.

[190] O. Bae and F. S. Kim, "Flexible Organic Electrolyte-Gated Transistors Based on Thin Polymer Blend Films of Crystalline C8-BTBT and Amorphous PTAA," *Macromolecular Research,* vol. 28, no. 7, p. 677, 2020.

[191] K. Hong, D. H. Choo, H. J. Lee, J. Y. Park, and J.-L. Lee, "Substrate-free, stretchable electrolyte gated transistors," *Organic Electronics,* vol. 87, p. 105936, 2020.

[192] C. C. Shih, W. Y. Lee, C. Lu, H. C. Wu, and W. C. Chen, "Enhancing the Mechanical Durability of an Organic Field Effect Transistor through a Fluoroelastomer Substrate with a Crosslinking-Induced Self-Wrinkled Structure," *Advanced Electronic Materials,* vol. 3, no. 5, p. 1600477, 2017.

[193] Y. Chen, X. Zhuang, E. A. Goldfine, V. P. Dravid, M. J. Bedzyk, W. Huang, A. Facchetti, and T. J. Marks, "Printable Organic-Inorganic Nanoscale Multilayer Gate Dielectrics for Thin-Film Transistors Enabled by a Polymeric Organic Interlayer," *Advanced Functional Materials,* vol. 30, no. 40, p. 2005069, 2020.

[194] M. Braendlein, T. Lonjaret, P. Leleux, J. M. Badier, and G. G. Malliaras, "Voltage amplifier based on organic electrochemical transistor," *Advanced science,* vol. 4, no. 1, p. 1600247, 2017.

[195] J. Pas, C. Pitsalidis, D. A. Koutsouras, P. P. Quilichini, F. Santoro, B. Cui, L. Gallais, R. P. O'Connor, G. G. Malliaras, and R. M. Owens, "Neurospheres on patterned PEDOT: PSS microelectrode arrays enhance electrophysiology recordings," *Advanced Biosystems,* vol. 2, no. 1, p. 1700164, 2018.

[196] S. Pecqueur, M. Mastropasqua Talamo, D. Guérin, P. Blanchard, J. Roncali, D. Vuillaume, and F. Alibart, "Neuromorphic time-dependent pattern classification with organic electrochemical transistor arrays," *Advanced Electronic Materials,* vol. 4, no. 9, p. 1800166, 2018.

[197] M. Braendlein, A. M. Pappa, M. Ferro, A. Lopresti, C. Acquaviva, E. Mamessier, G. G. Malliaras, and R. M. Owens, "Lactate detection in tumor cell cultures using organic transistor circuits," *Advanced Materials,* vol. 29, no. 13, p. 1605744, 2017.

[198] Y. Liang, T. Guo, L. Zhou, A. Offenhäusser, and D. Mayer, "Label-free split aptamer sensor for femtomolar detection of dopamine by means of flexible organic electrochemical transistors," *Materials,* vol. 13, no. 11, p. 2577, 2020.

[199] J. Rivnay, S. Inal, A. Salleo, R. M. Owens, M. Berggren, and G. G. Malliaras, "Organic electrochemical transistors," *Nature Reviews Materials,* vol. 3, no. 2, p. 1, 2018.

[200] Y. Li, X. Li, S. Zhang, L. Liu, N. Hamad, S. R. Bobbara, D. Pasini, and F. Cicoira, "Autonomic self-healing of PEDOT: PSS achieved via polyethylene glycol addition," *Advanced Functional Materials,* vol. 30, no. 30, p. 2002853, 2020.

[201] Y. Li, S. Zhang, N. Hamad, K. Kim, L. Liu, M. Lerond, and F. Cicoira, "Tailoring the Self-Healing Properties of Conducting Polymer Films," *Macromolecular Bioscience,* vol. 20, no. 11, p. 2000146, 2020.

[202] S. Zhang, E. Hubis, G. Tomasello, G. Soliveri, P. Kumar, and F. Cicoira, "Patterning of stretchable organic electrochemical transistors," *Chemistry of Materials,* vol. 29, no. 7, p. 3126, 2017.

[203] S. Zhang, E. Hubis, C. Girard, P. Kumar, J. DeFranco, and F. Cicoira, "Water stability and orthogonal patterning of flexible micro-electrochemical transistors on plastic," *Journal of Materials Chemistry C,* vol. 4, no. 7, p. 1382, 2016.

[204] V. Kaphle, S. Liu, A. Al-Shadeedi, C. M. Keum, and B. Lüssem, "Contact resistance effects in highly doped organic electrochemical transistors," *Advanced Materials,* vol. 28, no. 39, p. 8766, 2016.

[205] X. Wu, M. Stephen, T. C. Hidalgo, T. Salim, J. Surgailis, A. Surendran, X. Su, T. Li, S. Inal, and W. L. Leong, "Ionic-Liquid Induced Morphology Tuning of PEDOT: PSS for High-Performance Organic Electrochemical Transistors," *Advanced Functional Materials,* vol. 32, no. 1, p. 2108510, 2022.

[206] L. Wang, Q. Sun, L. Zhang, J. Wang, G. Ren, L. Yu, K. Wang, Y. Zhu, G. Lu, and H. D. Yu, "Realizing Ultrahigh Transconductance in Organic Electrochemical Transistor by Co-Doping PEDOT: PSS with Ionic Liquid and Dodecylbenzenesulfonate," *Macromolecular Rapid Communications,* vol. 43, no. 17, p. 2200212, 2022.

[207] P. D'Angelo, S. L. Marasso, A. Verna, A. Ballesio, M. Parmeggiani, A. Sanginario, G. Tarabella, D. Demarchi, C. F. Pirri, and M. Cocuzza, "Scaling organic electrochemical transistors down to nanosized channels," *Small,* vol. 15, no. 41, p. 1902332, 2019.

[208] J. Kawahara, P. A. Ersman, K. Katoh, and M. Berggren, "Fast-switching printed organic electrochemical transistors including electronic vias through plastic and paper substrates," *IEEE transactions on electron devices,* vol. 60, no. 6, p. 2052, 2013.

[209] X. Luan, J. Liu, and H. Li, "Electrolyte-gated vertical organic transistor and circuit," *The Journal of Physical Chemistry C,* vol. 122, no. 26, p. 14615, 2018.

[210] D. B. Shah, K. R. Olson, A. Karny, S. J. Mecham, J. M. DeSimone, and N. P. Balsara, "Effect of anion size on conductivity and transference number of perfluoroether electrolytes with lithium salts," *Journal of The Electrochemical Society,* vol. 164, no. 14, p. A3511, 2017.

[211] S. Yamamoto, A. G. Polyravas, S. Han, and G. G. Malliaras, "Correlation between Transient Response and Neuromorphic Behavior in Organic Electrochemical Transistors," *Advanced Electronic Materials,* vol. 8, no. 4, p. 2101186, 2022.

[212] T. Nguyen-Dang, K. Harrison, A. Lill, A. Dixon, E. Lewis, J. Vollbrecht, T. Hachisu, S. Biswas, Y. Visell, and T. Q. Nguyen, "Biomaterial-Based Solid-Electrolyte Organic Electrochemical Transistors for Electronic and Neuromorphic Applications," *Advanced Electronic Materials,* vol. 7, no. 12, p. 2100519, 2021.

[213] H. Yang and N. Wu, "Ionic conductivity and ion transport mechanisms of solid-state lithium-ion battery electrolytes: A review," *Energy Science & Engineering,* vol. 10, no. 5, p. 1643, 2022.

[214] H. Zhang, H. Xia, and Y. Zhao, "Poly (vinyl alcohol) hydrogel can autonomously self-heal," *ACS Macro Letters,* vol. 1, no. 11, p. 1233, 2012.

[215] Y. Wu, Y. Li, Y. Wang, Q. Liu, Q. Chen, and M. Chen, "Advances and prospects of PVDF based polymer electrolytes," *Journal of Energy Chemistry,* vol. 64, p. 62, 2022.

[216] J. Fan, C. Montemagno, and M. Gupta, "3D printed high transconductance organic electrochemical transistors on flexible substrates," *Organic Electronics,* vol. 73, p. 122, 2019.

[217] S. Demuru, C.-H. Huang, K. Parvez, R. Worsley, G. Mattana, B. Piro, V. Noël, C. Casiraghi, and D. Briand, "All-Inkjet-Printed Graphene-Gated Organic Electrochemical Transistors on Polymeric Foil as Highly Sensitive Enzymatic Biosensors," *ACS Applied Nano Materials,* vol. 5, no. 1, p. 1664, 2022.

[218] M. Zabihipour, D. Tu, J. Strandberg, M. Berggren, I. Engquist, and P. Andersson Ersman, "Designing Inverters Based on Screen Printed Organic Electrochemical Transistors Targeting Low-Voltage and High-Frequency Operation," *Advanced Materials Technologies,* vol. 6, no. 12, p. 2100555, 2021.

[219] M. Sensi, G. Migatti, V. Beni, T. M. D'Alvise, T. Weil, M. Berto, P. Greco, C. Imbriano, F. Biscarini, and C. A. Bortolotti, "Monitoring DNA Hybridization with Organic Electrochemical Transistors Functionalized with Polydopamine," *Macromolecular Materials and Engineering,* vol. 307, no. 5, p. 2100880, 2022.

[220] L. S. McCarty and G. M. Whitesides, "Electrostatic charging due to separation of ions at interfaces: contact electrification of ionic electrets," *Angewandte Chemie International Edition,* vol. 47, no. 12, p. 2188, 2008.

[221] V. Lockett, R. Sedev, J. Ralston, M. Horne, and T. Rodopoulos, "Differential capacitance of the electrical double layer in imidazolium-based ionic liquids: influence of potential, cation size, and temperature," *The Journal of Physical Chemistry C,* vol. 112, no. 19, p. 7486, 2008.

[222] M. Saito, S. Kawaharasaki, K. Ito, S. Yamada, K. Hayamizu, and S. Seki, "Strategies for fast ion transport in electrochemical capacitor electrolytes from diffusion coefficients, ionic conductivity, viscosity, density and interaction energies based on HSAB theory," *RSC advances,* vol. 7, no. 24, p. 14528, 2017.

[223] K. Tang, W. Miao, and S. Guo, "Crosslinked PEDOT: PSS organic electrochemical transistors on interdigitated electrodes with improved stability," *ACS Applied Polymer Materials,* vol. 3, no. 3, p. 1436, 2021.

[224] H. Huang, C. Ge, Z. Liu, H. Zhong, E. Guo, M. He, C. Wang, G. Yang, and K. Jin, "Electrolyte-gated transistors for neuromorphic applications," *Journal of Semiconductors,* vol. 42, no. 1, p. 013103, 2021.

[225] C. Eckel, J. Lenz, A. Melianas, A. Salleo, and R. T. Weitz, "Nanoscopic electrolyte-gated vertical organic transistors with low operation voltage and five orders of magnitude switching range for neuromorphic systems," *Nano Letters,* vol. 22, no. 3, p. 973, 2022.

[226] D. Wang, V. Noël, and B. Piro, "Electrolytic gated organic field-effect transistors for application in biosensors—A Review," *Electronics,* vol. 5, no. 1, p. 9, 2016.

[227] H. Liu, D. Liu, J. Yang, H. Gao, and Y. Wu, "Flexible Electronics Based on Organic Semiconductors: from Patterned Assembly to Integrated Applications," *Small,* vol. 19, no. 11, p. 2206938, 2023.

APPENDIX A SUPPLEMENTARY INFORMATION FOR ARTICLE 1 : FLEXIBLE ORGANIC ION-GATED TRANSISTOR WITH LOW OPERATING VOLTAGE AND LIGHT-SENSING APPLICATION

*Mona Azimi[1], Arunprabaharan Subramanian[1], Nur Adilah Roslan[2], Fabio Cicoira[1]**

[1] Polytechnique Montréal, Department of Chemical Engineering, H3T 1J4, Canada.

[2] Department of Physics, University of Malaya, 50603, Kuala Lumpur, Malaysia

* Corresponding author: fabio.cicoira@polymtl.ca

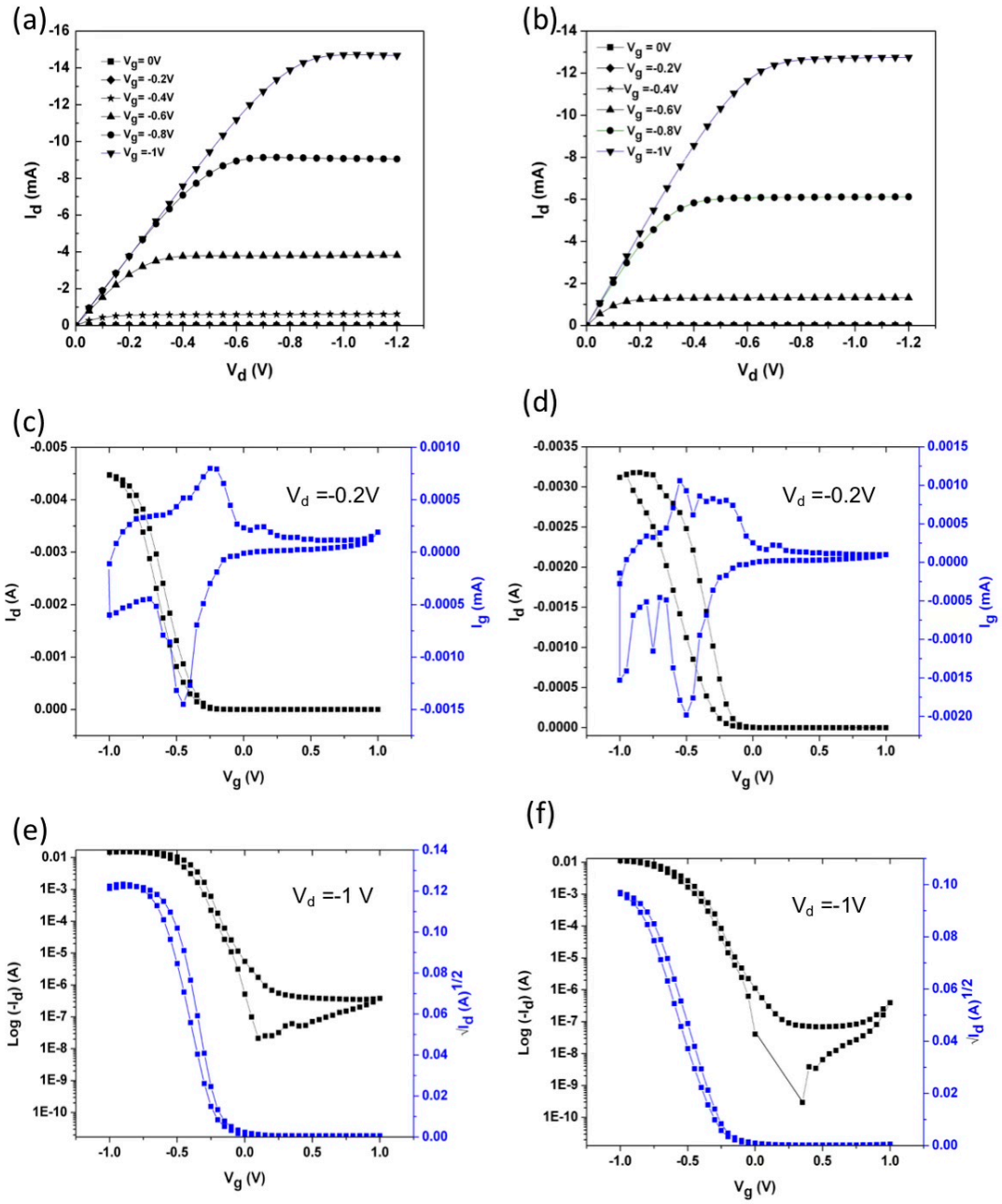

Figure S1. Output (a,b) and transfer curves in linear region (V_d= -0.2 V) (c,d) and transfer curves in saturation region(V_d= -1 V)(e,f) for two [EMIM][TFSI] gated PCDTPT transistors fabricated on SiO_2/Si substrate and measured in N_2-purged glovebox (O_2 and H_2O < 3 ppm) with a scan rate of 50 mV/s.

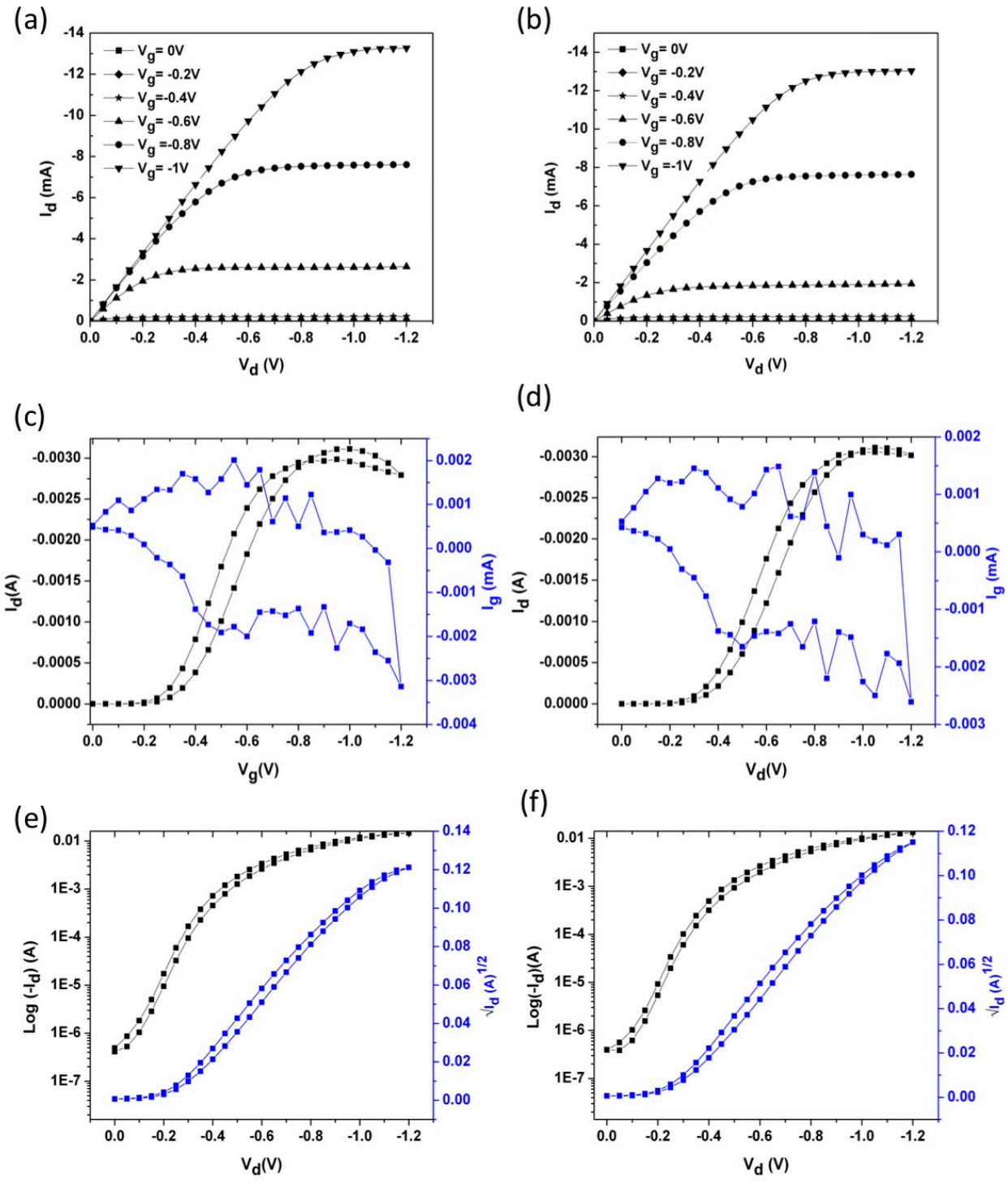

Figure S2. Figure S1. Output (a,b) and transfer curves in linear region (V_d= -0.2 V) (c,d) and transfer curves in saturation region(V_d= -1 V)(e,f) for two [EMIM][TFSI] gated PCDTPT transistors fabricated on PI substrate and measured in N_2-purged glovebox (O_2 and H_2O < 3 ppm) with a scan rate of 50 mV/s.

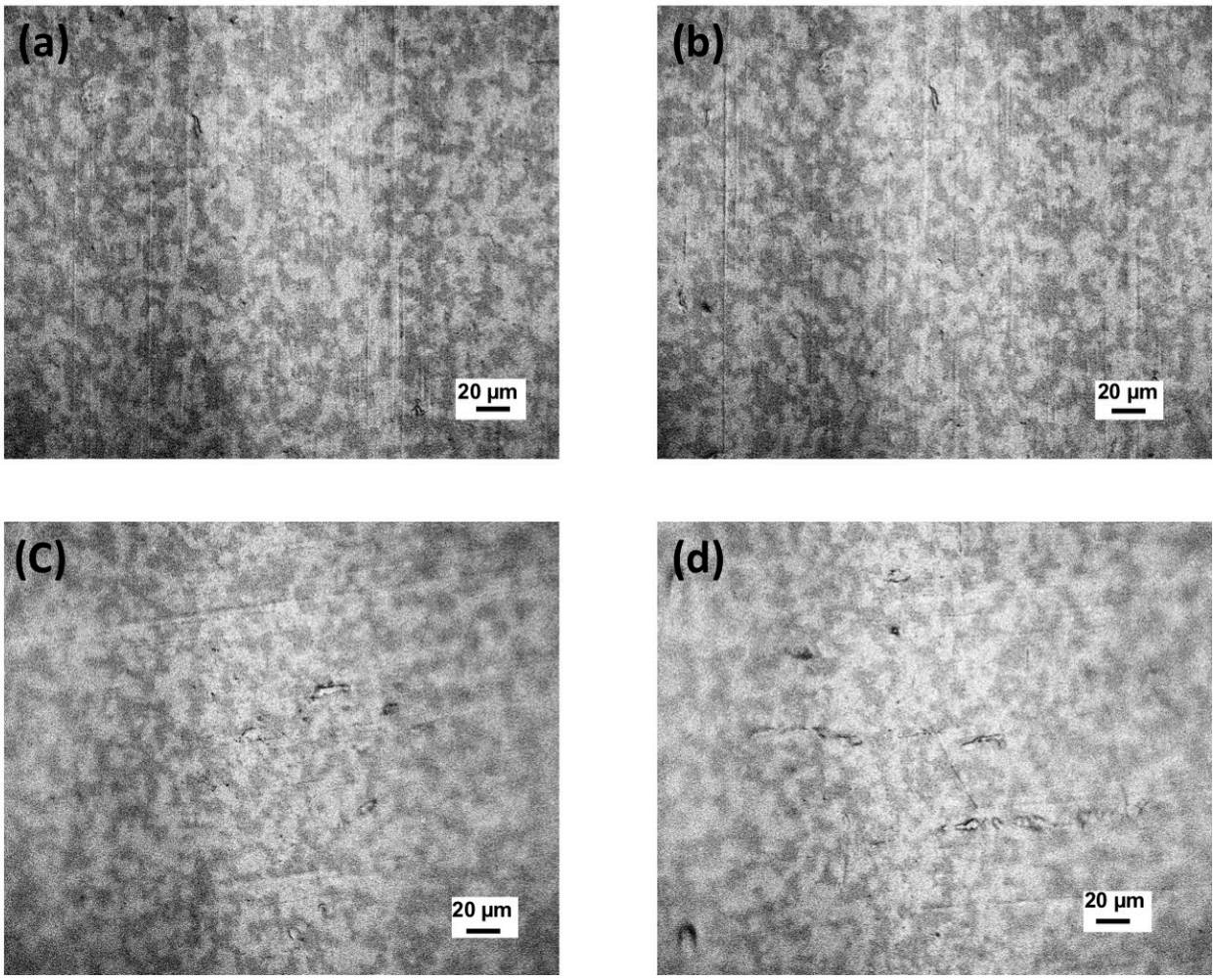

Figure S3. Optical microscopy images of PCDTPT film on PI substrate bended for 1 time(a), 10 times(b), 100 times (c), 1000 times(d).

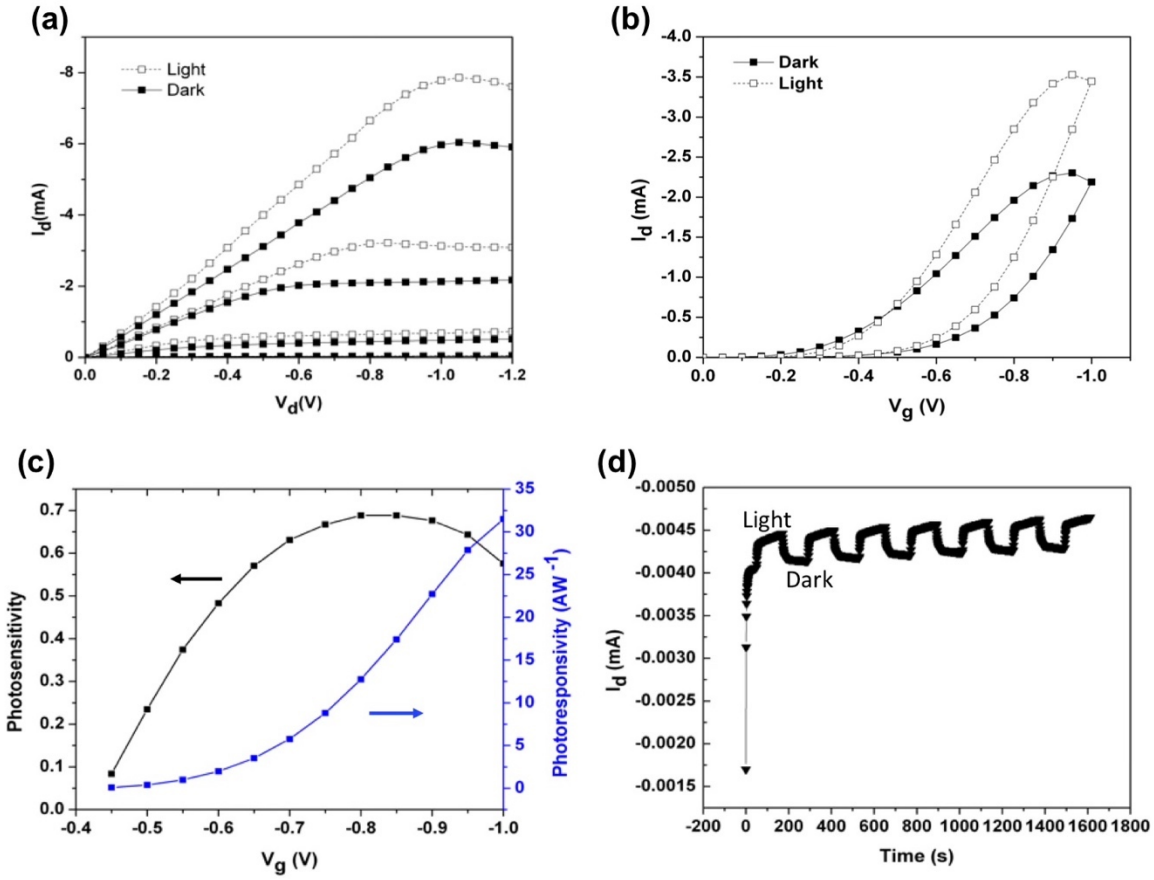

Figure S4. Output characteristic of phototransistor fabricated on SiO_2/Si substrate at V_g = -1, -0.8, -0.6, -0.4 V in dark and under solar simulator light in vacuum condition (a), transfer characteristic at V_d = -0.5 V in dark and light condition (b), photosensitivity and photoresponsivity curves versus gate voltage at V_d = -0.5 V(c), and dynamic photoresponse behavior at V_g = -0.2 V and V_d = -0.2V (d).

APPENDIX B SUPPLEMENTARY INFORMATION FOR ARTICLE 2 : ELECTRICAL AND MECHANICAL STABILITY OF FLEXIBLE, ORGANIC ELECTROLYTE-GATED TRANSISTORS BASED ON ION GEL AND HYDROGELS

Mona Azimi[1], Arunprabaharan Subramanian[1], Jiaxin Fan[1], Francesca Soavi[2] and Fabio Cicoira[*1]

[1] Department of Chemical Engineering, Polytechnique Montréal, H3T 1J4, Montreal, Canada.

[2] Dipartimento di Chimica "Giacomo Ciamician", Università di Bologna, Via Selmi 2, Bologna 40126, Italy.

* Corresponding author: fabio.cicoira@polymtl.ca

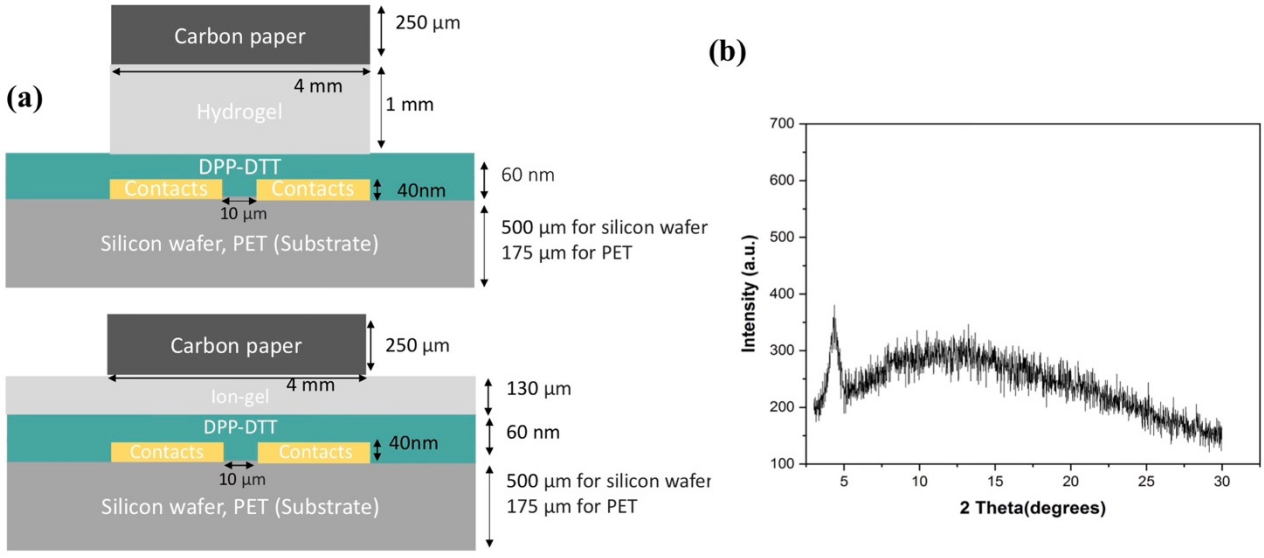

Figure S1. Side view of structure of EGTs (a) using hydrogel gating media (top) and ion-gel gating media (bottom), XRD Pattern of spin coated DPP-DTT film on Si/SiO_2 substrate (b).

Table S1. Specific capacitance of reported MIM structures with different electrolytes.

Gel	**MIM structure**	**Specific capacitance ($\mu F\ cm^{-2}$)**	**Ref**
Biocampatible and biodegradable ionic gel ([CH][MA]:Levan[a])	Dry casting of gel on SUS stainless steel coin cell electrode (diameter:	1.39 to 40.0 at 10 Hz	[54]
[EMIM][TFSI]:PVDF-HFP	ITO/Ion gel/ Al	8.39 (±0.38) (at 20 Hz)	[80]
[EMIM][TFSI]:PVDF-HFP	Au/Ion gel/Au	0.167 ± 0.03 - 4.16 ± 0.15 (at 1 KHz)	[79]
[EMIM][TFSI]: SEAS-N3[b]	Au/Ion gel/Au	24	[121]
[EMIM][TFSI]:PVDF-HFP	Au/Ion gel/Au	13.26 ± 1.26- 21.82 ± 0.92	[175]

a: [CH]: Choline bicarbonate, [MA]: malic acid, Levan: polysaccharide (matrix)

b: SEAS-N3: Poly[(styrene-r-vinylbenzyl azide)-b-poly(ethyl acrylate)-b-poly(styrene-r-vinylbenzyl azide)

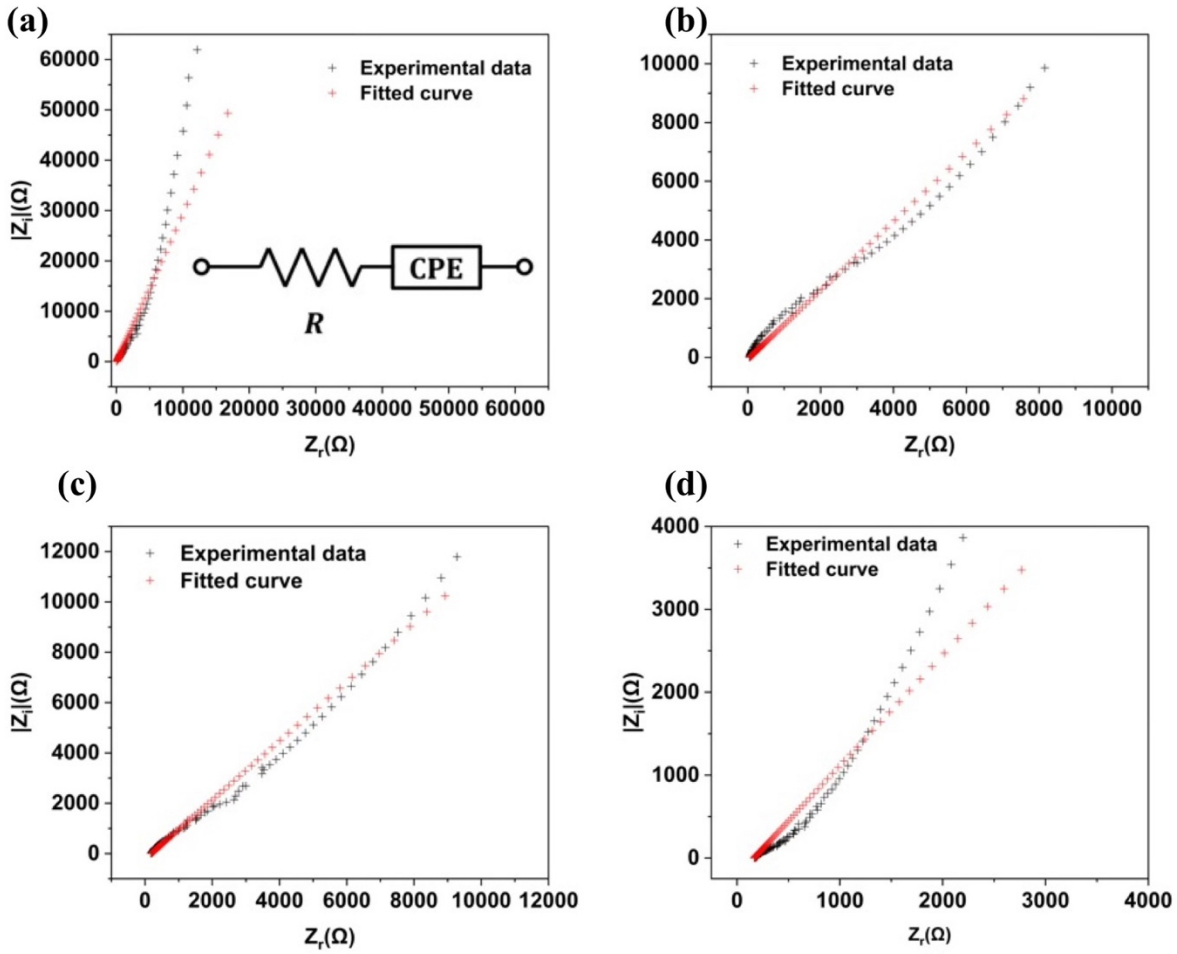

Figure S2. Fitted Nyquist curves (a) for ion-gel (a), PVA/W(0.5) (b), PVA/W+Gl (0.5) (c) and PVA/W+Gl (0.7) (d). (Inset of figure (a) represents the equivalent circuit use for fitting.

Table S2. Parameters obtained from fitting of equivalent circuit.

Sample	R (Ω)	CPE (F.s^(α-1))	α
Ion-gel	55	3.139e-6	0.82
PVA/W(0.5)	50	31.41e-6	0.55
PVA/W+Gl (0.5)	180	27.03e-6	0.55
PVA/W+Gl (0.7)	166	77.75e-6	0.59

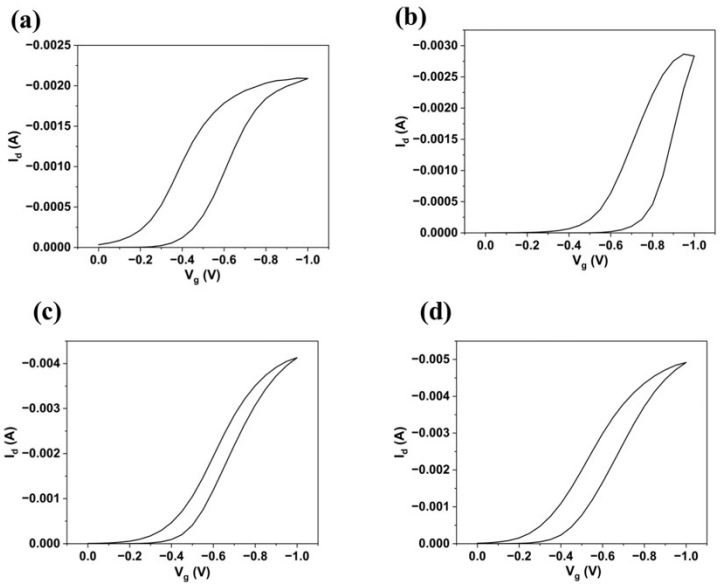

Figure S3. Transfer curves in linear region (V_d= -0.2 V) for PVDF-HFP/IL, PVA/W (0.5), PVA/W+Gl (0.5), and PVA/W+Gl (0.7) gated transistors (a, b, c, d). Scan rate is 50 mV s^{-1}.

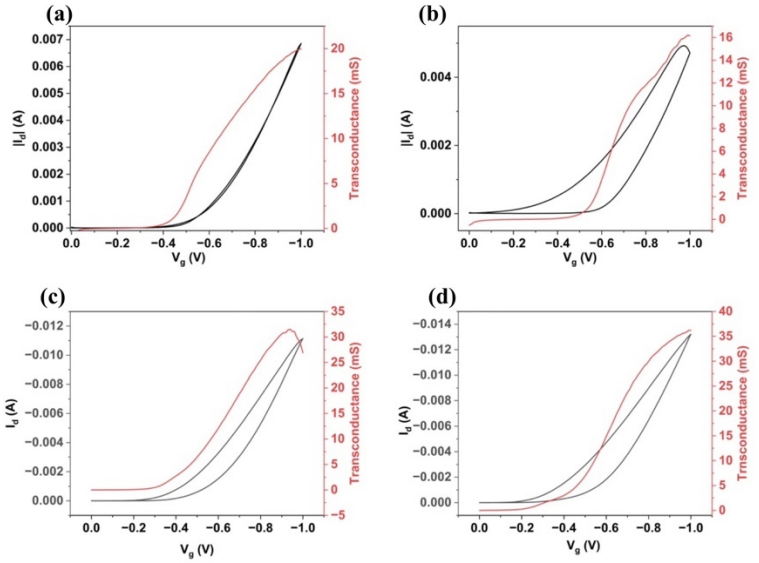

Figure S4. Transfer curves in saturation region (V_d= -0.8 V) for PVDF-HFP/IL, PVA/W (0.5), PVA/W+Gl (0.5), and PVA/W+Gl (0.7) gated transistors (a, b, c, d) (right Y axis represents transconductance. Scan rate is 10 mV s^{-1}

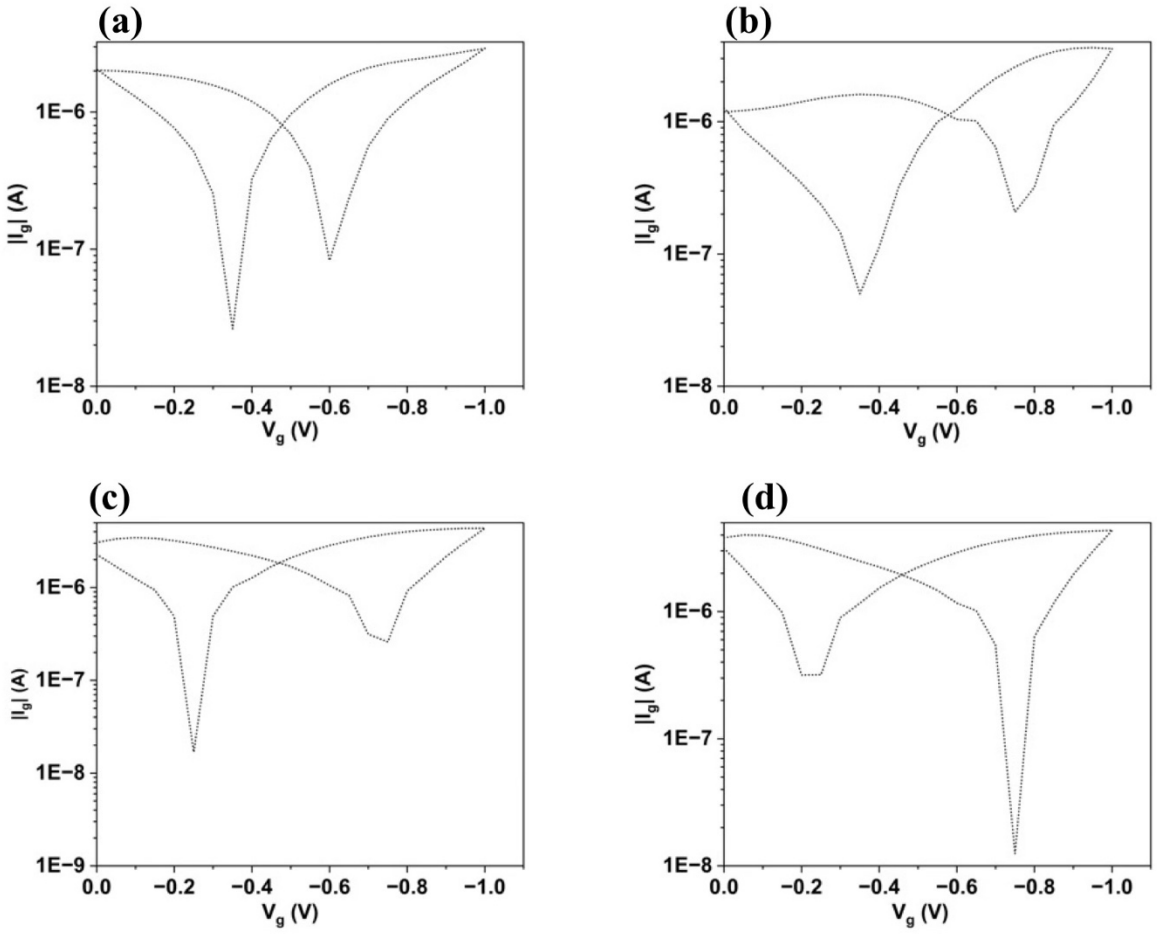

Figure S5. Gate current versus gate voltage for PVDF-HFP/IL, PVA/W (0.5), PVA/W+Gl (0.5), and PVA/W+Gl (0.7) gated transistors (a, b, c, d).

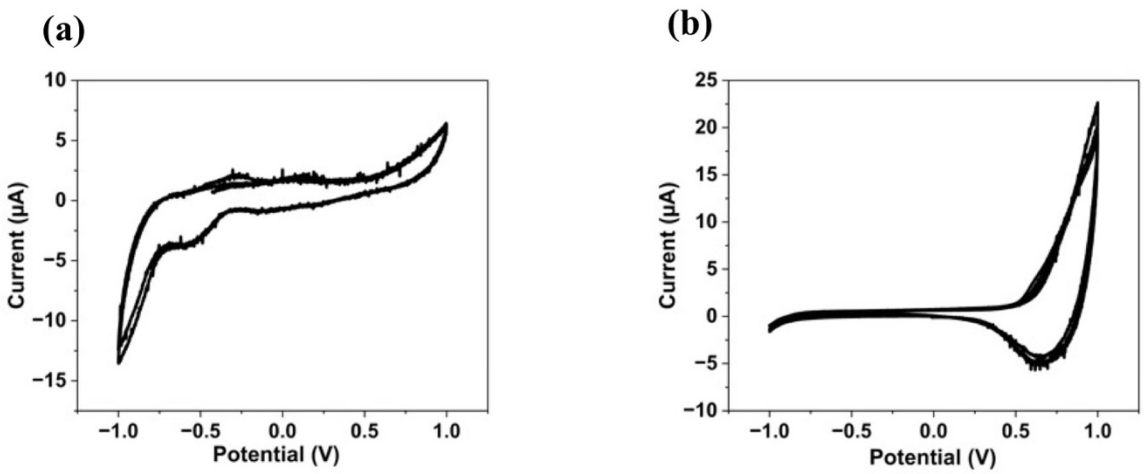

Figure S6. CVs of MIM structure (a), and MIS structure (b).

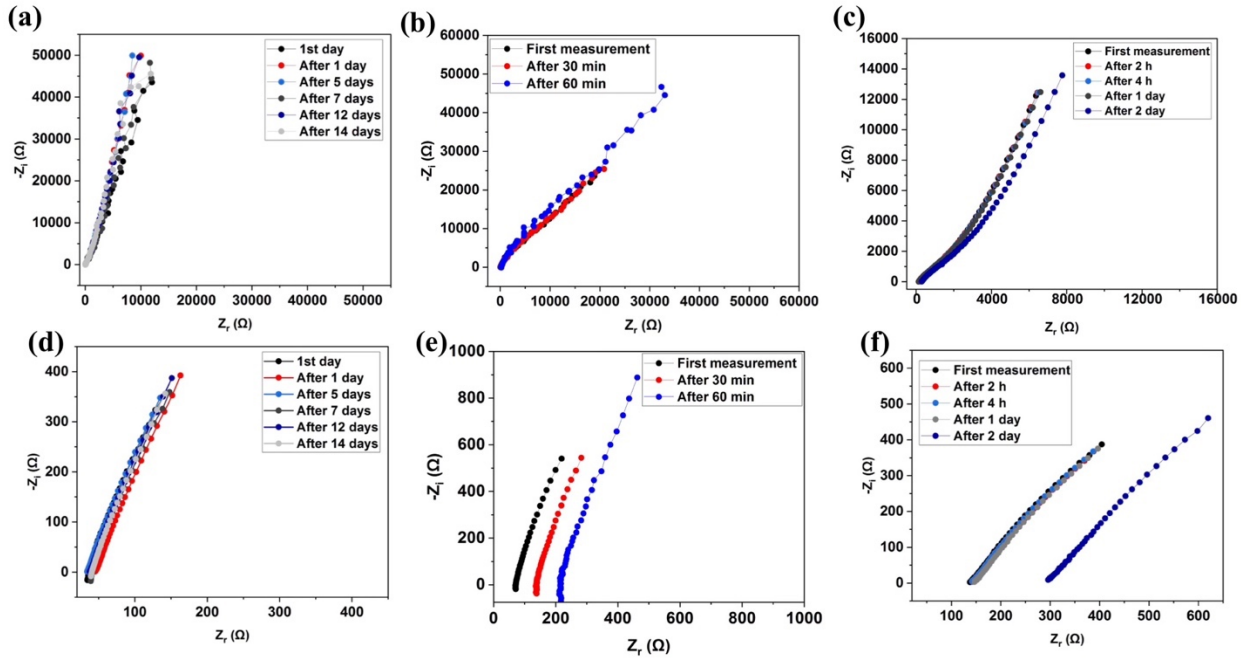

Figure S7. Nyquist curves for MIM structures of PVDF-HFP/IL (a), PVA/W(0.5) (b), , and PVA/W+Gl (0.7) (C). Magnified Nyquist plots at high frequencies related to PVDF-HFP/IL (d), PVA/W(0.5) (e), and PVA/W+Gl (0.7) (f).

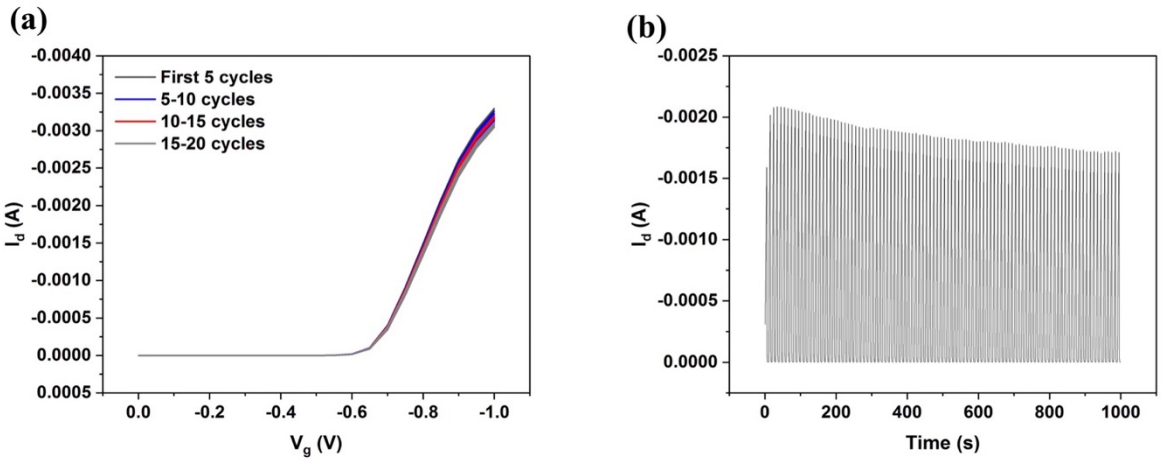

Figure S8. Transfer curves in 20 cycles (V_d= −0.2 V) (a), Pulse measurements with V_d= −0.2 V and square pulse V_g varied from 0 to -0.8 V (pulse width = 5 s) for PVA/W+Gl (0.5) gated transistor (b).

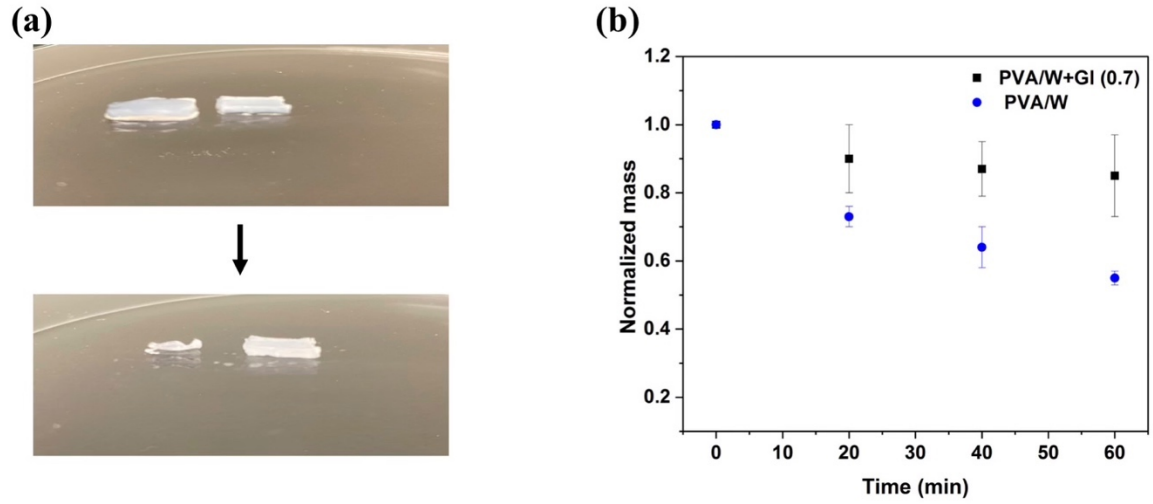

Figure S9. Optical images of PVA/W hydrogel (left) and PVA/W+Gl (0.7) hydrogel (right) directly after taking out from saline solution (top) and after 24 hours in ambient (bottom) (a) and normalized mass of two types of hydrogels after removal from the swelling solution during 60 minutes (values measured every 20 minutes).

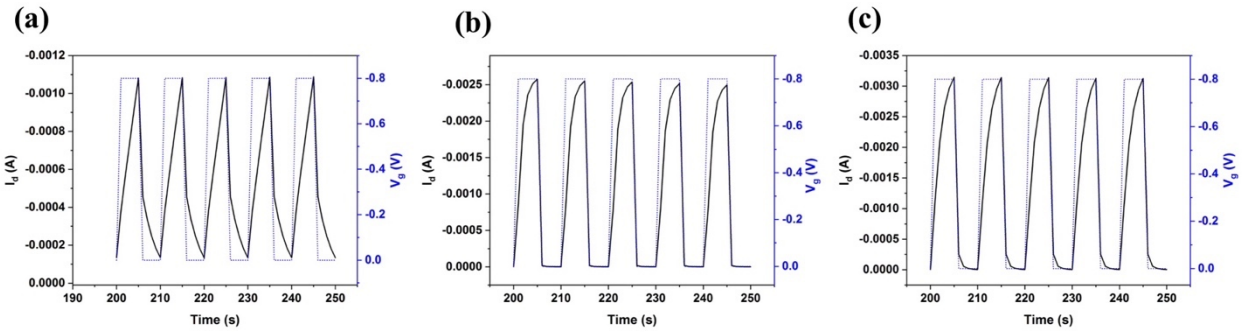

Figure S10. Magnified five cycles of pulse measurements in time scale of 200-250 s for PVDF-HFP/IL (a), PVA/W (0.5) (b) and PVA/W+Gl (0.7) (c) gated transistors.

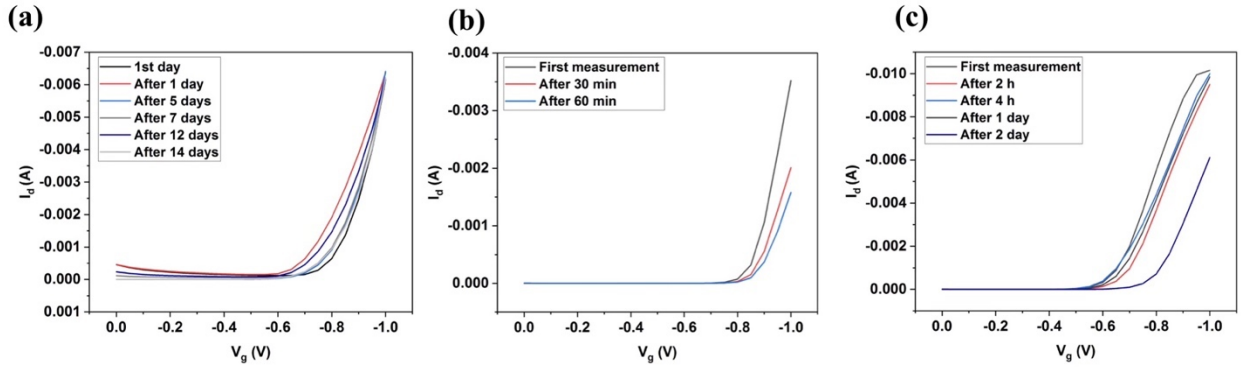

Figure S11: Stability of EGTs for PVDF-HFP/IL (a), PVA/W(0.5) (b), , and PVA/W+Gl (0.7) gated transistors (C).

APPENDIX C SUPPLEMENTARY INFORMATION FOR ARTICLE 3 : EFFECT OF IONIC CONDUCTIVITY OF ELECTROLYTE ON PRINTED PLANAR AND VERTICAL ORGANIC ELECTROCHEMICAL TRANSISTORS

Mona Azimi[1], Chi-hyeong Kim[1], Jiaxin Fan[1], Fabio Cicoira[1*]

[1] Department of Chemical Engineering, Polytechnique Montréal, Montreal, Quebec, Canada

[*] Corresponding Author: fabio.cicoira@polymtl.ca

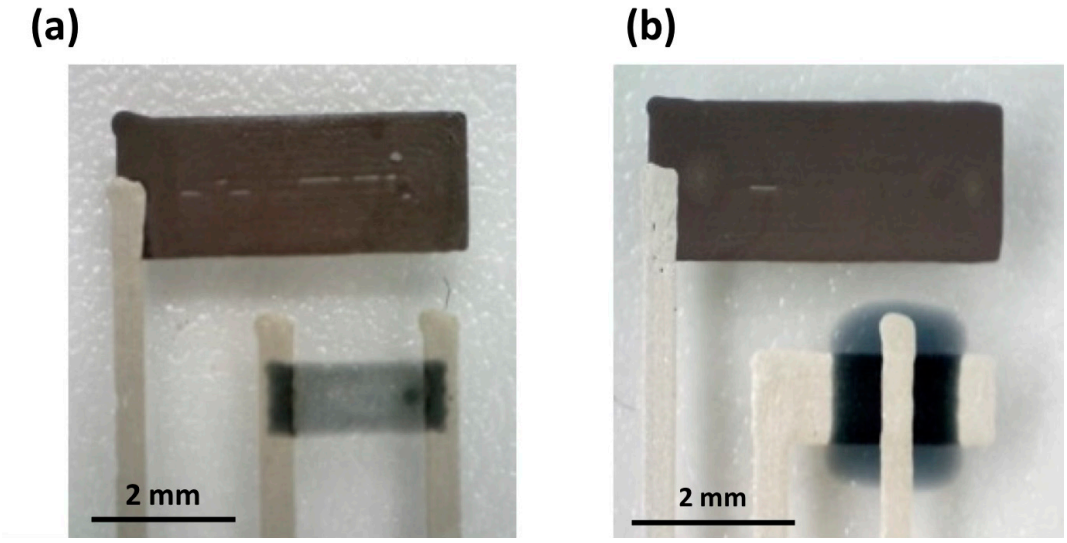

Figure S1. optical images of printed planar device (a), and vertical structure (b).

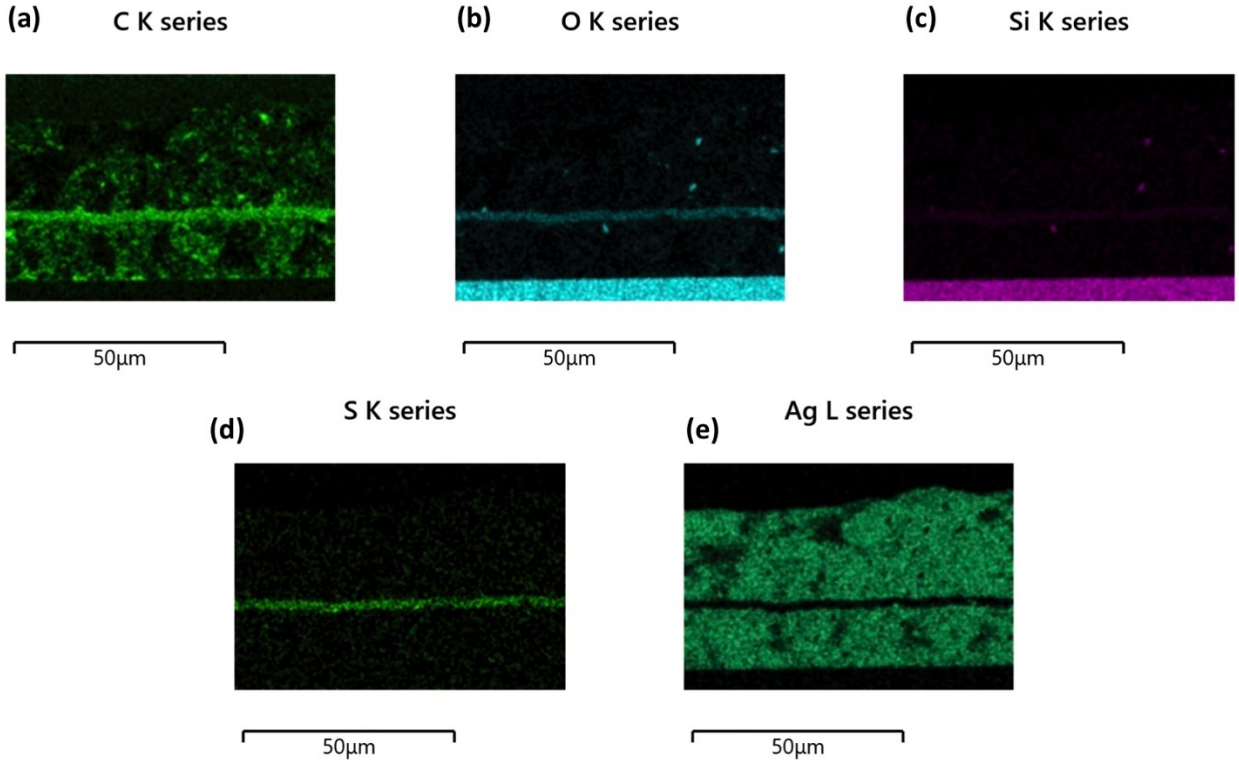

Figure S2. EDX results for printed vertical OECTs.

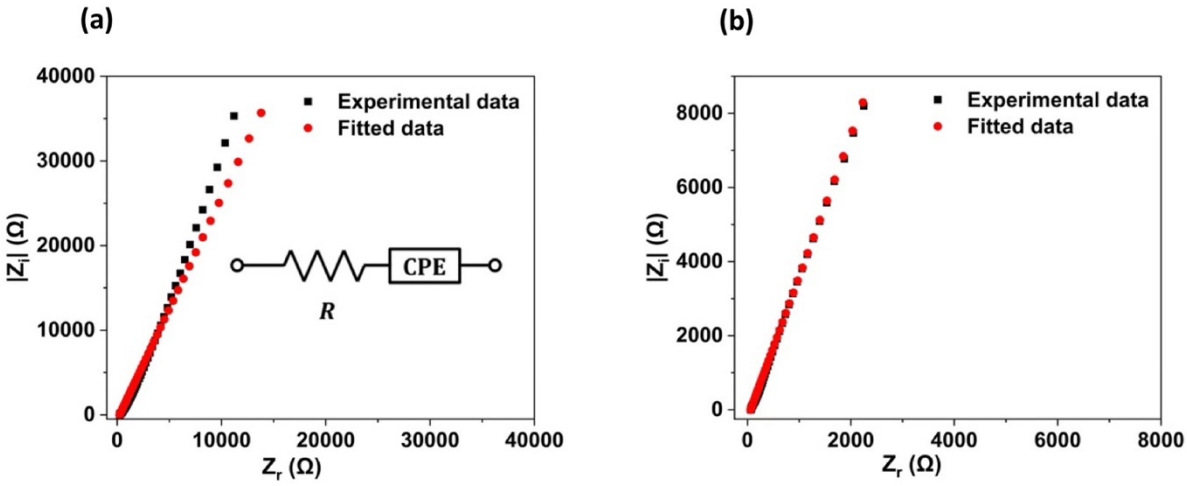

Figure S3. Fitted Nyquist plots for ion gel (a), and organogel(b).

Table S1. Fitted parameters for EIS results.

Gel	R(Ω)	CPE ($F.s^{\alpha-1}$)	α
Ion gel	234	$6.37E^{-6}$	0.78
Organogel	60	$25.06E^{-6}$	0.83

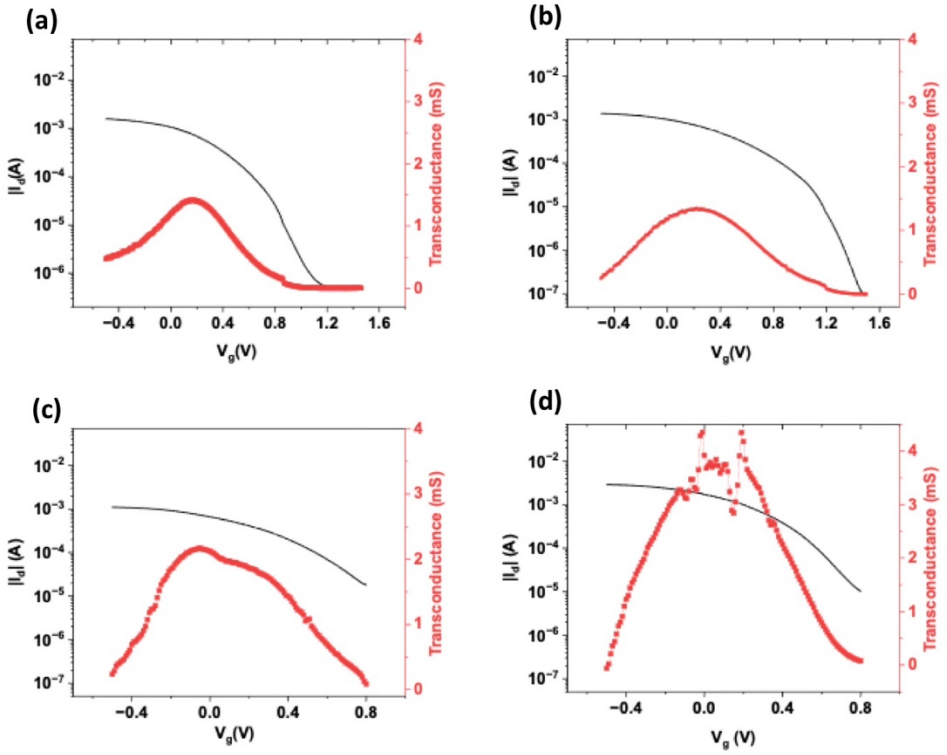

Figure S4. Transfer curves (V_d= -0.2 V) of planar OECTs with ion gel (a,b) and organogel (c,d).

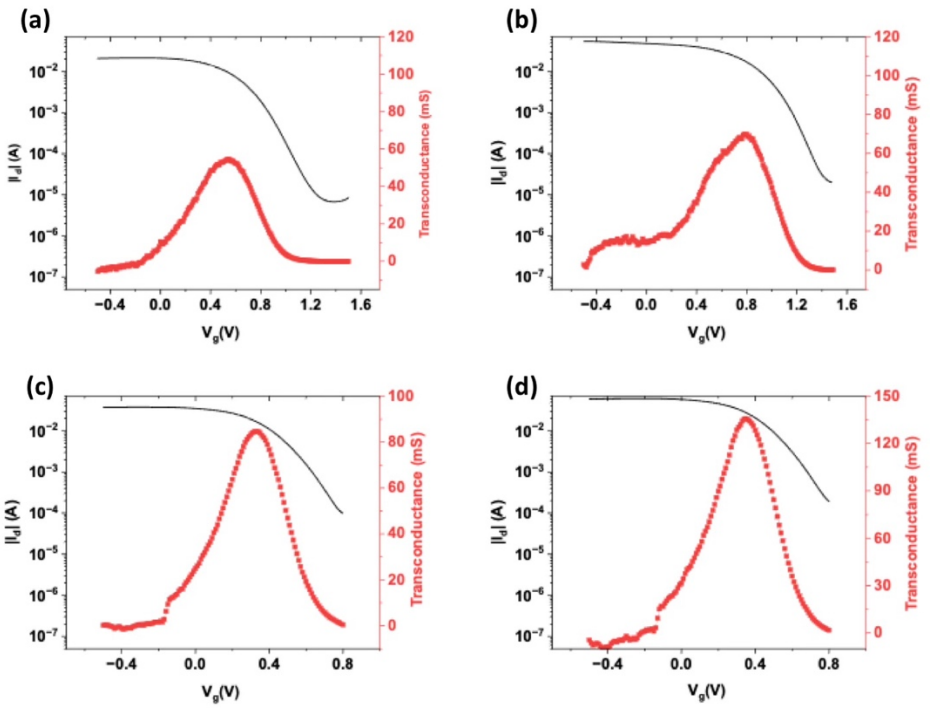

Figure S5. Transfer curves (V_d= -0.2 V) of vertical OECTs with ion gel (a,b) and organogel (c,d).

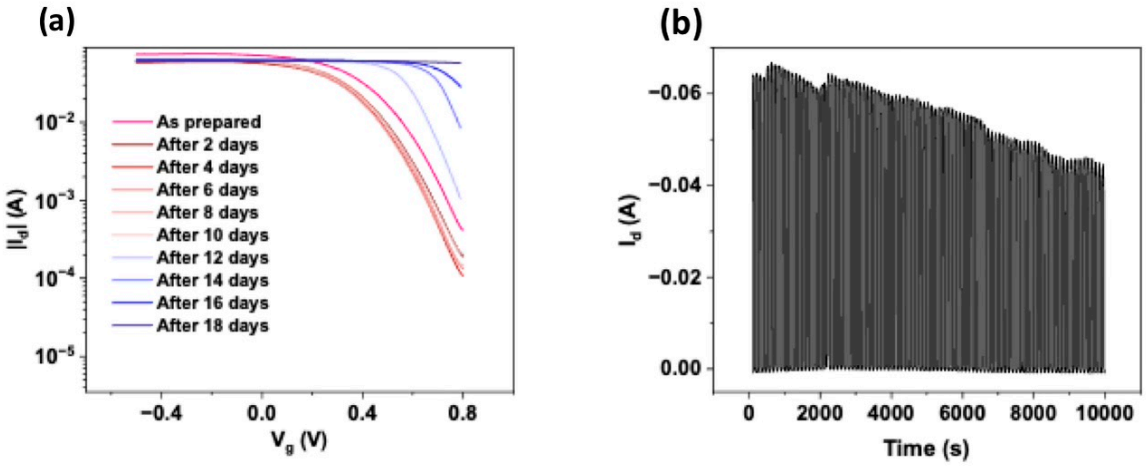

Figure S6. Transfer curves (V_d= -0.2 V) of vertical OECT gated by organogel over 18 days (a), transient response of vertical OECT gated by organogel (V_g was pulsed from 0 V to 0.8 V for 50 s) (b).

APPENDIX D LIST OF PUBLICATIONS AT POLYTECHNIQUE MONTREAL NOT INCLUDED IN THE THESIS

1. Arunprabaharan Subramanian, **Mona Azimi**, Clara Santato and Fabio Cicoira, Combining Aqueous Solution Processing and Printing for Fabrication of Flexible and Sustainable Tin Dioxide Ion-Gated Transistors, *Advanced Materials Technologies*, **2021**, DOI: 10.1002/admt.202100843.
2. Arunprabaharan Subramanian, **Mona Azimi**, Cheng Yee Leong, Siew Ling Lee, Clara Santato and Fabio Cicoira, Solution- processed titanium dioxide ion-gated transistors (IGTs) and pH sensors using ionic liquid and aqueous saline solution, *Frontiers In Electronics*, **2021**, DOI**:**10.3389/felec.2022.813535.
3. Chi-Hyeong Kim, **Mona Azimi**, Jiaxin Fan, Harini Nagarajan, Meijing Wang, and Fabio Cicoira, All-printed and stretchable organic electrochemical transistors using a hydrogel electrolyte, *Nanoscale*, **2023**, DOI: 10.1039/D2NR06731E.

APPENDIX E PARTICIPATION TO CONFERENCES

1. **Mona Azimi**, and Fabio Cicoira, Organic field effect transistors based on carbon nanotube electrodes, 21st IEEE International Conference on Nanotechnology, Montreal, Quebec, Canada, July 2021.
2. **Mona Azimi**, and Fabio Cicoira, Flexible tin dioxide ion-gated transistors (IGTs) using room temperature ionic liquid and aqueous saline solution, Canadian Chemical Engineering Conference (CCEC), Montreal, Quebec, Canada, October 2021.
3. **Mona Azimi**, Arunprabaharan Subramanian, and Fabio Cicoira, Electrochemical and operational stability of ion-gel gated organic transistors, MRS Fall Meeting, Boston, Massachusetts, USA, December 2021.
4. **Mona Azimi**, and Fabio Cicoira, Printed vertical organic electrochemical transistor, MRS Fall Meeting, Boston, Massachusetts, USA, December 2022.

APPENDIX F SCHOLARSHIPS AND AWARDS RECEIVED AT POLYTECHNIQUE MONTREAL

1. Trottier Scholarship (2018-2021), Trottier Energy Institute
2. Micro-Nanotechnology Award (August 2019, August 2020, February 2021), CMC Microsystems